

NASA TECHNICAL NOTE



NASA TN D-5935

2.1

NASA TN D-5935

LOAN COPY: RETURN
AFWL (WLOL)
KIRTLAND AFB, N

0132700



TECH LIBRARY KAFB, NM

AERODYNAMIC CHARACTERISTICS OF VEHICLE BODIES AT CROSSWIND CONDITIONS IN GROUND PROXIMITY

by Kalman J. Grunwald

Langley Research Center

Hampton, Va. 23365



0132700

1. Report No. NASA TN D-5935	2. Government Accession No.	3. Recipient's Catalog No.	
4. Title and Subtitle AERODYNAMIC CHARACTERISTICS OF VEHICLE BODIES AT CROSSWIND CONDITIONS IN GROUND PROXIMITY		5. Report Date August 1970	
		6. Performing Organization Code	
7. Author(s) Kalman J. Grunwald		8. Performing Organization Report No. L-7088	
		10. Work Unit No. 126-63-11-01	
9. Performing Organization Name and Address NASA Langley Research Center Hampton, Va. 23365		11. Contract or Grant No.	
		13. Type of Report and Period Covered Technical Note	
12. Sponsoring Agency Name and Address National Aeronautics and Space Administration Washington, D.C. 20546		14. Sponsoring Agency Code	
15. Supplementary Notes			
16. Abstract <p>A series of force tests was conducted on unpowered, high-speed ground-vehicle model configurations to provide information on shapes of this type very near the ground. Of particular interest were the crosswind effects on the aerodynamic forces and moments of the six models tested. These tests were conducted over the moving-belt ground plane in the 17-foot (5.18-m) test section of the Langley 300-MPH 7- by 10-foot tunnel at free-stream dynamic pressure values of 10 lb/ft² (478.8 N/m²).</p> <p>The results indicate that the half-circle configuration is desirable because of the low rolling moments it experienced; however, it did have higher lift values than the other configurations and, from a utility standpoint, could be impractical. The half-circle configurations with extended sides may make good compromise configurations.</p> <p>All the ground-simulation techniques employed — moving ground belt, fixed ground belt, and image model — gave reasonable representations of the overall aerodynamic trends.</p>			
17. Key Words (Suggested by Author(s)) Vehicle bodies in crosswind Ground proximity		18. Distribution Statement Unclassified — Unlimited	
19. Security Classif. (of this report) Unclassified	20. Security Classif. (of this page) Unclassified	21. No. of Pages 140	22. Price* \$3.00

AERODYNAMIC CHARACTERISTICS OF VEHICLE BODIES AT CROSSWIND CONDITIONS IN GROUND PROXIMITY

By Kalman J. Grunwald
Langley Research Center

SUMMARY

A series of force tests was conducted on unpowered, high-speed ground-vehicle model configurations to provide information on shapes of this type very near the ground. Of particular interest were the crosswind effects on the aerodynamic forces and moments of the six models tested. These tests were conducted over the moving-belt ground plane in the 17-foot (5.18-m) test section of the Langley 300-MPH 7- by 10-foot tunnel at free-stream dynamic pressure values of 10 lb/ft² (478.8 N/m²).

The results indicate that the half-circle configuration is desirable because of the low rolling moments it experienced; however, it did have higher lift values than the other configurations and, from a utility standpoint, could be impractical. The half-circle configurations with extended sides may make good compromise configurations.

All the ground-simulation techniques employed – moving ground belt, fixed ground belt, and image model – gave reasonable representations of the overall aerodynamic trends.

INTRODUCTION

The U.S. Department of Transportation has been given the immediate responsibility of providing improved passenger transportation service in the Northeast Corridor from Boston to Washington. (See refs. 1 and 2.) In the area of train transport, they have provided impetus and support for improved passenger trains, such as the Metroliner and the Turbo train (refs. 3 and 4). Although not completely new systems, such as the Japanese National Railways system (appendix B of ref. 5), these trains do offer high speed and modern luxury conveniences.

New concepts in high-speed ground systems such as the air-cushion vehicle are also being considered. (Some limitations of high-speed steel-wheel vehicles on steel rails are discussed in ref. 6.) The French are presently incorporating their Aerotrain (ref. 7) concept into a ground transportation system, and the British (ref. 8) are considering a similar air-cushion vehicle for intercity use.

The Office of High-Speed Ground Transportation of the U.S. Department of Transportation has been sponsoring research on the air-cushion vehicle. The purpose of this work at present is to design, construct, and test a tracked air-cushion research vehicle from which data can be fed into the design and evaluation of operational 300-mph (483-km/hr) transportation systems.

At the request of the U.S. Department of Transportation, the NASA Langley Research Center has been conducting supporting research. A series of force tests was conducted on unpowered vehicle model configurations to provide information on shapes of this type very near the ground. Of particular interest were the crosswind effects on the aerodynamic forces and moments of the six models tested. These tests were conducted over the moving-belt ground plane in the 17-foot (5.18-m) test section of the Langley 300-MPH 7- by 10-foot tunnel at free-stream dynamic pressure values of 10 lb/ft² (478.8 N/m²). Included in this investigation were the effects of small changes in height and small changes in angle of attack. Different methods of ground simulation, including moving ground belt, stopped ground belt, and image model, were also examined.

SYMBOLS

An axis-system drawing indicating the positive direction of forces, moments, and angles is presented in figure 1. All the data have been presented about the moment reference center, shown in figures 2 to 7.

A maximum cross-sectional area of models, feet² (meters²)

C_D' drag coefficient, $\frac{\text{Drag}}{qA}$

$C_{D,c}'$ drag coefficient corrected for base pressure

C_L lift coefficient, $\frac{\text{Lift}}{qA}$

$C_{L\alpha}$ lift-curve slope, $\frac{\Delta C_L}{\Delta \alpha}$

C_l rolling-moment coefficient, $\frac{\text{Rolling moment}}{qA d_e}$

$C_{l\beta}$ rolling moment due to sideslip, $\frac{\Delta C_l}{\Delta \beta}$

C_m pitching-moment coefficient, $\frac{\text{Pitching moment}}{qAl}$

$C_{m,c}$	pitching-moment coefficient corrected for base pressure
$C_{m\alpha}$	static pitching derivative, $\frac{\Delta C_m}{\Delta \alpha}$
C_n	yawing-moment coefficient, $\frac{\text{Yawing moment}}{qAd_e}$
$C_{n\beta}$	directional stability parameter, $\frac{\Delta C_n}{\Delta \beta}$
C_Y	side-force coefficient, $\frac{\text{Side force}}{qA}$
$C_{Y\beta}$	side-force derivative, $\frac{\Delta C_Y}{\Delta \beta}$
d_e	diameter of a circle with cross-sectional area equivalent to maximum cross-sectional area of models tested, inches (centimeters)
H	nominal height setting of model from ground belt or effective ground height for image models, inches (centimeters)
l	length (all models 72 inches (183 cm)), inches (centimeters)
q	dynamic pressure, pounds/foot ² (newtons/meter ²)
r	radius, inches (centimeters)
V	free-stream velocity, feet/second (meters/second)
α	angle of attack, degrees
β	angle of sideslip, degrees

MODEL AND APPARATUS

Drawings of the six configurations are presented in figures 2 to 7, and photographs of the half-circle and square-type configurations are presented in figure 8. The surface of each model was constructed of glass fiber and was supported by wood bulkheads for bracing. The bulkheads were mounted to an aluminum strongback which fastened to a six-component internal strain-gage balance. In order to prevent excessive vibration of the model, a set of pitch and roll dampers was mounted inside the model. These dampers

were of the piston type, in which a steel ball acting as a piston was immersed in oil inside a closely fitting cylinder. The piston was attached to the rigid model support sting, and the cylinder was attached to the model. A checkload calibration revealed that no interaction effects from the dampers were in evidence on the balance readings.

The basic cross-sectional shapes of the configurations were chosen as follows: Two of the shapes, the square-type configuration (fig. 3) and the triangular-type configuration (fig. 4), were based on shapes tested in reference 9; the circular (fig. 2) and half-circle (fig. 5) shapes were considered as other possible vehicle configurations. A preliminary series of tests on these configurations indicated the desirability of testing shapes based on the half-circle design. The two half-circle configurations with extended sides (figs. 6 and 7) were then constructed, and the entire group of models was tested over the moving belt.

Some tests were conducted by using the image technique. In order to conduct these tests, image models for three of the configurations were constructed from the same basic construction molds as the originals. A drawing and a photograph of the image-test setup are presented in figures 9 and 10, respectively. These models were mounted near the center of the tunnel from identically shaped support stings. A splitter plate was used to control the intermixing of the separated flow at the rear of the models, as suggested in reference 10.

TESTS AND CORRECTIONS

Test Procedure

This investigation was conducted in the 17-foot (5.18-m) test section of the Langley 300-MPH 7- by 10-foot tunnel. Tests were conducted over the moving-belt ground plane described in reference 11. Data were also obtained for the circular, square-type, and half-circle configurations by using the image technique.

For the tests over the ground belt, the model was set at an effective height at $\alpha = 0^\circ$; then the tunnel dynamic pressure was brought to 10 lb/ft² (478.8 N/m²), and the model was yawed from -10° to $+20^\circ$. The effective height was determined from a systematic measurement of the distance from the model to the ground at discrete locations under the model. From these measurements, a simple arithmetic average height was determined and called the effective height. The effective height at which the models were tested varied from 36 inches (91.4 cm), which can be considered out of ground effect, to 0.1 inch (0.254 cm). At all heights except 36 inches (91.4 cm), data were recorded with the ground belt moving and stopped. The effect of angle of attack was also examined over the moving belt. For these tests, the model was set at an effective height then pitched about the 50-percent-chord station of the model lower surface until the desired angle of

attack was attained. This angle was held constant, and the model was yawed from -10° to 20° .

For the image tests, it was necessary to separate the test model and the image model by a distance equal to twice the effective height. This separation is required because the effective ground location for these tests is halfway between the models. The models were then yawed from -10° to 20° .

Because of the small size of the models with respect to the tunnel and the low lift values, no corrections for blockage and wall interference were applied, since these effects would be insignificant.

The Reynolds number, based on free-stream velocity and the model length of 6 feet (1.83 m), was approximately 3.7×10^6 . The maximum crosswind Reynolds number, based on an effective model diameter of 9 inches (0.229 m), was approximately 0.2×10^6 . For long slender bodies of the type tested and presented in this paper, references 12 and 13 state that the Reynolds number should be based on body length not body effective diameter associated with the cross-sectional area because at low angles of sideslip the boundary layer is primarily dependent on the axial flow. The Reynolds number of 3.7×10^6 is considered to be supercritical, and therefore, the data would be representative of data for larger scale vehicles.

Problems in Maintaining Effective Height

Although the moving belt has been used as a research tool and the image technique has been employed in the past for ground simulation, neither technique has been used at such low heights or with models so close together. The moving belt, its backing plate, and the lower surfaces of the models introduced minor inaccuracies in setting the height because of their surface irregularities. At the higher height settings, these inaccuracies were only a small percentage of the height setting. But at the 0.100-inch (0.254-cm) setting, a change of 0.010 inch (0.025-cm) in the backing plate and a 0.007-inch (0.0178-cm) variation in belt thickness represent a sizable percentage of the effective height. During belt operation another source of height error is introduced by the belt lifting off the backing plate. The belt was observed while operating and was found to be lifting by as much as 0.030 inch (0.076 cm) at some speeds. This 0.030-inch (0.076-cm) variation was determined by the use of a height gage placed at the edge of the belt away from the model. Visual observation of the height under the model indicated that the belt was not lifting the full 0.030 inch (0.076 cm). The pressures acting on the lower surface of the model may have pushed the belt down and thereby decreased the amount of belt lifting. In any case, precise knowledge of the height setting was not possible. For this paper, no adjustment was made to the data for the belt lifting.

The image models, which were sting mounted, also introduced both height setting problems and symmetrical mounting problems. Although the models were made from the same basic mold, minor construction differences in external shape caused difficulty in mounting the models at a uniform height setting over their length.

An additional complication in maintaining effective height resulted from the severe buffeting experienced by the models during the image tests. Although some buffeting was in evidence during the tests over the belt, the magnitude was considerably lower than buffeting during the image tests, which was, in some cases, severe enough to cause premature run terminations. This condition is most probably a result of the unsteady flow created in the mixing region between the two models. A more complete discussion of this phenomenon is presented subsequently.

PRESENTATION OF RESULTS

Figures 11 to 25 are presented for discussion and analysis. Figure 26 is a sketch of a representative vehicle. The rest of the figures (figs. 27 to 51) are basic data figures for all tests conducted during this investigation. The following table presents the principal variables in each data figure.

Figure

Effect of configuration:

Longitudinal data:

$\alpha = 0^0$; $\frac{H}{d_e} \approx \text{Range}$; ground belt moving 11

Lateral data:

$\alpha = 0^0$; $\frac{H}{d_e} \approx \text{Range}$; ground belt moving 12

Lateral effectiveness:

$\alpha = 0^0$; $\frac{H}{d_e} \approx \text{Range}$; ground belt moving 13

Stability derivatives:

$\beta = 0^0$; $\frac{H}{d_e} \approx 0.03$; ground belt moving 14

$\beta = 12^0$; $\frac{H}{d_e} \approx 0.03$; ground belt moving 15

$\beta = 12^0$; $\frac{H}{d_e} \approx 0.03$; ground belt stopped 16

Effect of ground simulation $\left(\alpha = 0^0; \frac{H}{d_e} \approx \text{Range} \right)$:

Circular configuration 17 to 19

Square-type configuration 20 to 22

Half-circle configuration 23 to 25

Effect of ground height $\left(\alpha = 0^\circ; \frac{H}{d_e} \approx \text{Range}\right)$:

Circular configuration:

Ground belt moving	27
Ground belt stopped	28

Square-type configuration:

Ground belt moving	29
Ground belt stopped	30

Triangular-type configuration:

Ground belt moving	31
Ground belt stopped	32

Half-circle configuration:

Ground belt moving	33
Ground belt stopped	34

Half-circle (short extended sides) configuration:

Ground belt moving	35
Ground belt stopped	36

Half-circle (long extended sides) configuration:

Ground belt moving	37
Ground belt stopped	38

Effect of angle of attack (all configurations; ground belt moving and stopped)

39 to 48

Effect of height $\left(\text{image technique; } \frac{H}{d_e} \approx \text{Range; } \alpha = 0^\circ\right)$:

Circular configuration	49
Square-type configuration	50
Half-circle configuration	51

DISCUSSION

The data presented in this paper could apply to the body aerodynamics of a tracked air-cushion vehicle on a flat guideway or a steel-wheel train on a steel track. In either case, the parameters of principal concern are those which might cause the vehicle to lift off its guideway as a result of a substantial crosswind. To evaluate the force and moment data in figures 11 to 25, a representative vehicle has been proposed and is sketched in figure 26. For this slender vehicle, the long pitching- and yawing-moment arms result in minimizing the effect of aerodynamic pitching moment and yawing moment. Aerodynamic side force resulting from a crosswind acting on either a rail vehicle or an air-cushion vehicle would increase the power required during acceleration and also to

maintain speed, but would not cause the vehicle to upset. The principal danger occurs when a combination of rolling moment and lift force could cause the vehicle to become airborne. This problem could be further aggravated by track irregularities which could result in the vehicle assuming a nose-up attitude during normal travel; under these circumstances, an additional increase in lift could occur.

Other factors, such as centrifugal loads experienced when rounding curves, may contribute to upsetting the vehicle. However, only the principal aerodynamic parameters are considered herein.

Configuration Effects

Lift. - The longitudinal aerodynamic coefficients are plotted as functions of sideslip (crosswind) and presented in figure 11 for the six basic cross-sectional shapes tested through a ground-height range with the ground belt moving. As expected, the symmetrical circular configuration develops little or no lift in the crosswind condition out of ground effect ($\frac{H}{d_e} \approx 3.3$). (See fig. 11(a).) The square-type configuration develops some negative lift due to its contoured nose shape, but this lift is still rather low. In general, for the configurations tested, there exists a systematic progression in lift coefficient from the symmetrical circular configuration to the low-aspect-ratio, winglike half-circle configuration. Although lift increases for all configurations as the models are moved nearer the ground, the lift-coefficient spread between the circular configuration and the half-circle configuration is reduced. Therefore, the effect of cross section decreases as the model moves into ground effect.

The maximum lift coefficient measured was 1.65 for the half-circle configuration at $\beta = 20^\circ$ and $\frac{H}{d_e} \approx 0.01$. (See fig. 11(h).) For the representative vehicle shown in figure 26 (64 feet (19.51 m) long and effectively 8 feet (2.44 m) wide, moving at 300 mph (483 km/hr) with a 110-mph (177-km/hr) crosswind, and weighing 30 000 pounds (133 kN)) this is equivalent to 19 000 pounds (85 kN) of lift. With a 60-mph (96.5-km/hr) crosswind, which is approximately 12° of sideslip, and at 300 mph (483 km/hr) forward speed, the maximum lift coefficient is 0.6, which for the representative vehicle would be 7000 pounds (31 kN) of lift. As far as the vehicle lifting off the track is concerned, these lift values do not appear to be excessive.

Rolling moment. - The lateral-directional coefficients are presented in figure 12. The slopes through zero sideslip angle C_{l_β} , C_{n_β} , and C_{Y_β} are presented as functions of ground height in figure 13. Since the vehicle is long and narrow, the significance of pitch and yaw is small and the effect of the roll input becomes substantial. At 20° of sideslip, the roll slopes C_{l_β} for the circular configuration very near the ground

approach a value of -0.048 per degree. For the representative vehicle traveling at 300 mph (483 km/hr), this 110-mph (177-km/hr) crosswind causes a rolling moment of approximately 90 000 ft-lb (122 018 m-N). If the lateral support points for the vehicle are 5 feet (1.52 m) apart, the vehicle would be required to offset approximately 18 000 pounds (80 kN) of force on the opposing side. At the more representative conditions of a 60-mph (96.5-km/hr) crosswind and $\beta = 12^\circ$, approximately 11 000 pounds (49 kN) of force would have to be offset. If these values are assumed to be representative, it is extremely important that the rolling moments be reduced. Of the models tested, the half-circle configuration exhibited significantly lower values of rolling moment, as can be seen in figure 13 where at $\frac{H}{d_e} \approx 0.01$, $C_{l\beta} = -0.004$. These values are equivalent to 5000 ft-lb (6779 m-N) of rolling moment for the 60-mph (96.5-km/hr) crosswind and would require only 1000 pounds (4448 N) of force on one side to compensate. This order-of-magnitude reduction in rolling moment makes the half-circle configuration highly desirable.

The main drawback of the half-circle configuration is that it tends to be inefficient for passenger loading and also for guide-pad mounting for an air-cushion vehicle. The half-circle configurations with extended sides represent compromise configurations; their shapes are more utilitarian, and their roll values are relatively low.

Angle of attack.- Thus far, lift and rolling moment have been mentioned as principal contributors to untracking; the third major contributor is a change in angle of attack. Under certain conditions, as a result of inertial effects caused by the vehicle passing over irregularities in the guideway, the vehicle may nose up and experience additional upsetting forces and moments. The aerodynamic parameters principally affected by angle of attack are rolling moment, pitching moment, and lift. Figures 14, 15, and 16, which have been derived from the basic data figures, present $\frac{\Delta C_l}{\Delta \alpha}$, $C_{m\alpha}$, and $C_{L\alpha}$ plotted as functions of configuration. By evaluating the design condition of an assumed 300-mph (483-km/hr) forward speed and a 60-mph (96.5-km/hr) crosswind, the relative significance of the angle of attack with respect to the parameters already discussed can be determined. On the representative vehicle a change of 1° in angle of attack would mean a 15-inch (0.381-m) movement of the nose with respect to the rear. This much change is unlikely. However, a 2- or 3-inch (5- or 7.6-cm) change is conceivable and corresponds to a change of approximately 0.2° in angle of attack. By evaluating the half-circle configuration which displays the largest effect of angle of attack, if $\Delta \alpha = 0.2^\circ$, then $\Delta C_L = 0.35$, which for the representative vehicle is equivalent to 4000 pounds (17.8 kN) of lift. From the data in figure 15 for the half-circle configuration and $\Delta \alpha = 0.2^\circ$, it can be found that $\Delta C_l = -0.056$, which results in an additional 5000 ft-lb (6779 m-N) of rolling moment. As was previously mentioned, these loads, although not excessive, do add to the overall forces acting on the vehicle and must be considered.

The half-circle configuration appears to be desirable because of the low basic rolling moments it experienced; however, it did have higher lift values than the other configurations, and from a utility standpoint, could contain wasted space. The half-circle configurations with extended sides may make good compromise configurations. These configurations also exhibit low values of rolling moment and are more compatible with a high-speed system from a utility standpoint.

Ground Simulation

The three types of ground simulation used during the testing were as follows: model over the moving ground belt, model over the stopped ground belt, and model with inverted image. These three types are compared at different ground heights for the circular configuration in figures 17 to 19, for the square-type configuration in figures 20 to 22, and for the half-circle configuration in figures 23 to 25.

Moving ground belt.- In order to simulate the proper relative velocity and direction of the airstream over the model in the yawed, or crosswind, condition in the tunnel, it would be necessary to have the moving ground belt traveling in the same direction as the model axis and at the same relative wind velocity. This condition could be met at all yawed model locations if the ground belt rotated with the model. However, the ground belt cannot be rotated, and therefore the only time this condition is met is at zero yaw angle, where the moving belt establishes the same relative velocity between the ground and the model as would be experienced by the full-scale vehicle moving over a guideway. In effect, during the yawed conditions, the crosswind boundary layer which, under actual operating conditions, would exist on the guideway has been eliminated. However, through the yaw-angle range of the tests, the difference can be considered negligible.

Stopped ground belt.- Tests were also conducted over the stopped ground belt. As was previously mentioned, the relative velocity difference that should exist between the ground and the model is equal to the effective velocity of the model. This condition is drastically violated in the wind tunnel when the ground belt is stopped. The primary purpose of these tests was to determine the significance of such a violation of the real conditions.

Image technique.- The image technique basically provides another form of proper relative-velocity simulation between the free air and the ground. As stated by Hoerner in reference 10, the image method, because of its symmetry, theoretically restricts air particles from penetrating the imaginary ground surface. In the actual condition the flow between the models is turbulent and separated, and the velocity components are crossing the plane of symmetry. It is also true that the formation of the vortex system aft of the vehicle may be affected by the nonexistence of the ground surface. Hoerner suggested that a plate be located behind the double model to prevent the motion of the larger

vortices across the plane of symmetry. Such a plate was installed (figs. 9 and 10) during the tests.

Effect of Ground Simulation

Model cross section.- Certain cross-sectional shapes, when tested over all three simulated grounds, showed greater differences than others. For example, in the tests of the circular configuration (figs. 17 to 19), the data revealed only a very limited difference regardless of which of the three techniques was employed. The square-type configuration (figs. 20 to 22) was more subject to differences in pitching moment and lift at the low heights, and the half-circle configuration showed large and significant changes in the longitudinal data (figs. 23 and 25) as a result of difference in technique.

There are two vehicle shape parameters which may be affecting the technique differences. They are the contour of the vehicle bottom and the sharpness of the corners on the bottom of the model. These points will be expanded when each technique is examined in the following sections.

Comparison of stopped belt with moving belt.- As has been previously discussed and as stated in reference 10, the moving ground belt provides the best simulation of real conditions that can be provided in the wind tunnel. The differences between the stopped-belt data and the moving-belt data (figs. 17 to 23) must, therefore, be a result of improper ground simulation. The significant and obvious difference in ground boundary-layer profile, coupled with the interaction of the flow about the model, results in the differences measured. The circular configuration is less affected by this interaction because of the generally smooth flow over and under the model. On the other hand, the half-circle configuration must cause a rather turbulent flow pattern from separations off its sharp sides. This flow then mixes with the unrealistic boundary-layer buildup from the floor and reacts on the bottom of the model in a fashion not representative of the real conditions. This boundary-layer buildup may also be responsible for basic flow changes across the model. In addition, the boundary-layer growth on the ground beneath the model would tend to reduce the velocity of the air passing across the bottom and could result in decreased pressure peaks. Furthermore, for this condition, more air would be forced to pass over the model and the higher velocities and greater suction pressures on the upper surface would result in the higher lift values that were measured. (See figs. 23(a), 24(a), and 25(a).)

Comparison of image technique with moving belt.- Reasons for the differences in the data between the image technique and the moving-belt technique are considerably more subtle than for the stopped belt. Theoretically, the image technique does present a fair representation of the real condition. Certainly, some of the model setup problems

contributed to the differences, as did model buffeting, which was considerably worse for image tests than for any other technique.

Perhaps the principal reason for the differences, when the models are very close together, is the intermixing of the flow between the models. This intermixing may cause an asymmetric flow region which would distort the imaginary ground and also change the effective ground height. Despite the observed differences in the data, all the techniques give reasonable representations of the existing trends.

CONCLUDING REMARKS

A series of force tests was conducted on unpowered, high-speed ground-vehicle model configurations to provide information on shapes of this type very close to the ground. Of particular interest were the crosswind effects on the aerodynamic forces and moments of the six models tested. These tests were conducted over the moving-belt ground plane in the 17-foot (5.18-m) test section of the Langley 300-MPH 7- by 10-foot tunnel at free-stream dynamic pressure values of 10 lb/ft² (478.8 N/m²).

The results indicate that the half-circle configuration is desirable because of the low rolling moments it experienced; however, it did have higher lift values than the other configurations, and from a utility standpoint, could be impractical. The half-circle configurations with extended sides may make good compromise configurations.

All the ground-simulation techniques employed – moving ground belt, fixed ground belt, and image model – gave reasonable representations of the overall aerodynamic trends.

Langley Research Center,
National Aeronautics and Space Administration,
Hampton, Va., May 4, 1970.

REFERENCES

1. Wheaton, Thomas R.; and Goodlatte, A. Richardson: Short Term Solutions to Northeast Corridor Transportation Needs. Paper presented at Sesquicentennial Forum on Transportation Engineering, N.Y. Acad. Sci., Aug. 28-30, 1967.
2. Boyd, Alan S.: National Transportation Policy and Planning. *Astronaut. Aeronaut.*, vol. 4, no. 11, Nov. 1966, pp. 112-116.
3. Anon.: Commercial Success for the Penn Central Metroliners. *Ry. Gaz.*, vol. 125, July 18, 1969, pp. 529-532.
4. Campbell, Garth: Marketing the CNR Turbo Train. *Ry. Gaz.*, vol. 125, no. 8, Apr. 18, 1969, pp. 295-299.
5. Anon.: Part I – Survey of Technology for High Speed Ground Transport. Contract C-85-65, Massachusetts Inst. Technol., June 15, 1965.
6. Anon.: Some Problems of Wheel/Rail Interaction Associated With High-Speed Trains. 06818-W318-R0-00 (Contract C-353-66(NEG)), TRW Systems, Mar. 1969.
7. Bertin; and Cié: Aerotrain – A New Concept. *High Speed Ground Transp. J.*, vol. I, no. 3, Sept. 1967, pp. 316-330.
8. Stevens, James Hay: HDL's Model Hovercar Presented. *Vertical World*, vol. 2, no. 2, Feb. 1967, pp. 16-18, 46.
9. Polhamus, Edward C.; Geller, Edward W.; and Grunwald, Kalman J.: Pressure and Force Characteristics of Noncircular Cylinders as Affected by Reynolds Number With a Method Included for Determining the Potential Flow About Arbitrary Shapes. NASA TR R-46, 1959.
10. Hoerner, Sighard F.: Fluid-Dynamic Drag. Publ. by the author (148 Busted Drive, Midland Park, New Jersey, 07432), 1965.
11. Turner, Thomas R.: A Moving-Belt Ground Plane for Wind-Tunnel Ground Simulation and Results for Two Jet-Flap Configurations. NASA TN D-4228, 1967.
12. Polhamus, Edward C.: Effect of Flow Incidence and Reynolds Number on Low-Speed Aerodynamic Characteristics of Several Noncircular Cylinders With Applications to Directional Stability and Spinning. NASA TR R-29, 1959. (Supersedes NACA TN 4176.)
13. Bursnall, William J.; and Loftin, Laurence K., Jr.: Experimental Investigation of the Pressure Distribution About a Yawed Circular Cylinder in the Critical Reynolds Number Range. NACA TN 2463, 1951.

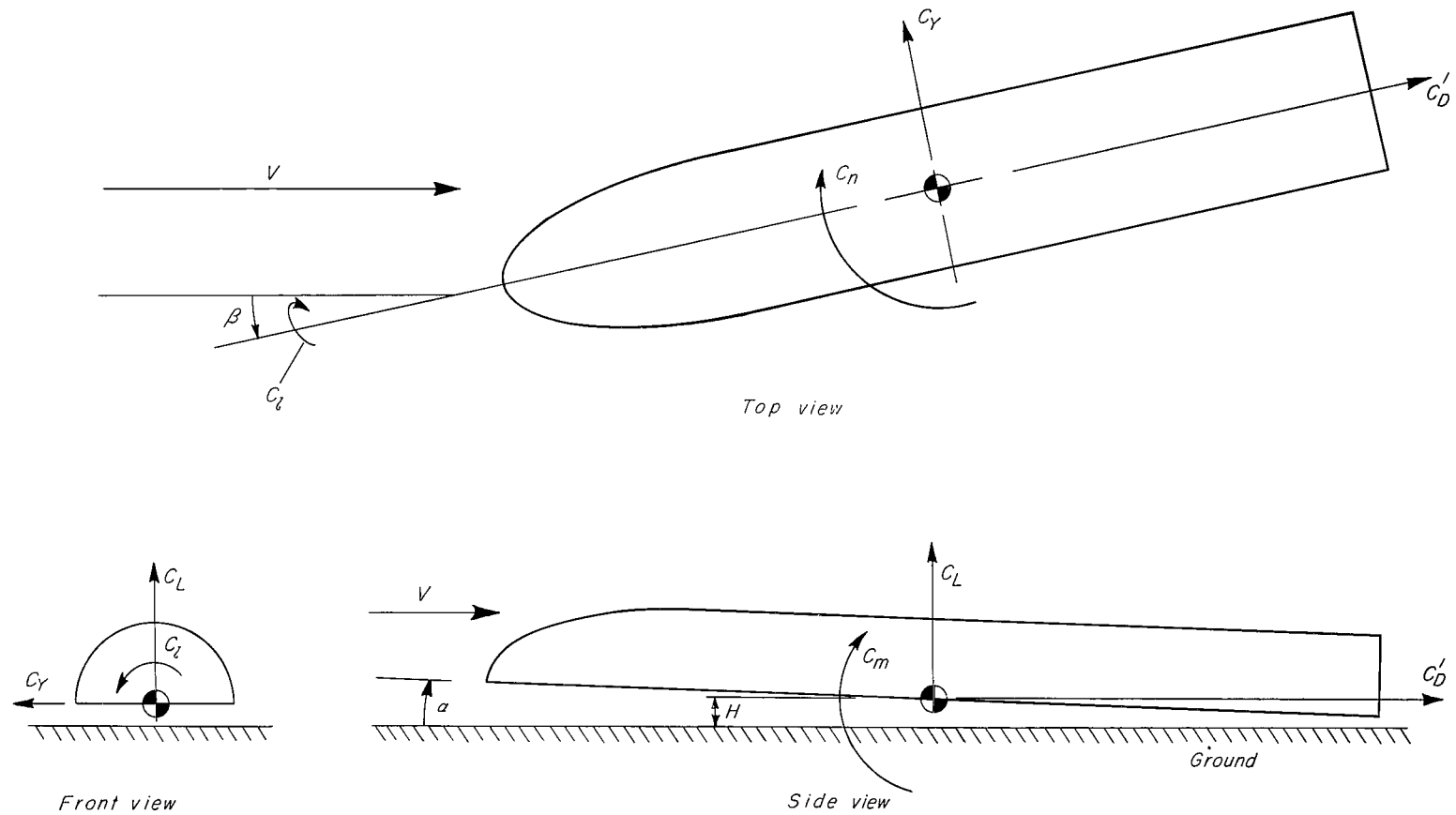
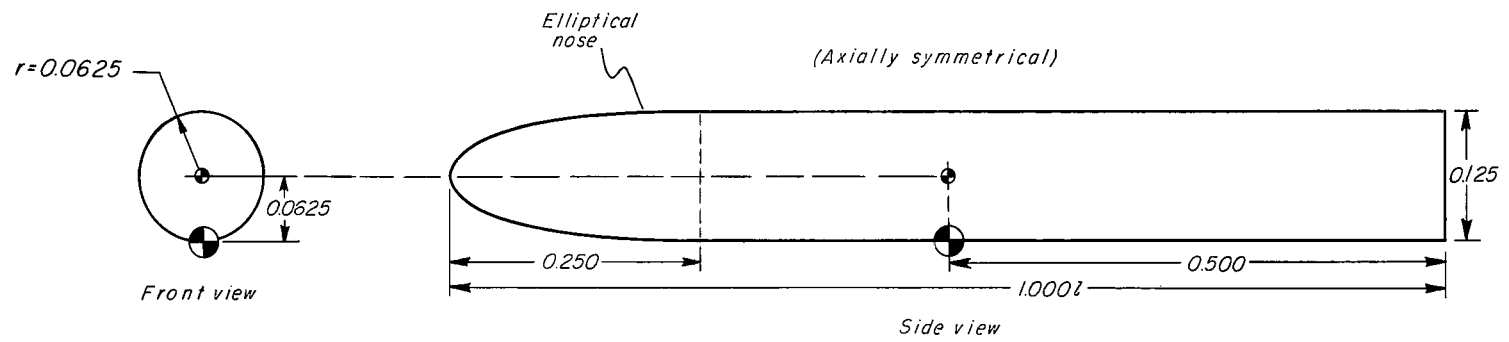


Figure 1.- Drawing of axis system showing positive direction of forces, moments, and angles.

Circular cross-section configuration





-  *Moment reference center*
-  *Sting balance center*

Figure 2.- Drawing of circular cross-section configuration. All dimensions based on vehicle length, $l = 72$ inches (183 cm).

Square-type cross-section configuration

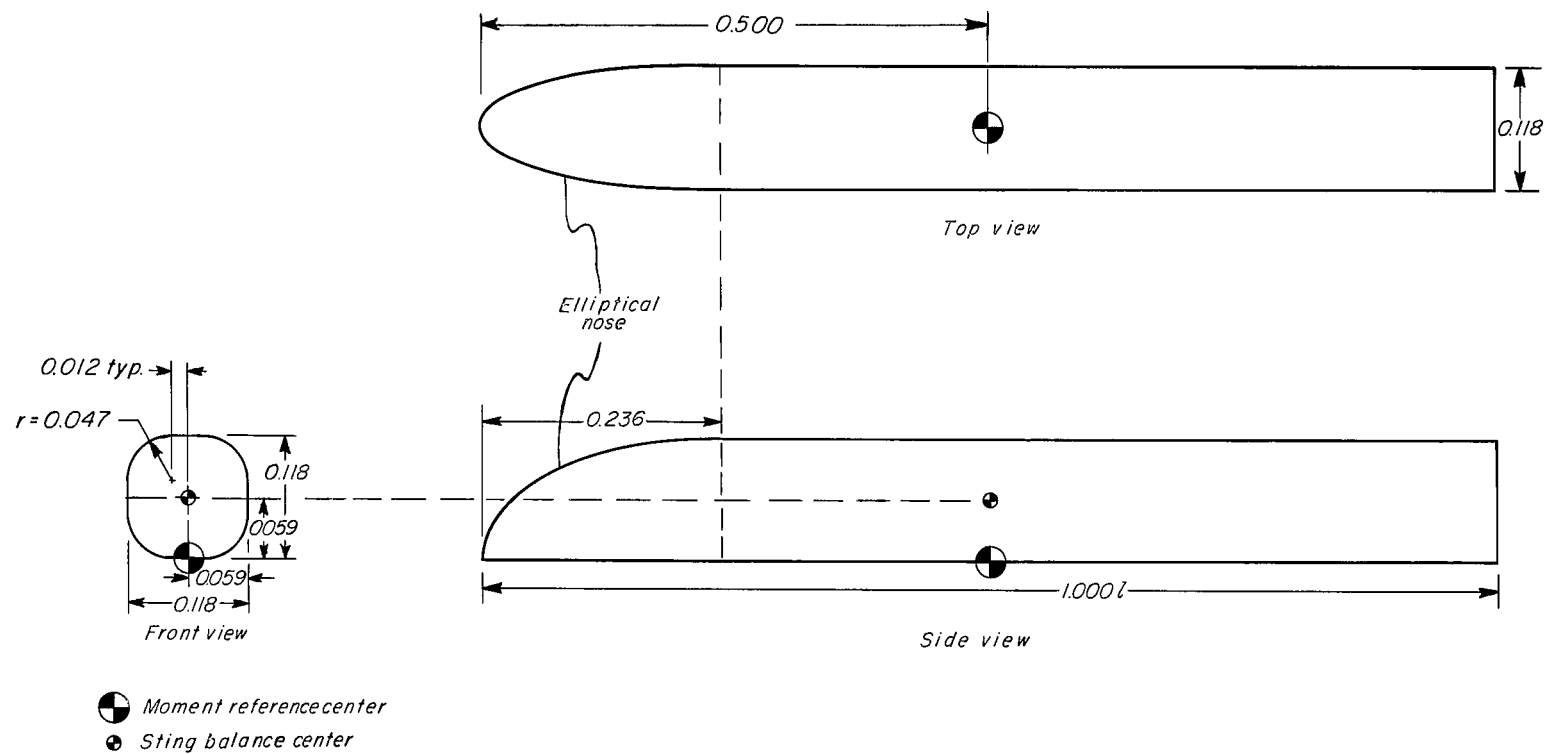


Figure 3.- Drawing of square-type cross-section configuration. All dimensions based on vehicle length, $l = 72$ inches (183 cm).

Triangular-type cross-section configuration

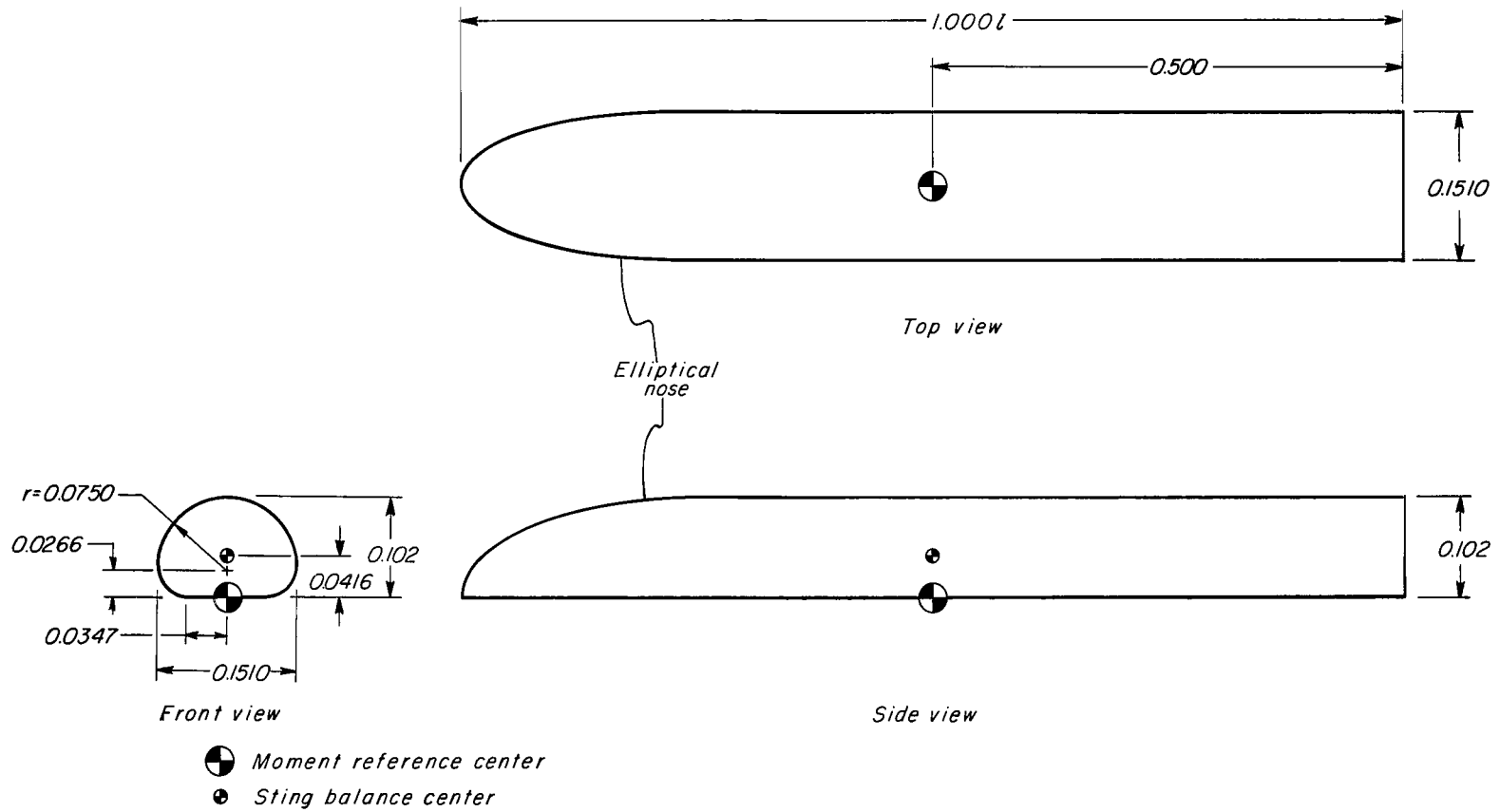


Figure 4.- Drawing of triangular-type cross-section configuration. All dimensions based on vehicle length, $l = 72$ inches (183 cm).

Half-circle cross-section configuration

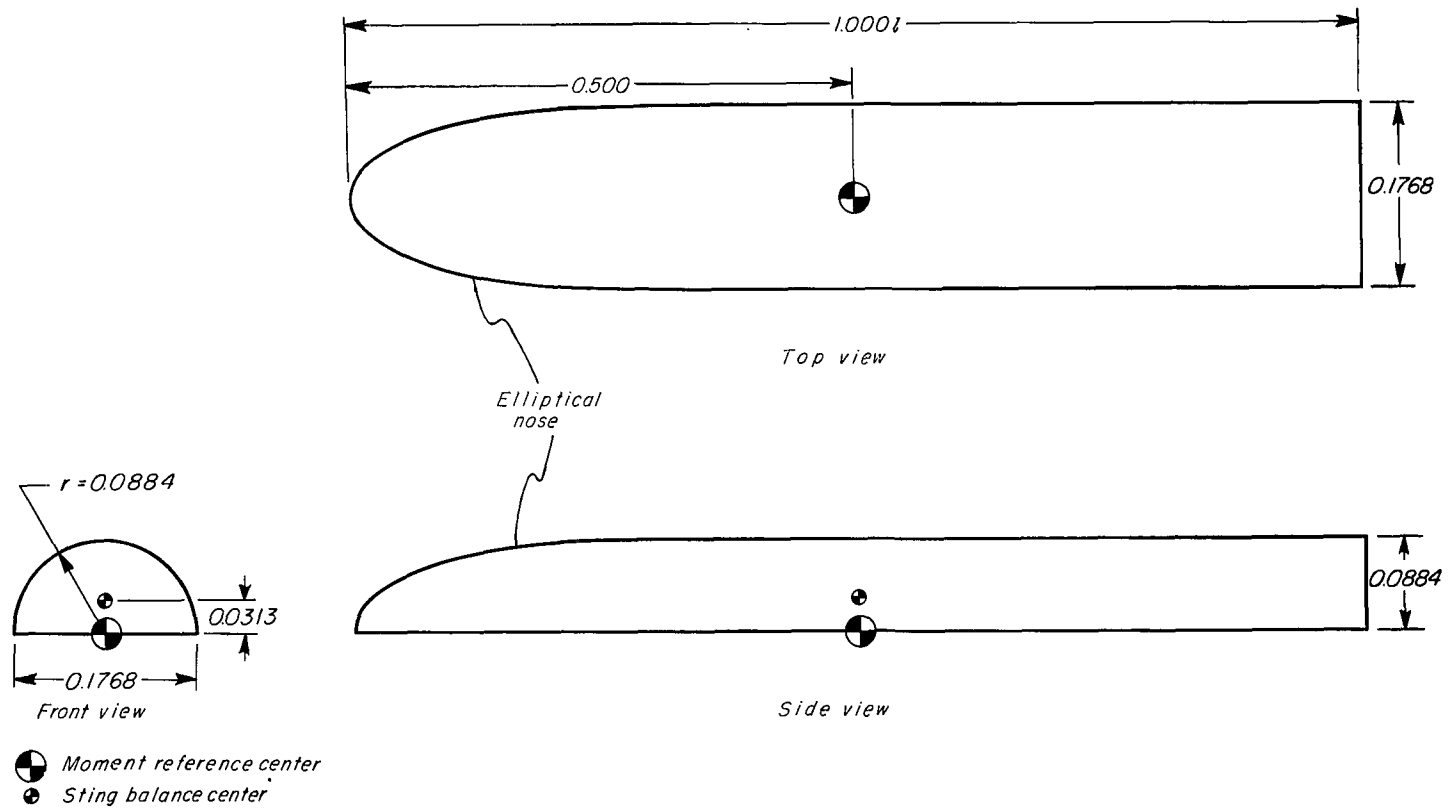


Figure 5.- Drawing of half-circle cross-section configuration. All dimensions based on vehicle length, $l = 72$ inches (183 cm).

Half-circle (short extended sides) cross-section configuration

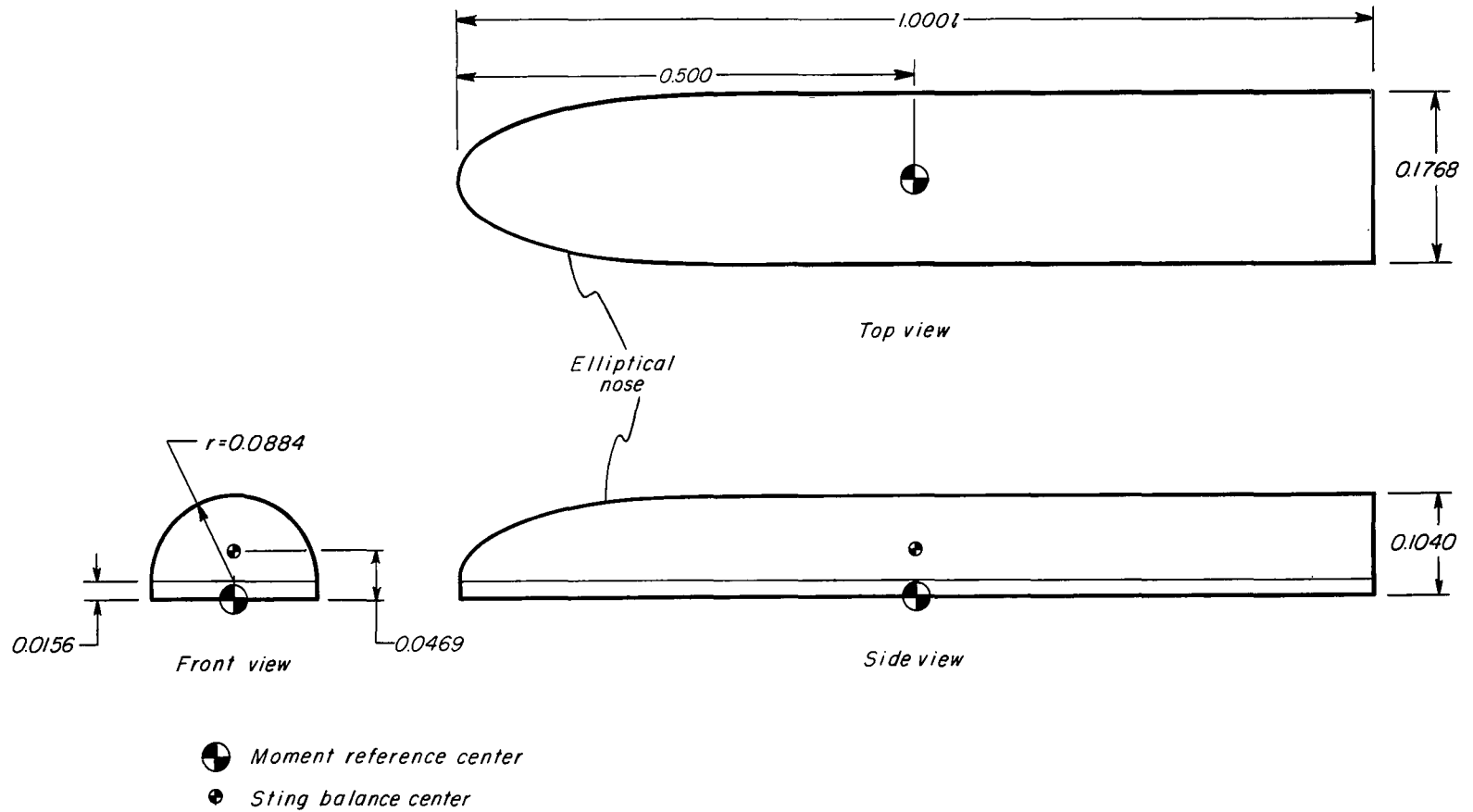


Figure 6.- Drawing of half-circle (short extended sides) cross-section configuration. All dimensions based on vehicle length, $l = 72$ inches (183 cm).

Half-circle (long extended sides) cross-section configuration

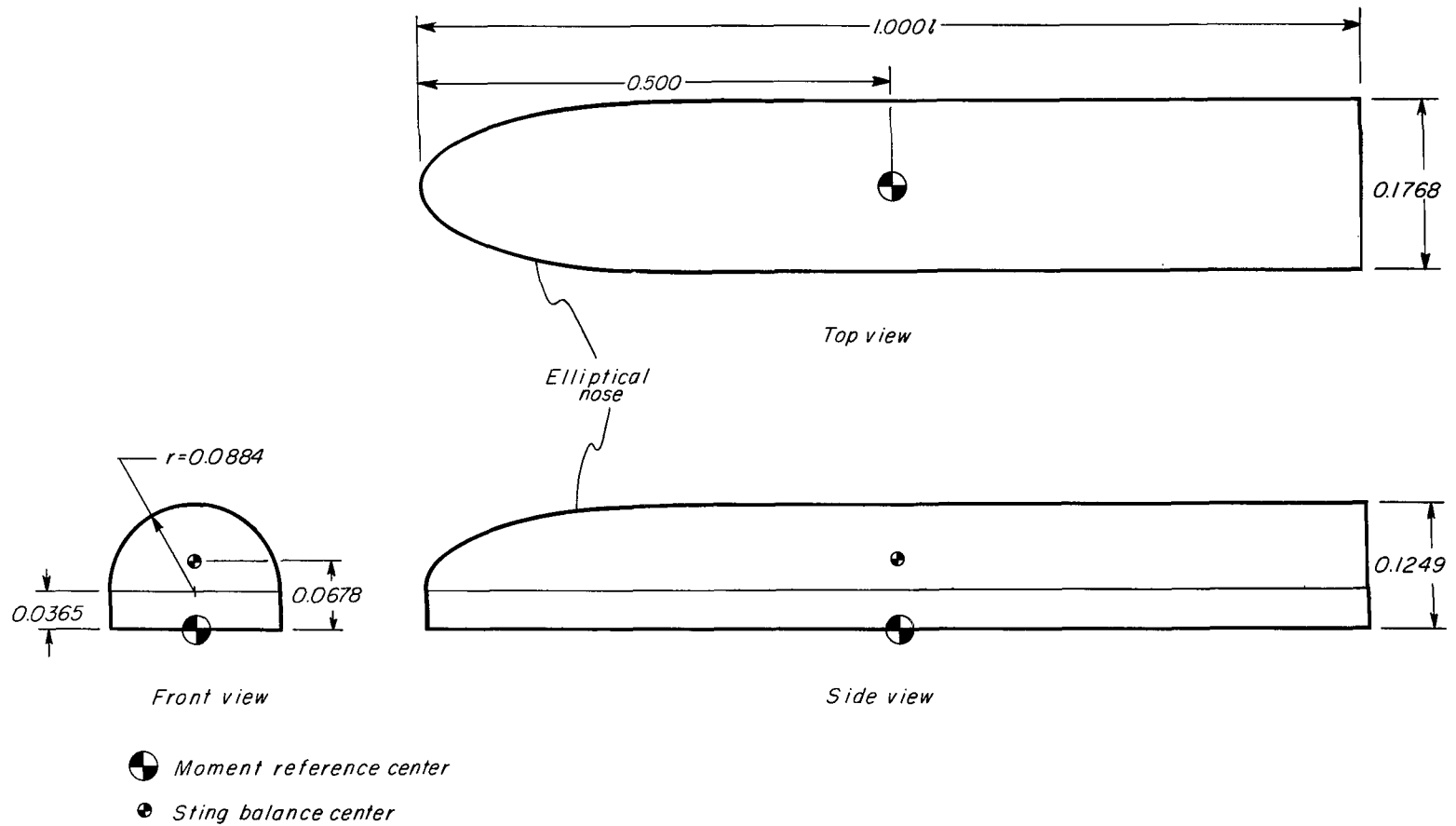
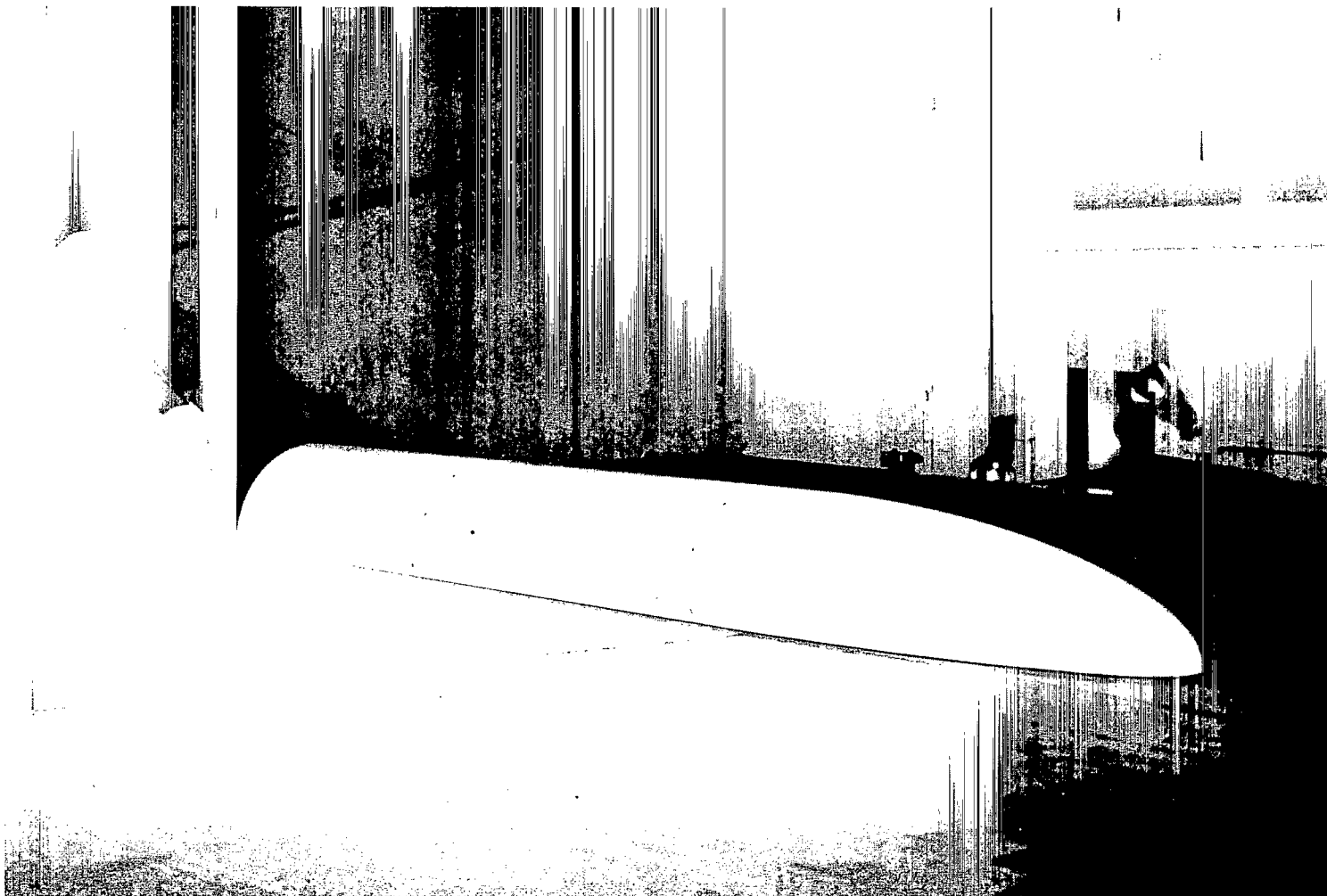


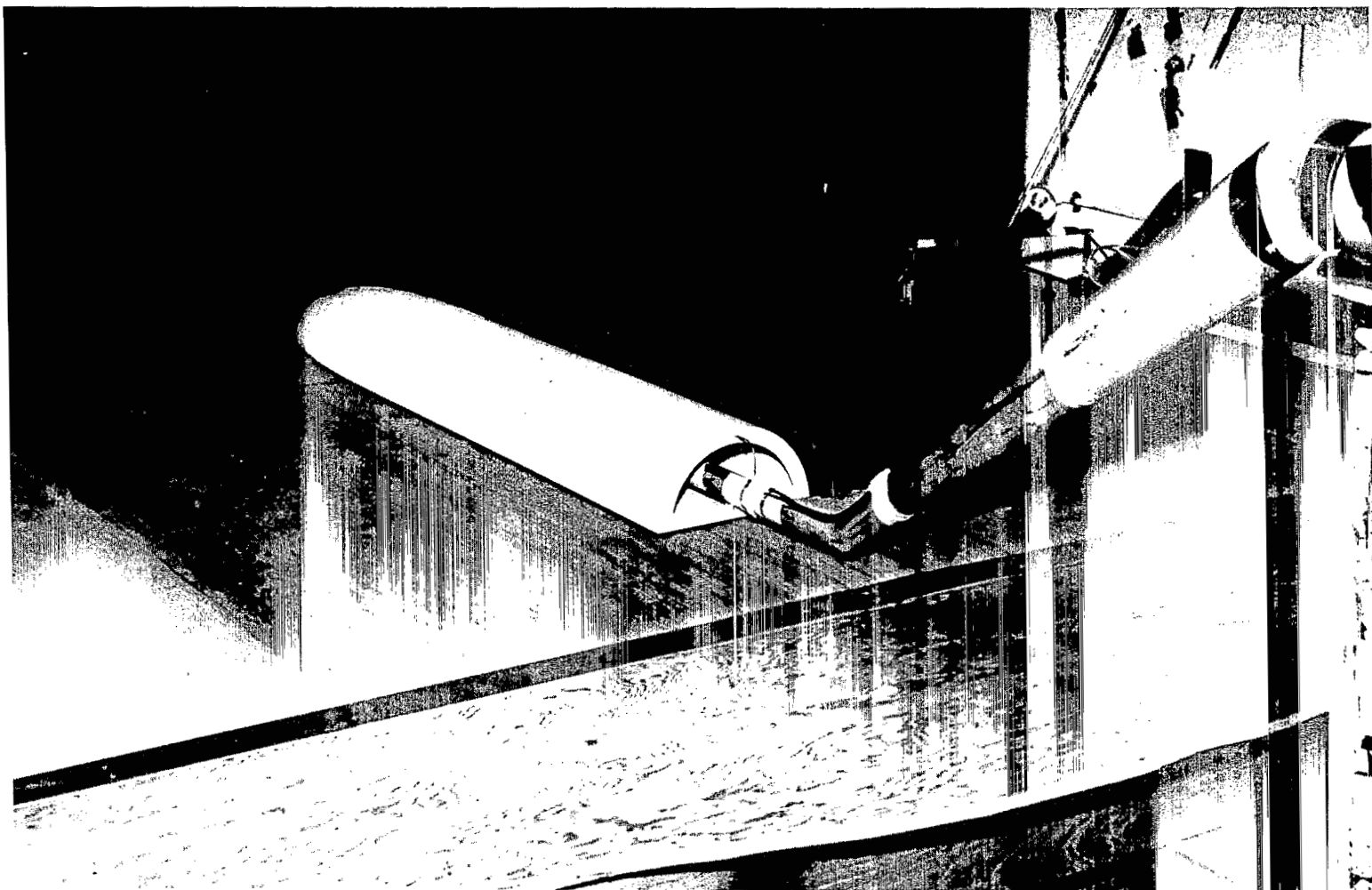
Figure 7.- Drawing of half-circle (long extended sides) cross-section configuration. All dimensions based on vehicle length, $l = 72$ inches (183 cm).



(a) Three-quarter front view of half-circle configuration.

L-67-6404

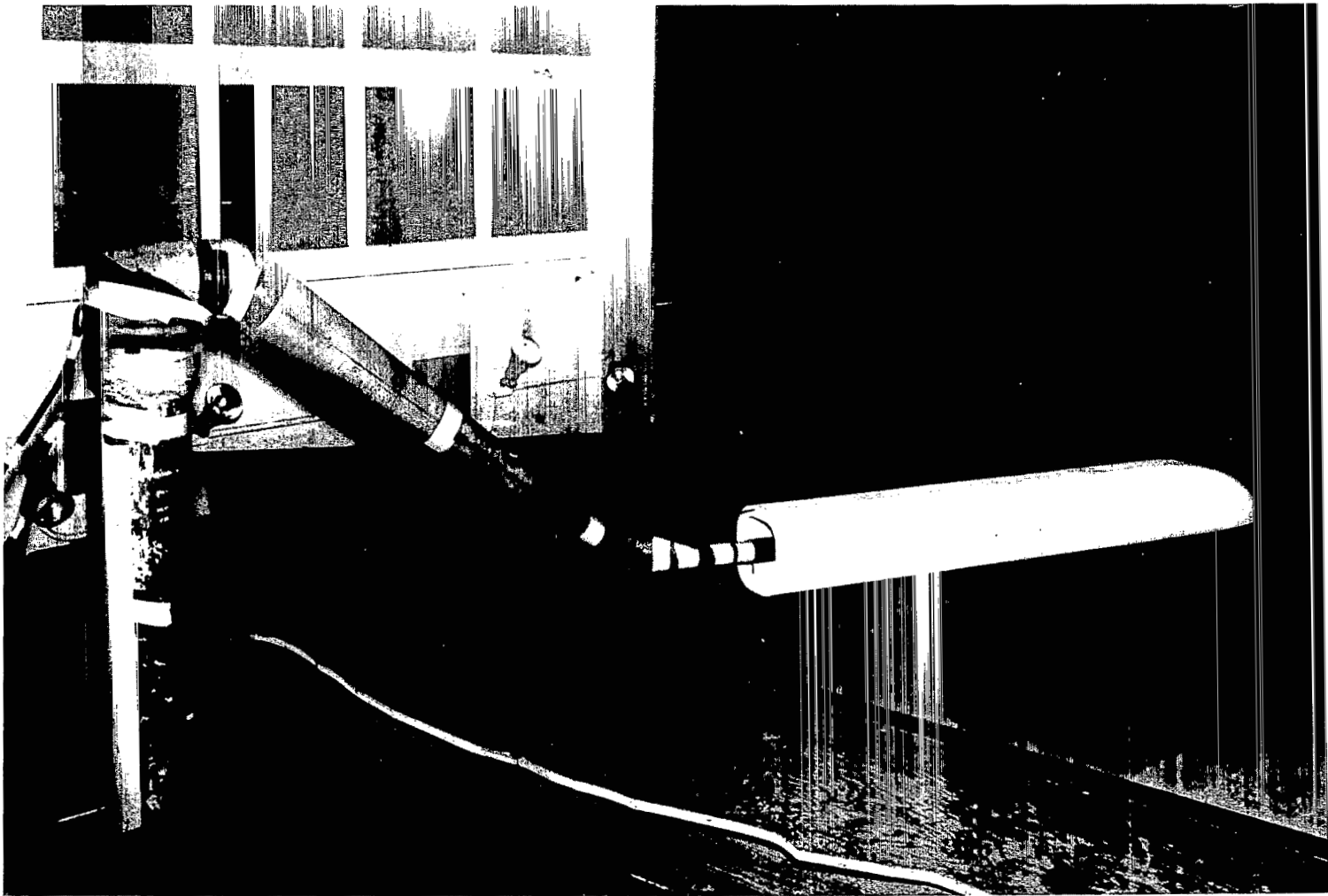
Figure 8.- Models over ground belt in tunnel.



(b) One-quarter rear view of half-circle configuration.

L-67-6405

Figure 8.- Continued.



(c) Three-quarter rear view of square-type configuration.

L-67-6789

Figure 8.- Concluded.

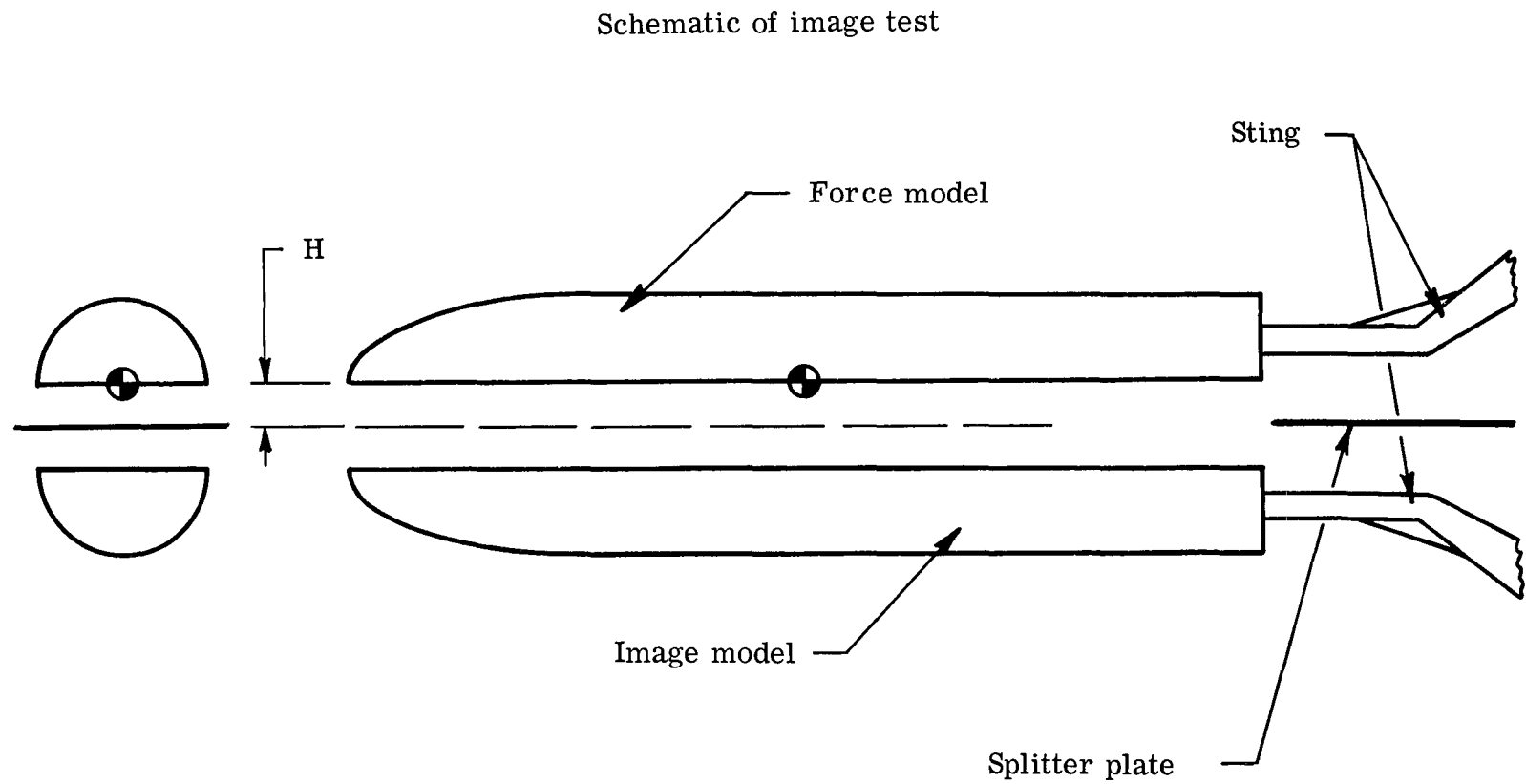
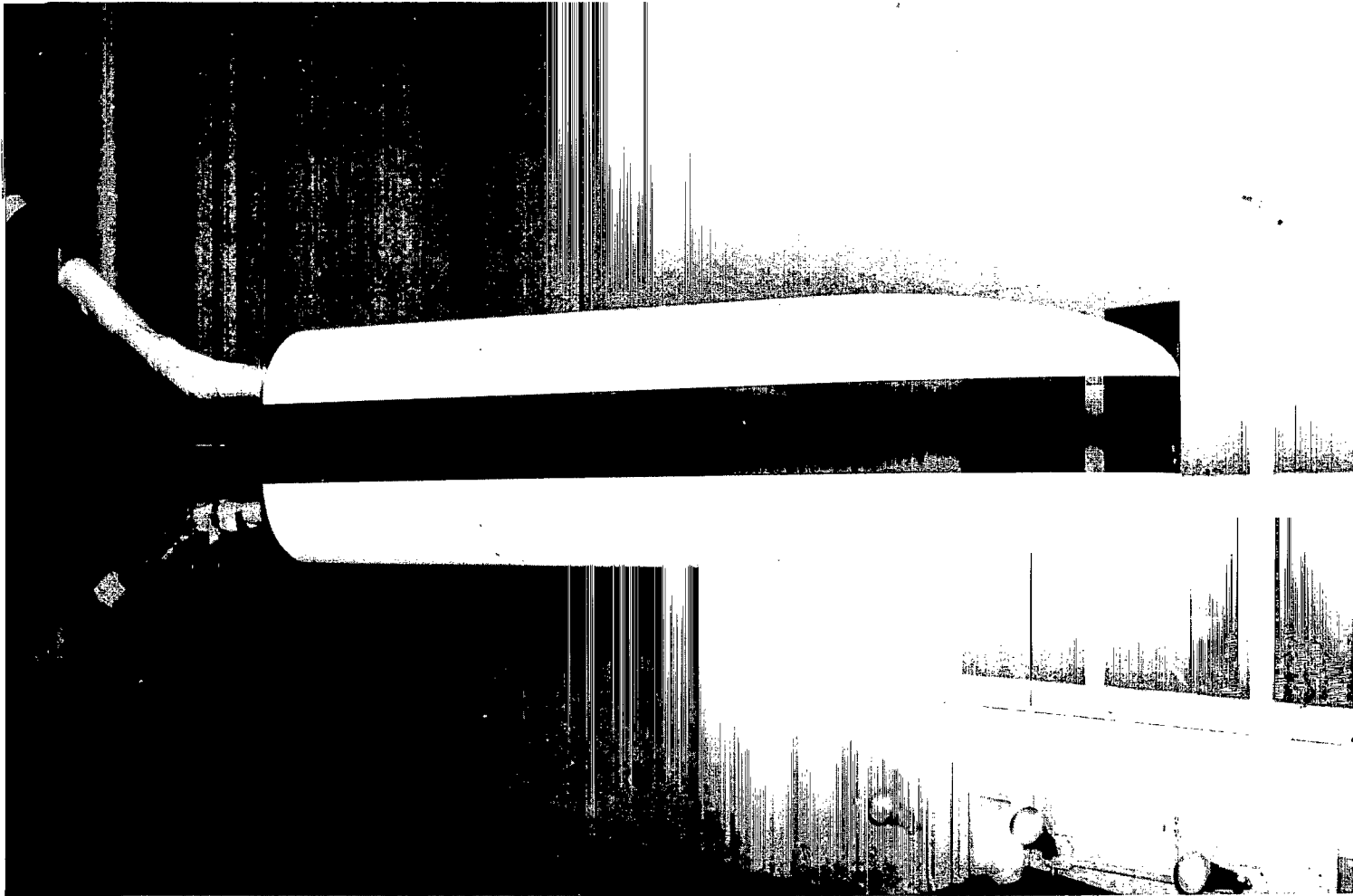


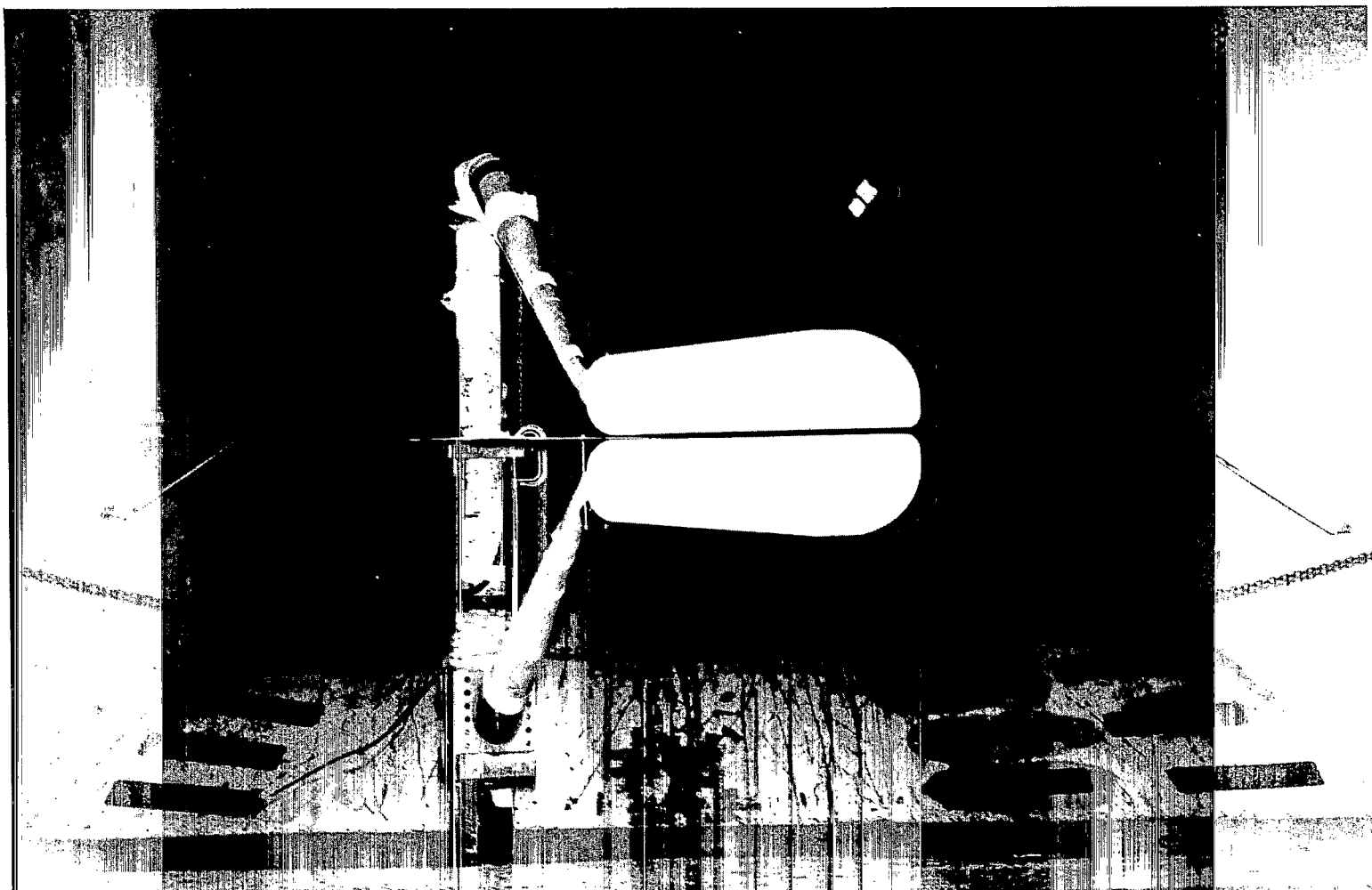
Figure 9.- Schematic representation of image-test setup.



(a) Half-circle configuration.

L-68-7954

Figure 10.- Image-test setup.



(b) Square-type configuration.

L-68-8071

Figure 10.- Concluded.

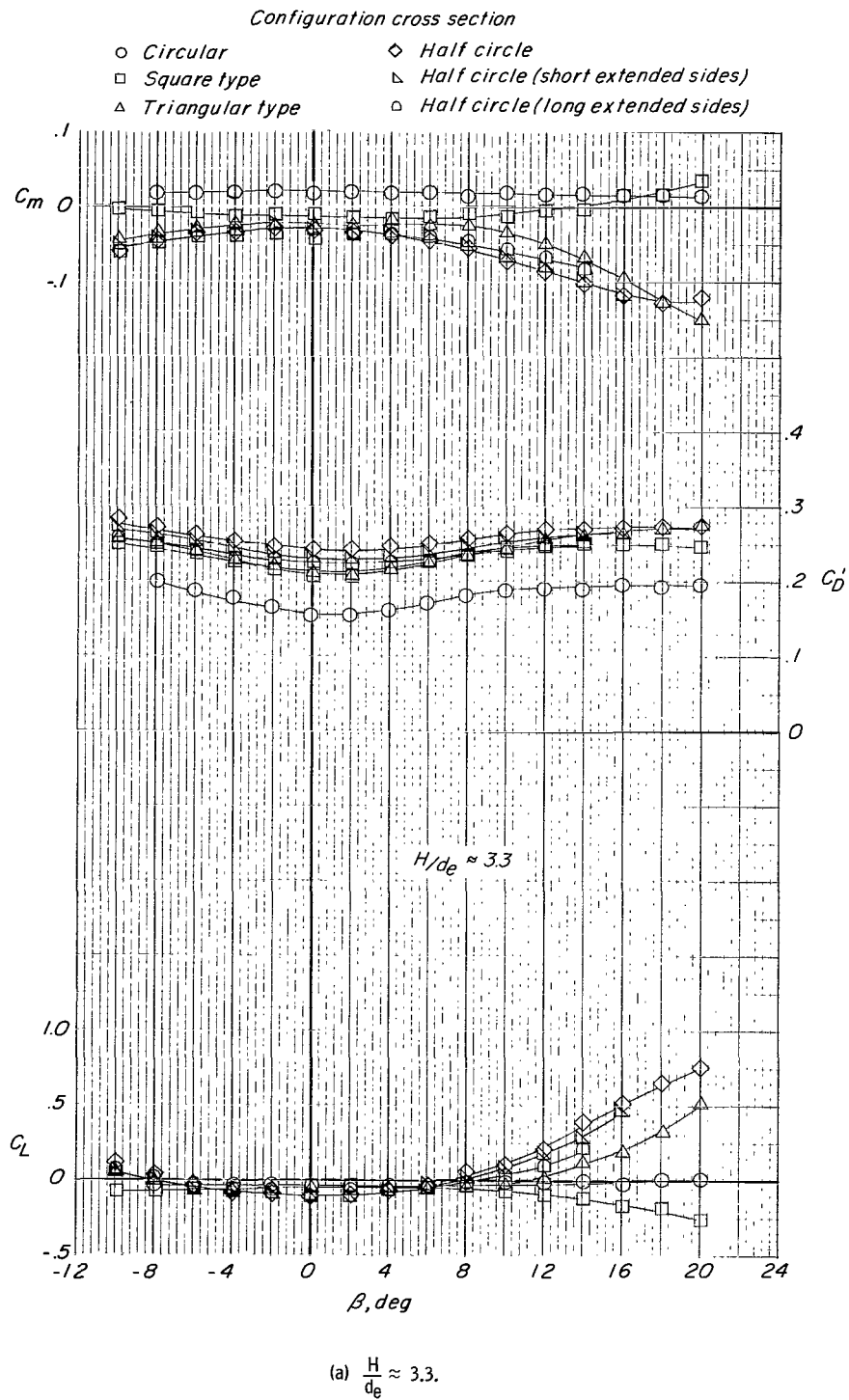
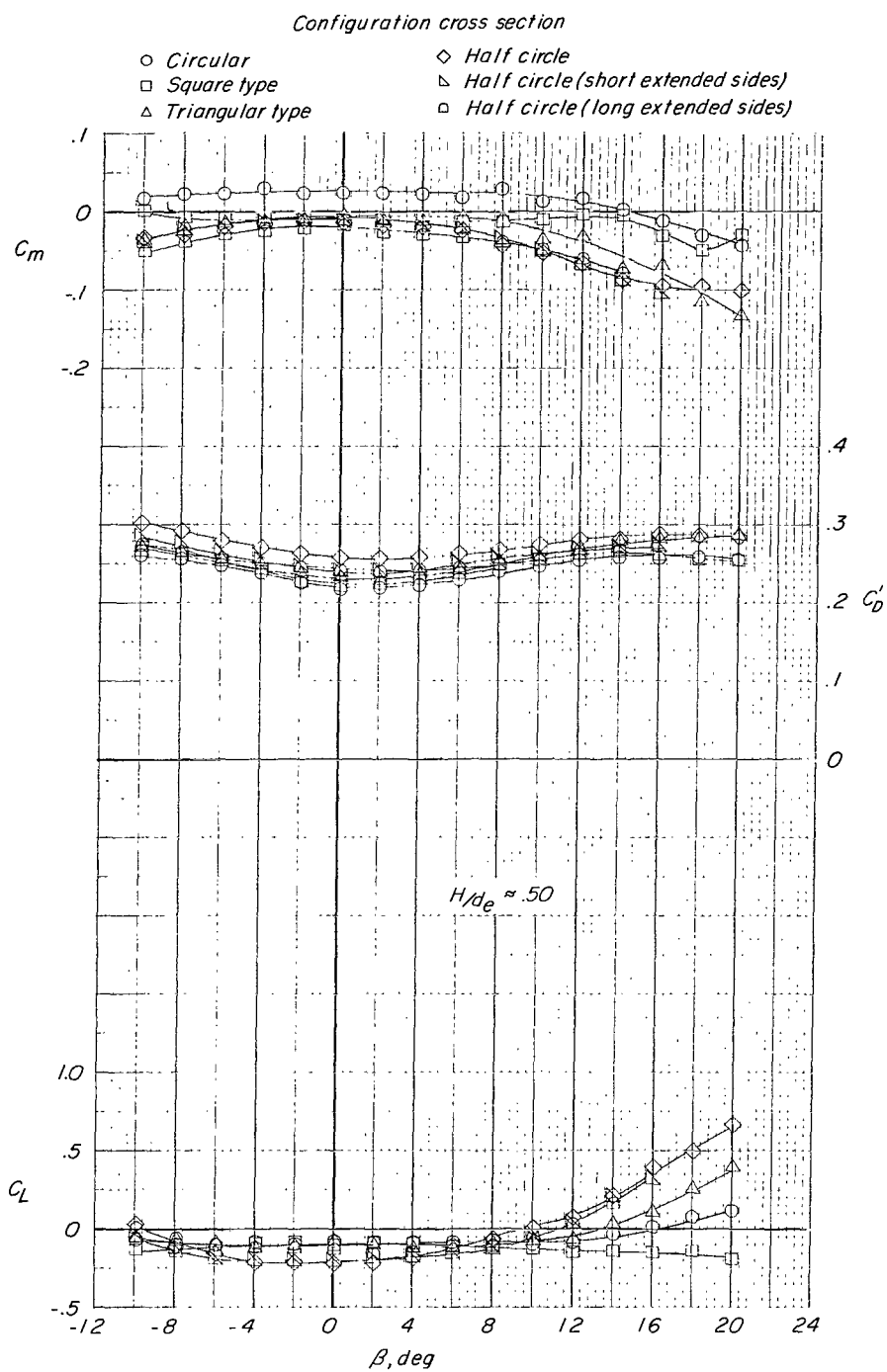
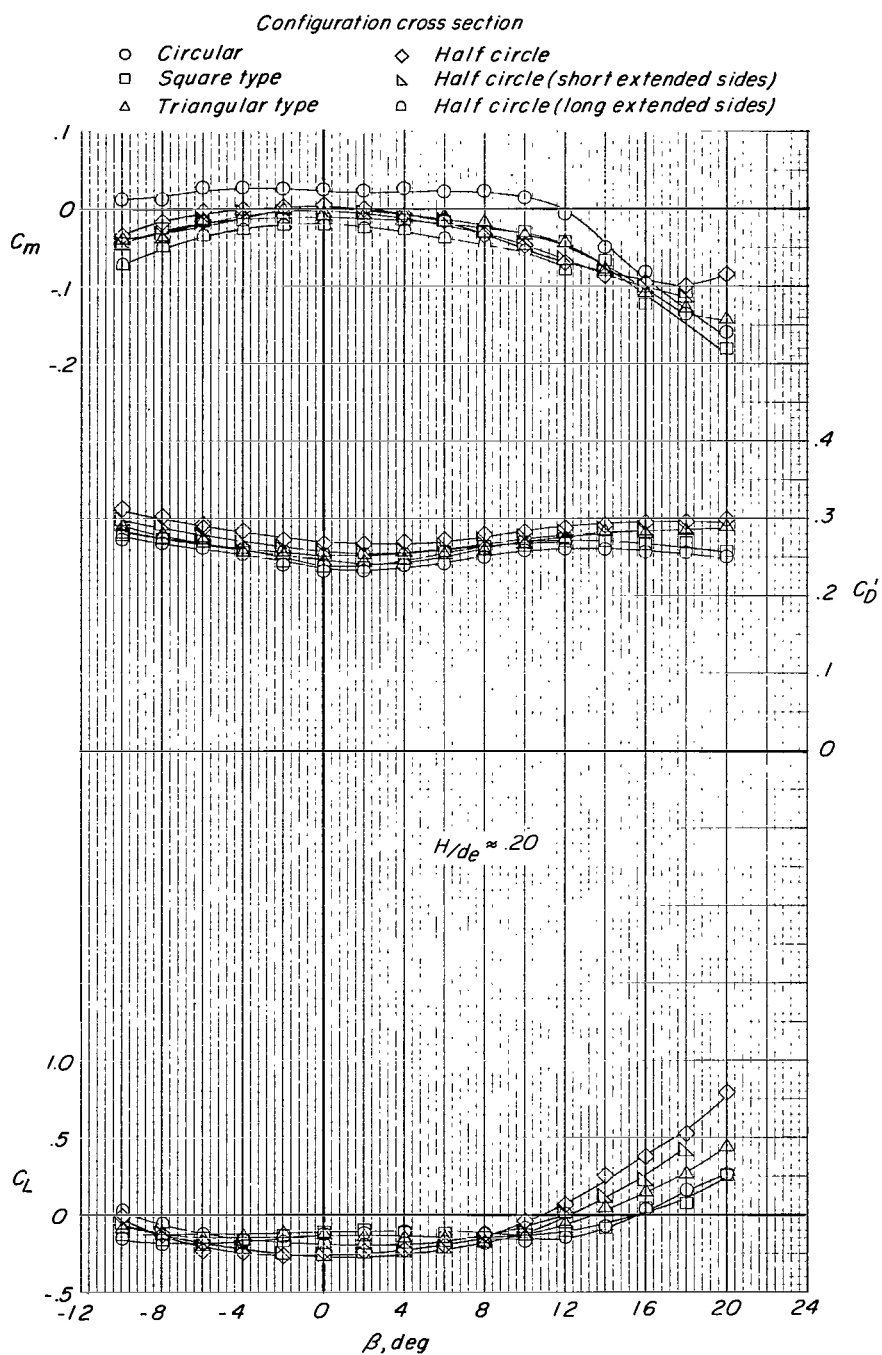


Figure 11.- Effect of configuration on lift, drag, and pitching moment. Ground belt moving; $\alpha = 0^\circ$.



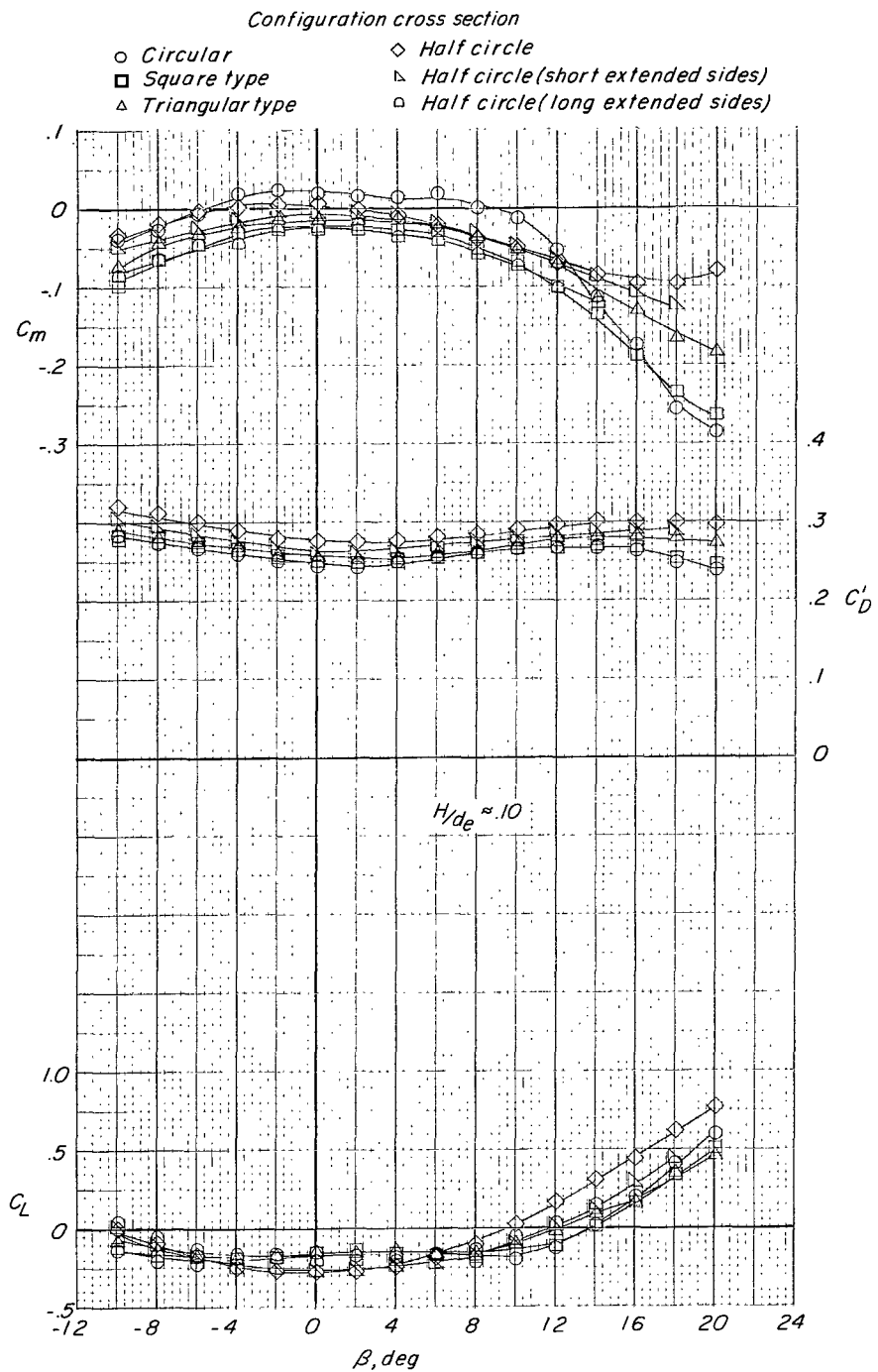
(b) $\frac{H}{d_e} \approx 0.50$.

Figure 11.- Continued.



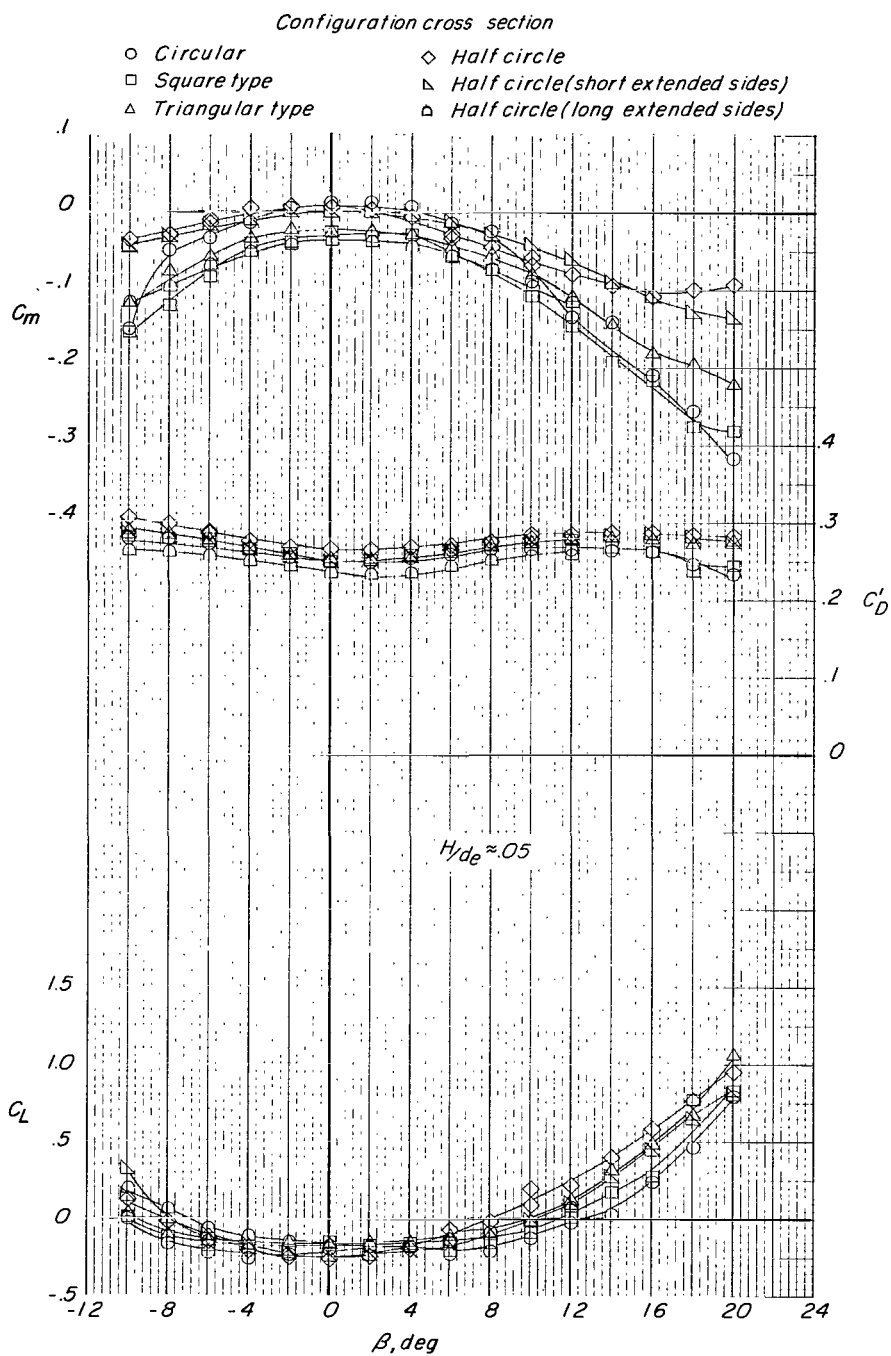
(c) $\frac{H}{d_e} \approx 0.20$.

Figure 11.- Continued.



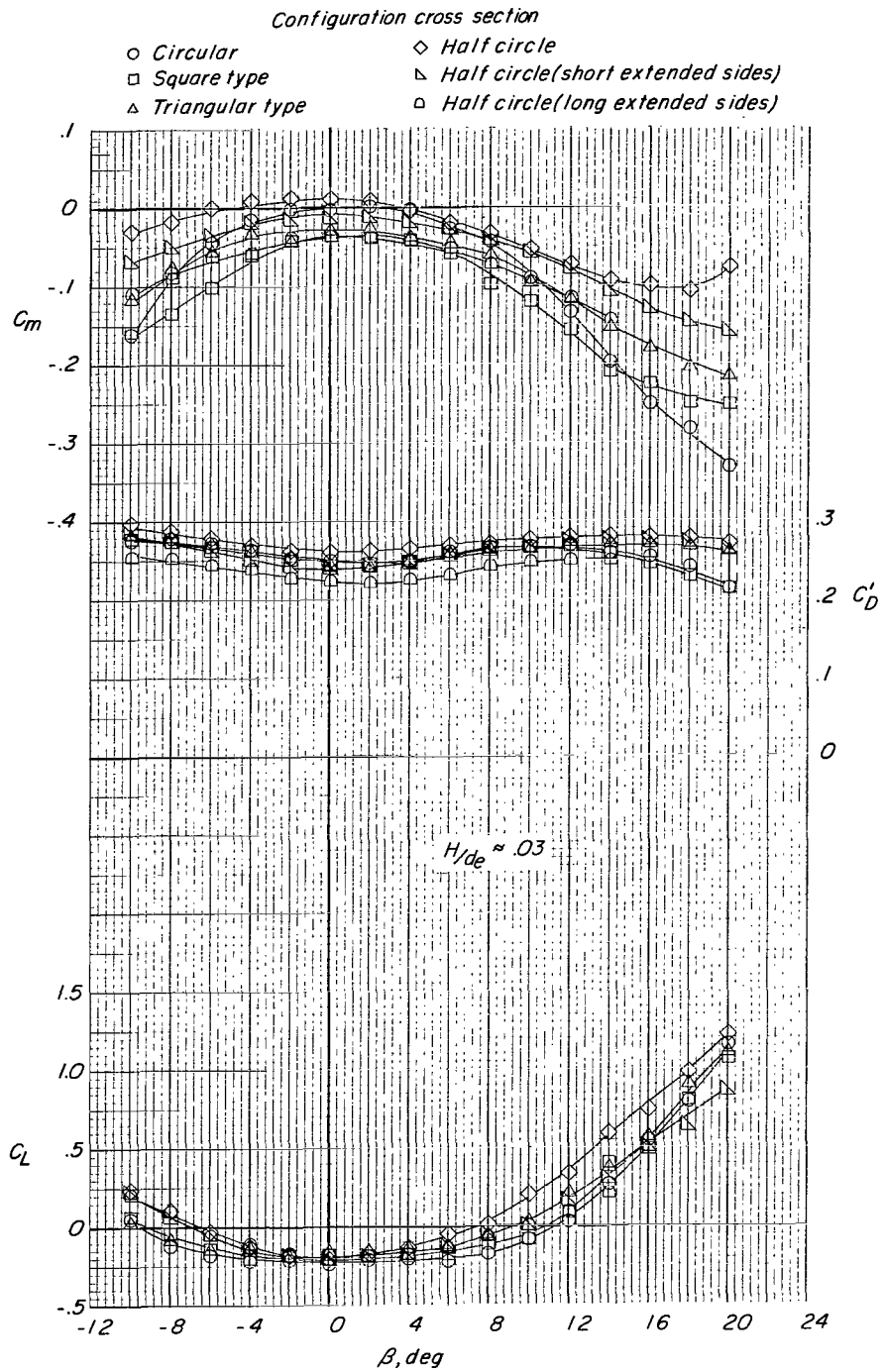
(d) $\frac{H}{d_e} \approx 0.10.$

Figure 11.- Continued.



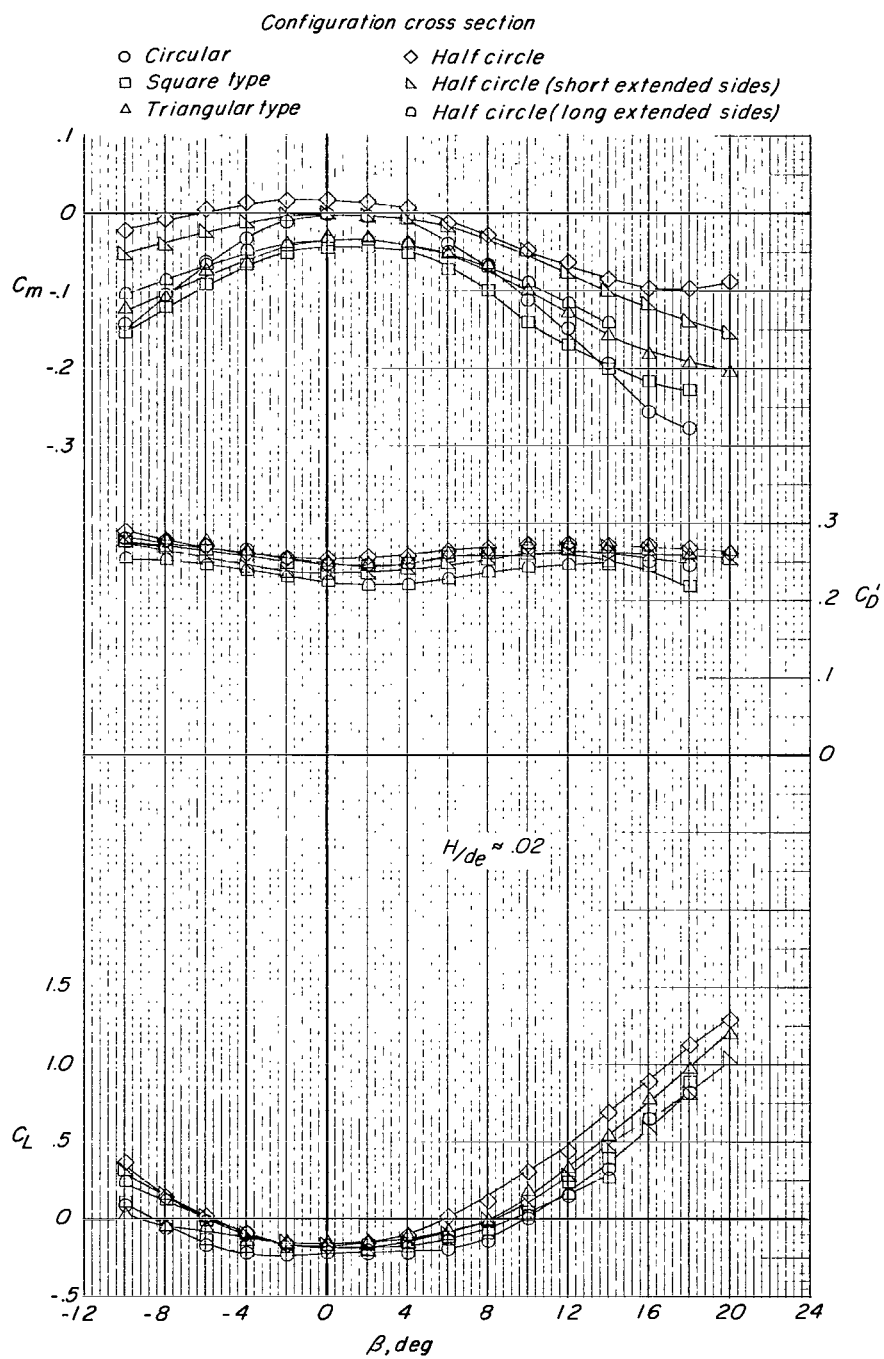
(e) $\frac{H}{d_e} \approx 0.05.$

Figure 11.- Continued.



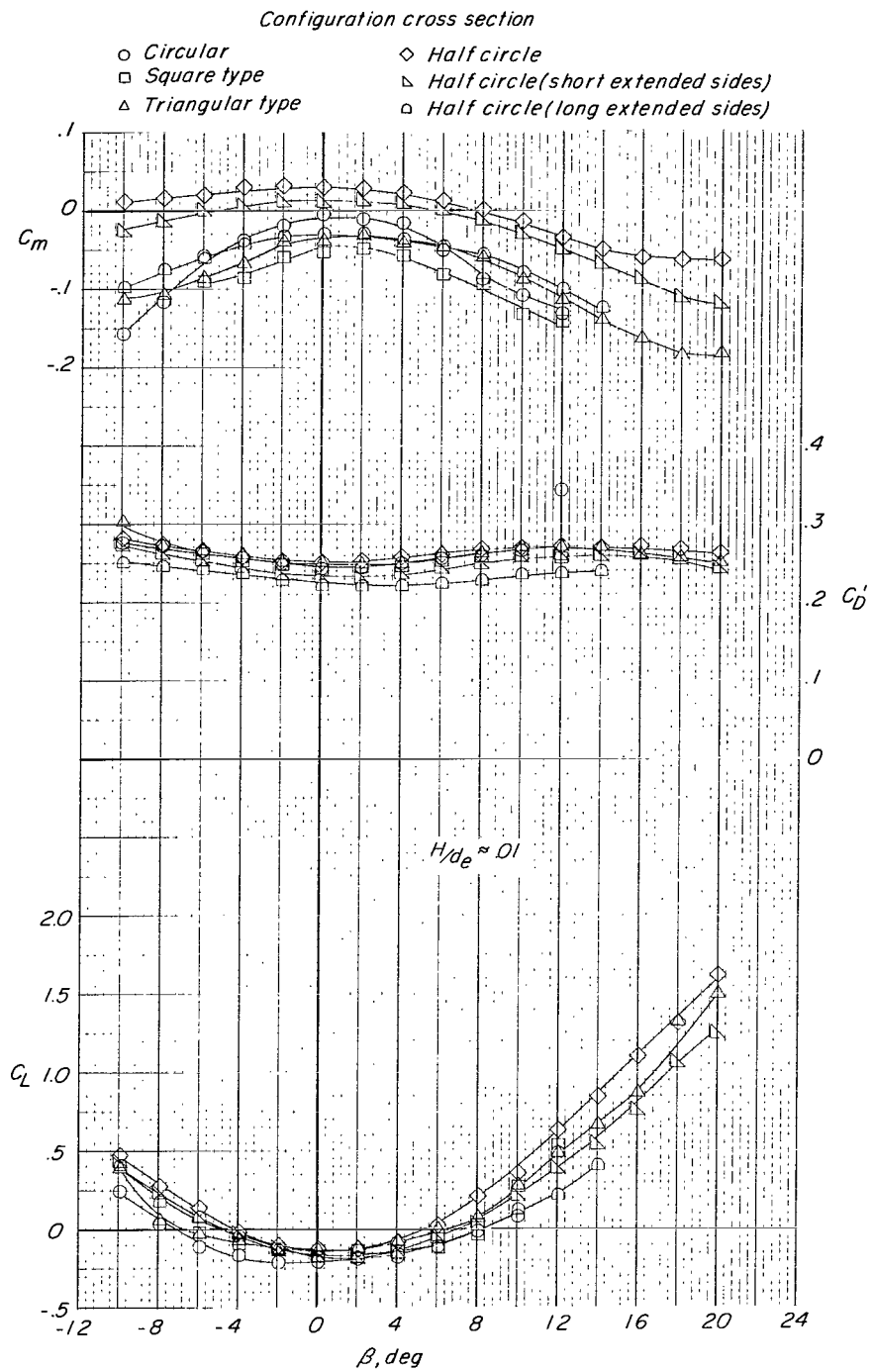
(f) $\frac{H}{d_e} \approx 0.03$.

Figure 11.- Continued.



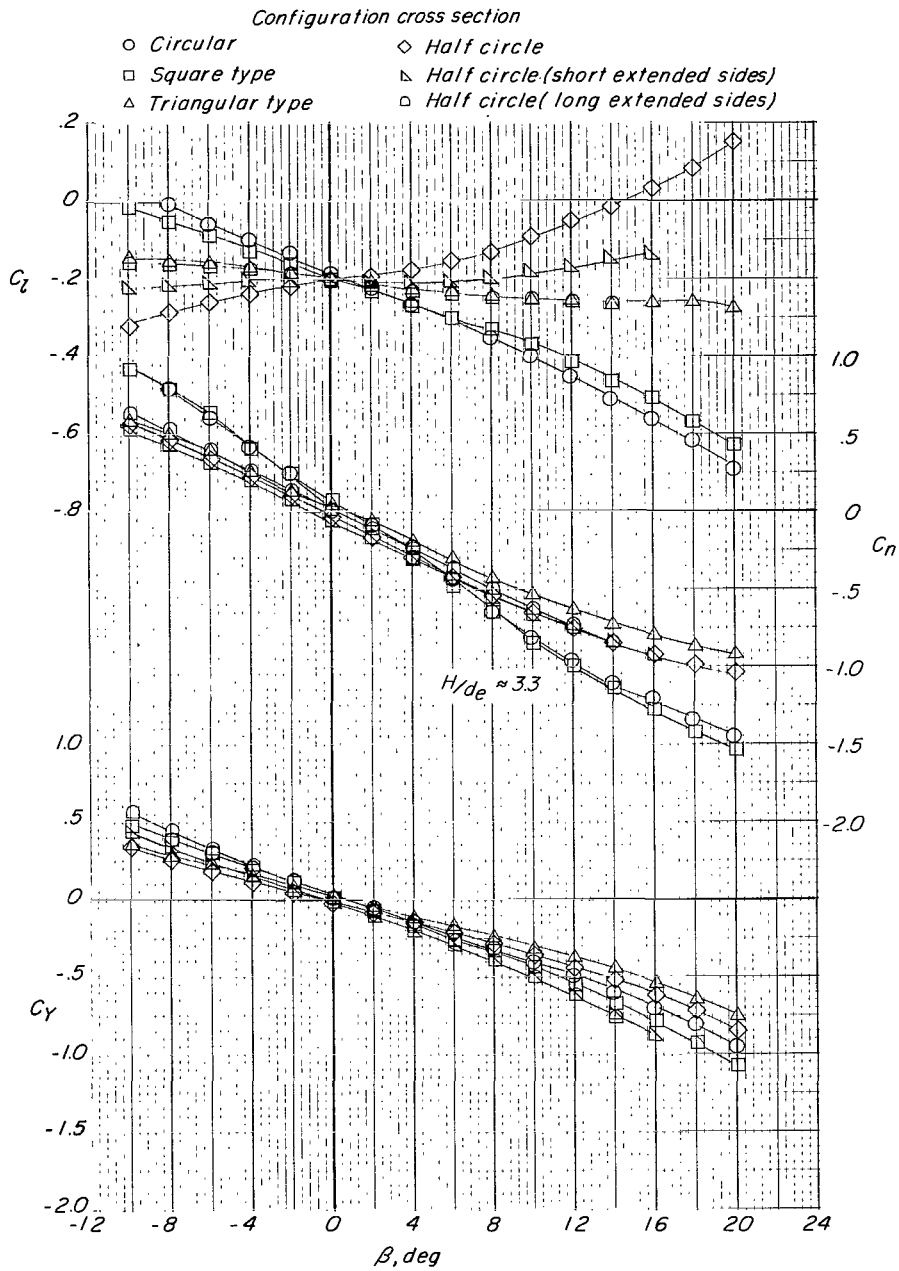
(g) $\frac{H}{d_e} \approx 0.02.$

Figure 11.- Continued.



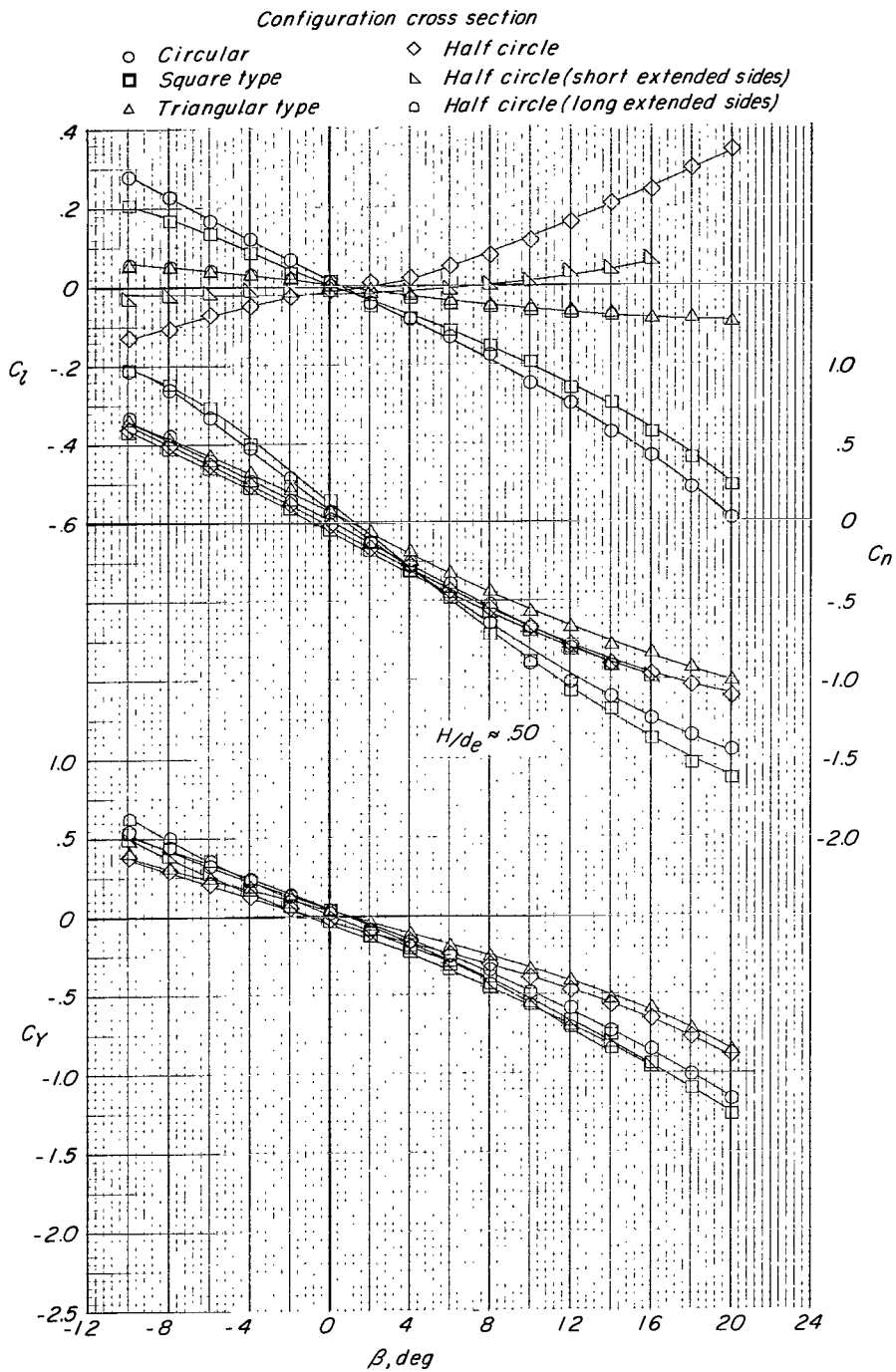
(h) $\frac{H}{d_e} \approx 0.01$.

Figure 11.- Concluded.



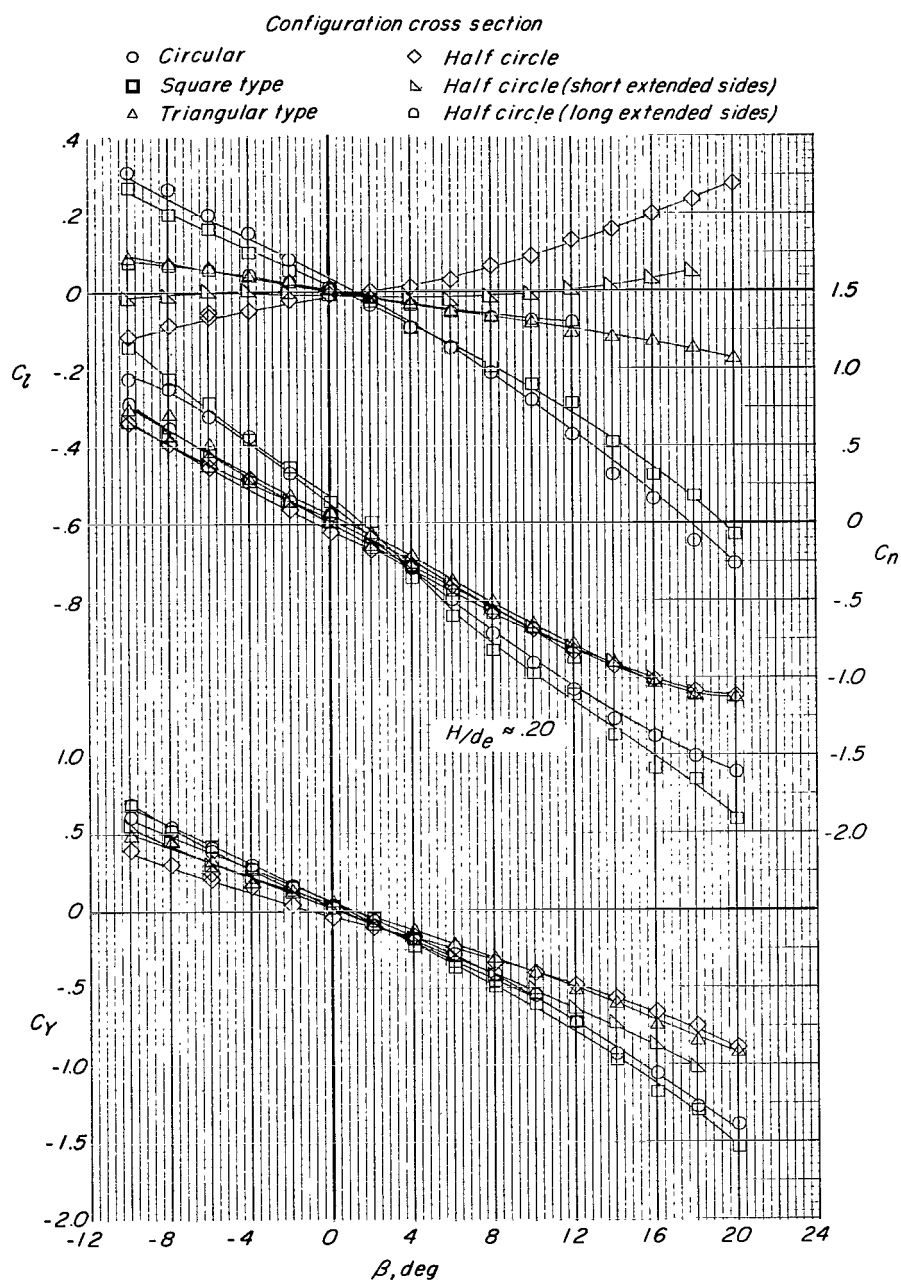
(a) $\frac{H}{d_e} \approx 3.3$.

Figure 12.- Effect of configuration on rolling moment, yawing moment, and side force. Ground belt moving; $\alpha = 0^\circ$.



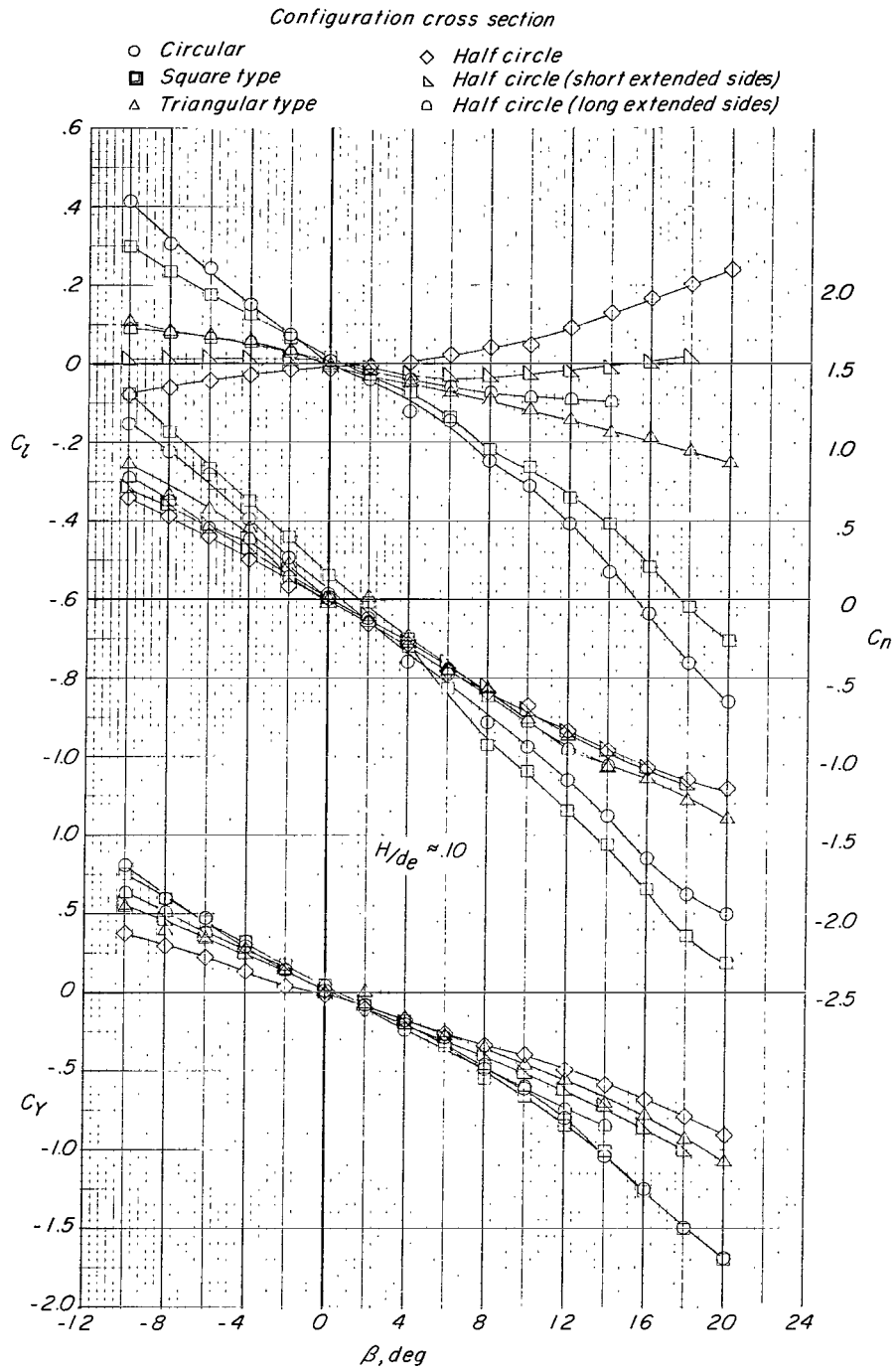
(b) $\frac{H}{d_e} \approx 0.50$.

Figure 12.- Continued.



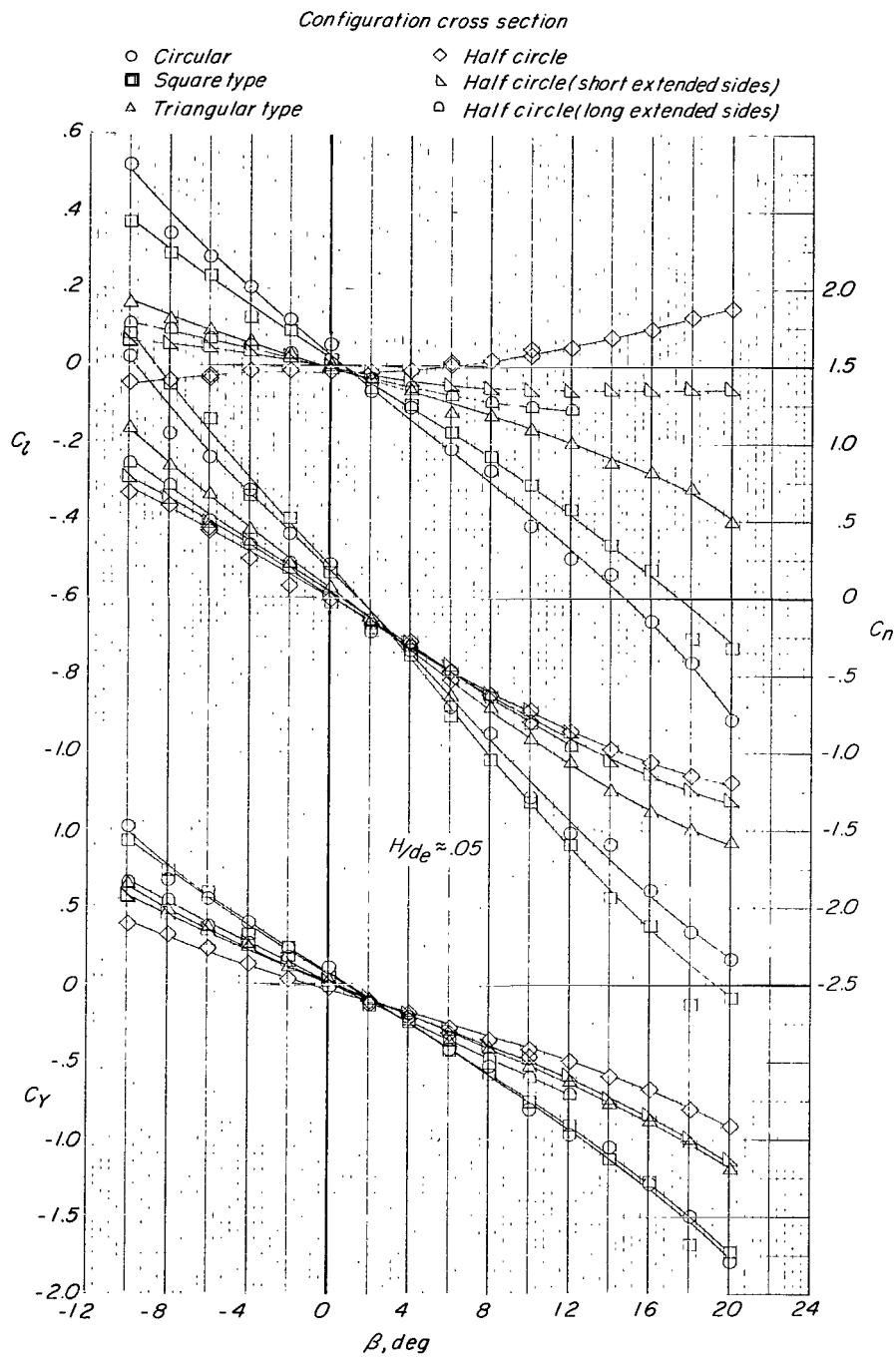
(c) $\frac{H}{d_e} \approx 0.20$.

Figure 12.- Continued.



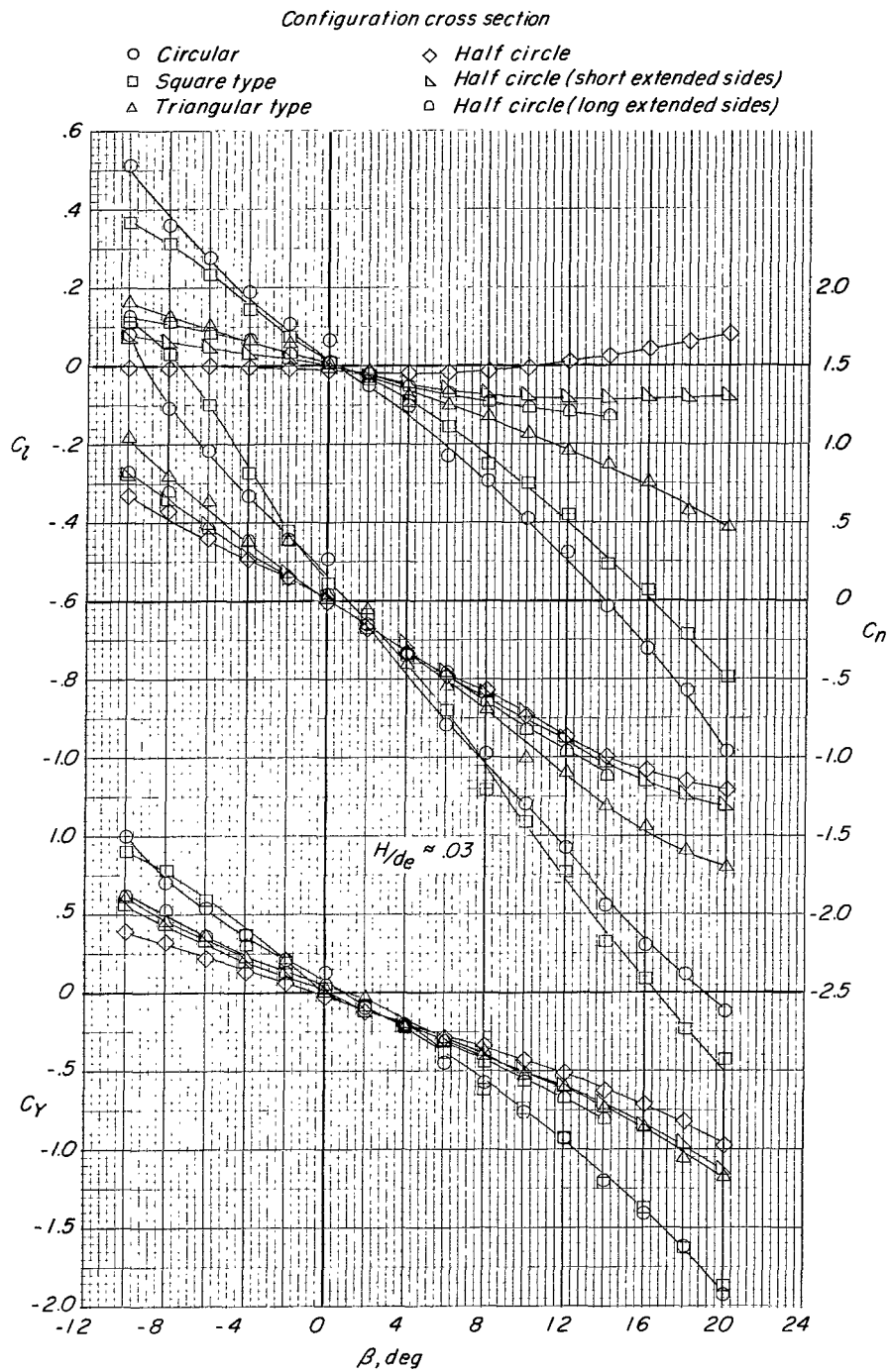
(d) $\frac{H}{d_e} \approx 0.10$.

Figure 12.- Continued.



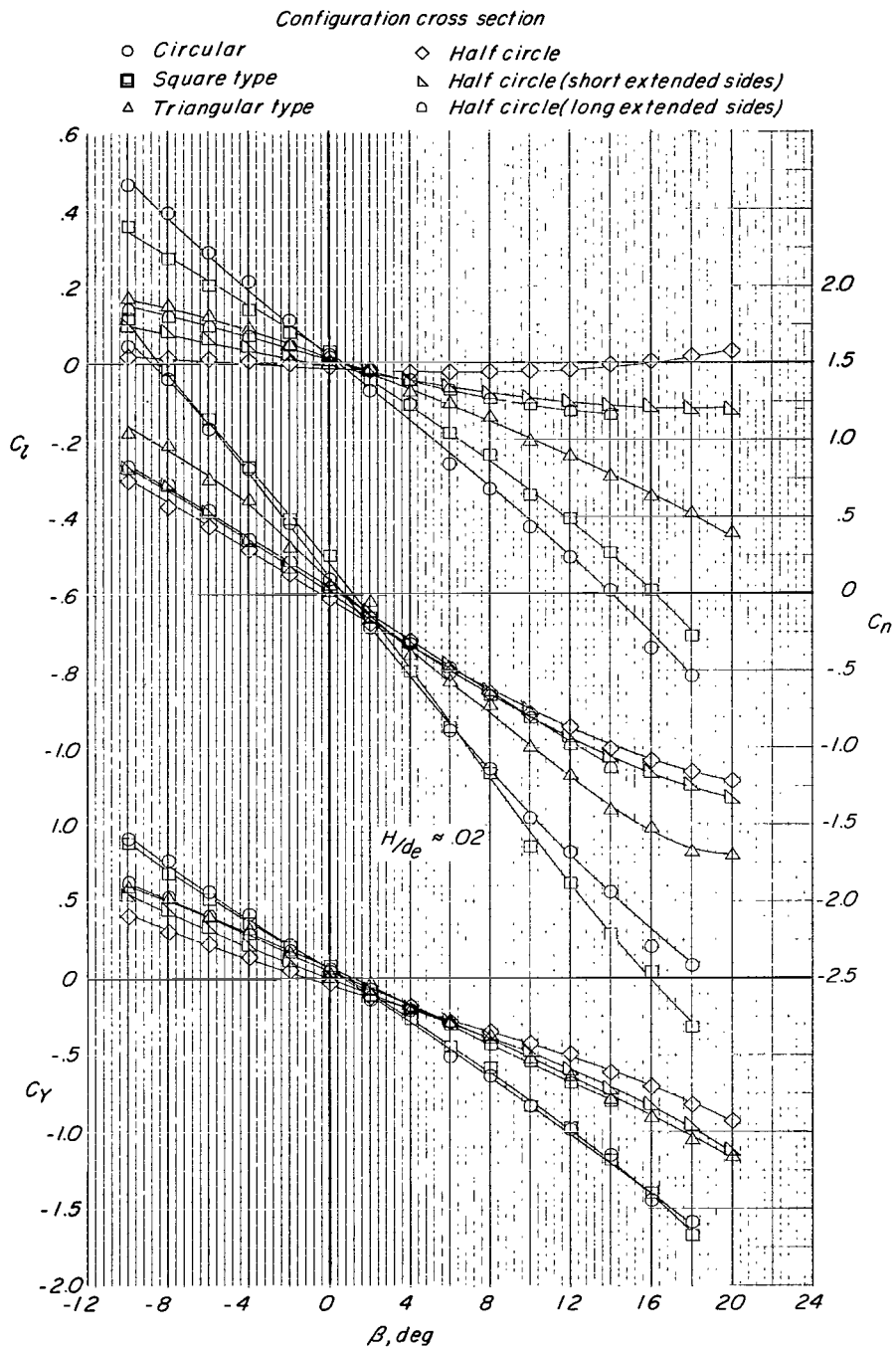
(e) $\frac{H}{d_e} \approx 0.05.$

Figure 12.- Continued.



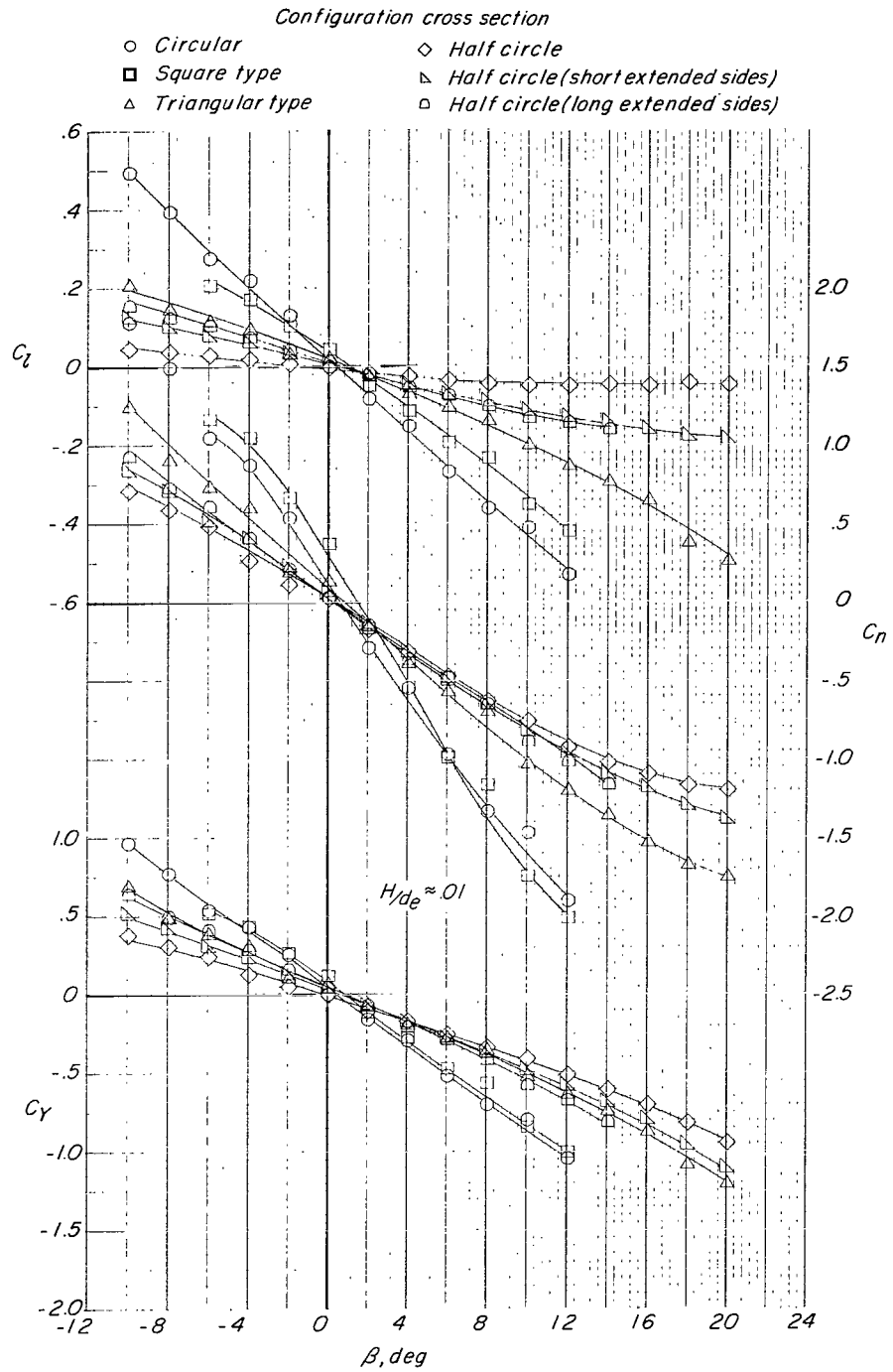
(f) $\frac{H}{d_e} \approx 0.03$.

Figure 12.- Continued.



(g) $\frac{H}{d_e} \approx 0.02.$

Figure 12.- Continued.



(h) $\frac{H}{d_e} \approx 0.01.$

Figure 12.- Concluded.

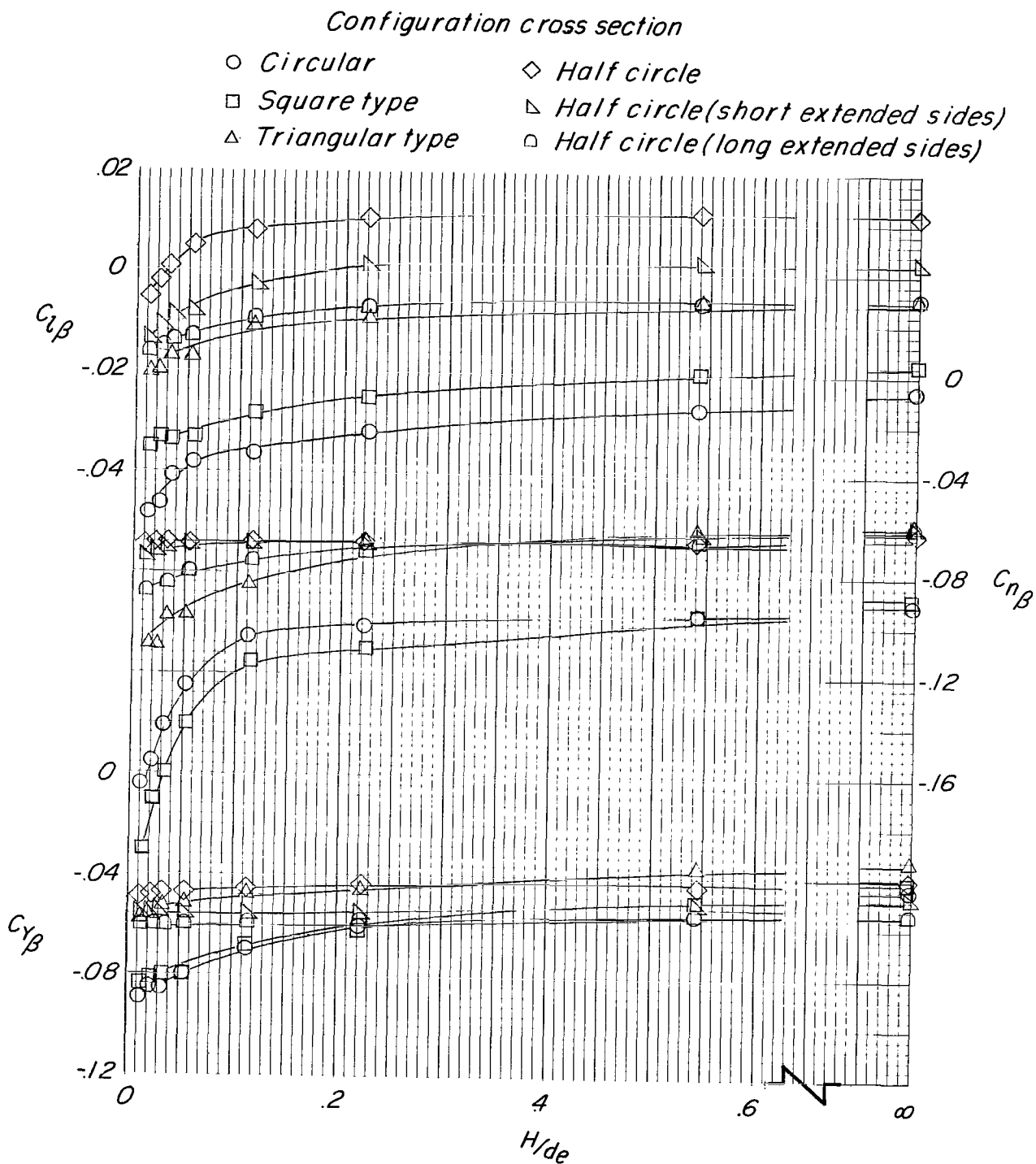


Figure 13.- The effect of height on the lateral effectiveness ($C_{l\beta}$, $C_{n\beta}$, $C_{y\beta}$) for all configurations. Ground belt moving; $\alpha = 0^\circ$.

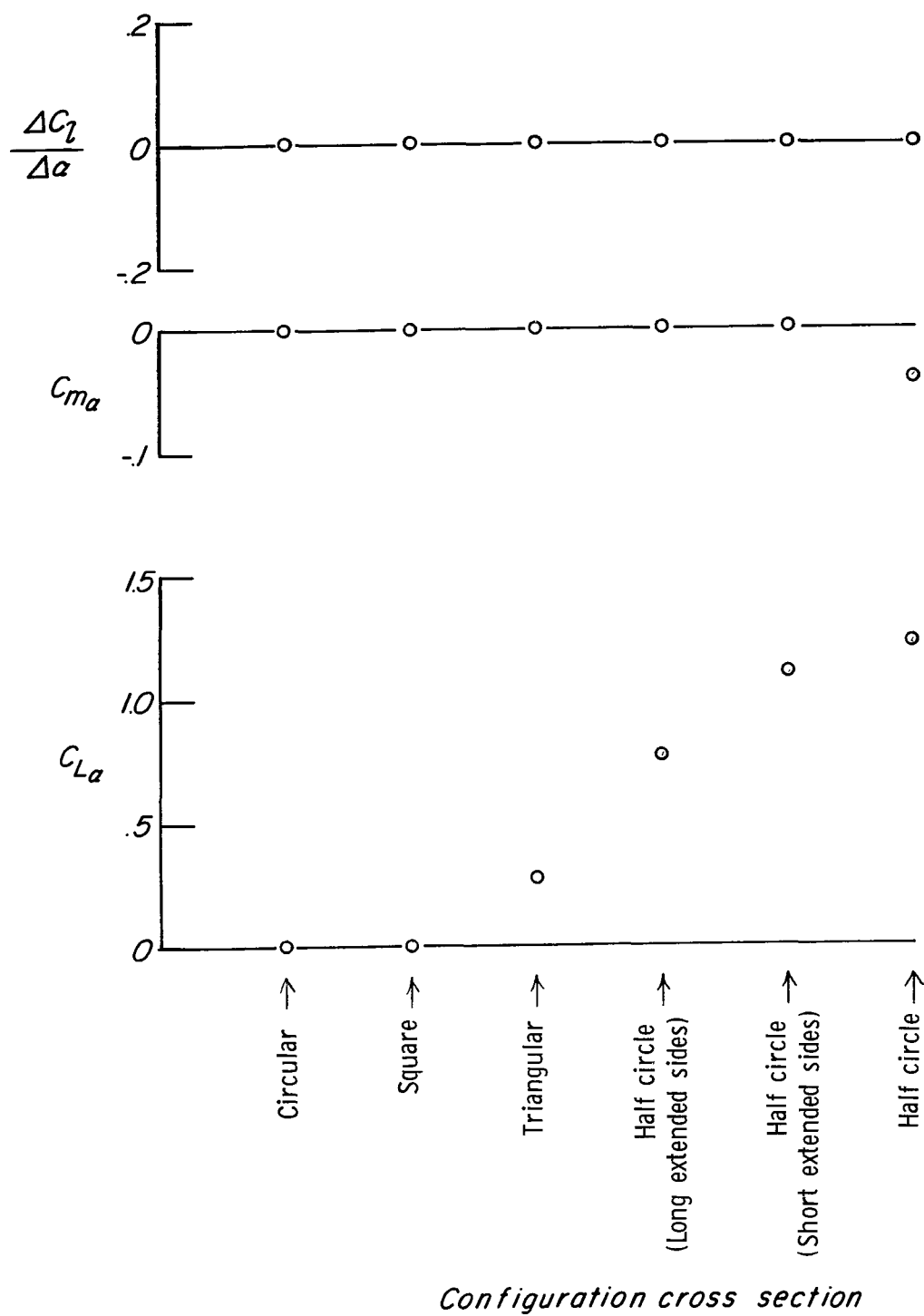


Figure 14.- Stability derivatives $\left(C_{L\alpha}, C_{m\alpha}, \frac{\Delta C_l}{\Delta \alpha}\right)$ plotted as functions of configuration cross section. $\beta = 0^\circ$; $\frac{H}{d_e} \approx 0.03$; ground belt moving.

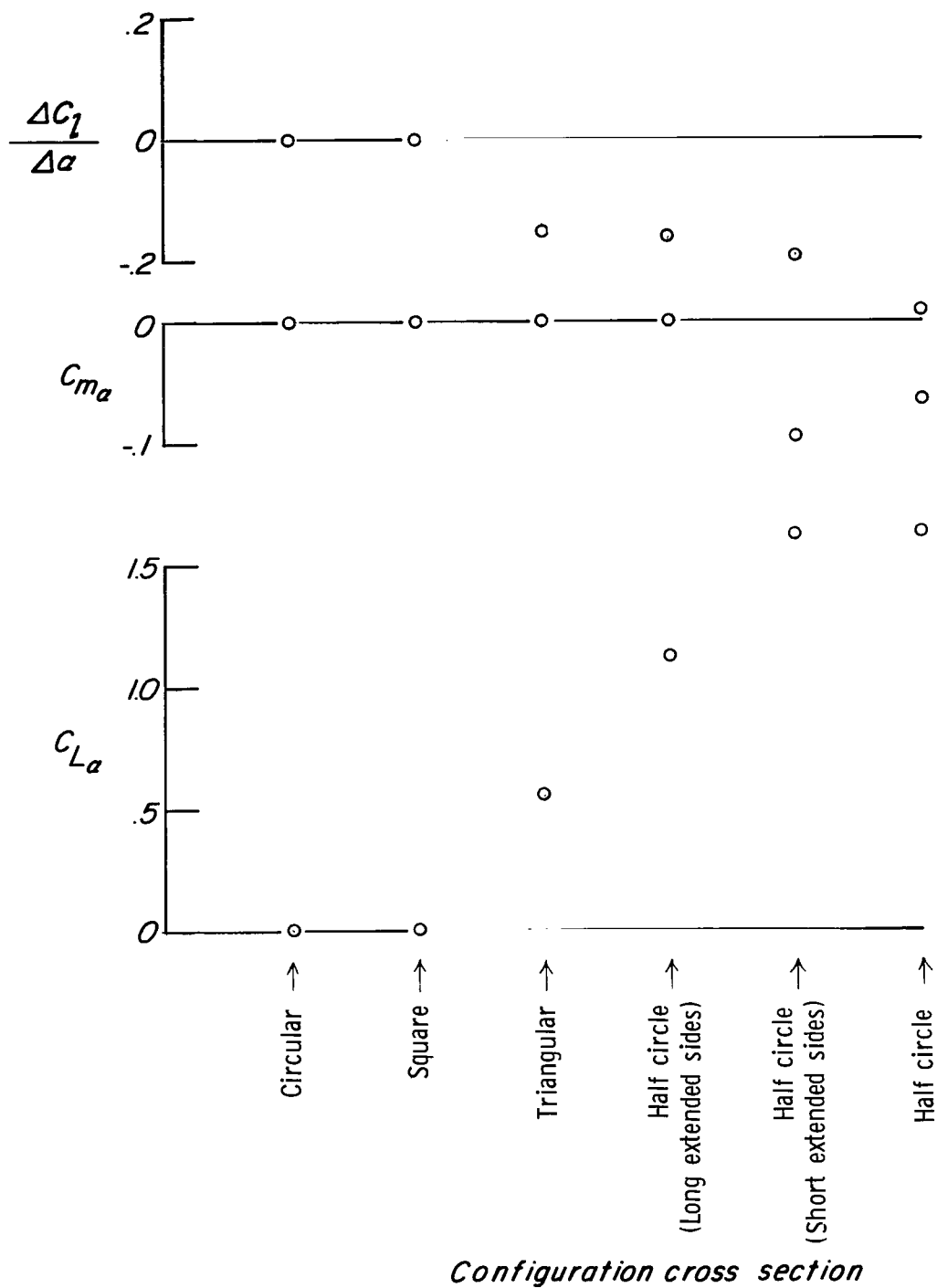


Figure 15.- Stability derivatives $\left(C_{L\alpha}, C_{m\alpha}, \frac{\Delta C_l}{\Delta \alpha} \right)$ plotted as functions of configuration cross section. $\beta = 12^\circ$; $\frac{H}{d_g} \approx 0.03$; ground belt moving.

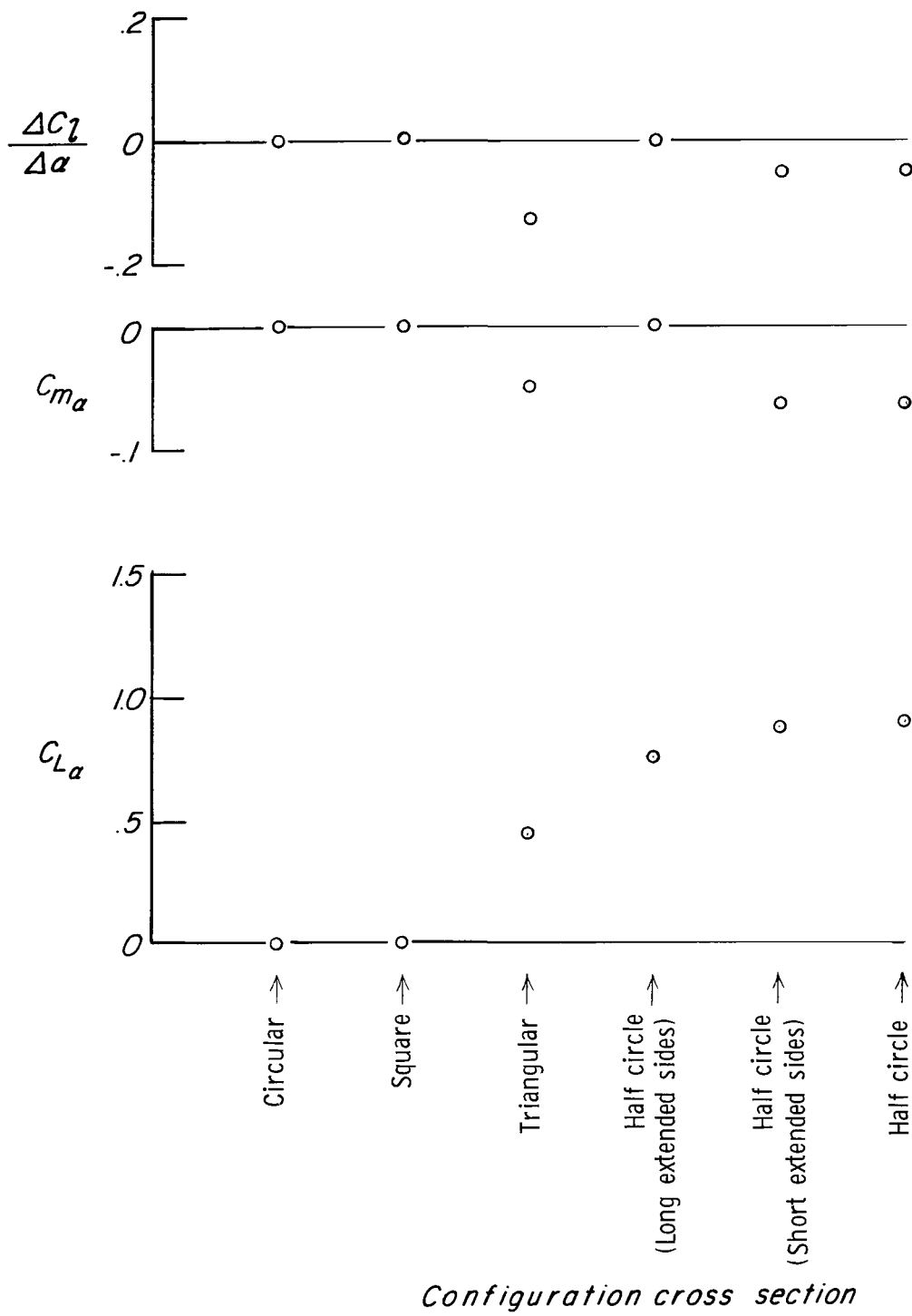


Figure 16.- Stability derivatives $\left(C_{L\alpha}, C_{m\alpha}, \frac{\Delta C_l}{\Delta \alpha}\right)$ plotted as functions of configuration cross section. $\beta = 12^\circ$; $\frac{H}{d_e} \approx 0.03$; ground belt stopped.

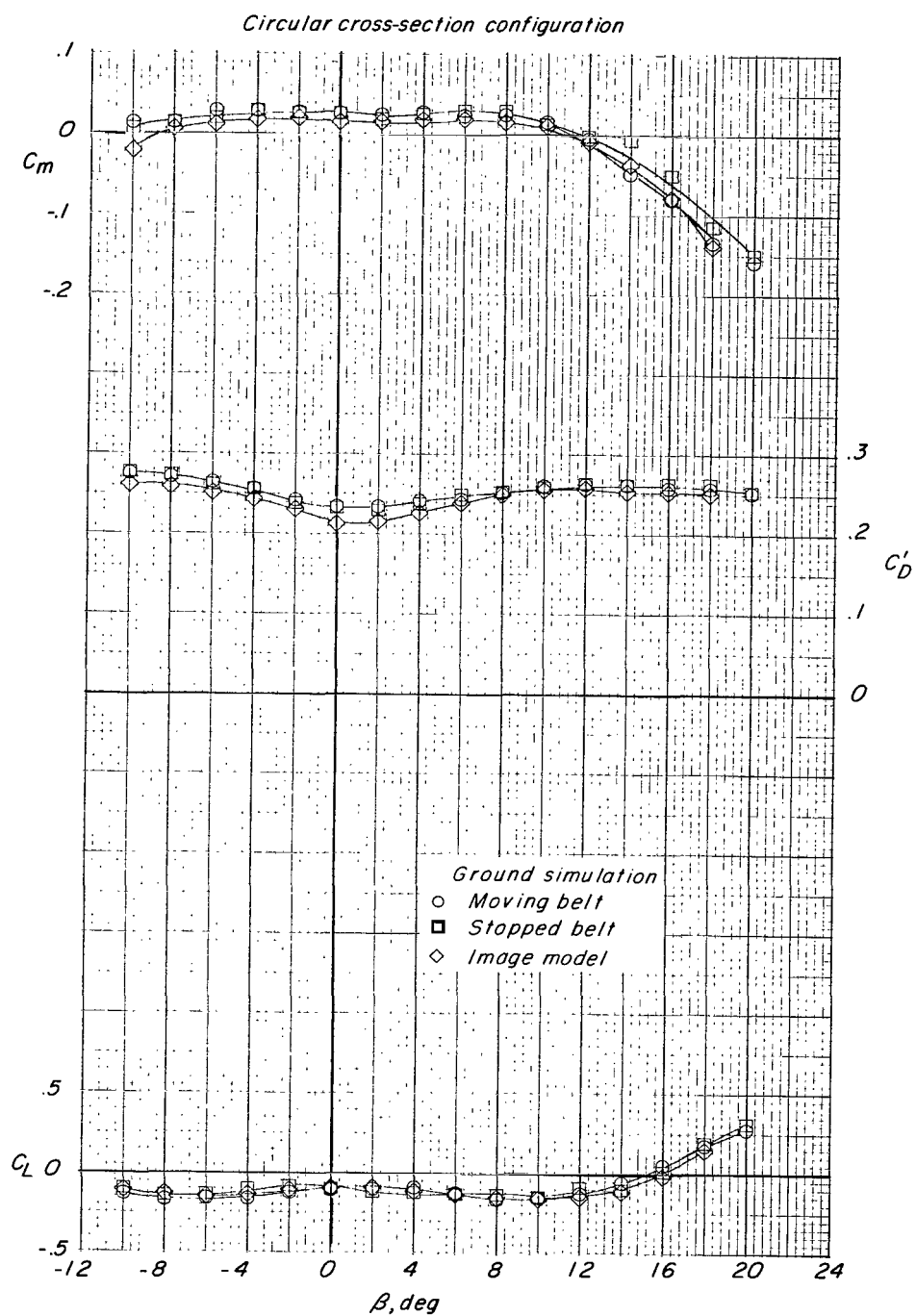
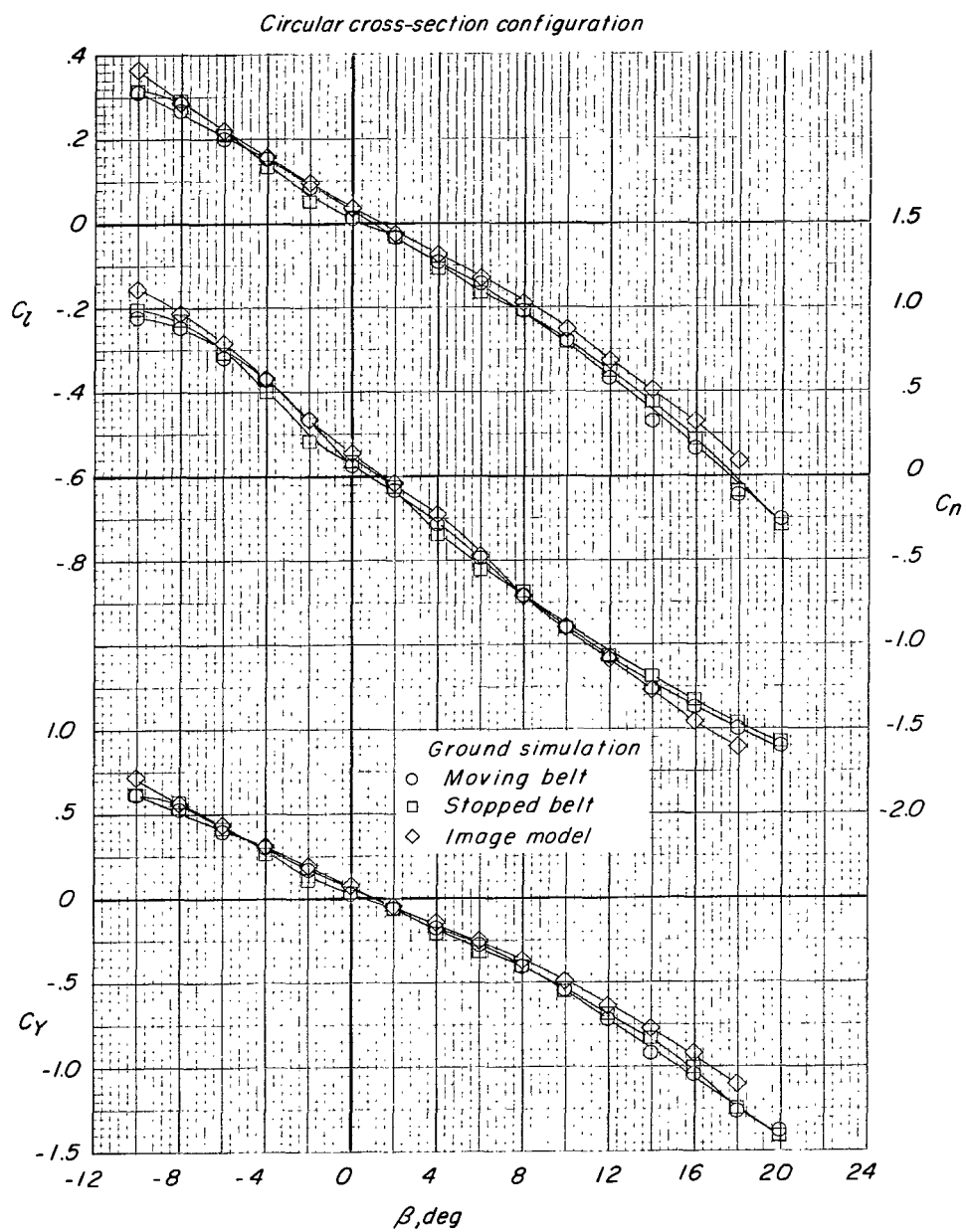
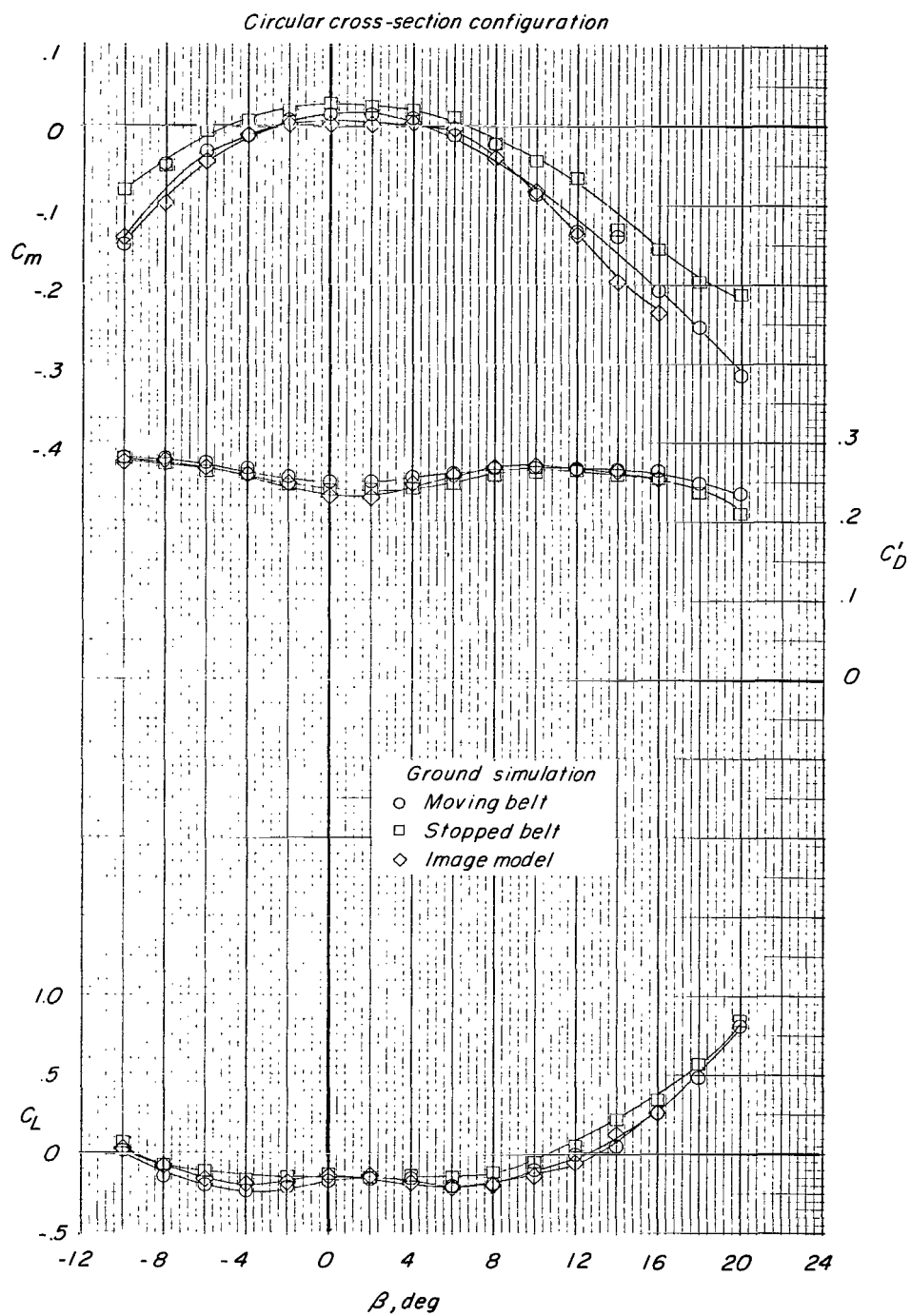


Figure 17.- Effect of ground-simulation technique on aerodynamic characteristics of circular configuration. $\frac{H}{d_g} \approx 0.20$; $\alpha = 0^\circ$.



(b) Rolling moment, yawing moment, and side force.

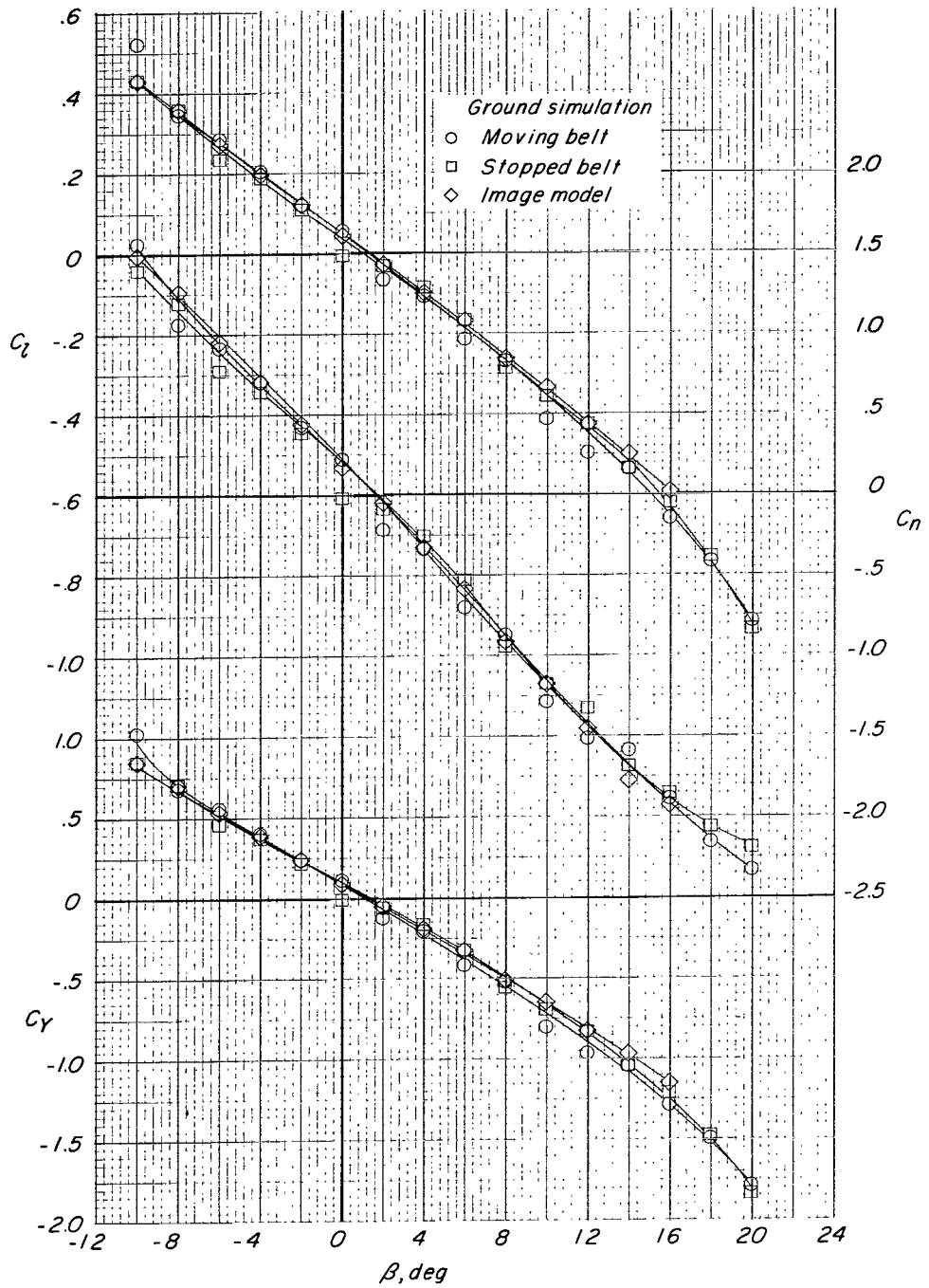
Figure 17.- Concluded.



(a) Lift, drag, and pitching moment.

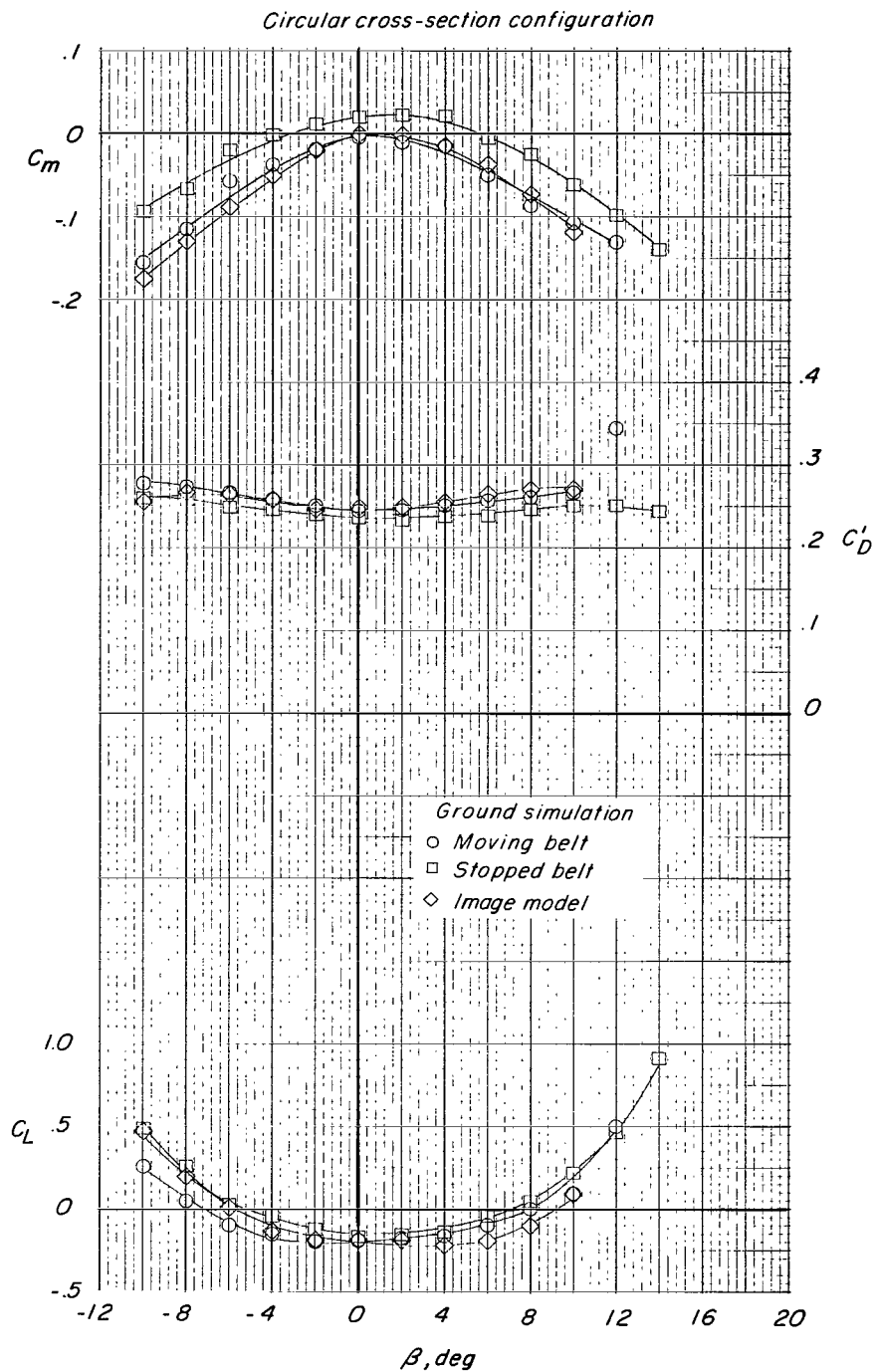
Figure 18.- Effect of ground-simulation technique on the aerodynamic characteristics of circular configuration. $\frac{H}{d_e} \approx 0.05$; $\alpha = 0^\circ$.

Circular cross-section configuration



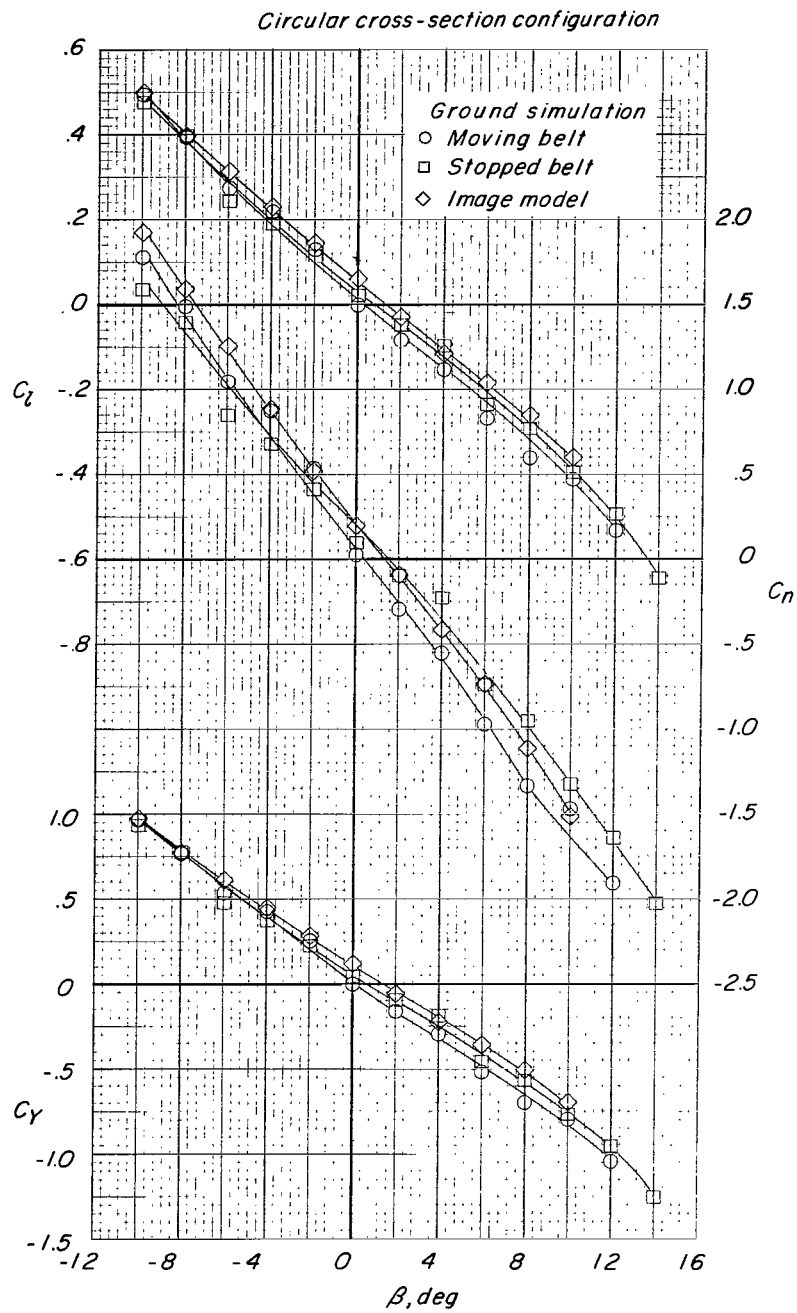
(b) Rolling moment, yawing moment, and side force.

Figure 18.- Concluded.



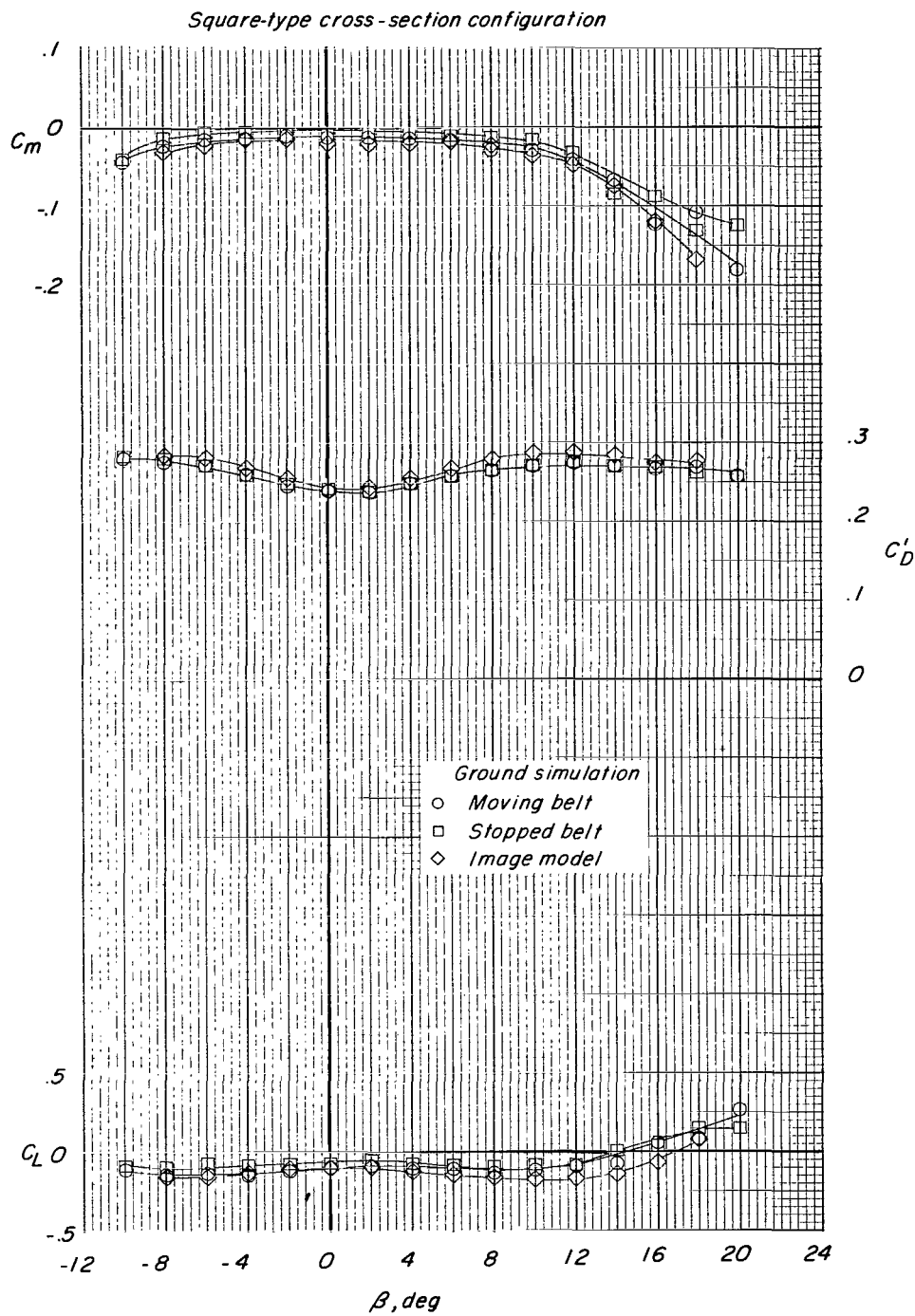
(a) Lift, drag, and pitching moment.

Figure 19.- Effect of ground-simulation technique on the aerodynamic characteristics of circular configuration. $\frac{H}{d_e} \approx 0.01$; $\alpha = 0^\circ$.



(b) Rolling moment, yawing moment, and side force.

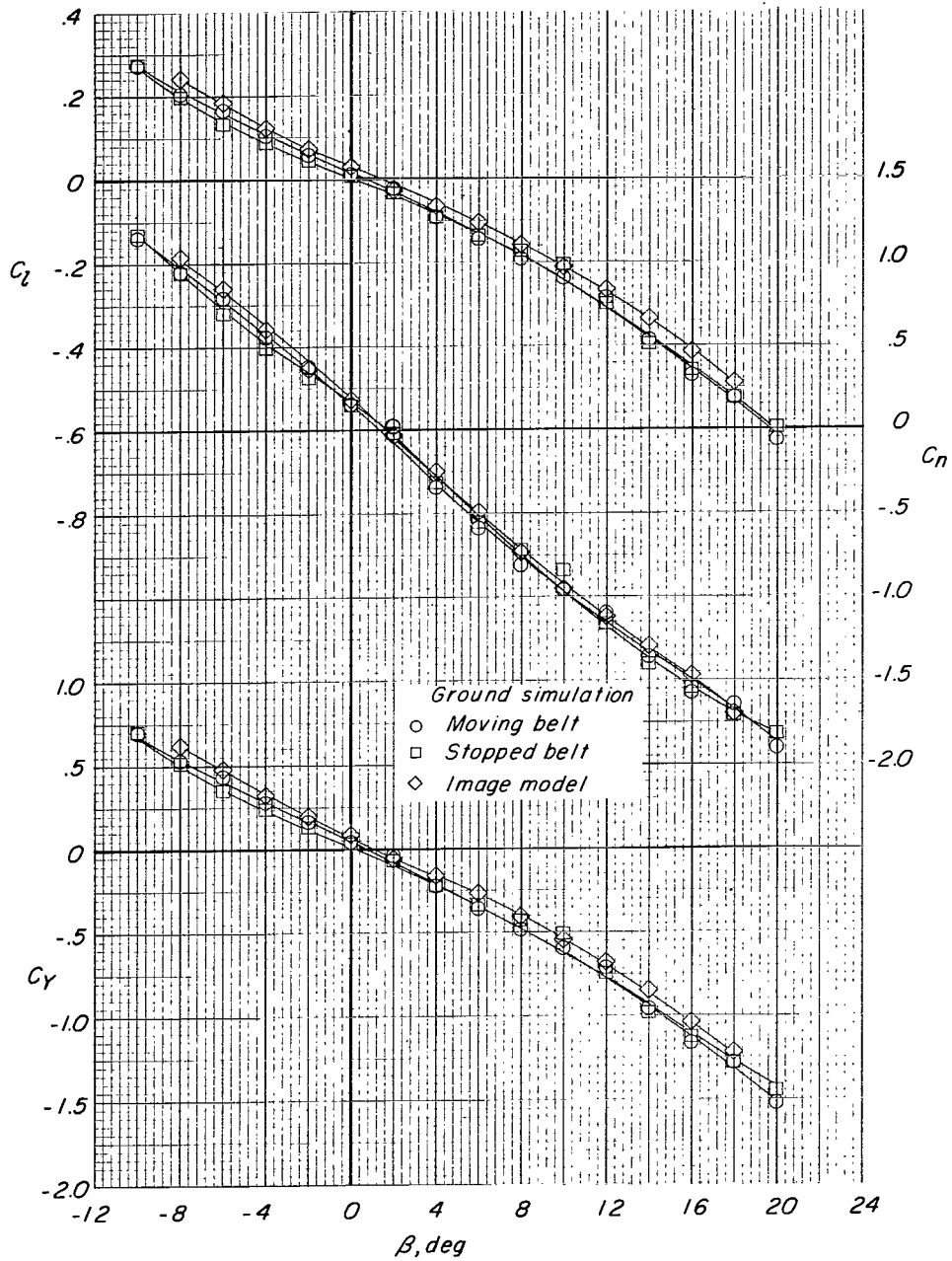
Figure 19.- Concluded.



(a) Lift, drag, and pitching moment.

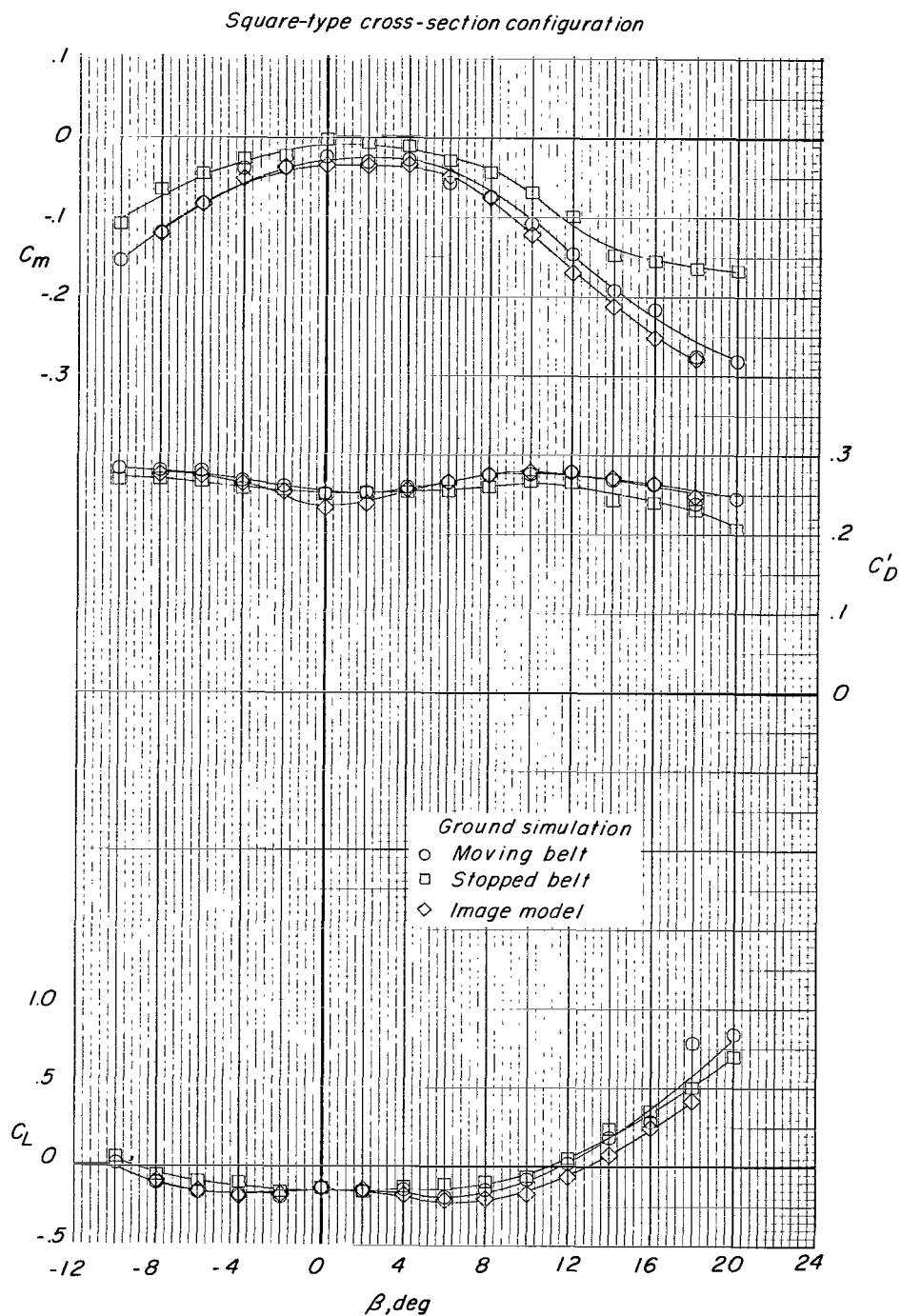
Figure 20.- Effect of ground-simulation technique on the aerodynamic characteristics of square-type configuration. $\frac{H}{d_g} \approx 0.20$; $\alpha = 0^\circ$.

Square-type cross-section configuration



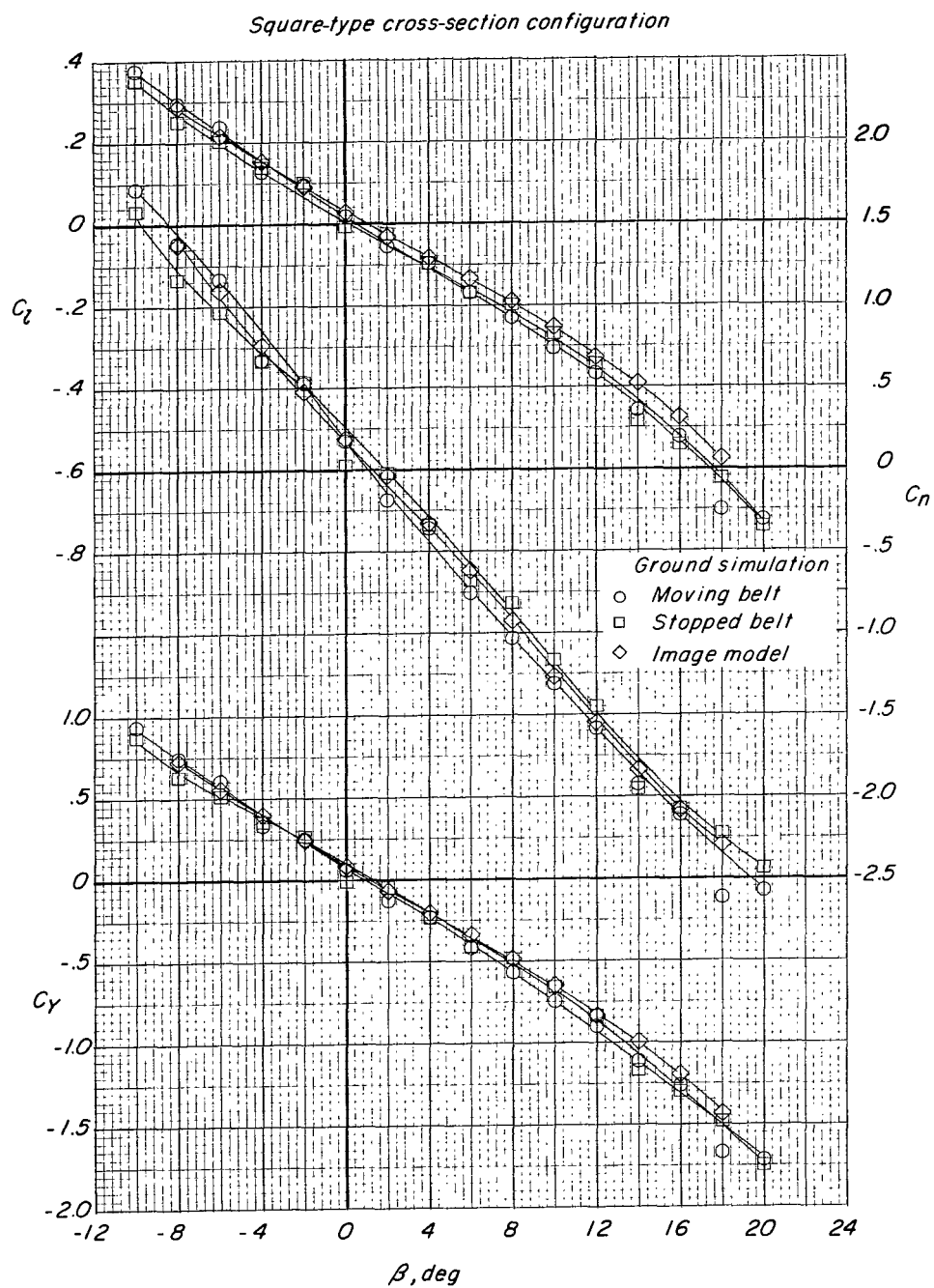
(b) Rolling moment, yawing moment, and side force.

Figure 20.- Concluded.



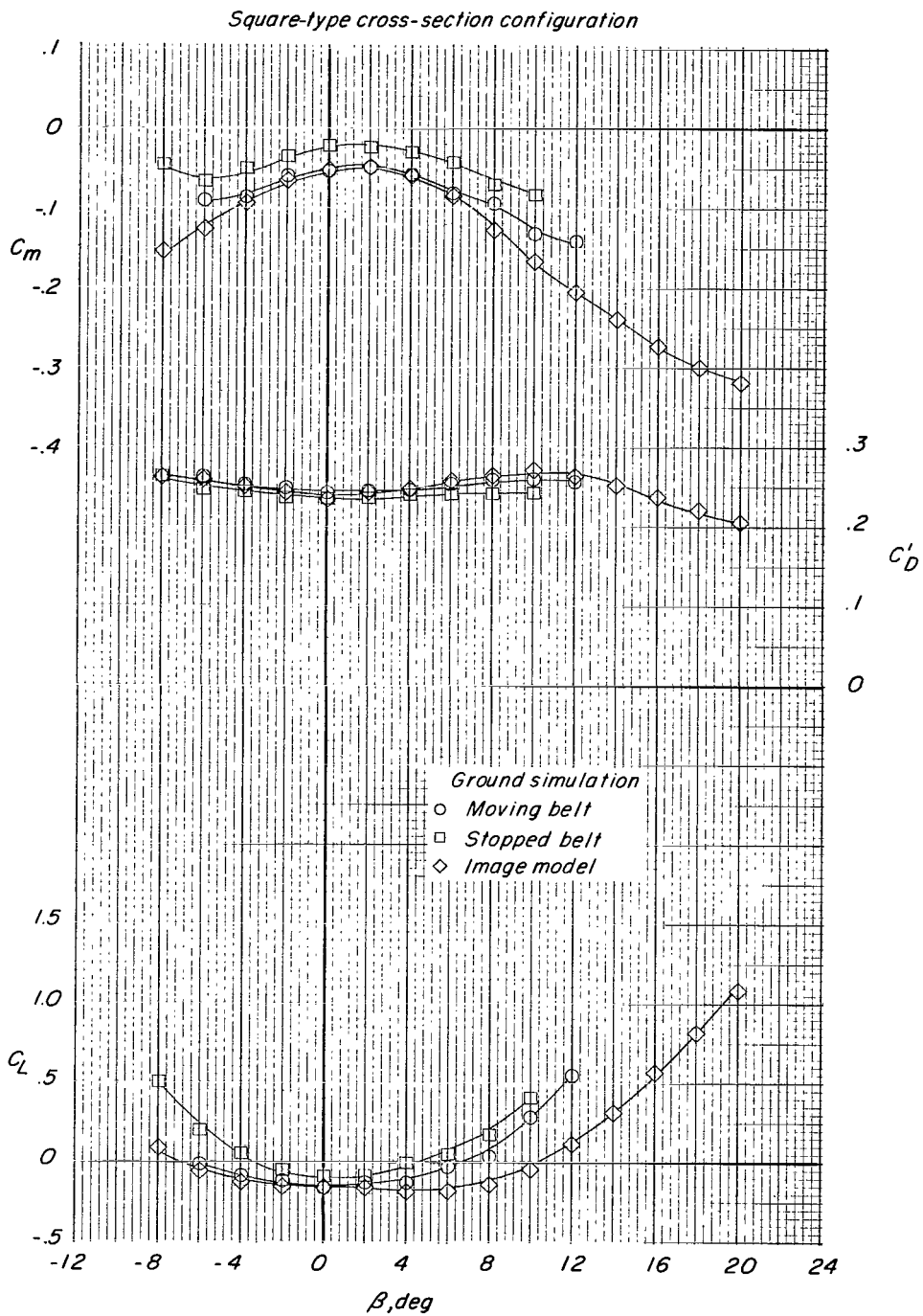
(a) Lift, drag, and pitching moment.

Figure 21.- Effect of ground-simulation technique on the aerodynamic characteristics of square-type configuration. $\frac{H}{d_0} \approx 0.05$; $\alpha = 0^\circ$.



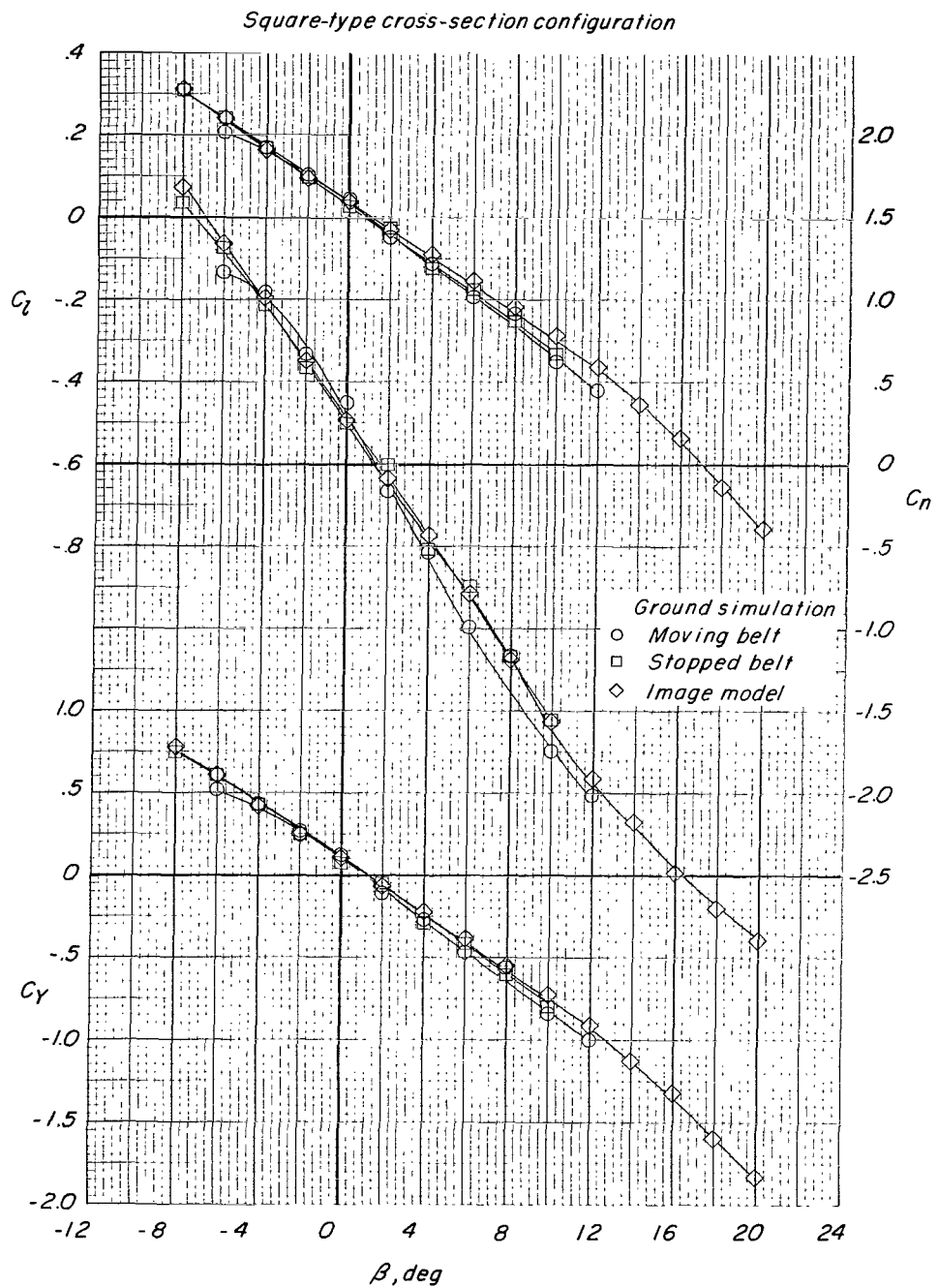
(b) Rolling moment, yawing moment, and side force.

Figure 21.- Concluded.



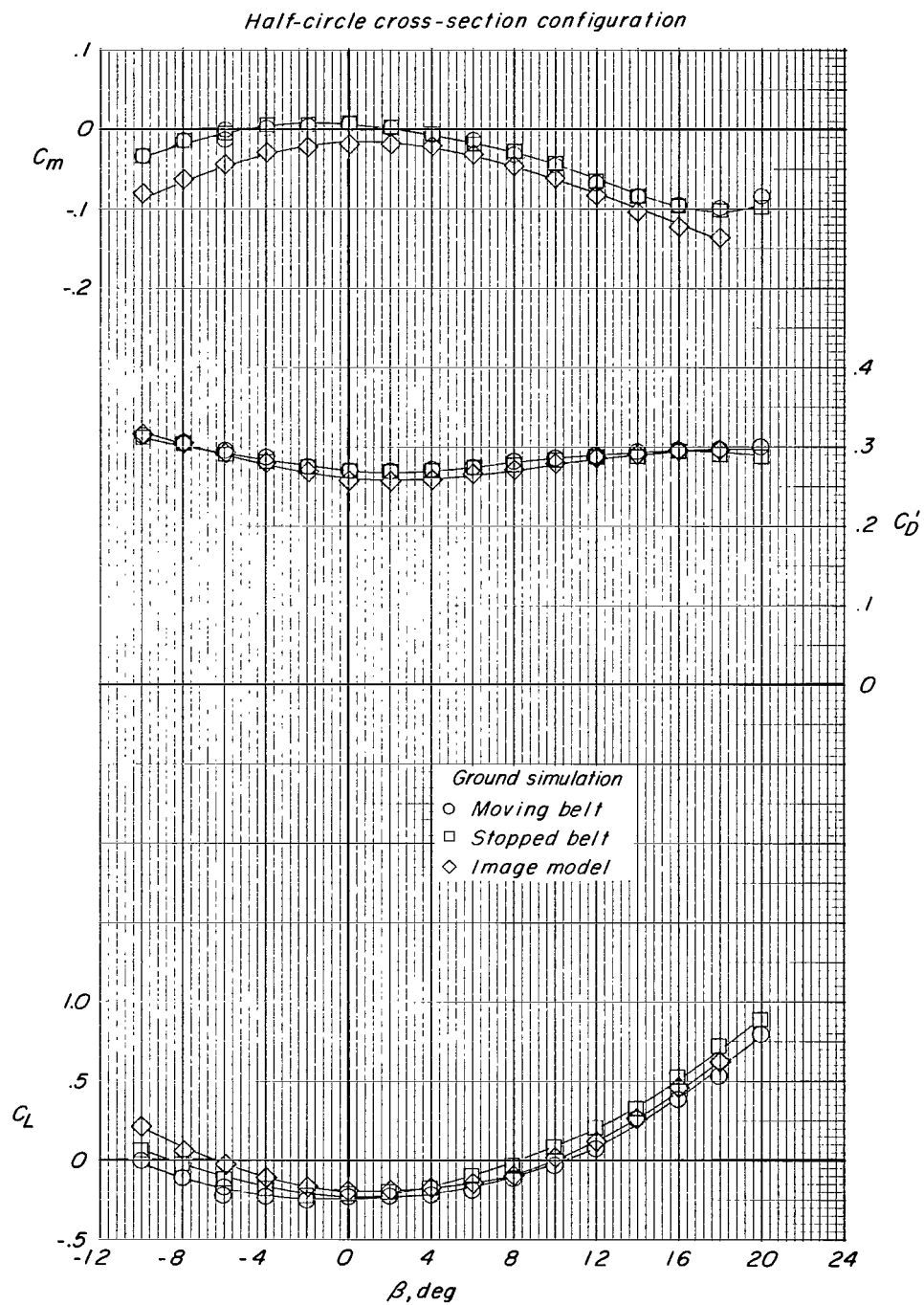
(a) Lift, drag, and pitching moment.

Figure 22.- Effect of ground-simulation technique on the aerodynamic characteristics of square-type configuration. $\frac{H}{d_e} \approx 0.01$; $\alpha = 0^\circ$.



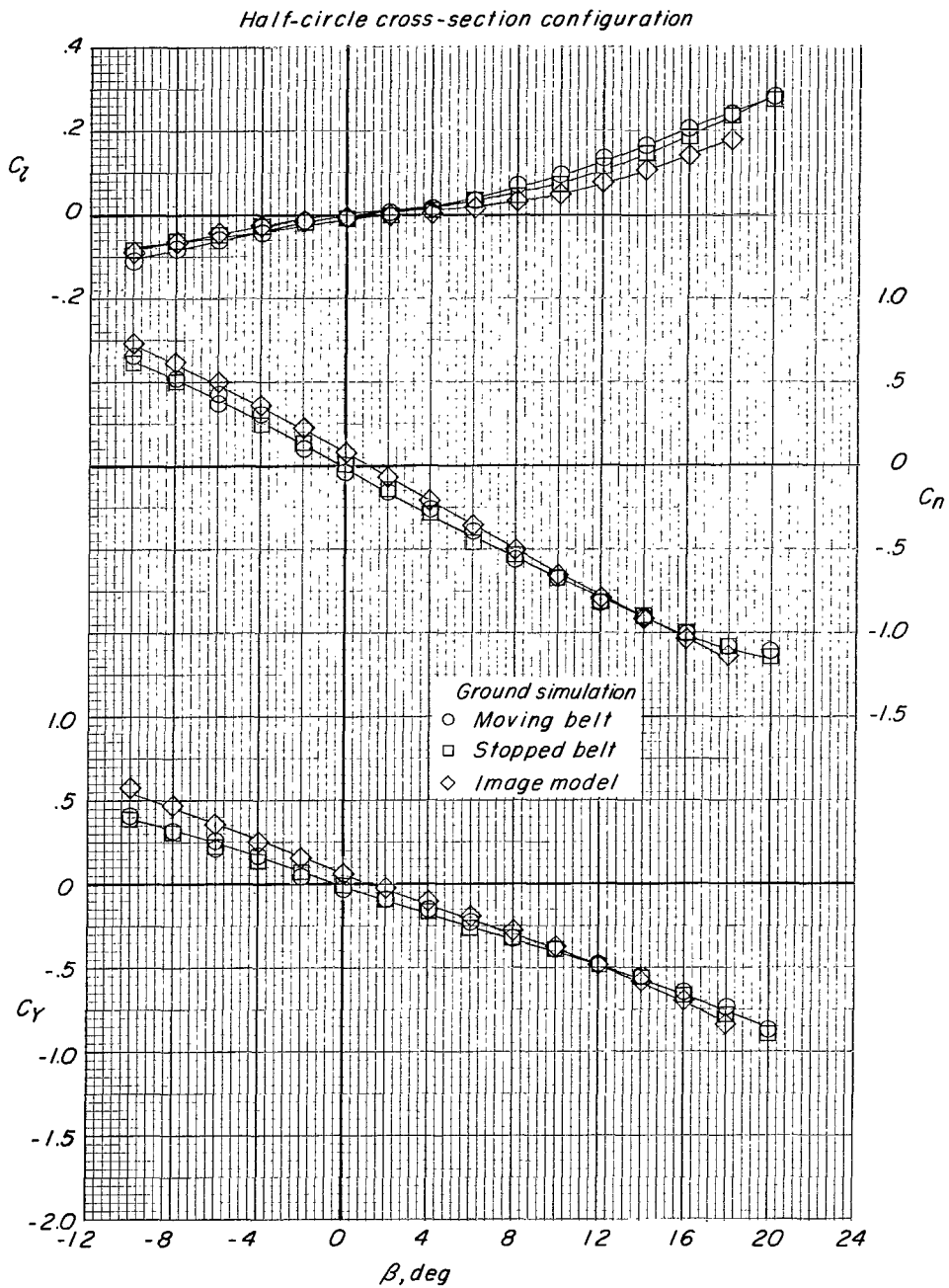
(b) Rolling moment, yawing moment, and side force.

Figure 22.- Concluded.



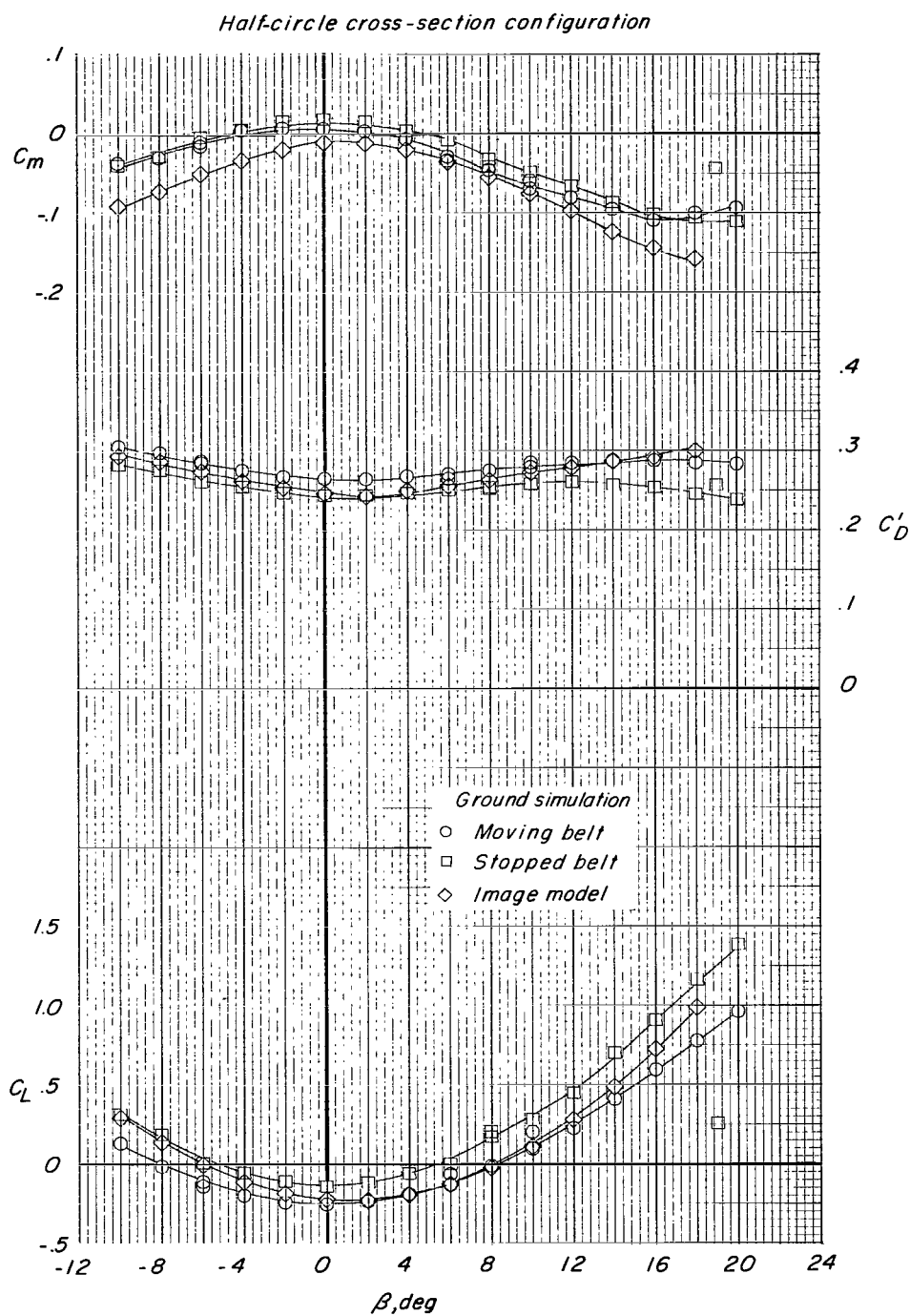
(a) Lift, drag, and pitching moment.

Figure 23.- Effect of ground-simulation technique on the aerodynamic characteristics of half-circle configuration. $\frac{H}{d_g} \approx 0.20$; $\alpha = 0^\circ$.



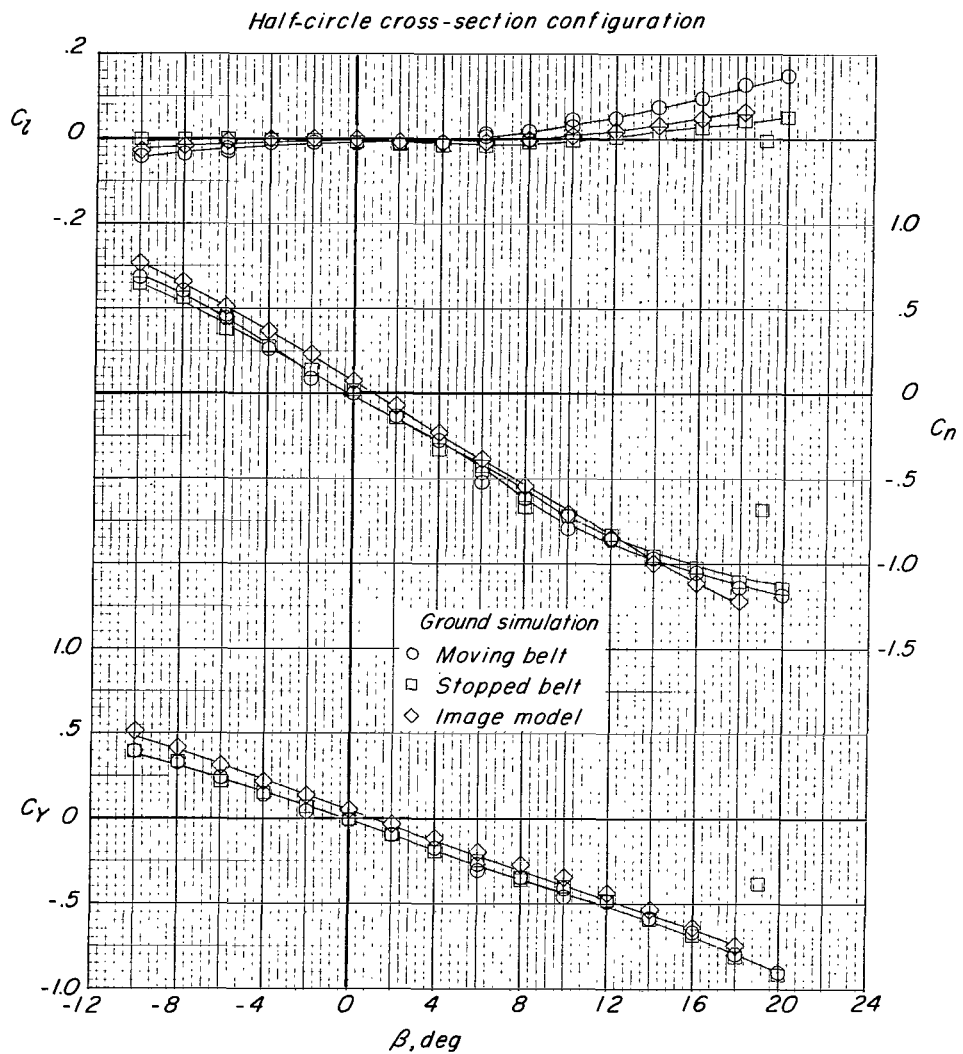
(b) Rolling moment, yawing moment, and side force.

Figure 23.- Concluded.



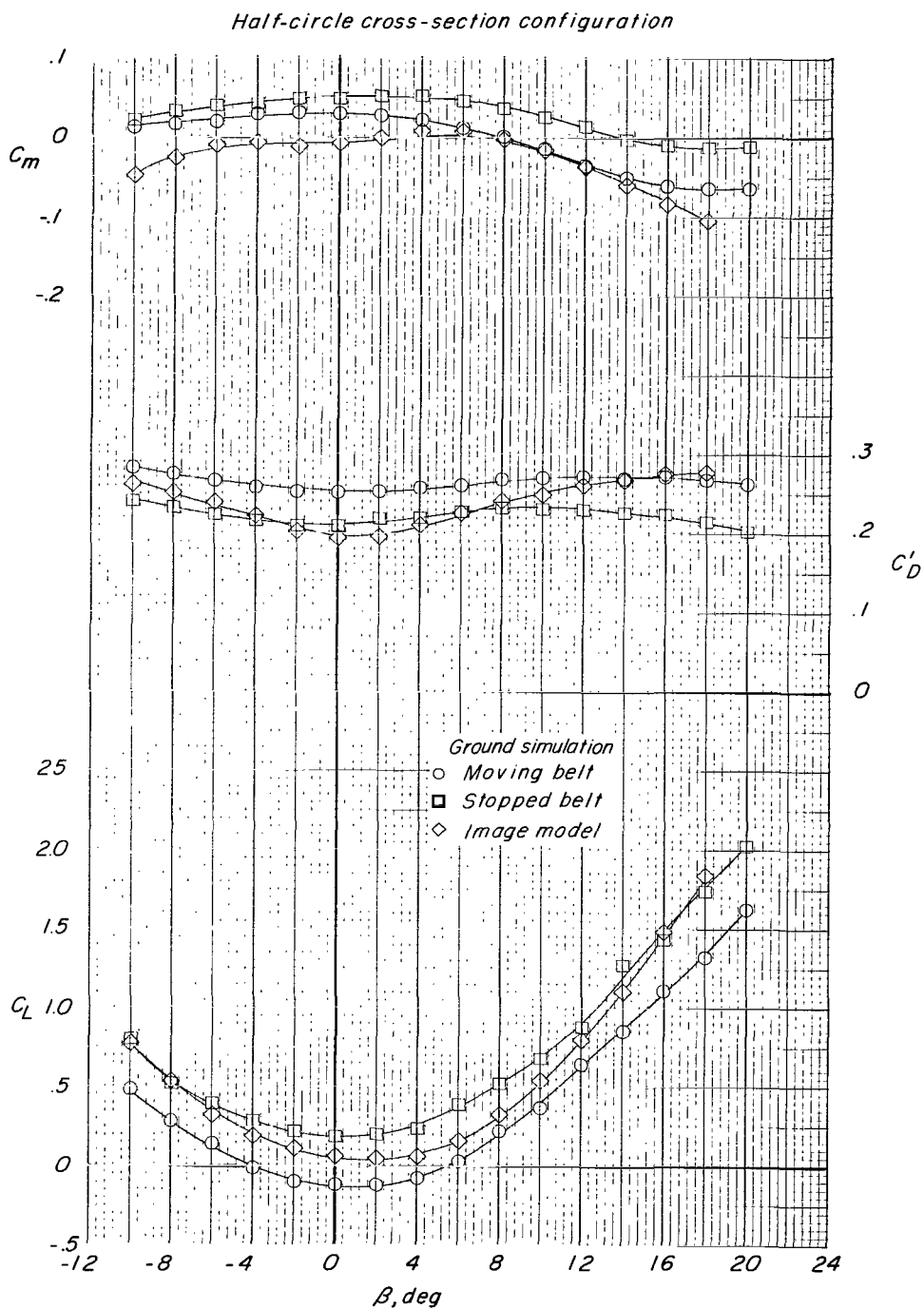
(a) Lift, drag, and pitching moment.

Figure 24.- Effect of ground-simulation technique on the aerodynamic characteristics of half-circle configuration. $\frac{H}{d_e} \approx 0.05$; $\alpha = 0^\circ$.



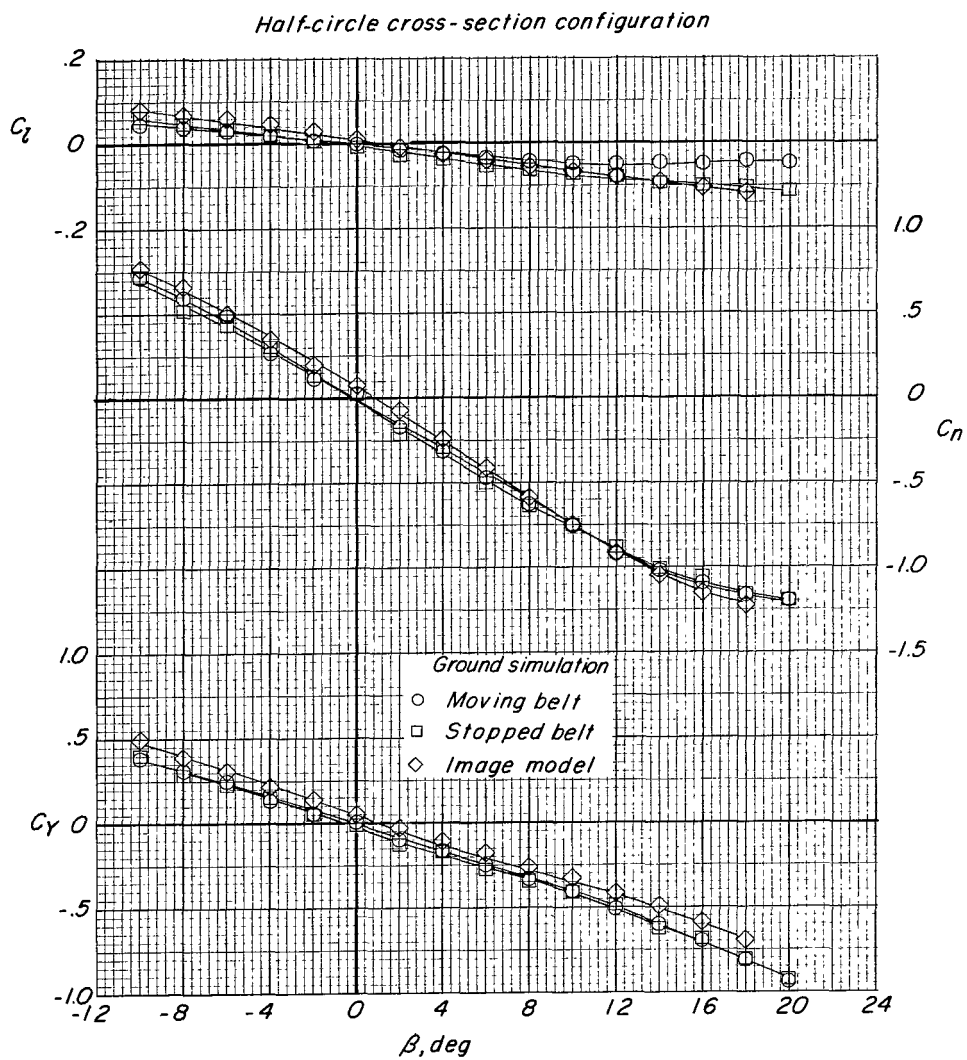
(b) Rolling moment, yawing moment, and side force.

Figure 24.- Concluded.



(a) Lift, drag, and pitching moment.

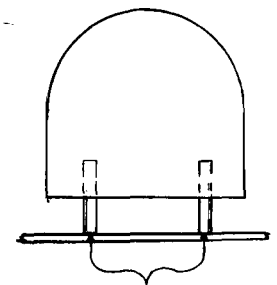
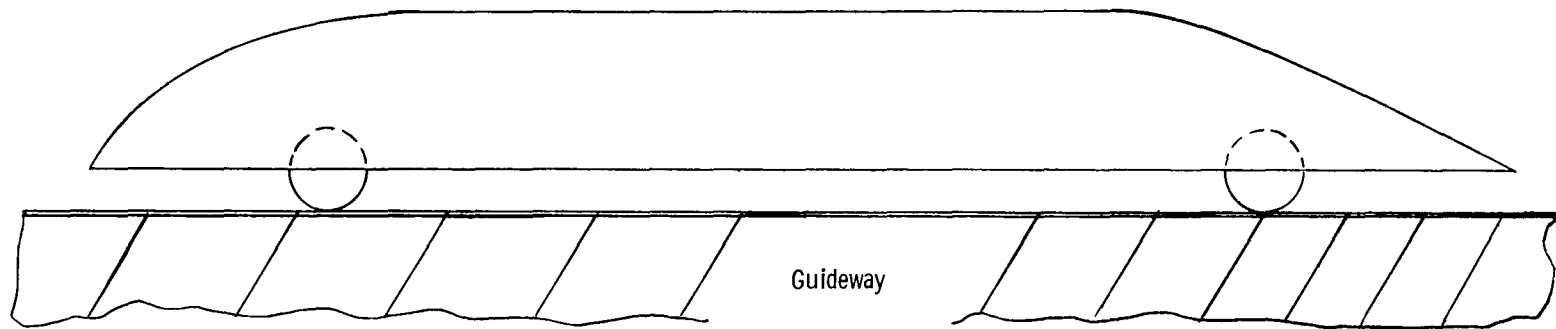
Figure 25.- Effect of ground-simulation technique on the aerodynamic characteristics of half-circle configuration, $\frac{H}{d_e} \approx 0.01$; $\alpha = 0^\circ$.



(b) Rolling moment, yawing moment, and side force.

Figure 25.- Concluded.

Representative vehicle

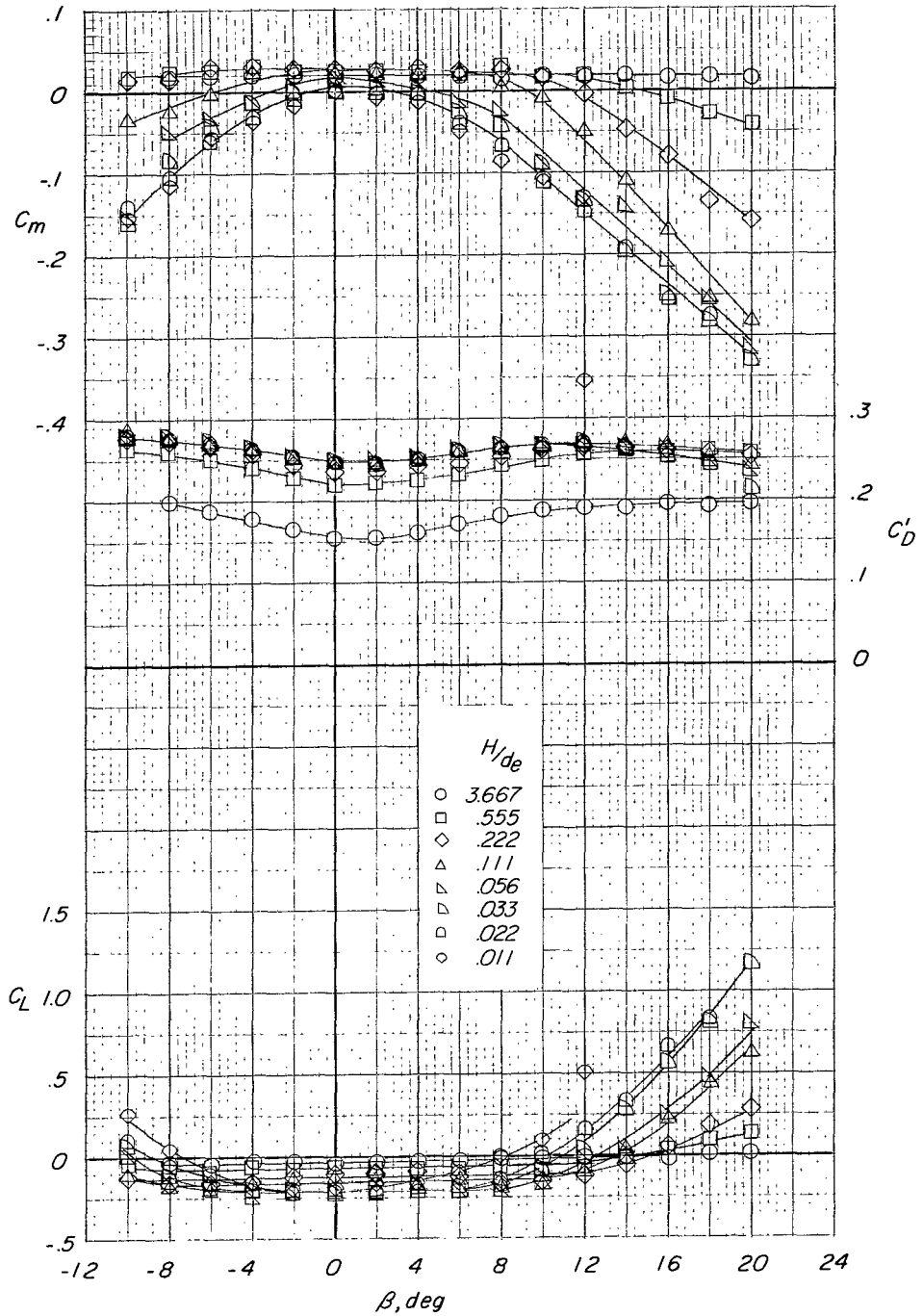


Support points
(Wheels or air cushions)

Weight	30 000 lb (133 447 newtons)
Length	64 feet (19.35 meters)
Width(effective)	8 feet (2.42 meters)
Distance between wheel or air-cushion support points:	
Lateral	5 feet (1.52 meters)
Longitudinal	40 feet (12.16 meters)

Figure 26.- Sketch and dimensions of a representative vehicle constructed for data analysis.

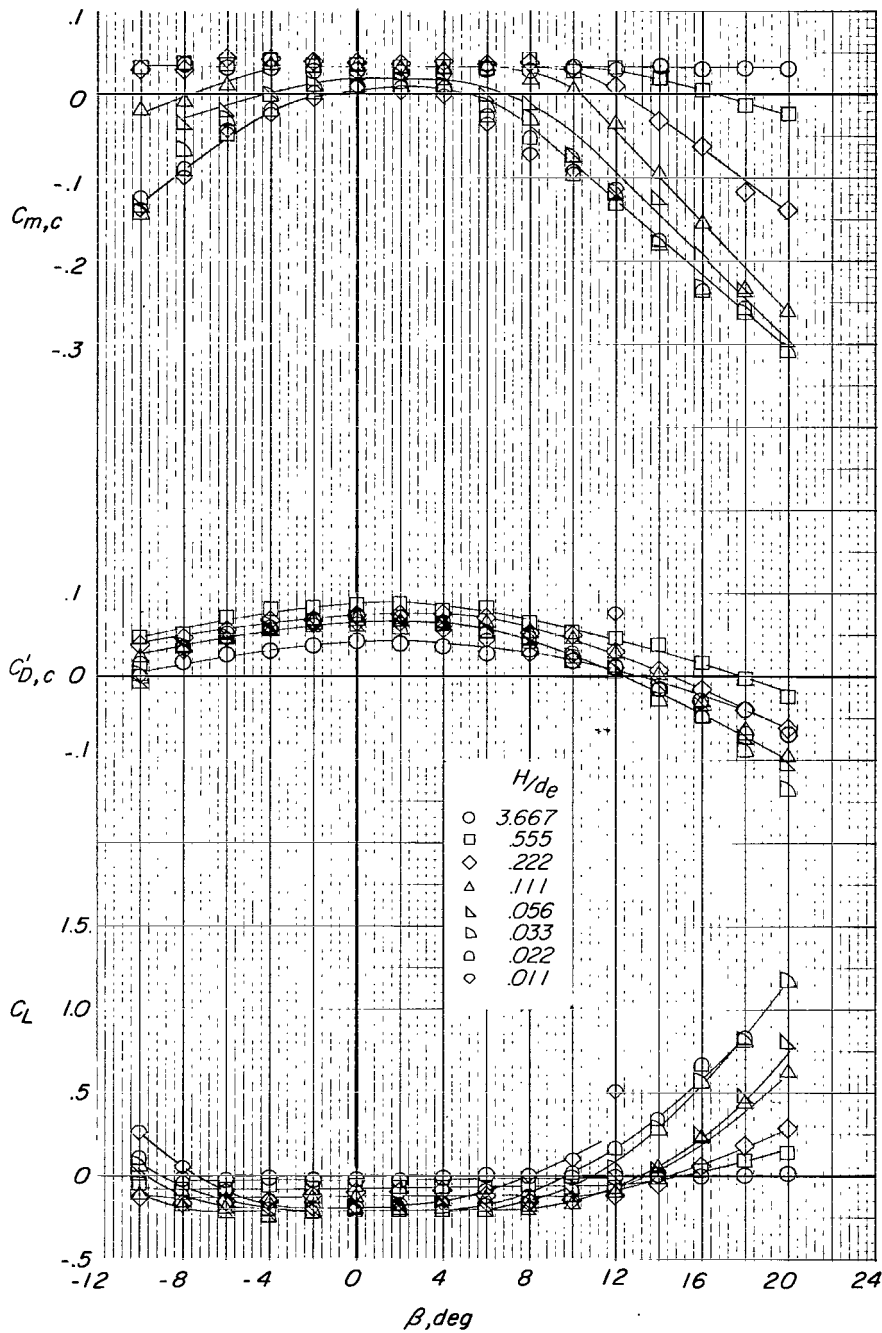
Circular cross-section configuration
Ground belt moving



(a) Lift, drag, and pitching-moment coefficients.

Figure 27.- Effect of ground height on the aerodynamic characteristics of circular configuration. Ground belt moving; $\alpha = 0^\circ$.

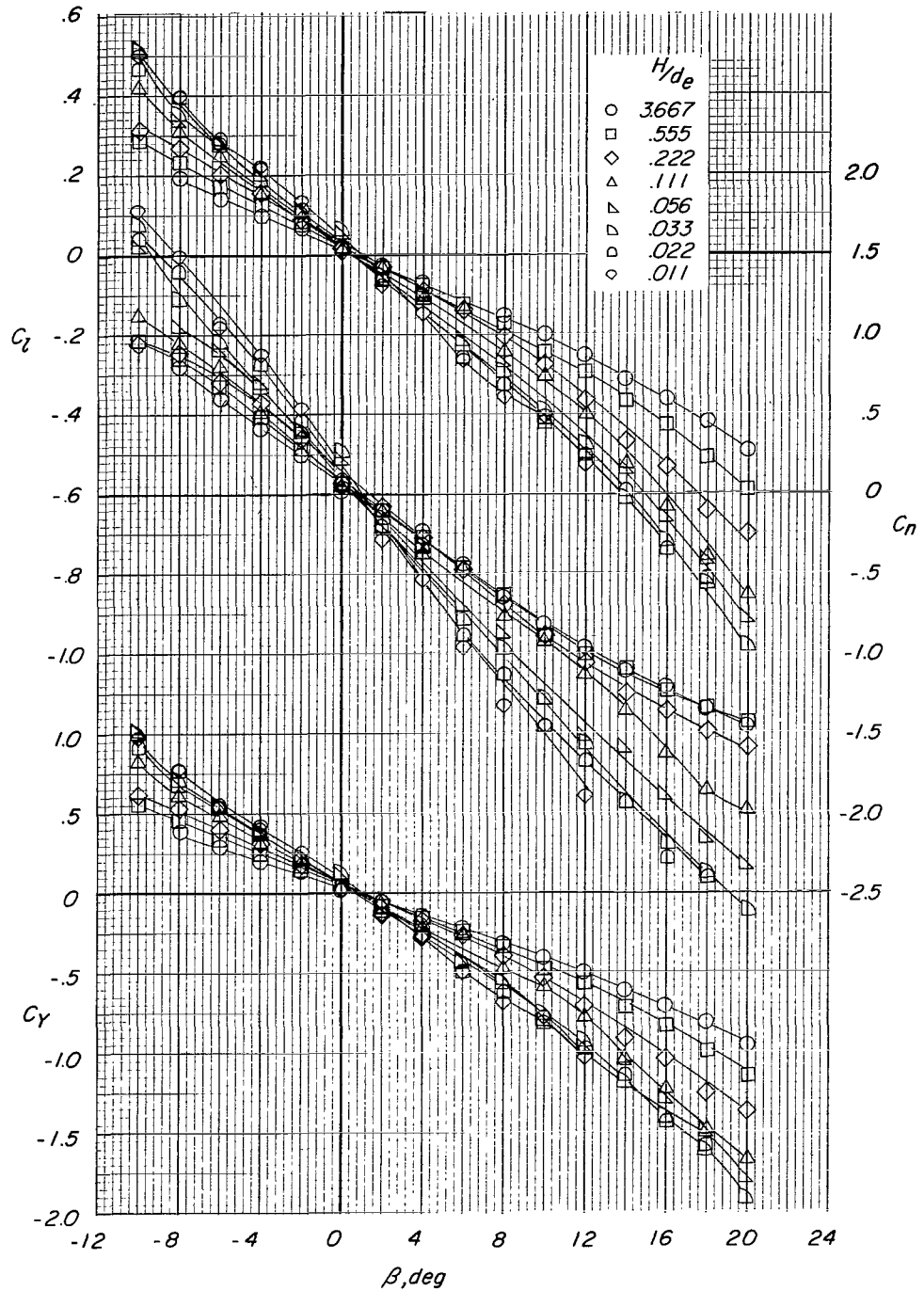
*Circular cross-section configuration
Ground belt moving*



(b) Lift, drag, and pitching-moment coefficients with base pressure corrections.

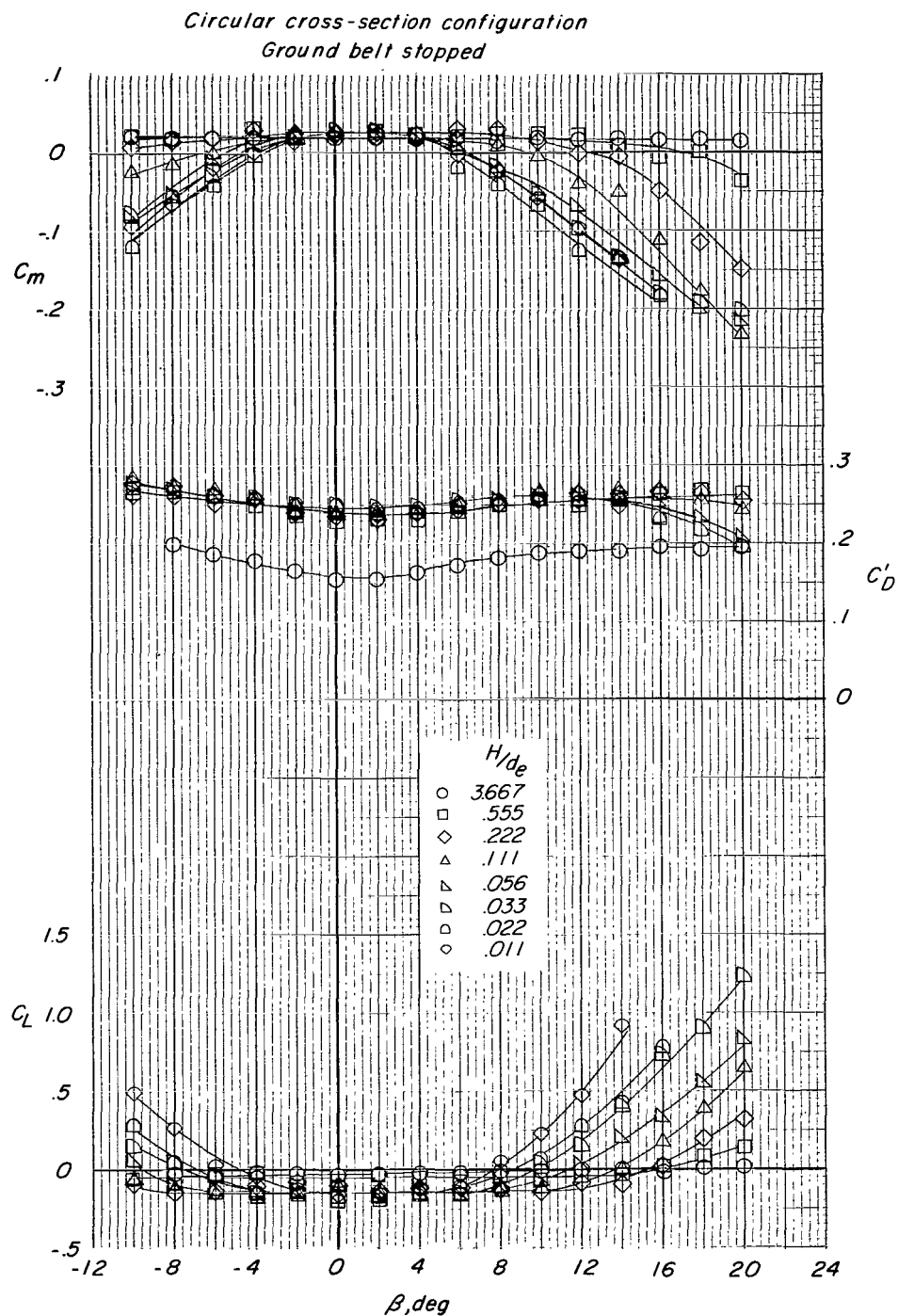
Figure 27.- Continued.

Circular cross-section configuration
Ground belt moving



(c) Rolling-moment, yawing-moment, and side-force coefficients.

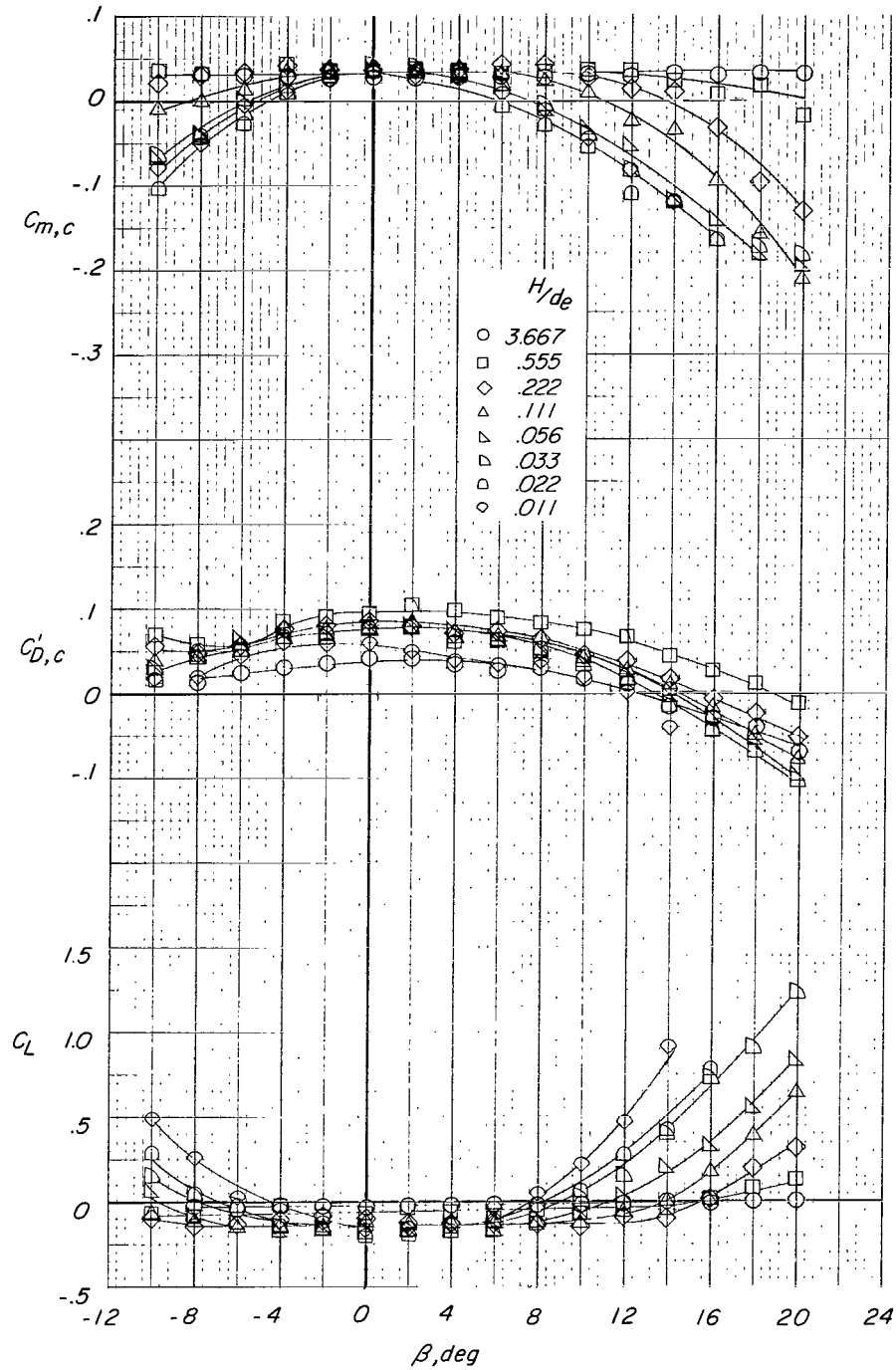
Figure 27.- Concluded.



(a) Lift, drag, and pitching-moment coefficients.

Figure 28.- Effect of ground height on the aerodynamic characteristics of circular configuration. Ground belt stopped; $\alpha = 0^\circ$.

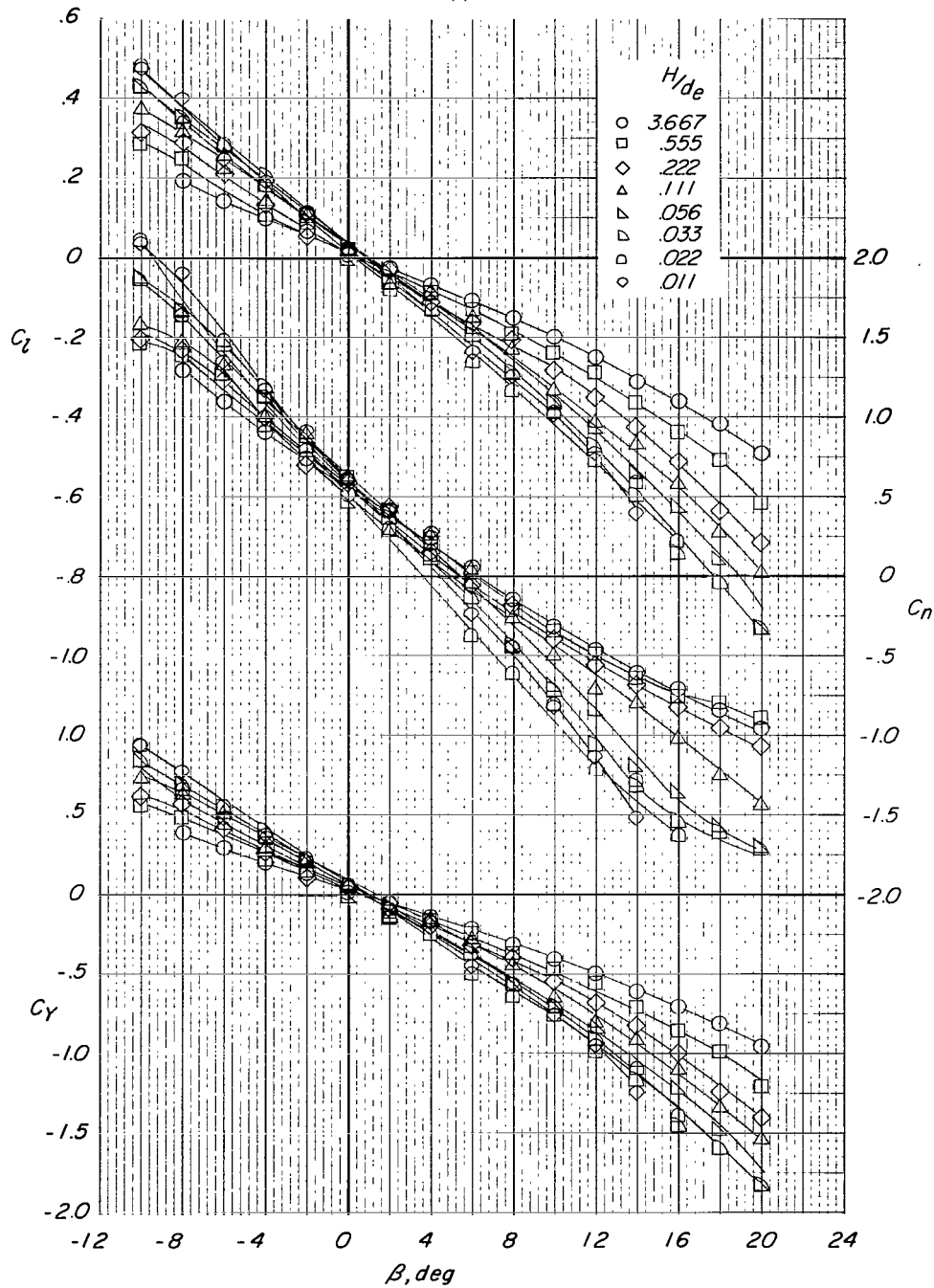
Circular cross-section configuration
Ground belt stopped



(b) Lift, drag, and pitching-moment coefficients with base pressure corrections.

Figure 28.- Continued.

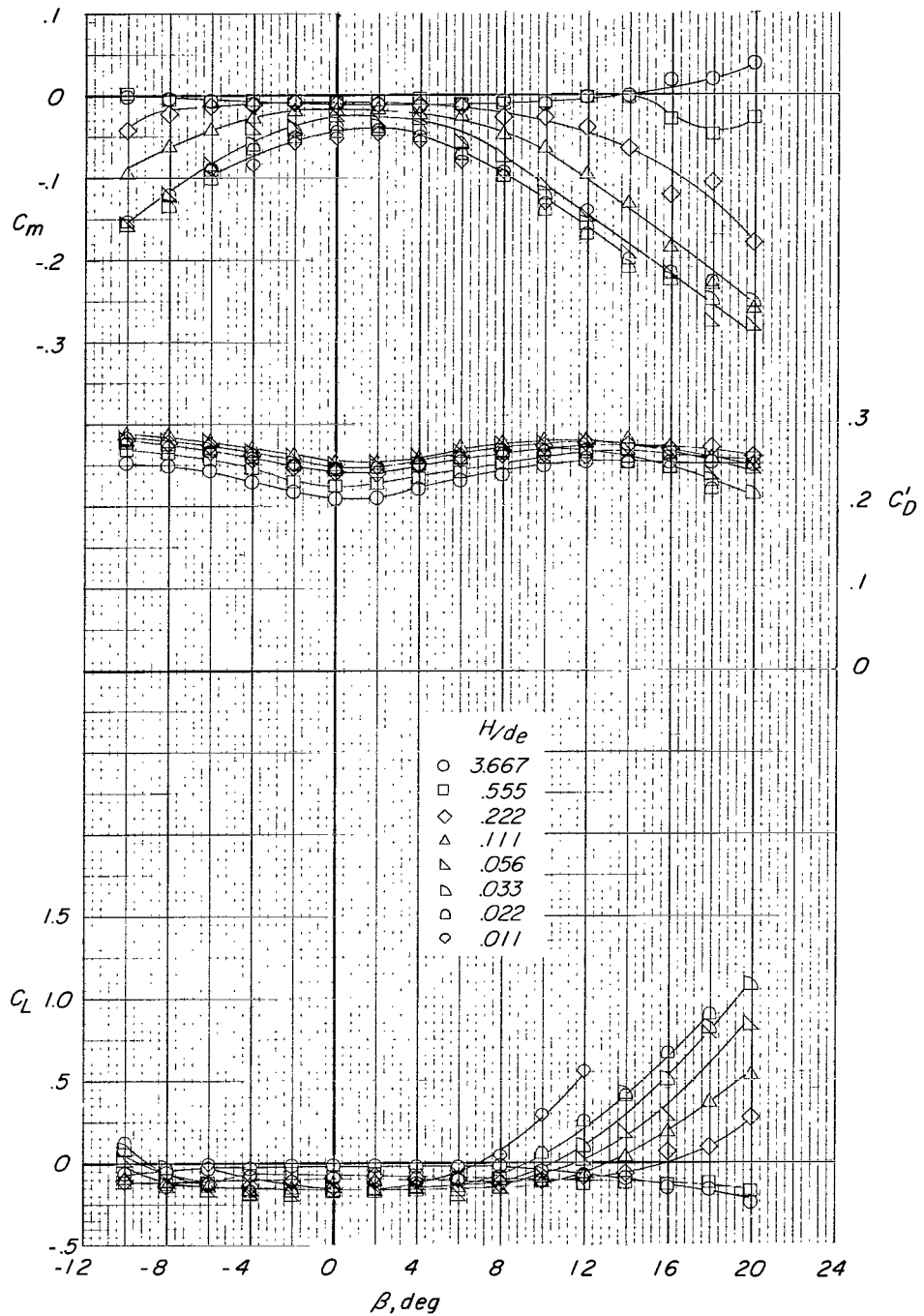
Circular cross-section configuration
Ground belt stopped



(c) Rolling-moment, yawing-moment, and side-force coefficients.

Figure 28.- Concluded.

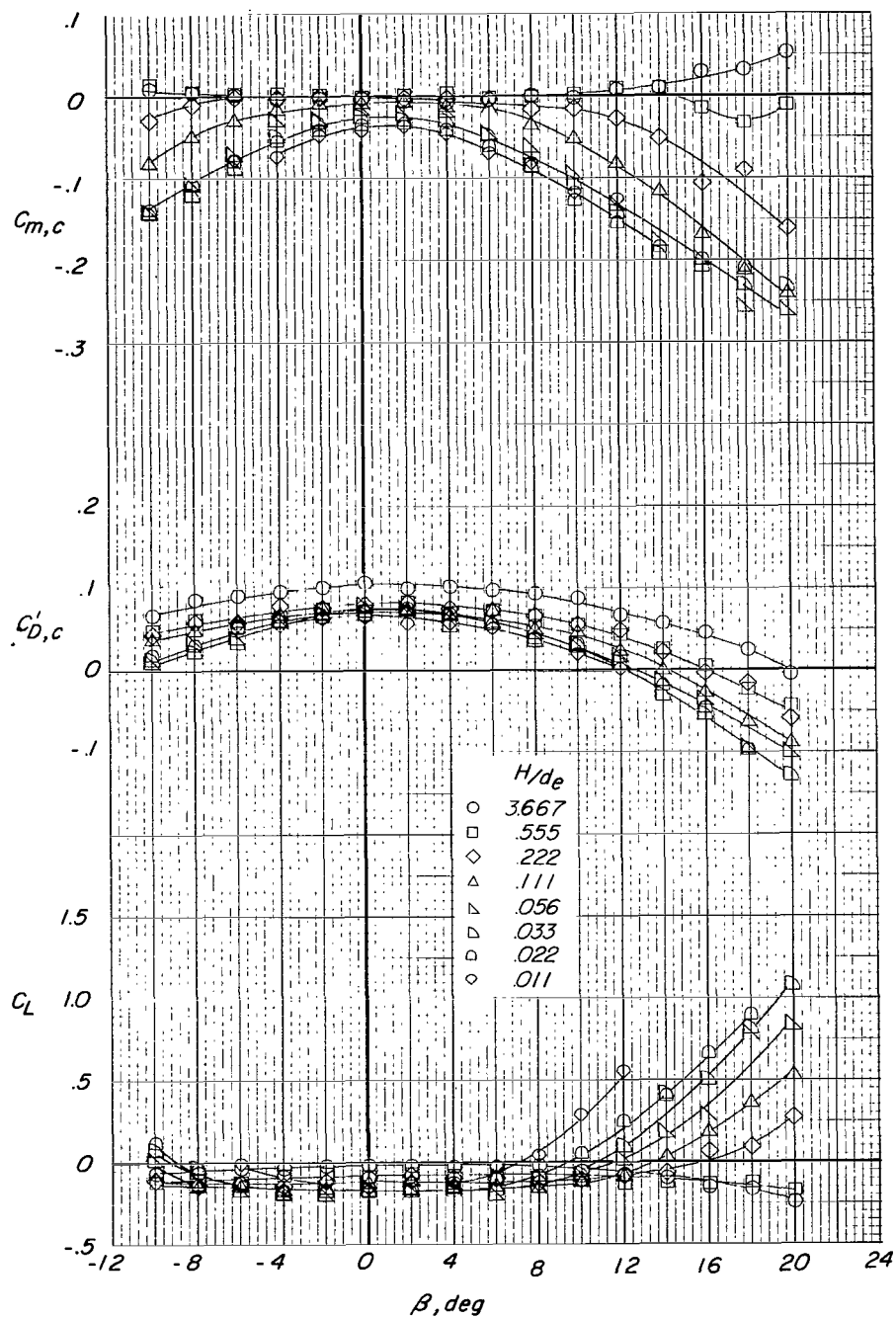
Square-type cross-section configuration
Ground belt moving



(a) Lift, drag, and pitching-moment coefficients.

Figure 29.- Effect of ground height on the aerodynamic characteristics of square-type configuration. Ground belt moving; $\alpha = 0^\circ$.

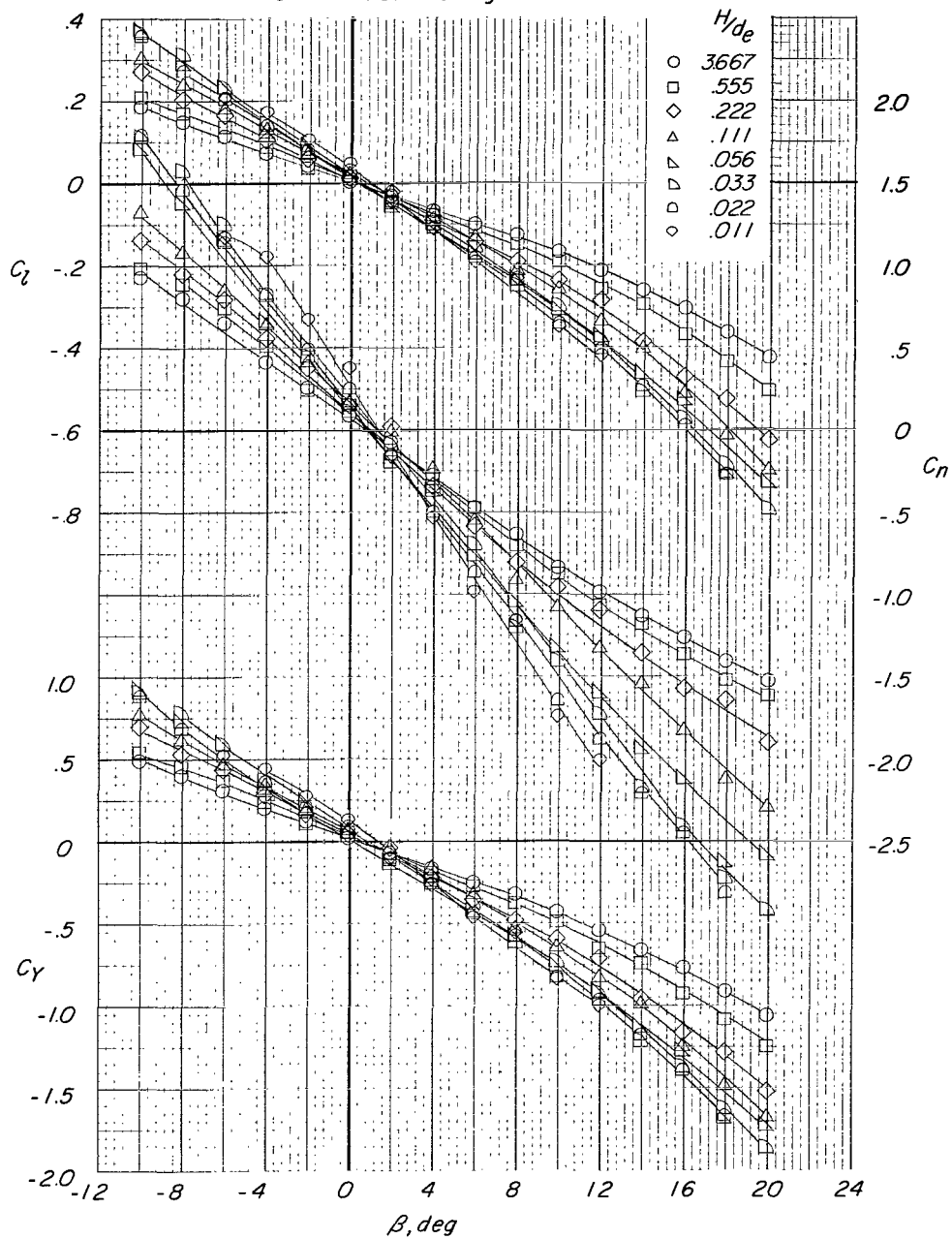
Square-type cross-section configuration
Ground belt moving



(b) Lift, drag, and pitching-moment coefficients with base pressure corrections.

Figure 29.- Continued.

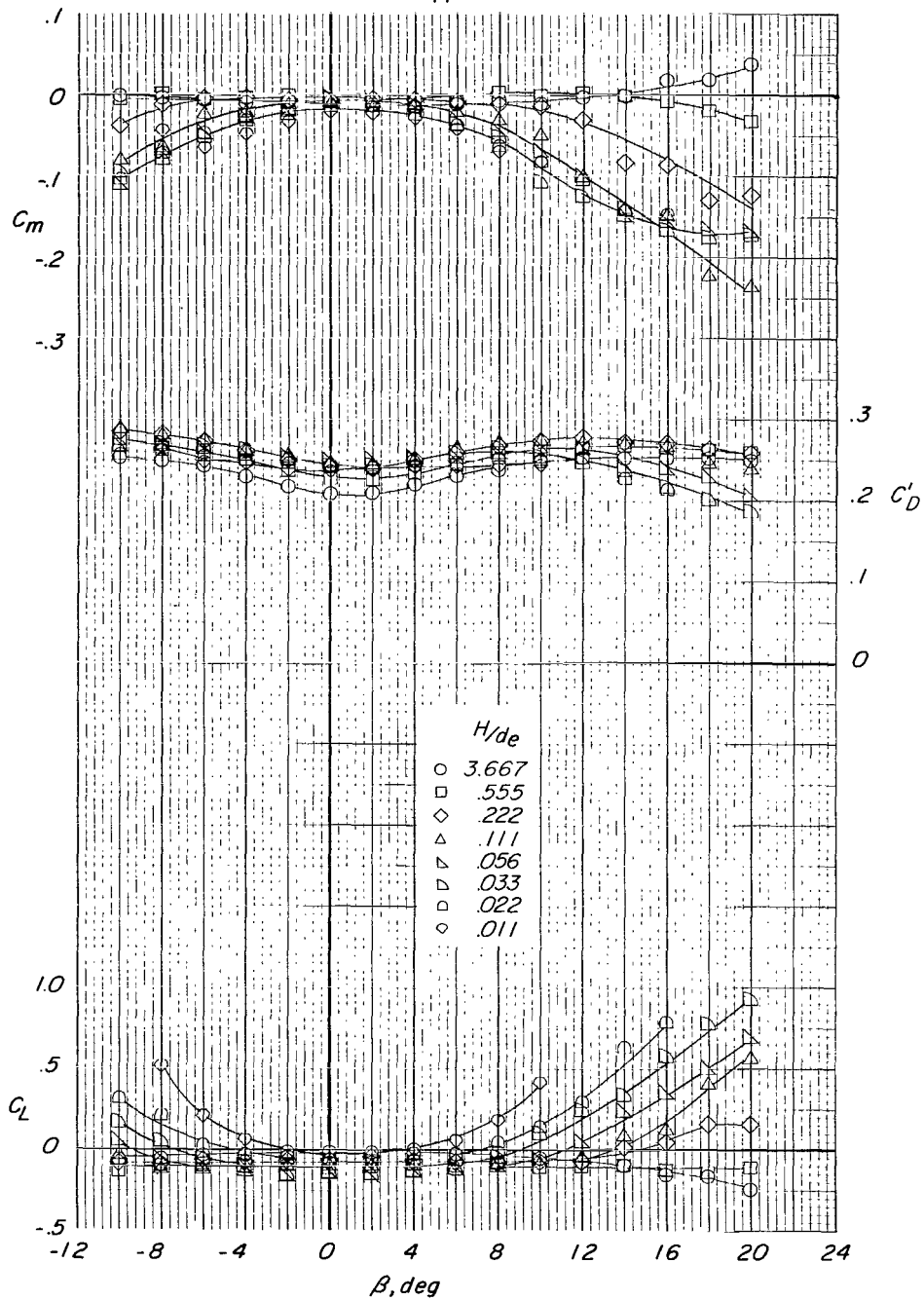
Square-type cross-section configuration
Ground belt moving



(c) Rolling-moment, yawing-moment, and side-force coefficients.

Figure 29.- Concluded.

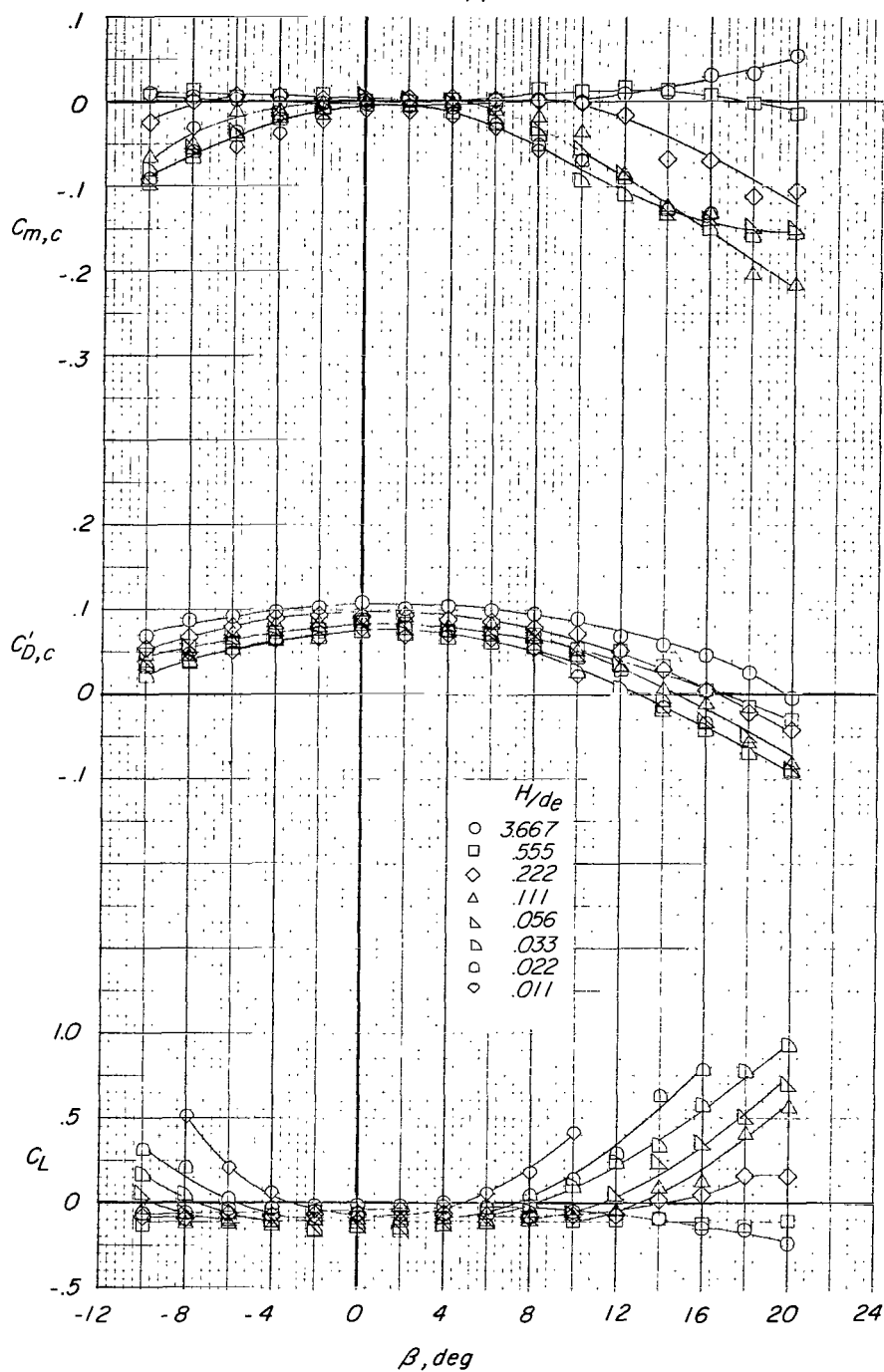
Square-type cross-section configuration
Ground belt stopped



(a) Lift, drag, and pitching-moment coefficients.

Figure 30.- Effect of ground height on the aerodynamic characteristics of square-type configuration. Ground belt stopped; $\alpha = 0^\circ$.

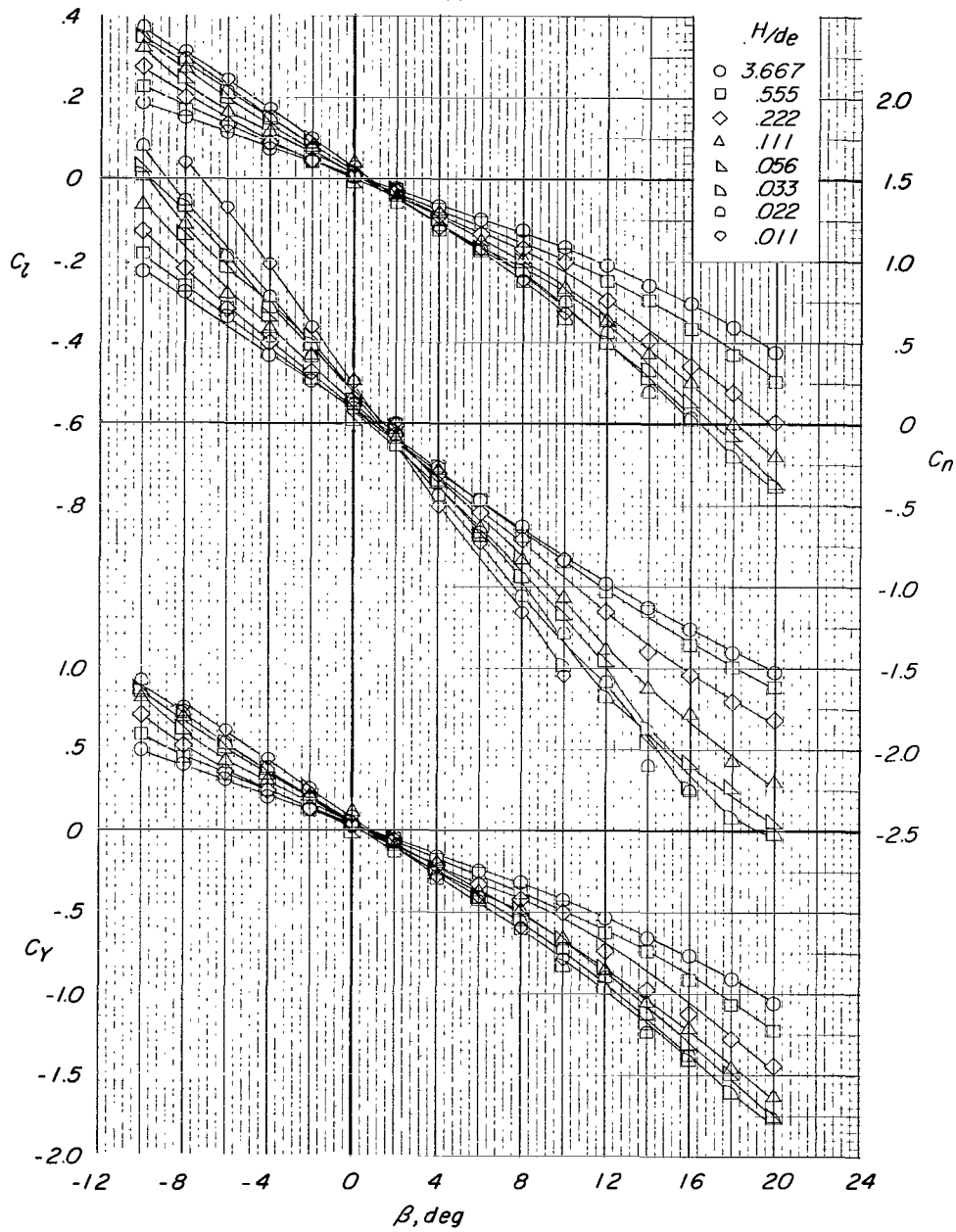
Square-type cross-section configuration
Ground belt stopped



(b) Lift, drag, and pitching-moment coefficients with base pressure corrections.

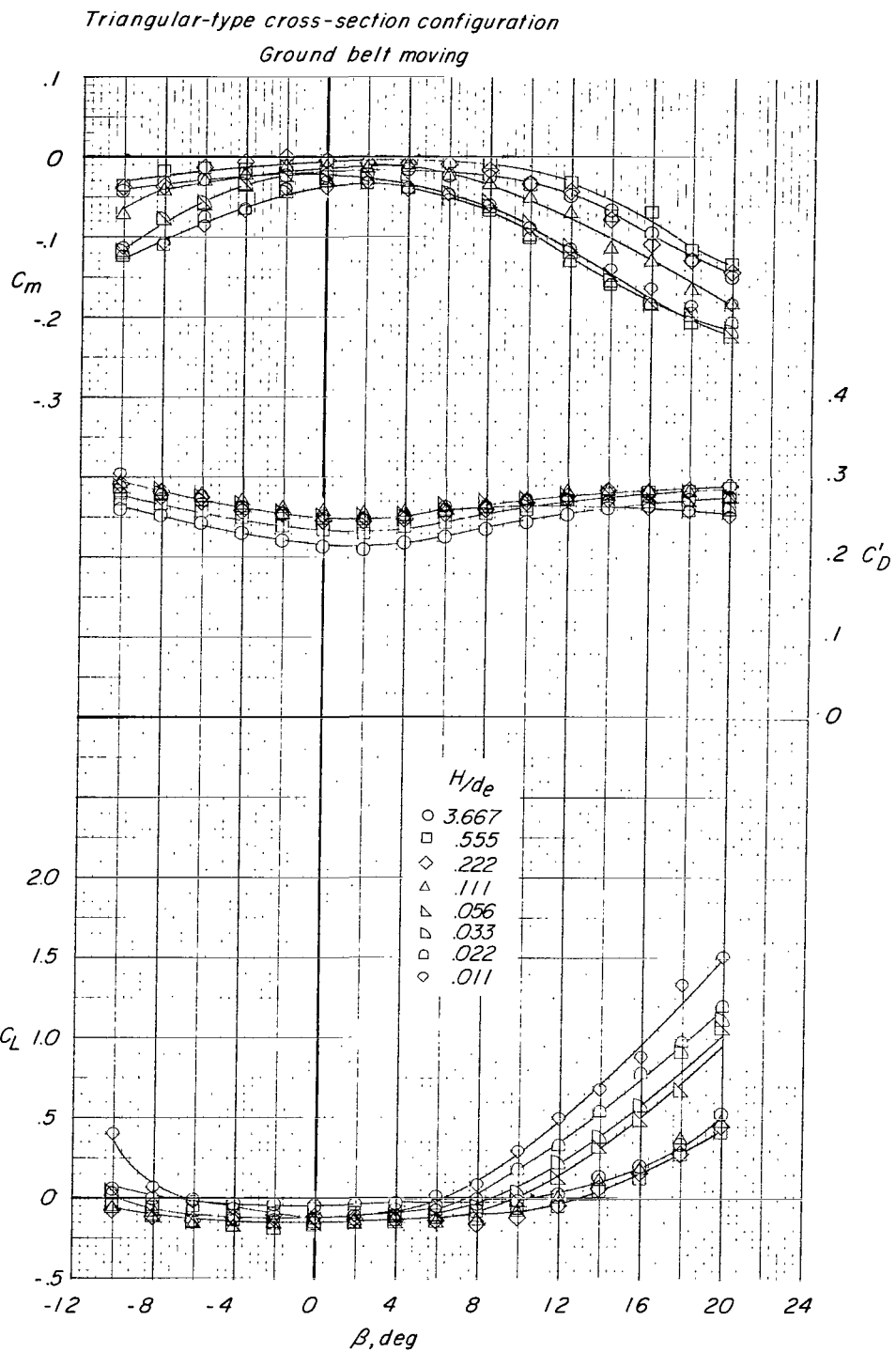
Figure 30.- Continued.

Square-type cross-section configuration
Ground belt stopped



(c) Rolling-moment, yawing-moment, and side-force coefficients.

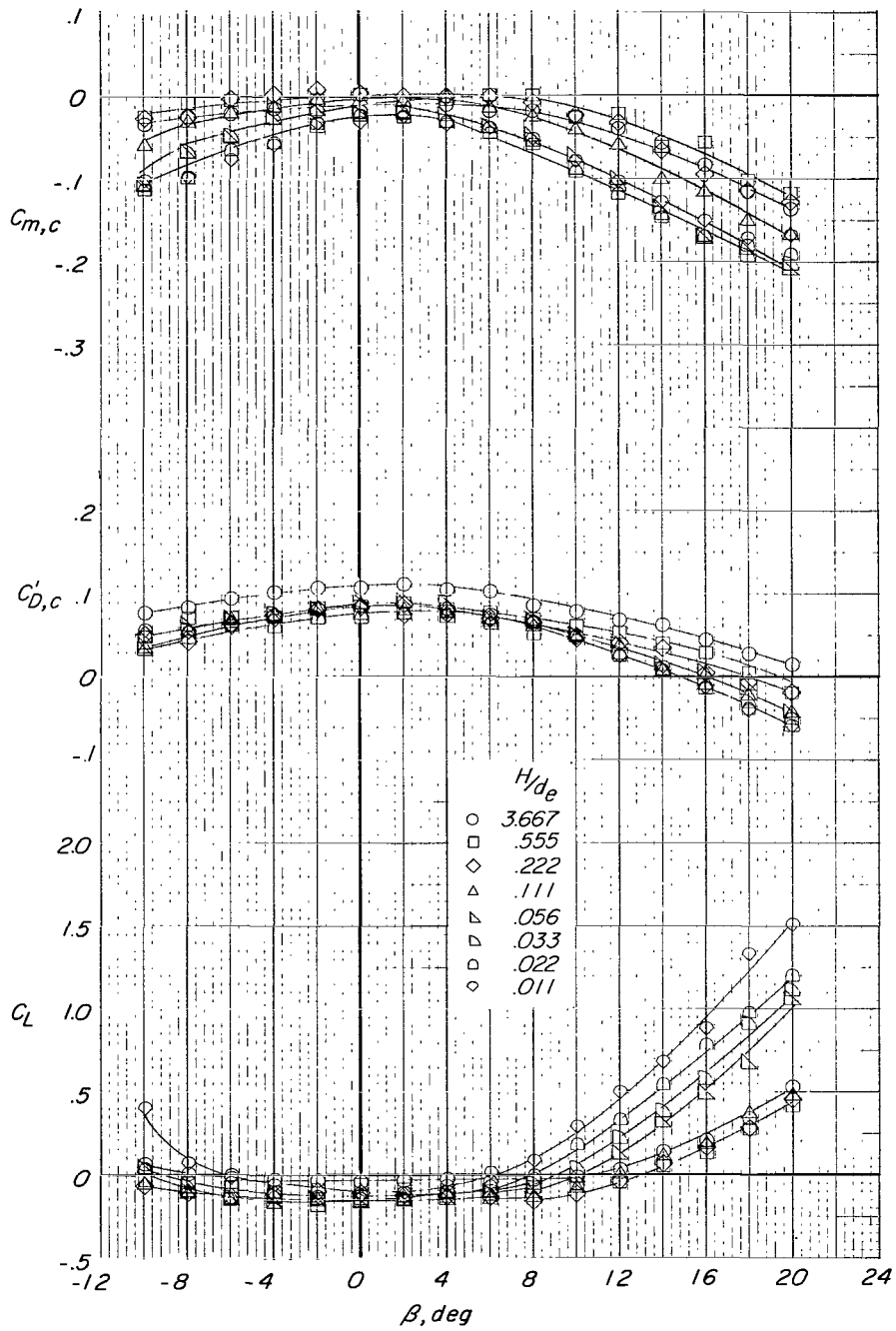
Figure 30.- Concluded.



(a) Lift, drag, and pitching-moment coefficients.

Figure 31.- Effect of ground height on the aerodynamic characteristics of triangular-type configuration. Ground belt moving; $\alpha = 0^\circ$.

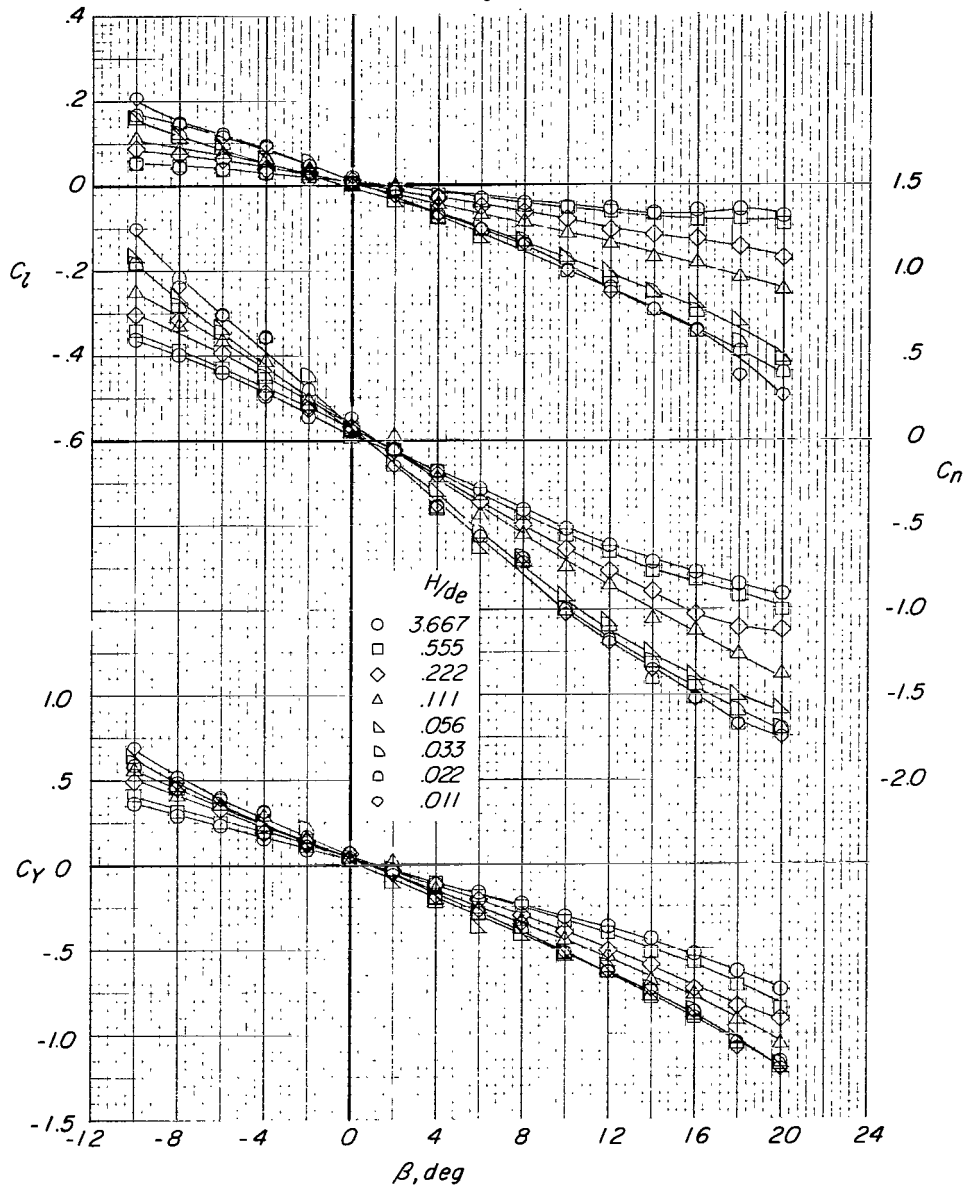
Triangular-type cross-section configuration
Ground belt moving



(b) Lift, drag, and pitching-moment coefficients with base pressure corrections.

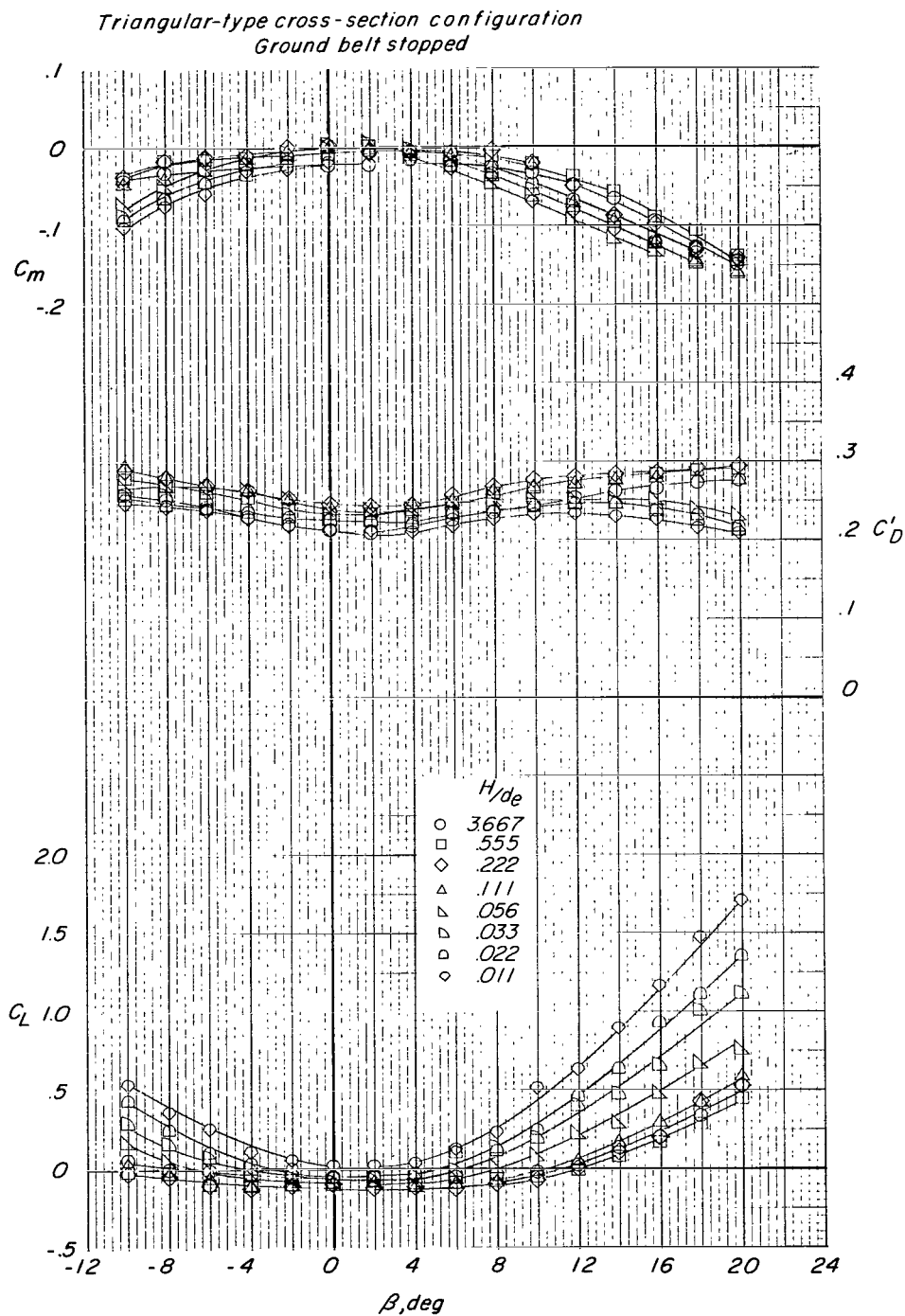
Figure 31.- Continued.

Triangular-type cross-section configuration
Ground belt moving



(c) Rolling-moment, yawing-moment, and side-force coefficients.

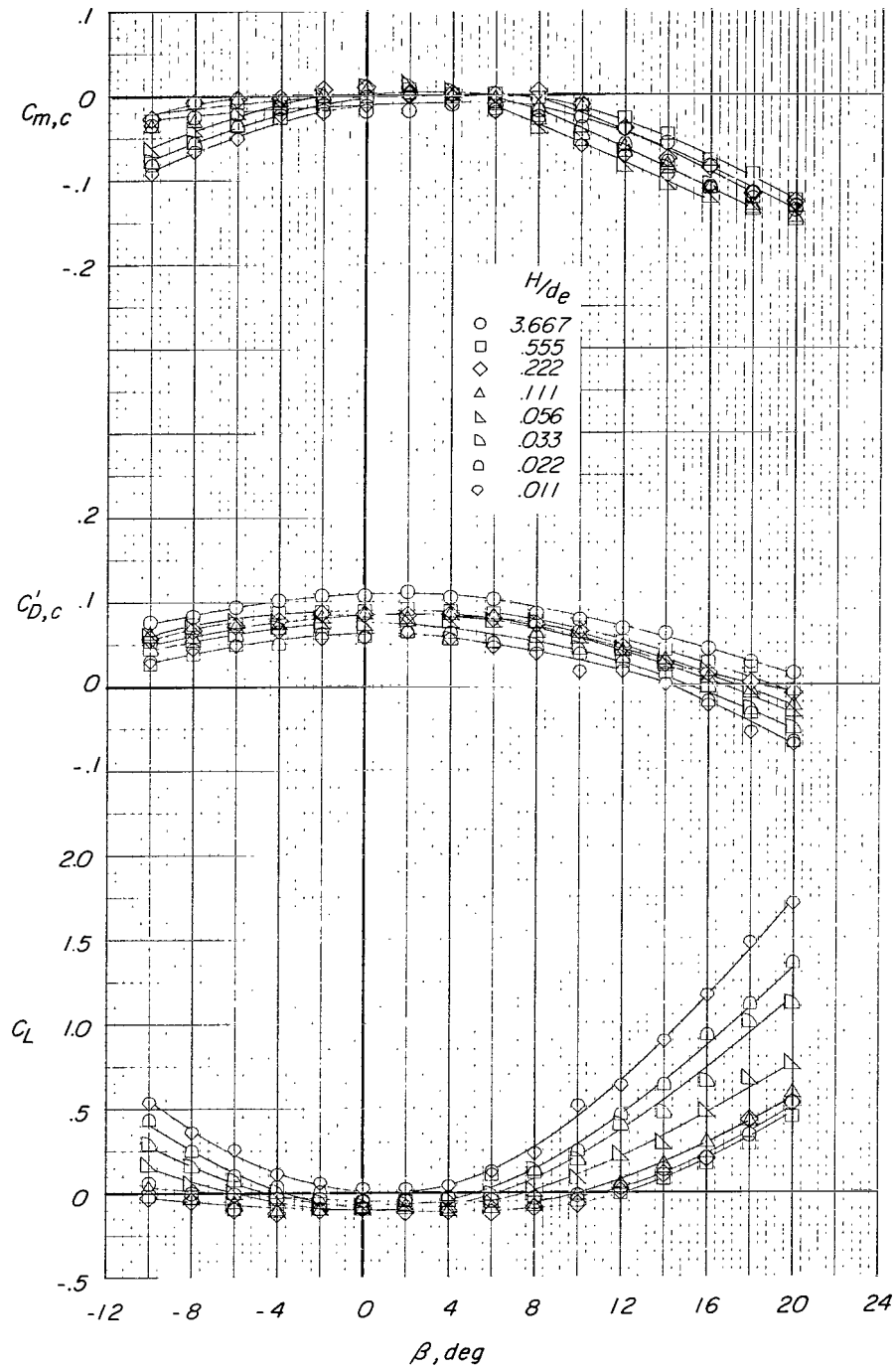
Figure 31.- Concluded.



(a) Lift, drag, and pitching-moment coefficients.

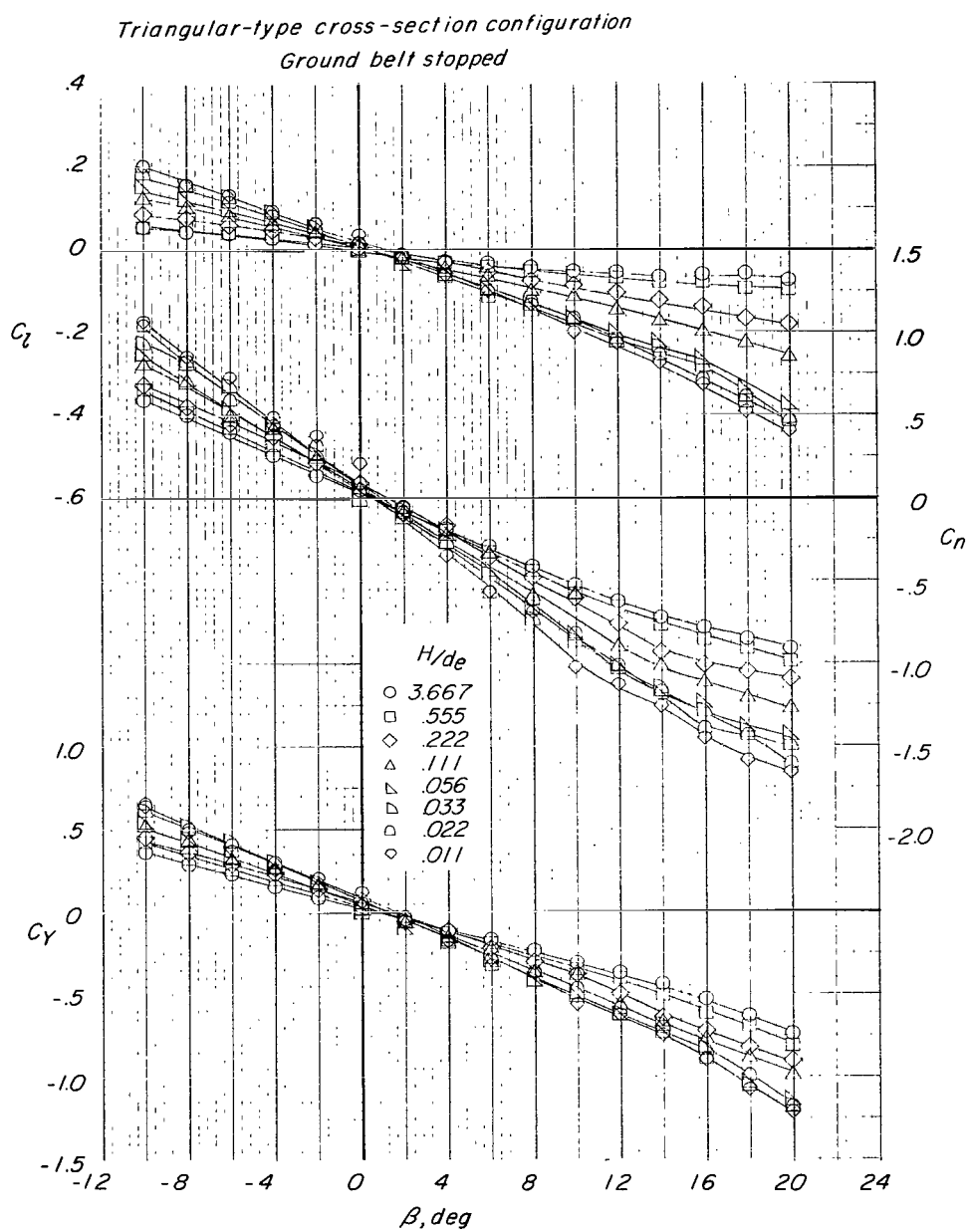
Figure 32.- Effect of ground height on the aerodynamic characteristics of triangular-type configuration. Ground belt stopped; $\alpha = 0^\circ$.

Triangular-type cross-section configuration
Ground belt stopped



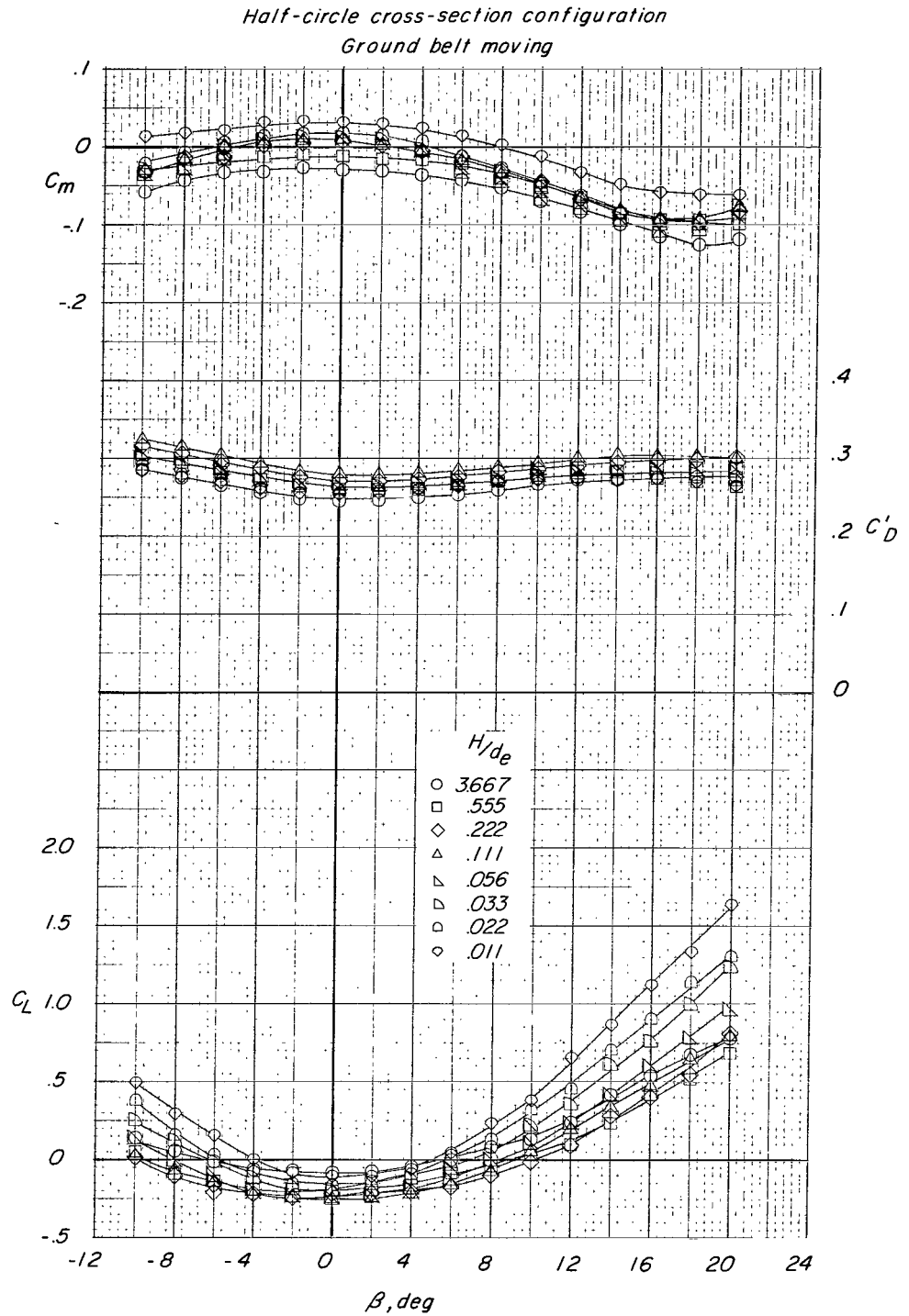
(b) Lift, drag, and pitching-moment coefficients with base pressure corrections.

Figure 32.- Continued.



(c) Rolling-moment, yawing-moment, and side-force coefficients.

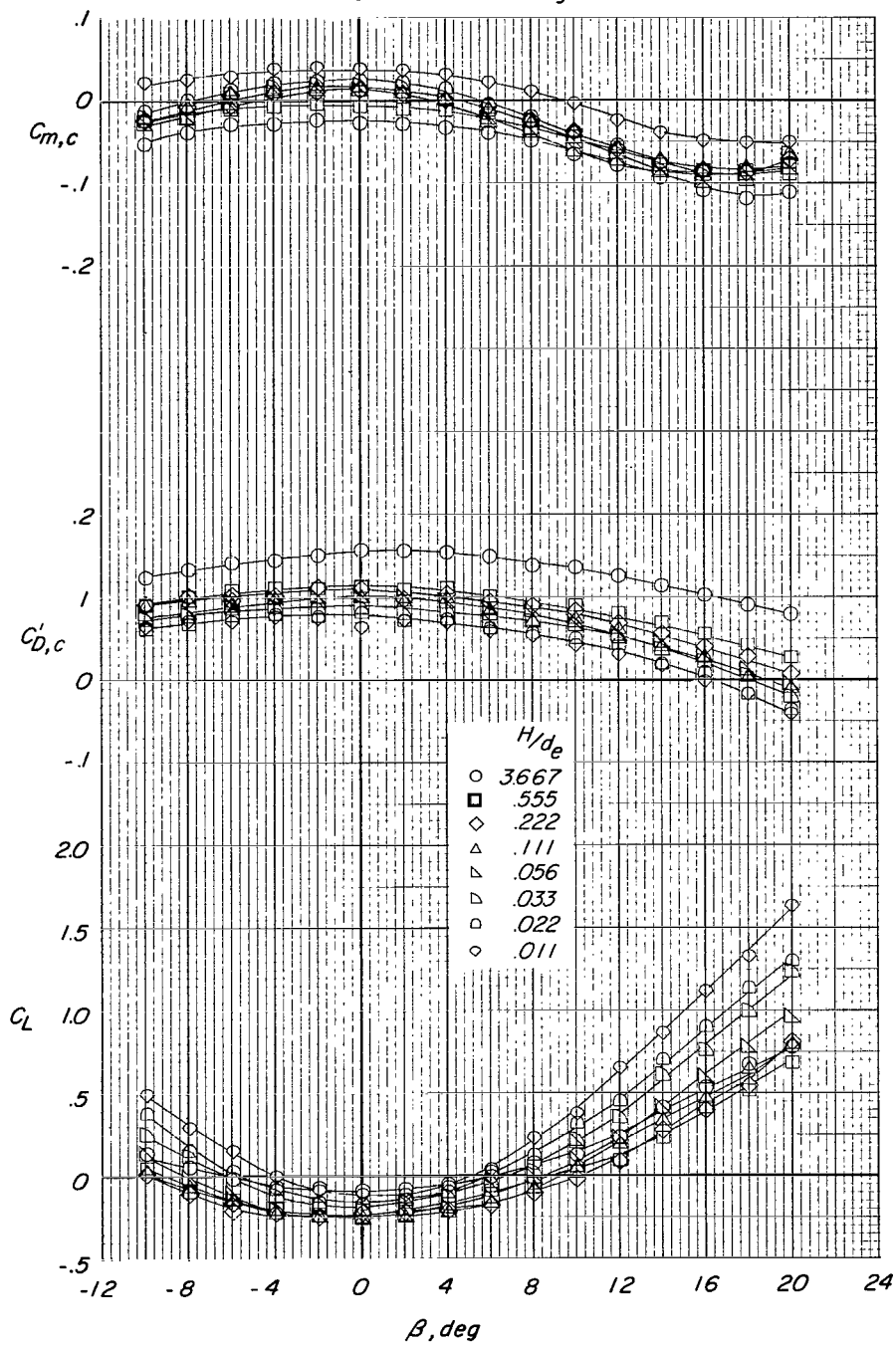
Figure 32.- Concluded.



(a) Lift, drag, and pitching-moment coefficients.

Figure 33.- Effect of ground height on the aerodynamic characteristics of half-circle configuration. Ground belt moving; $\alpha = 0^\circ$.

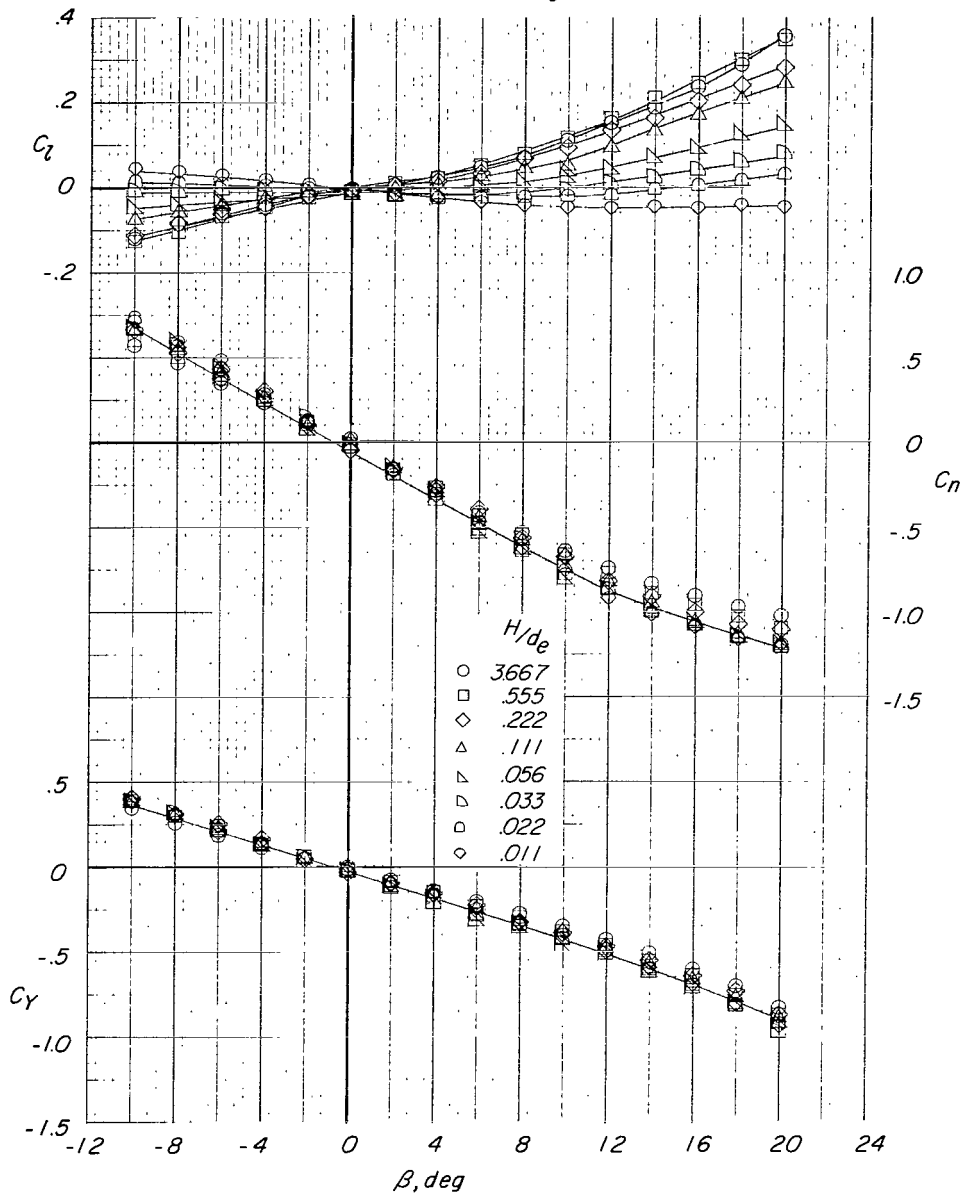
Half-circle cross-section configuration
Ground belt moving



(b) Lift, drag, and pitching-moment coefficients with base pressure corrections.

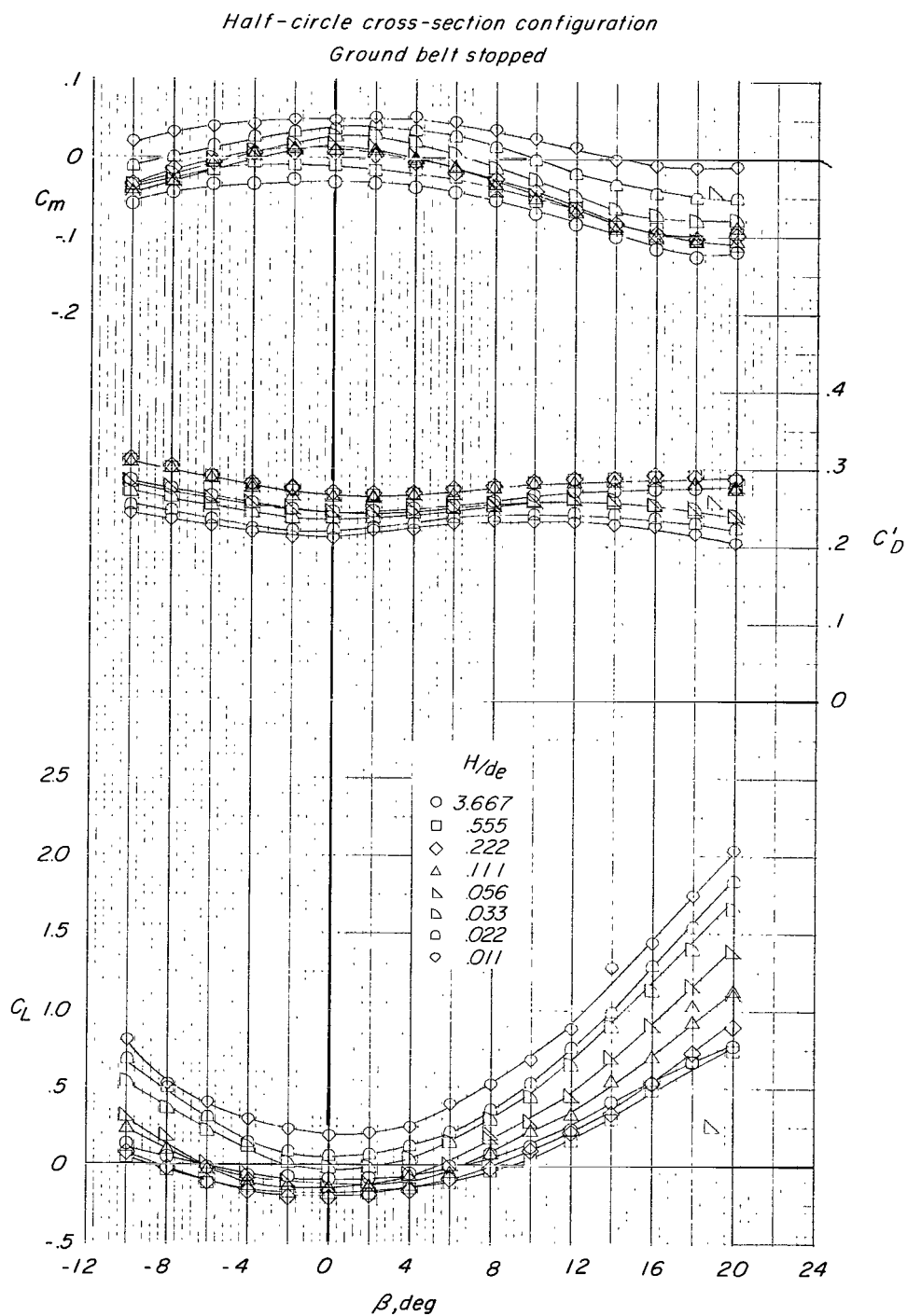
Figure 33.- Continued.

Half-circle cross-section configuration
Ground belt moving



(c) Rolling-moment, yawing-moment, and side-force coefficients.

Figure 33.- Concluded.

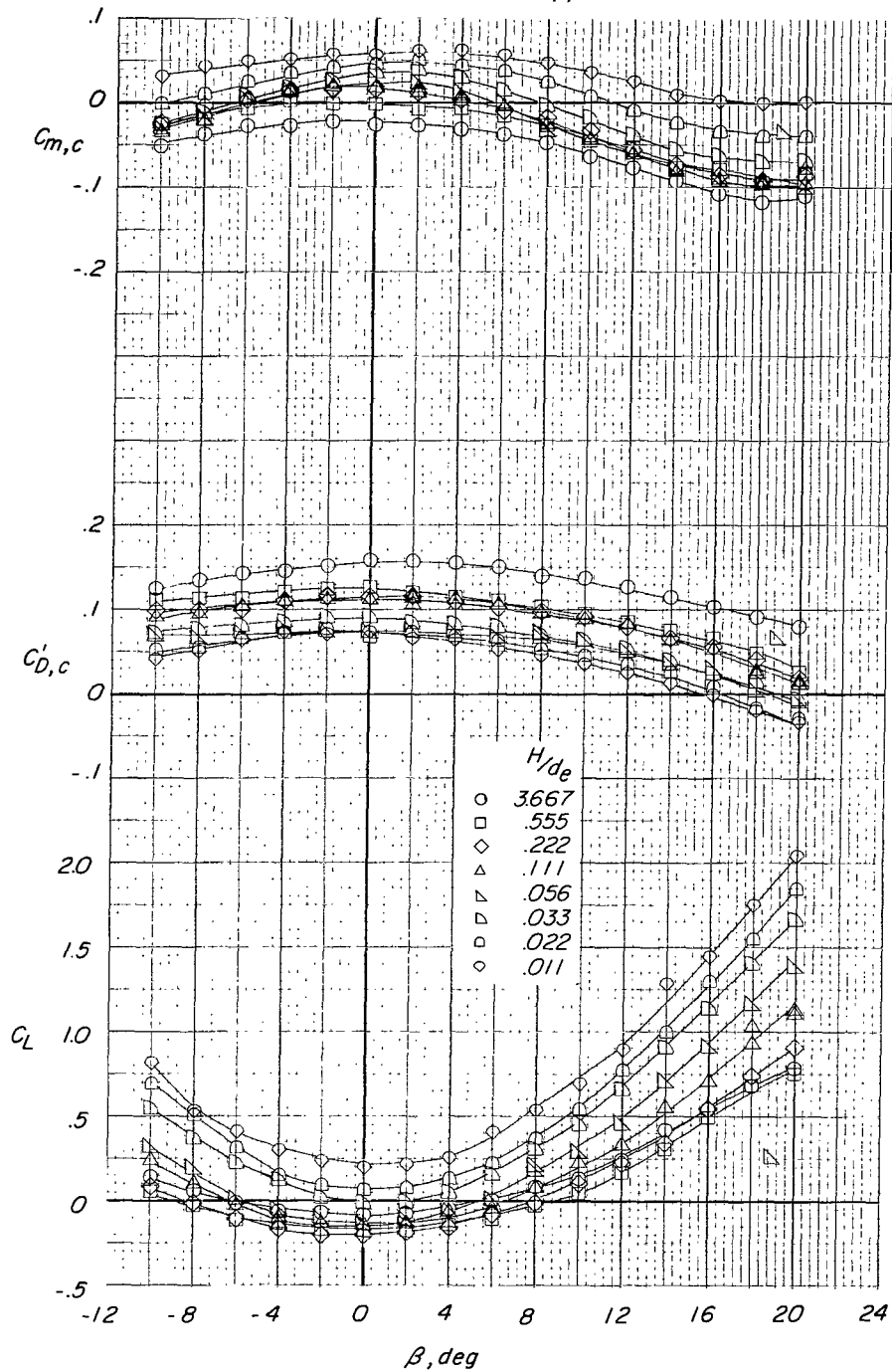


(a) Lift, drag, and pitching-moment coefficients.

Figure 34.- Effect of ground height on the aerodynamic characteristics of half-circle configuration. Ground belt stopped; $\alpha = 0^\circ$.

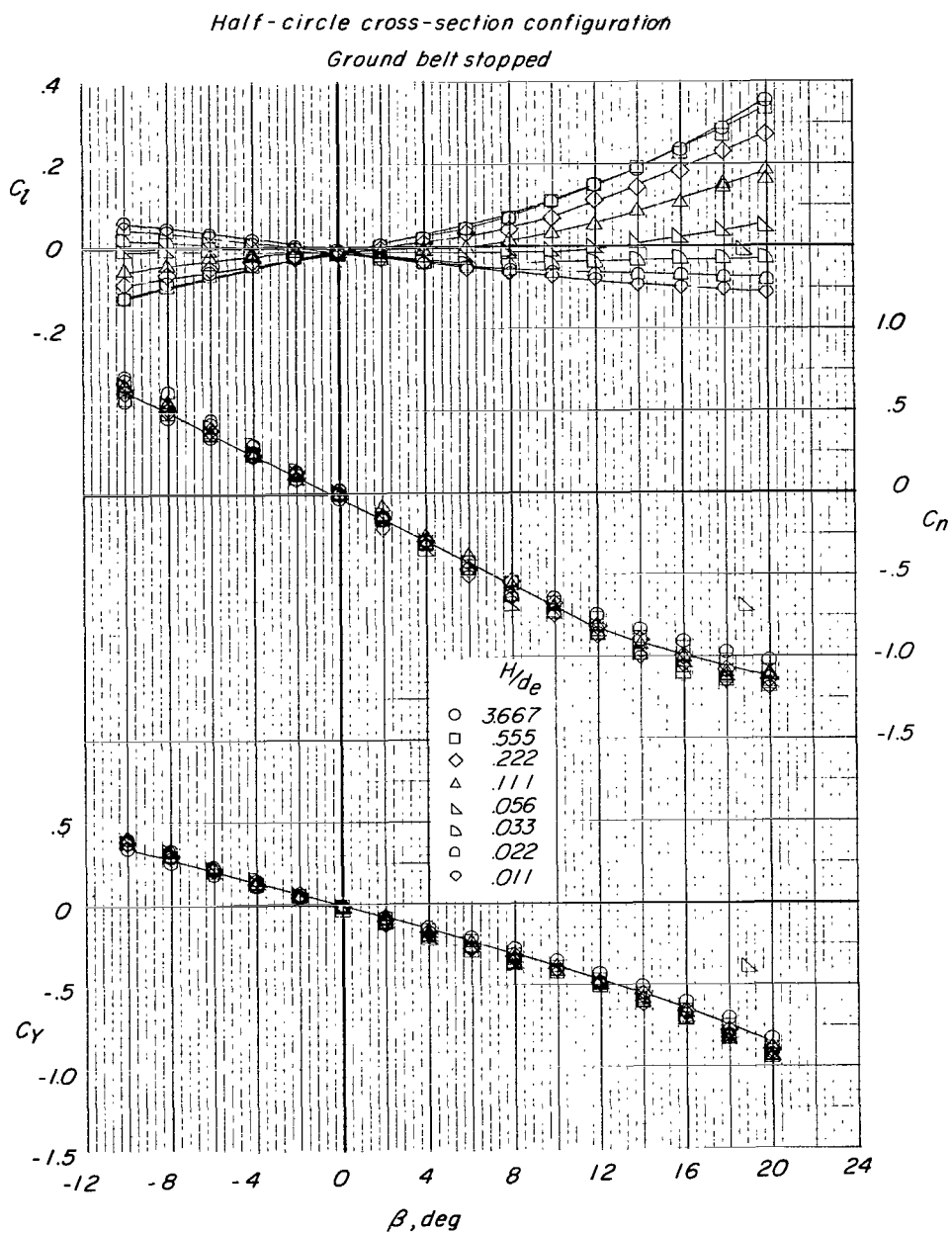
Half-circle cross-section configuration

Ground belt stopped



(b) Lift, drag, and pitching-moment coefficients with base pressure corrections.

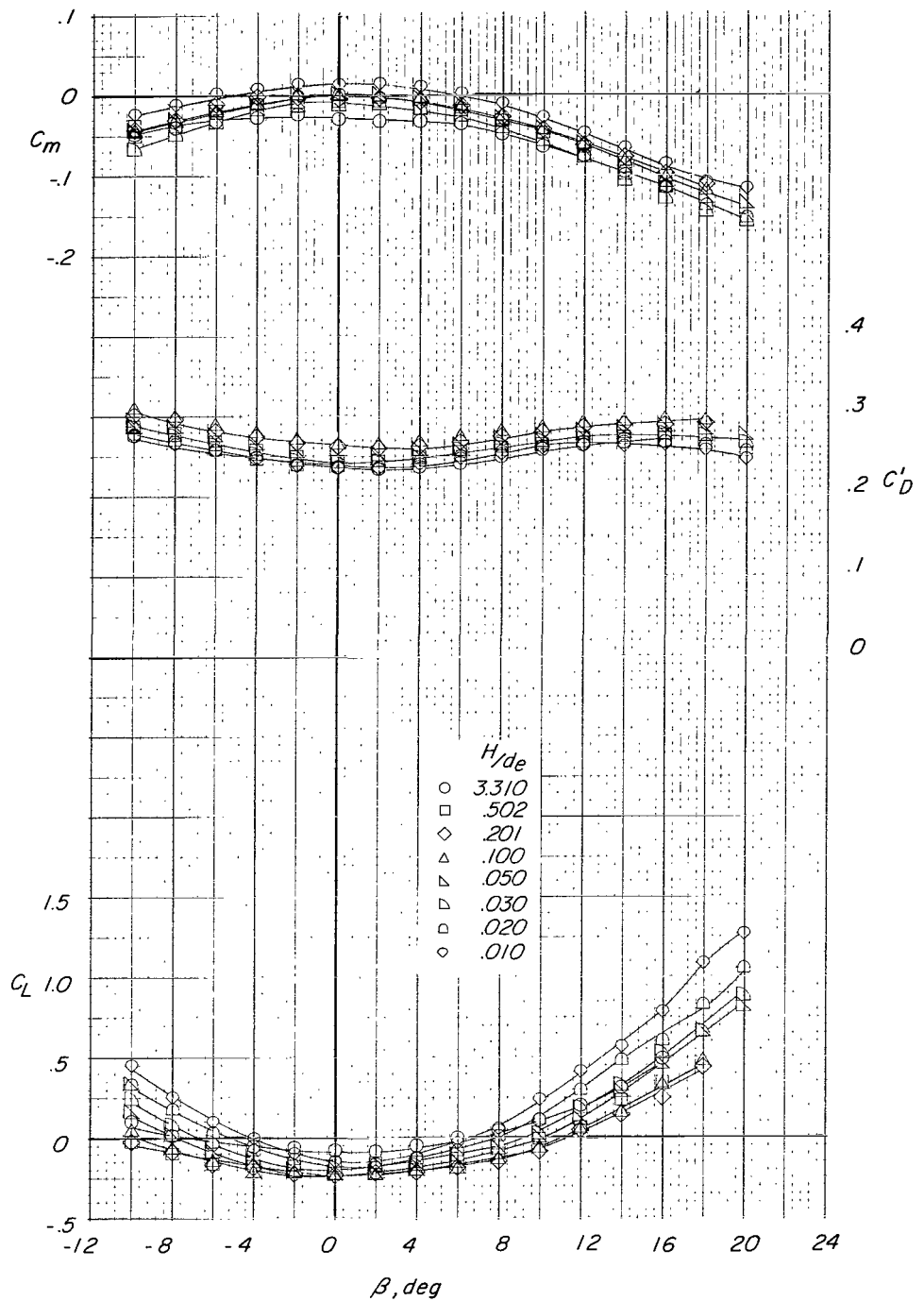
Figure 34.- Continued.



(c) Rolling-moment, yawing-moment, and side-force coefficients.

Figure 34.- Concluded.

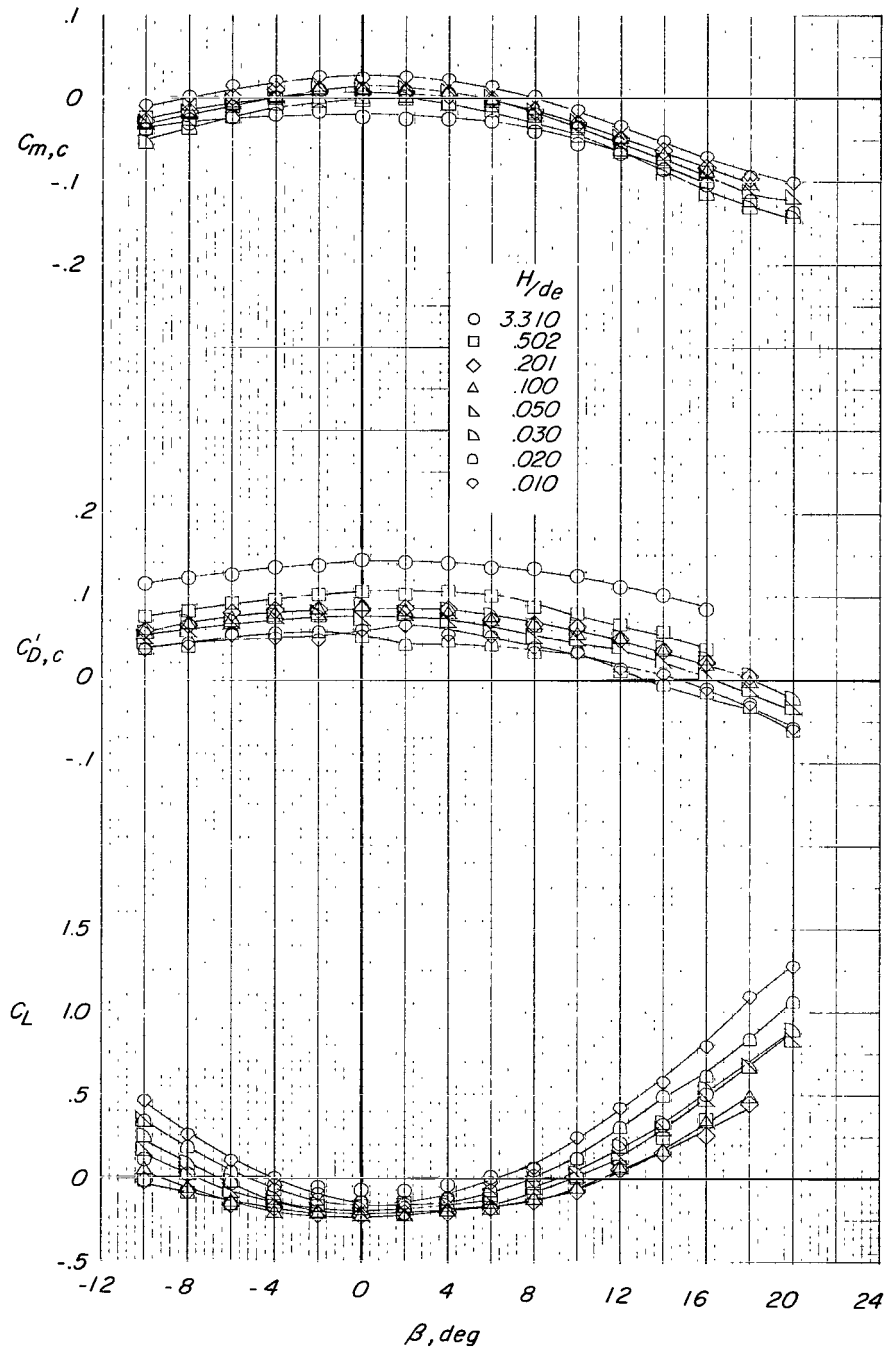
Half-circle (short extended sides) cross-section configuration
Ground belt moving



(a) Lift, drag, and pitching-moment coefficients.

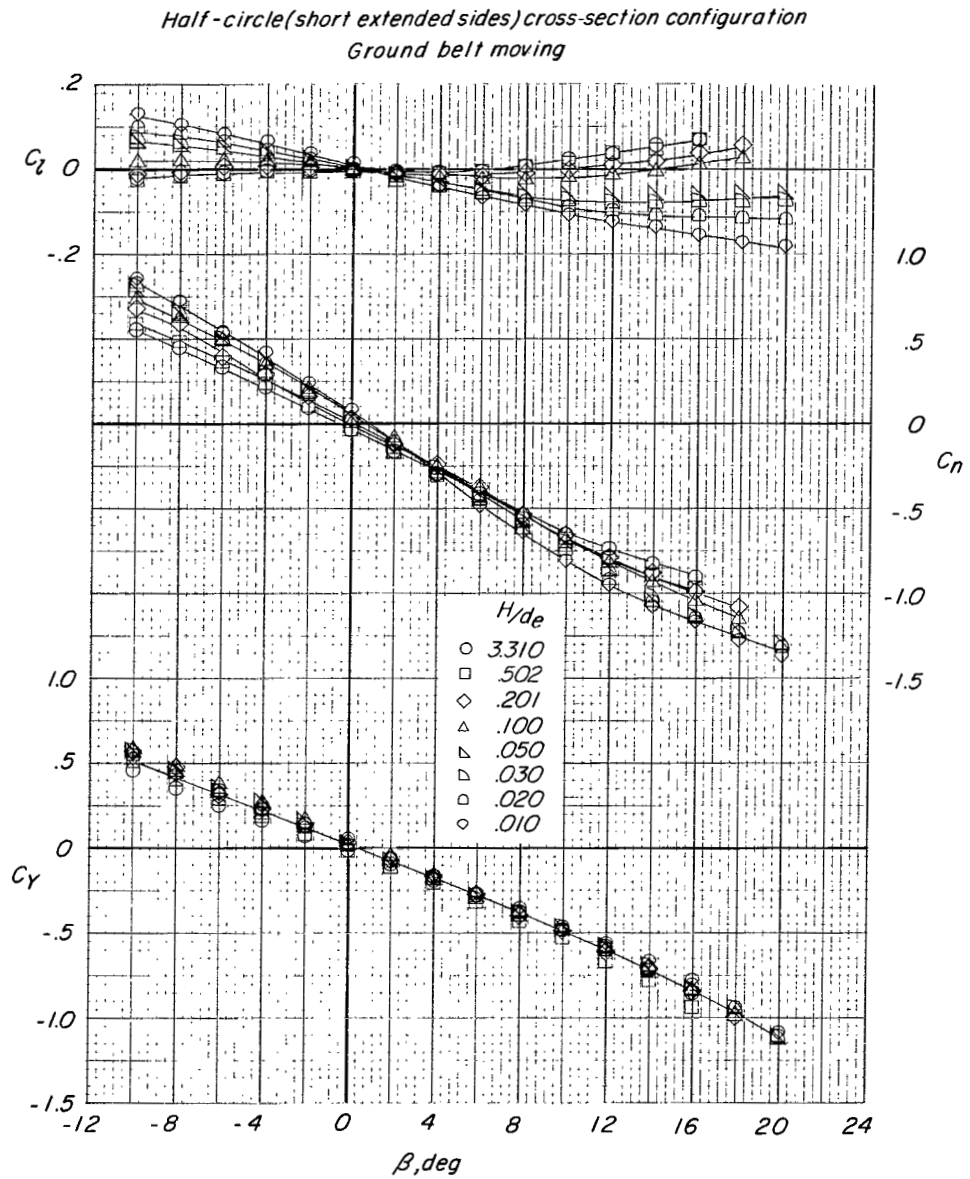
Figure 35.- Effect of ground height on the aerodynamic characteristics of half-circle (short extended sides) configuration.
Ground belt moving; $\alpha = 0^\circ$.

Half-circle (short extended sides) cross-section configuration
Ground belt moving



(b) Lift, drag, and pitching-moment coefficients with base pressure corrections.

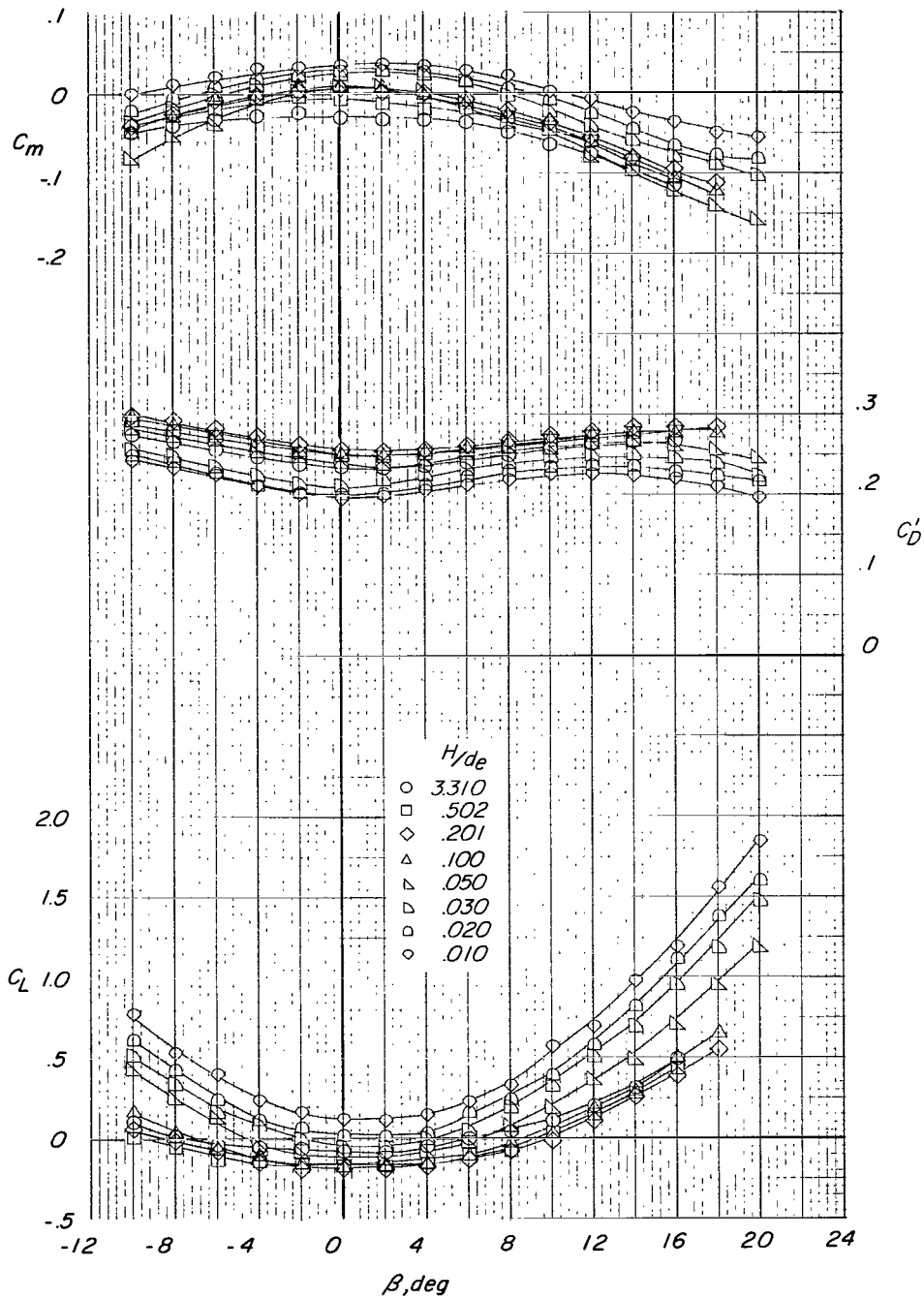
Figure 35.- Continued.



(c) Rolling-moment, yawing-moment, and side-force coefficients.

Figure 35.- Concluded.

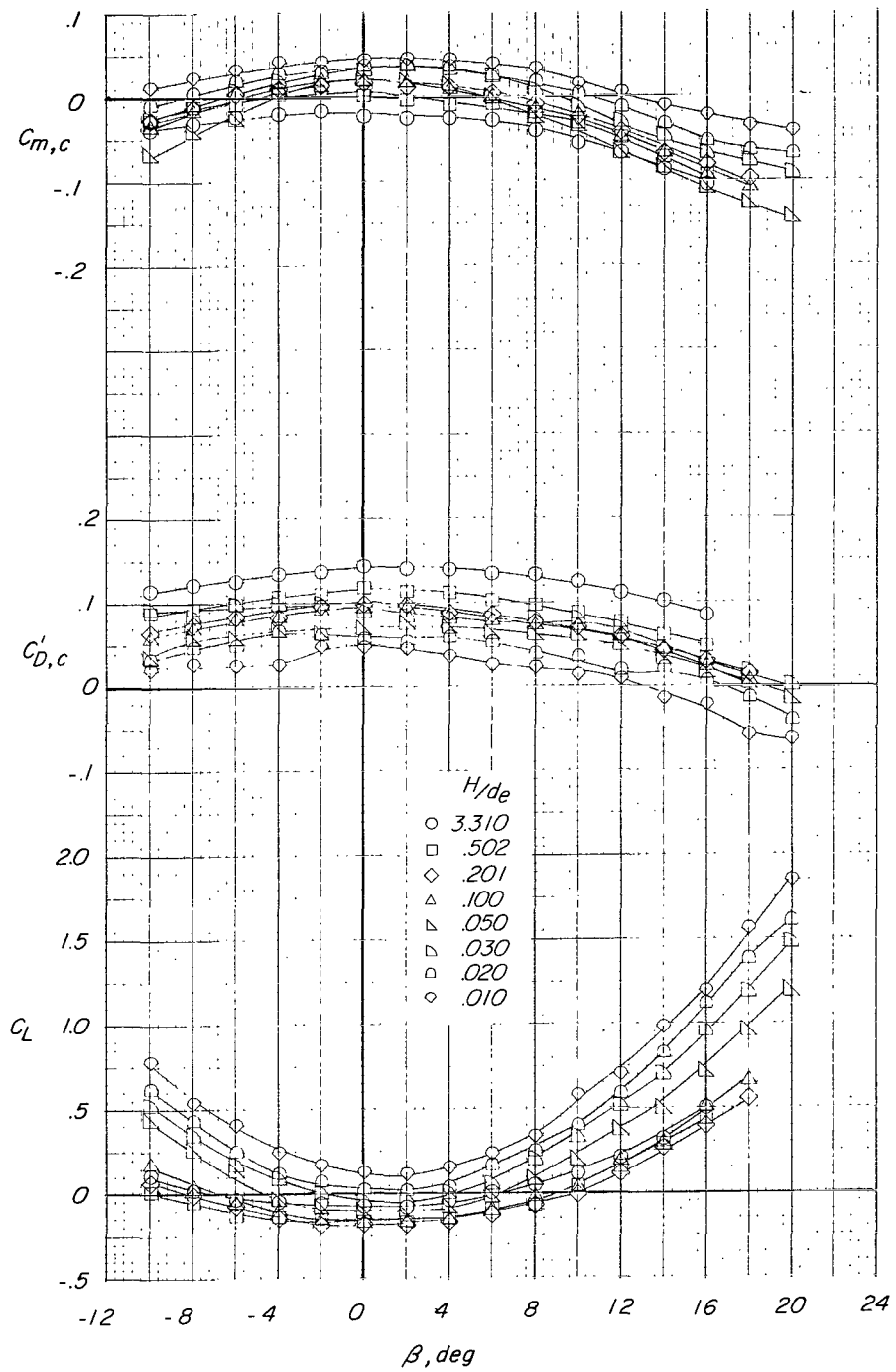
Half-circle (short extended sides) cross-section configuration
Ground belt stopped



(a) Lift, drag, and pitching-moment coefficients.

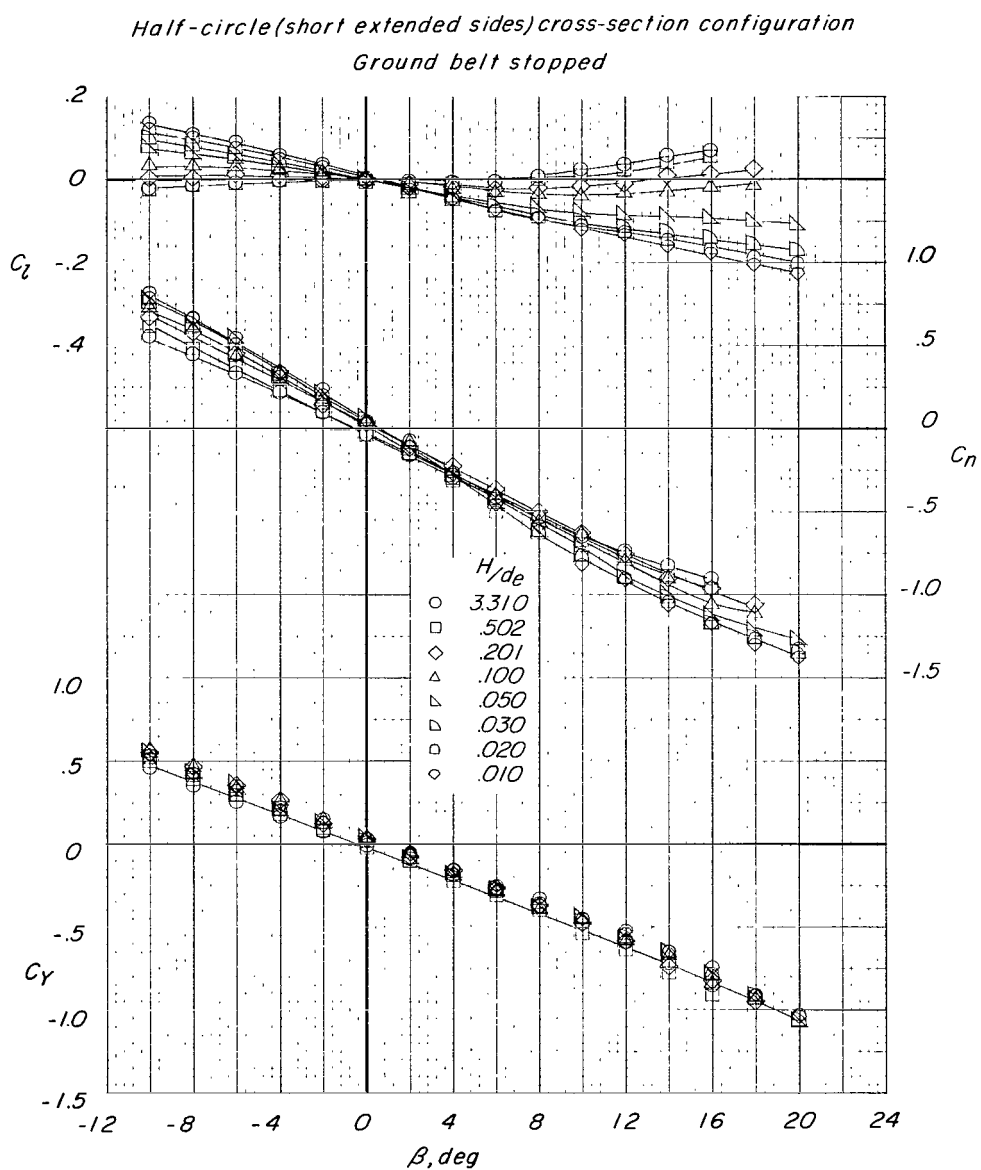
Figure 36.- Effect of ground height on the aerodynamic characteristics of half-circle (short extended sides) configuration.
Ground belt stopped; $\alpha = 0^\circ$.

Half-circle(short extended sides)cross-section configuration
Ground belt stopped



(b) Lift, drag, and pitching-moment coefficients with base pressure corrections.

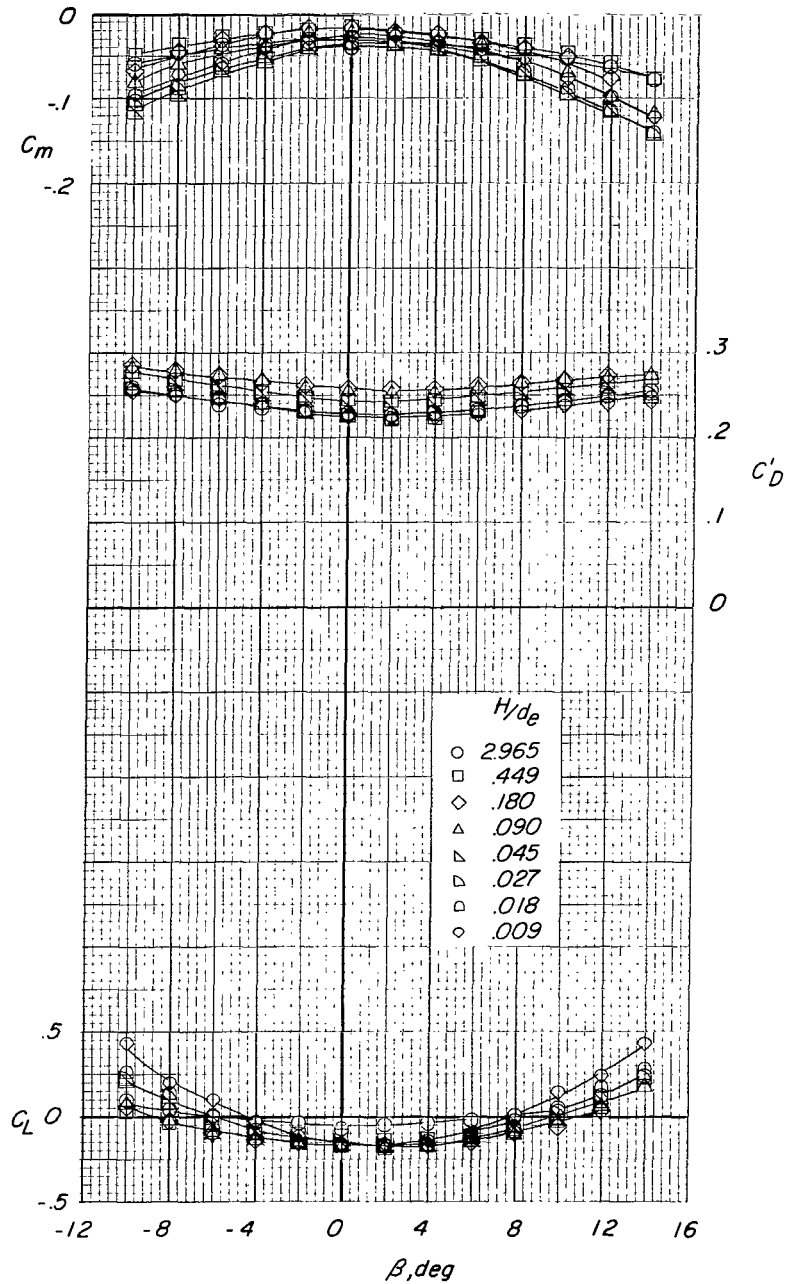
Figure 36.- Continued.



(c) Rolling-moment, yawing-moment, and side-force coefficients.

Figure 36.- Concluded.

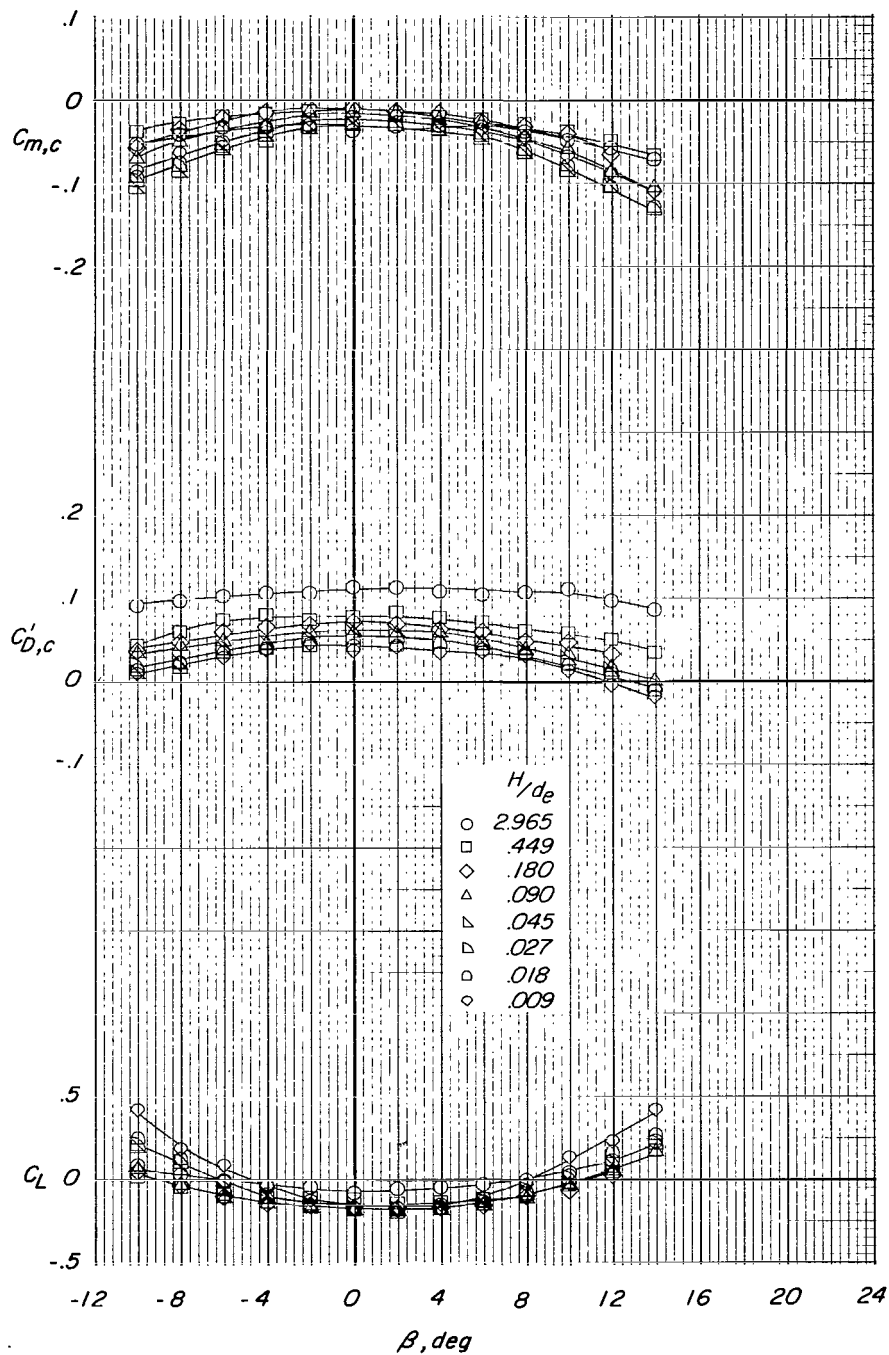
Half-circle (long extended sides) cross-section configuration
Ground belt moving



(a) Lift, drag, and pitching-moment coefficients.

Figure 37.- Effect of ground height on the aerodynamic characteristics of half-circle (long extended sides) configuration.
Ground belt moving; $\alpha = 0^\circ$.

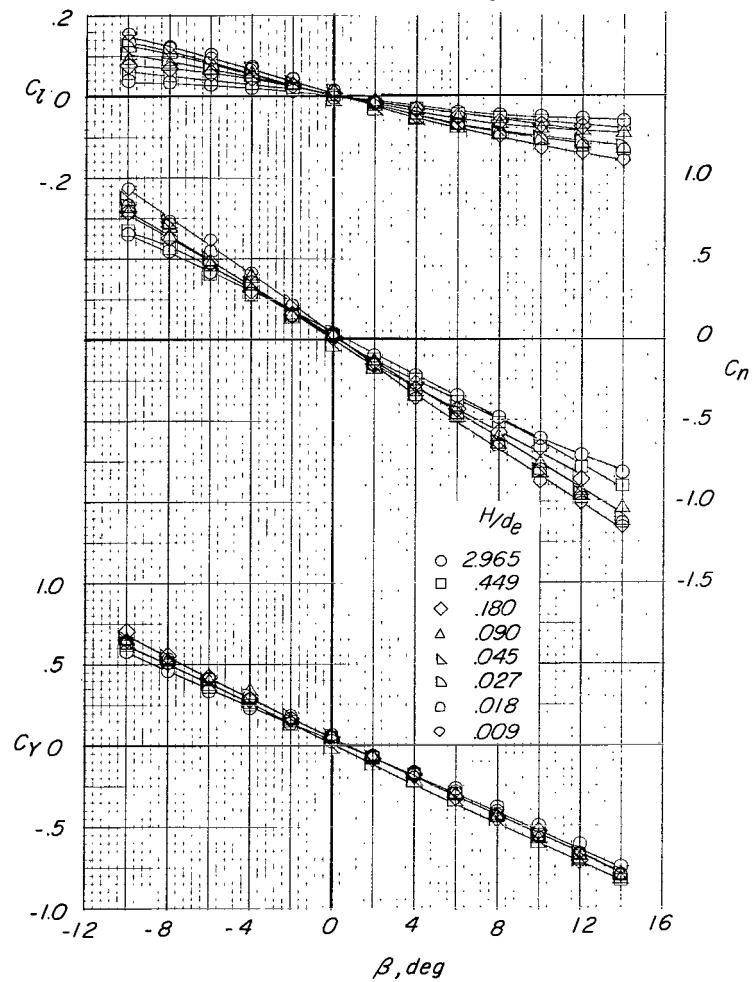
Half-circle (long extended sides) cross-section configuration
Ground belt moving



(b) Lift, drag, and pitching-moment coefficients with base pressure corrections.

Figure 37.- Continued.

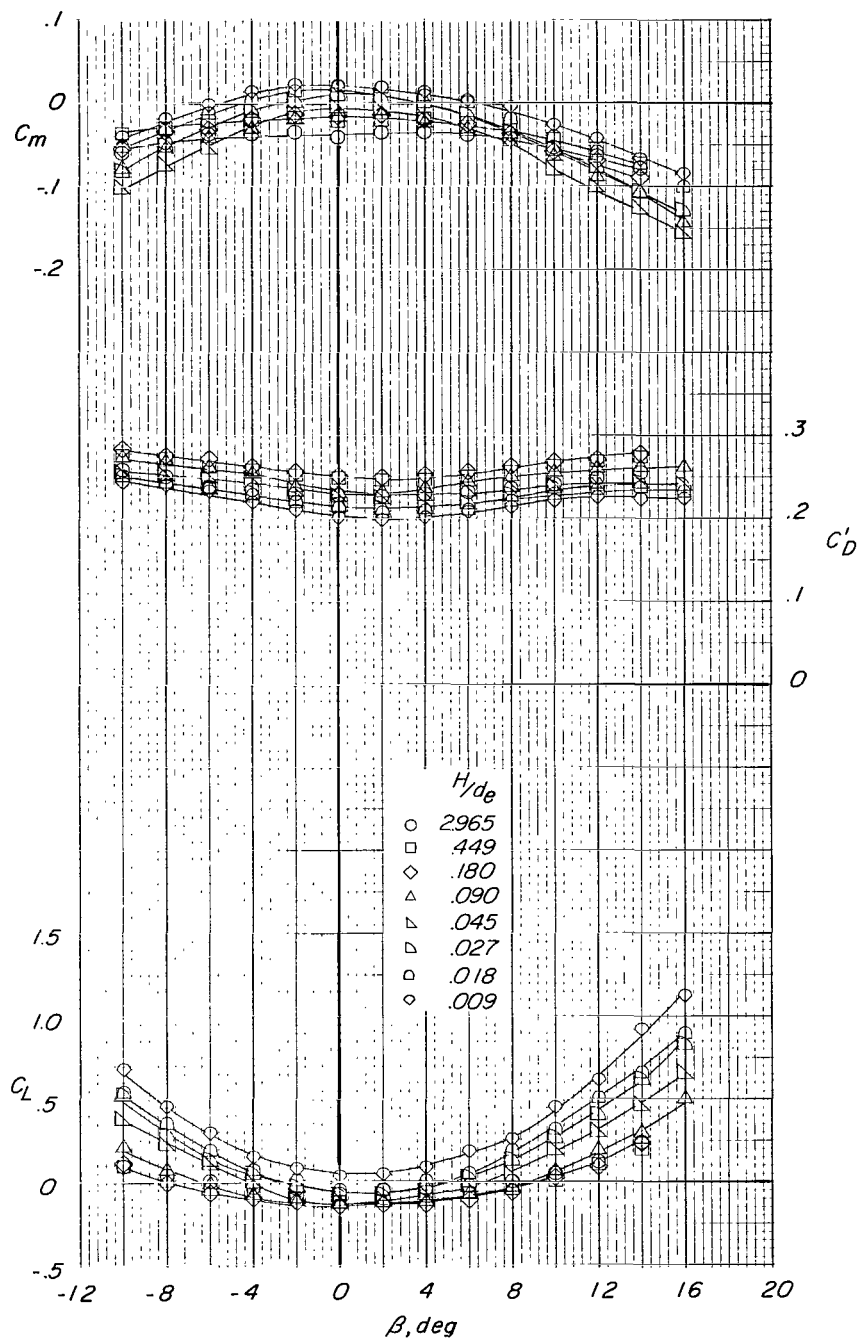
Half-circle (long extended sides) cross-section configuration
Ground belt moving



(c) Rolling-moment, yawing-moment, and side-force coefficients.

Figure 37.- Concluded.

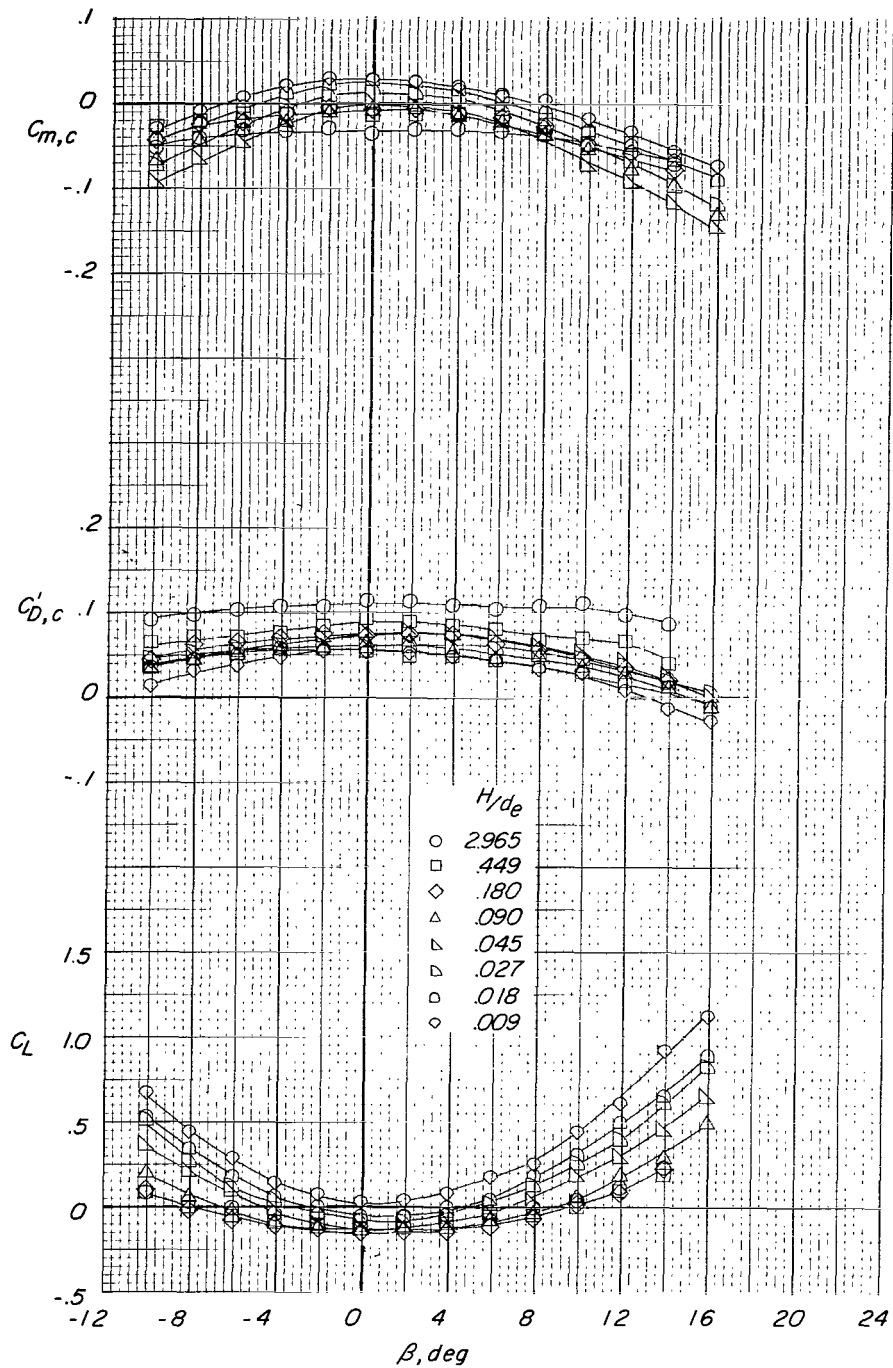
Half-circle (long extended sides) cross-section configuration
Ground belt stopped



(a) Lift, drag, and pitching-moment coefficients.

Figure 38.- Effect of ground height on the aerodynamic characteristics of half-circle (long extended sides) configuration.
Ground belt stopped; $\alpha = 0^\circ$.

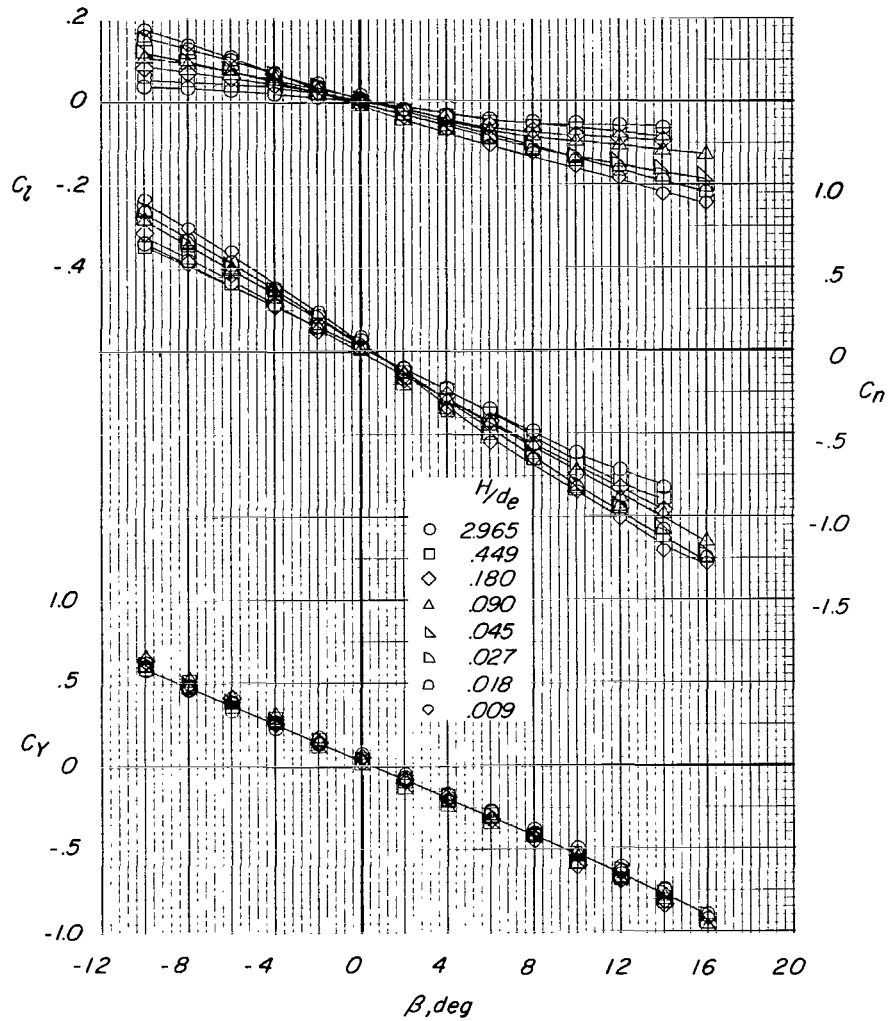
Half-circle (long extended sides) cross-section configuration
Ground belt stopped



(b) Lift, drag, and pitching-moment coefficients with base pressure corrections.

Figure 38.- Continued.

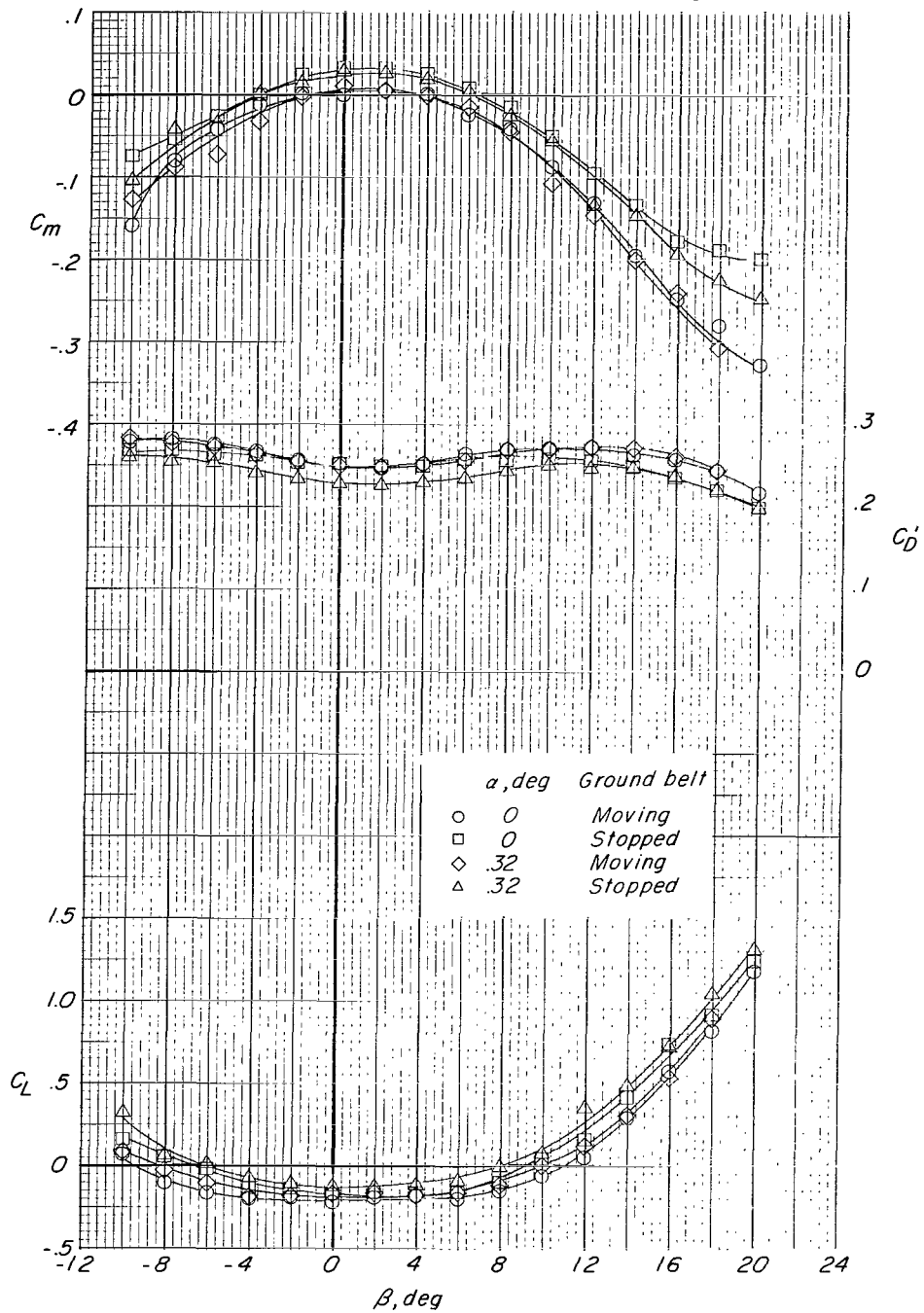
Half-circle (long extended sides) cross-section configuration
Ground belt stopped



(c) Rolling-moment, yawing-moment, and side-force coefficients.

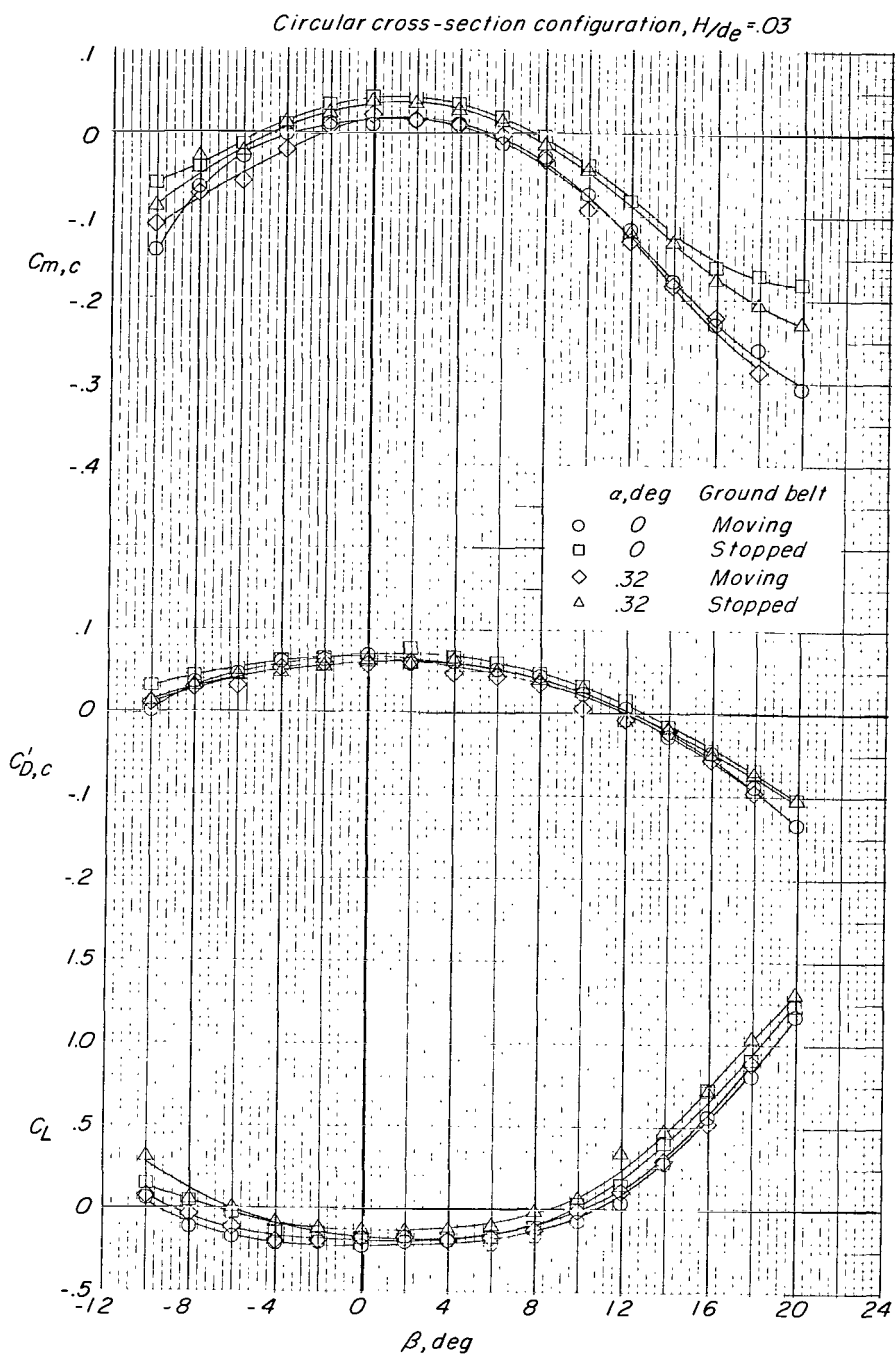
Figure 38.- Concluded.

Circular cross-section configuration, $H/d_e = .03$



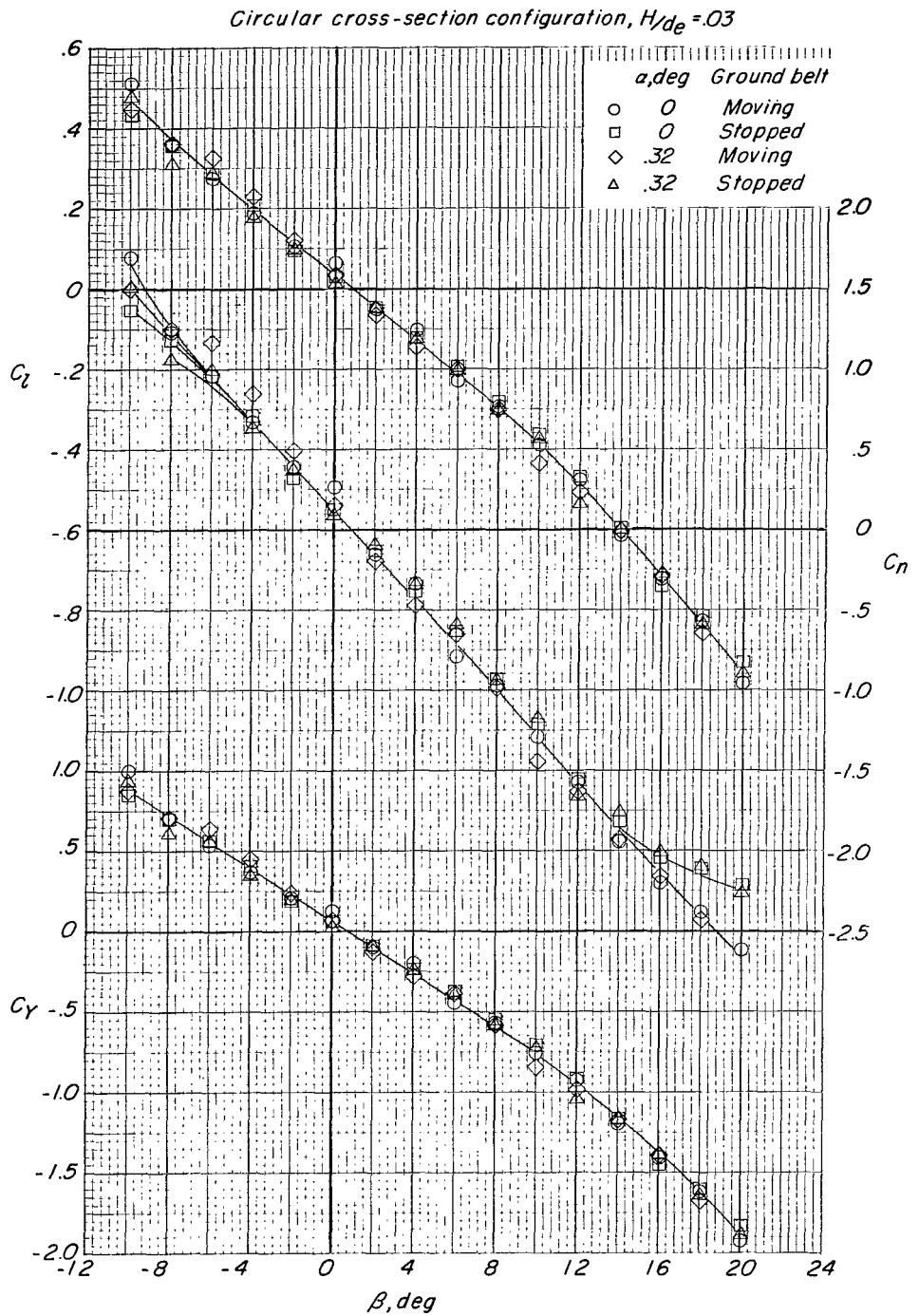
(a) Lift, drag, and pitching-moment coefficients.

Figure 39.- Effect of angle of attack α on the aerodynamic characteristics of circular configuration.



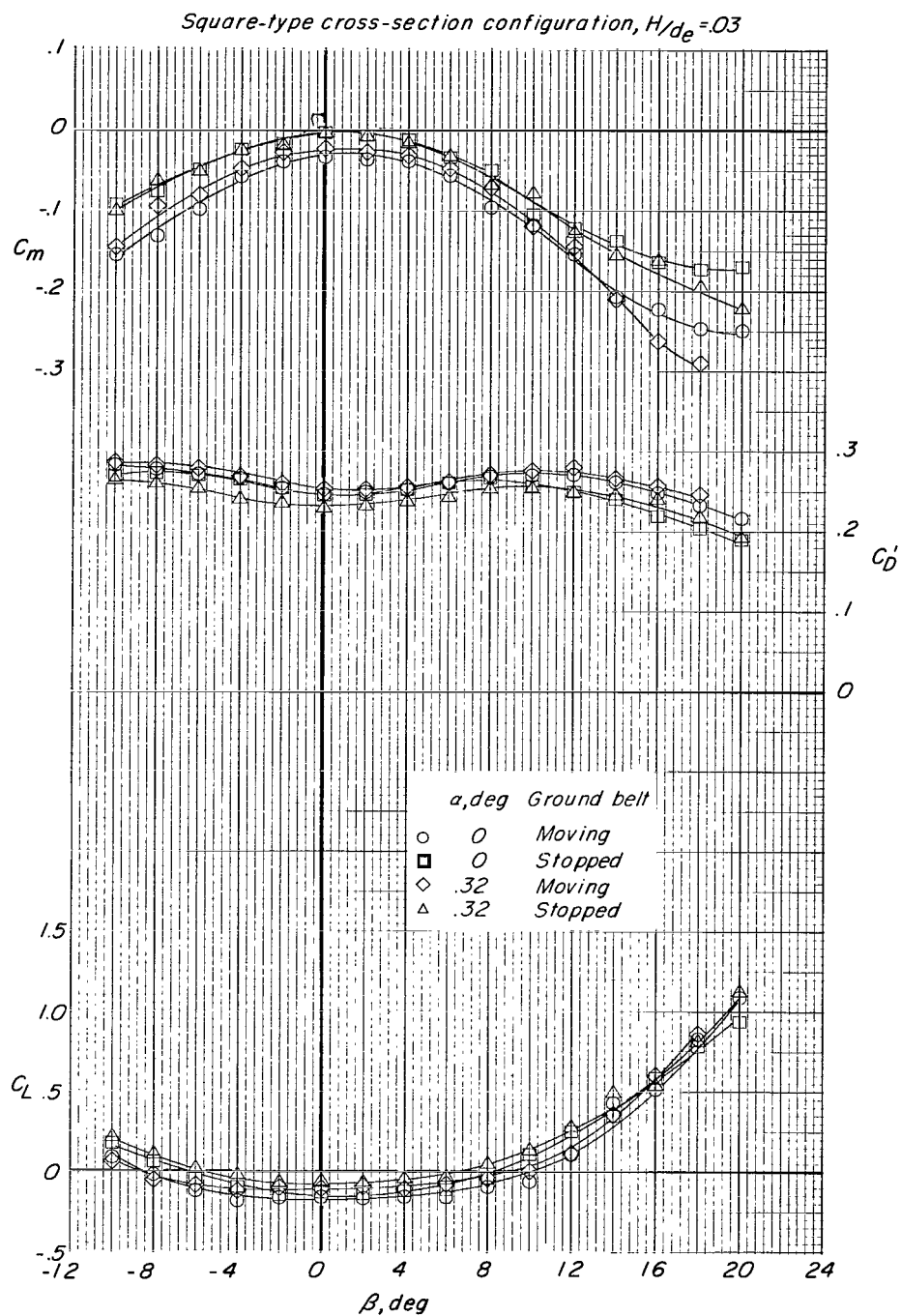
(b) Lift, drag, and pitching-moment coefficients with base pressure corrections.

Figure 39.- Continued.



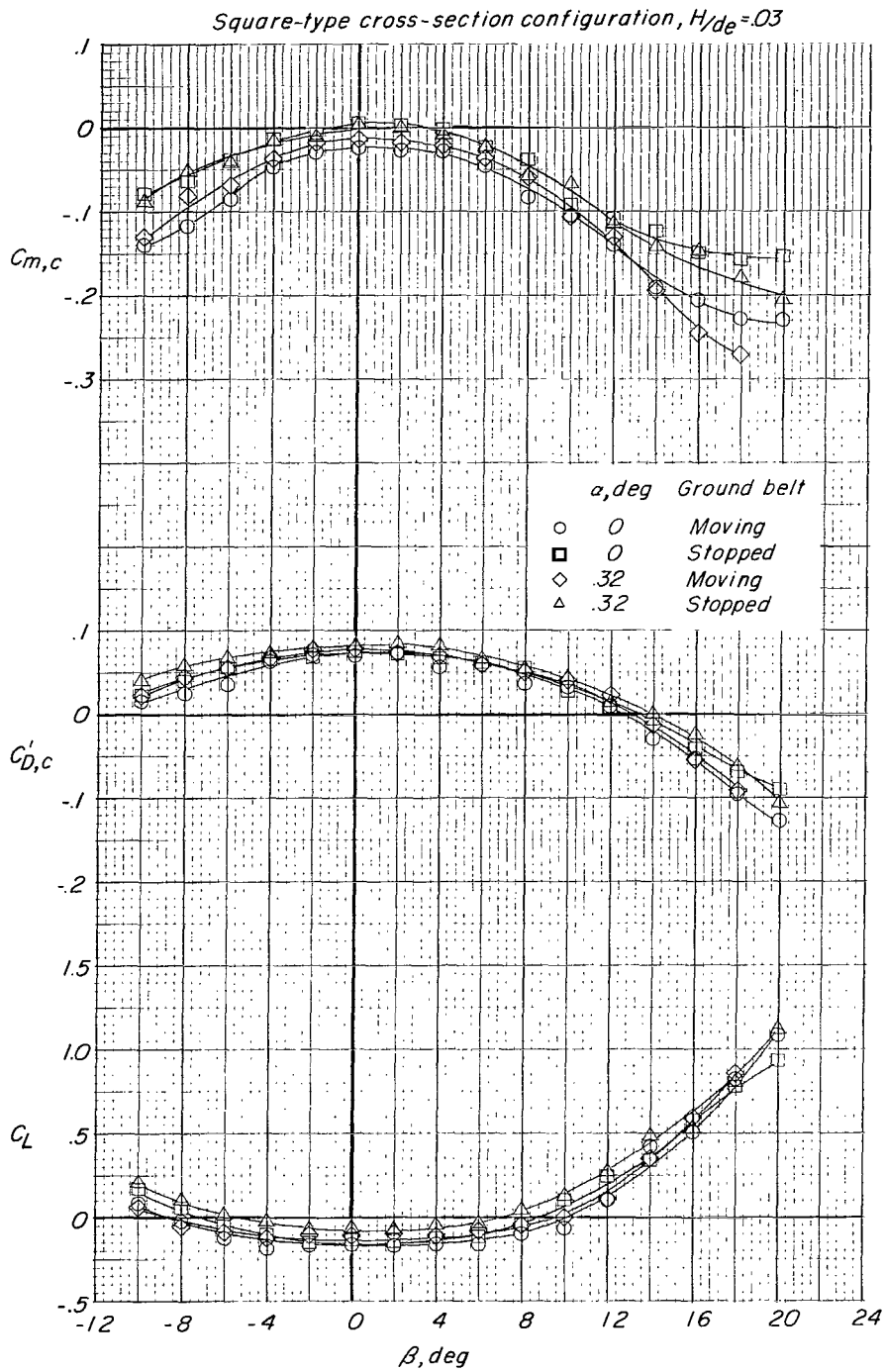
(c) Rolling-moment, yawing-moment, and side-force coefficients.

Figure 39.- Concluded.



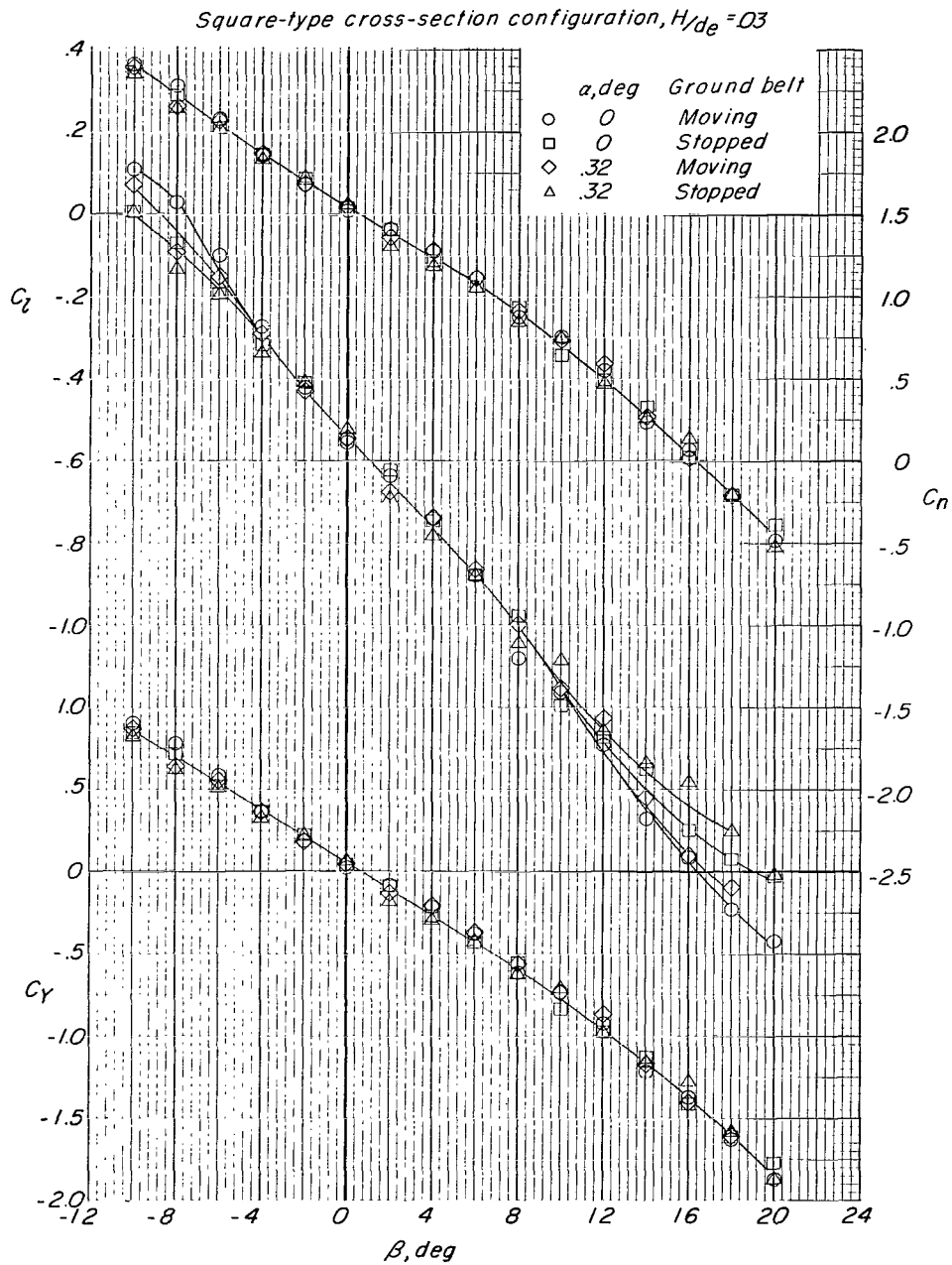
(a) Lift, drag, and pitching-moment coefficients.

Figure 40.- Effect of angle of attack α on the aerodynamic characteristics of square-type configurations.



(b) Lift, drag, and pitching-moment coefficients with base pressure corrections.

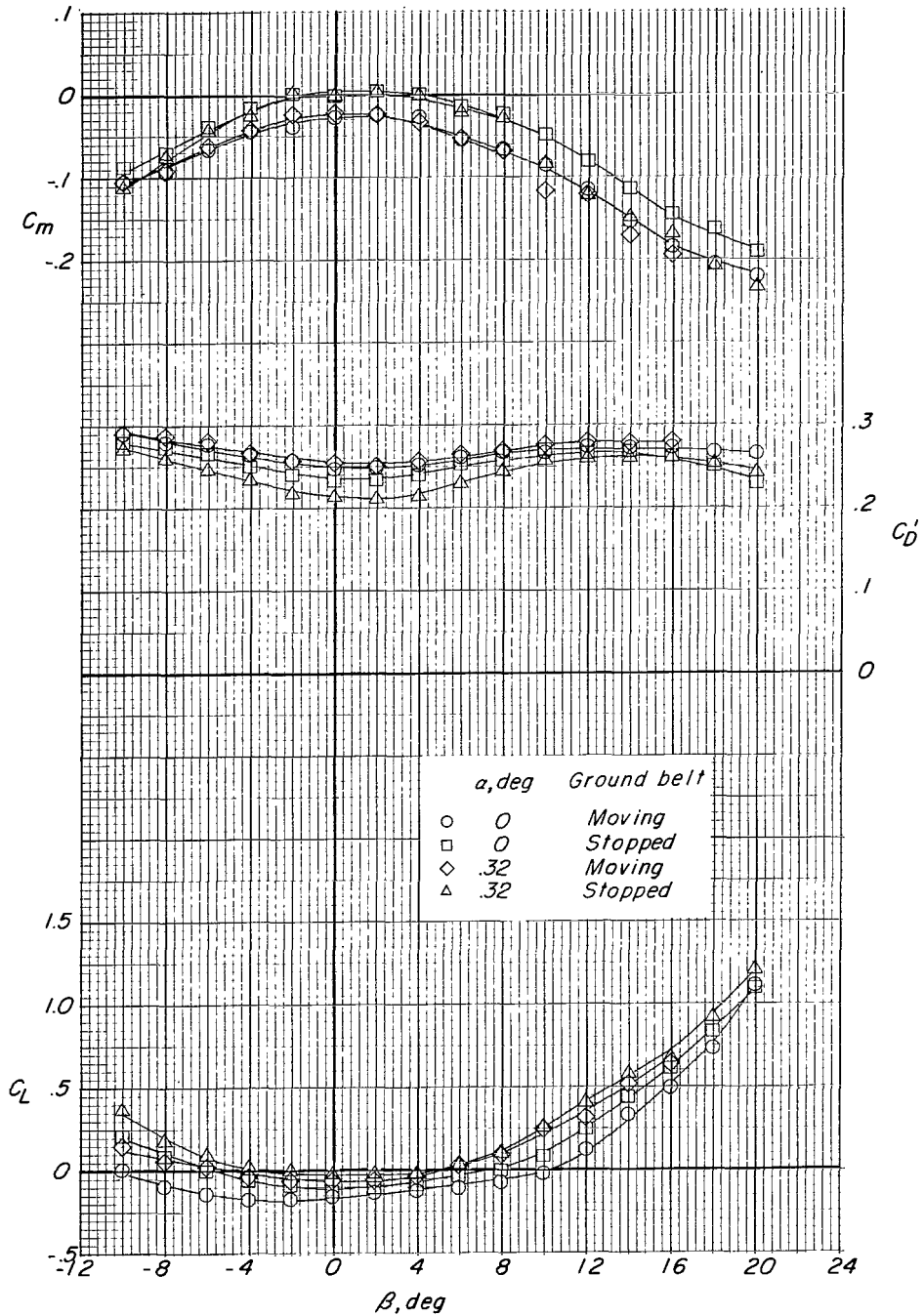
Figure 40.- Continued.



(c) Rolling-moment, yawing-moment, and side-force coefficients.

Figure 40.- Concluded.

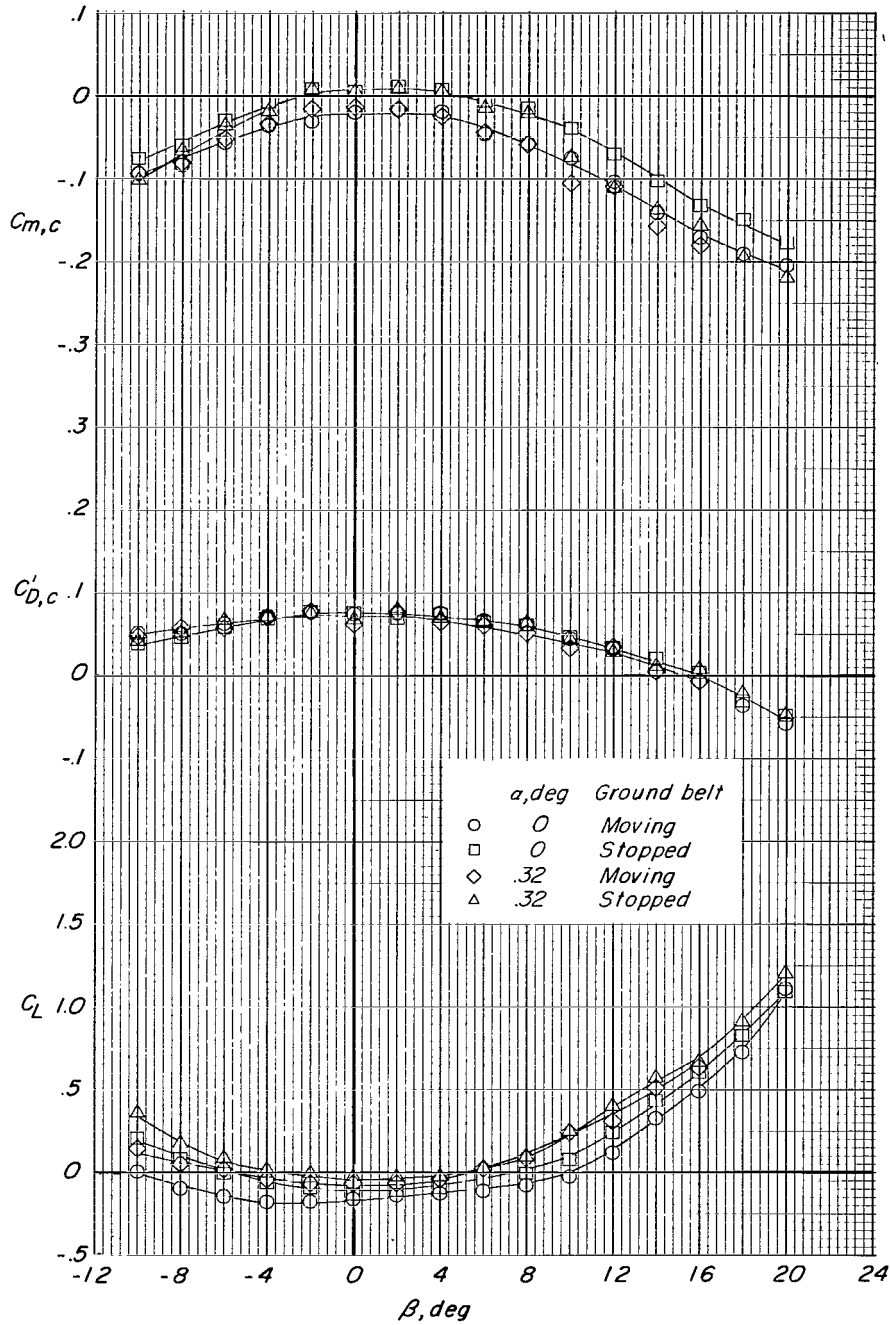
Triangular-type cross-section configuration, $H/d_e = .03$



(a) Lift, drag, and pitching-moment coefficients.

Figure 41.- Effect of angle of attack α on the aerodynamic characteristics of triangular-type configuration.

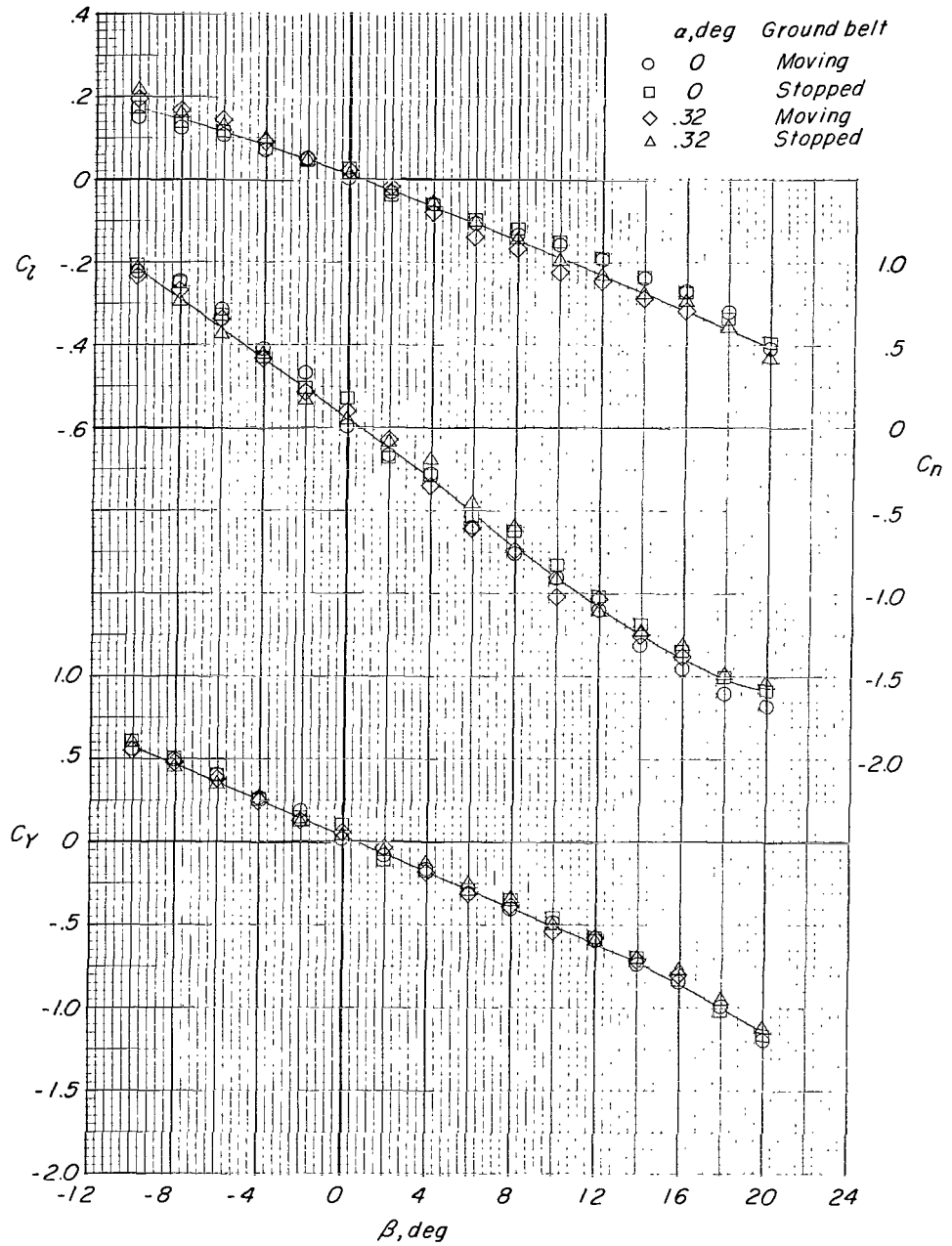
Triangular-type cross-section configuration, $H/d_e = .03$



(b) Lift, drag, and pitching-moment coefficients with base pressure corrections.

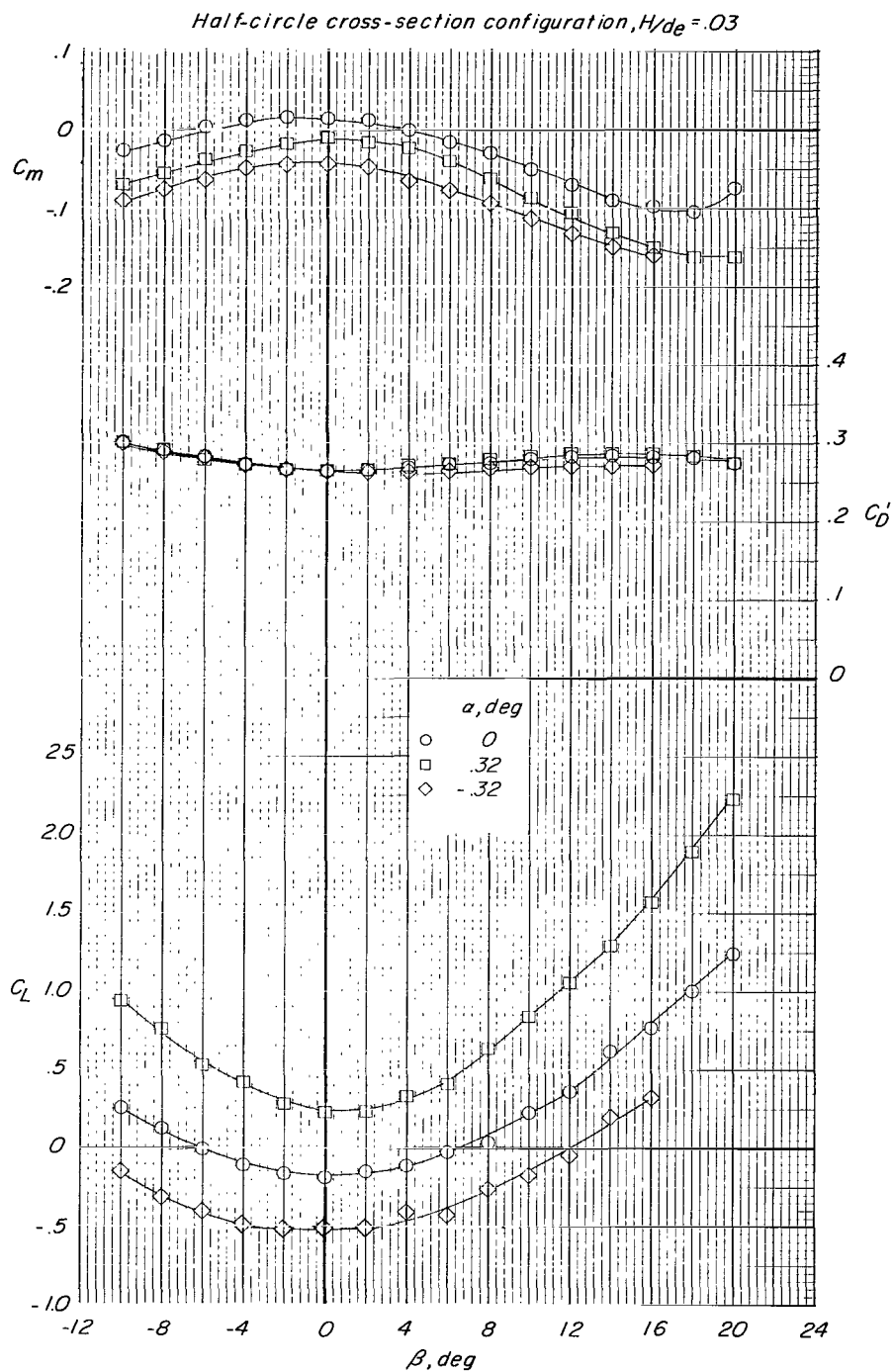
Figure 41.- Continued.

Triangular-type cross-section configuration, $H/d_e = 0.3$



(c) Rolling-moment, yawing-moment, and side-force coefficients.

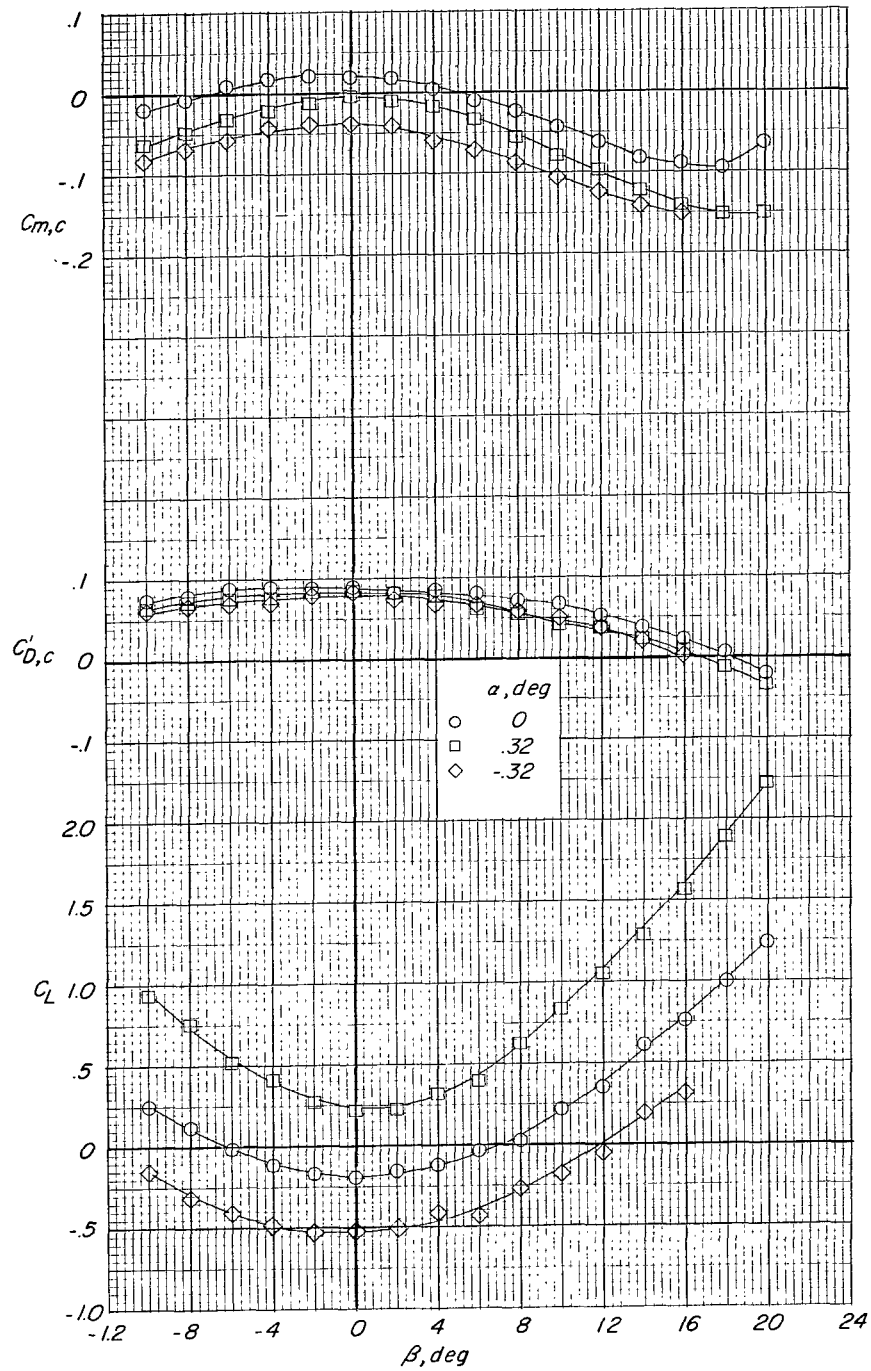
Figure 41.- Concluded.



(a) Lift, drag, and pitching-moment coefficients.

Figure 42.- Effect of angle of attack α on the aerodynamic characteristics of half-circle configuration. Ground belt moving.

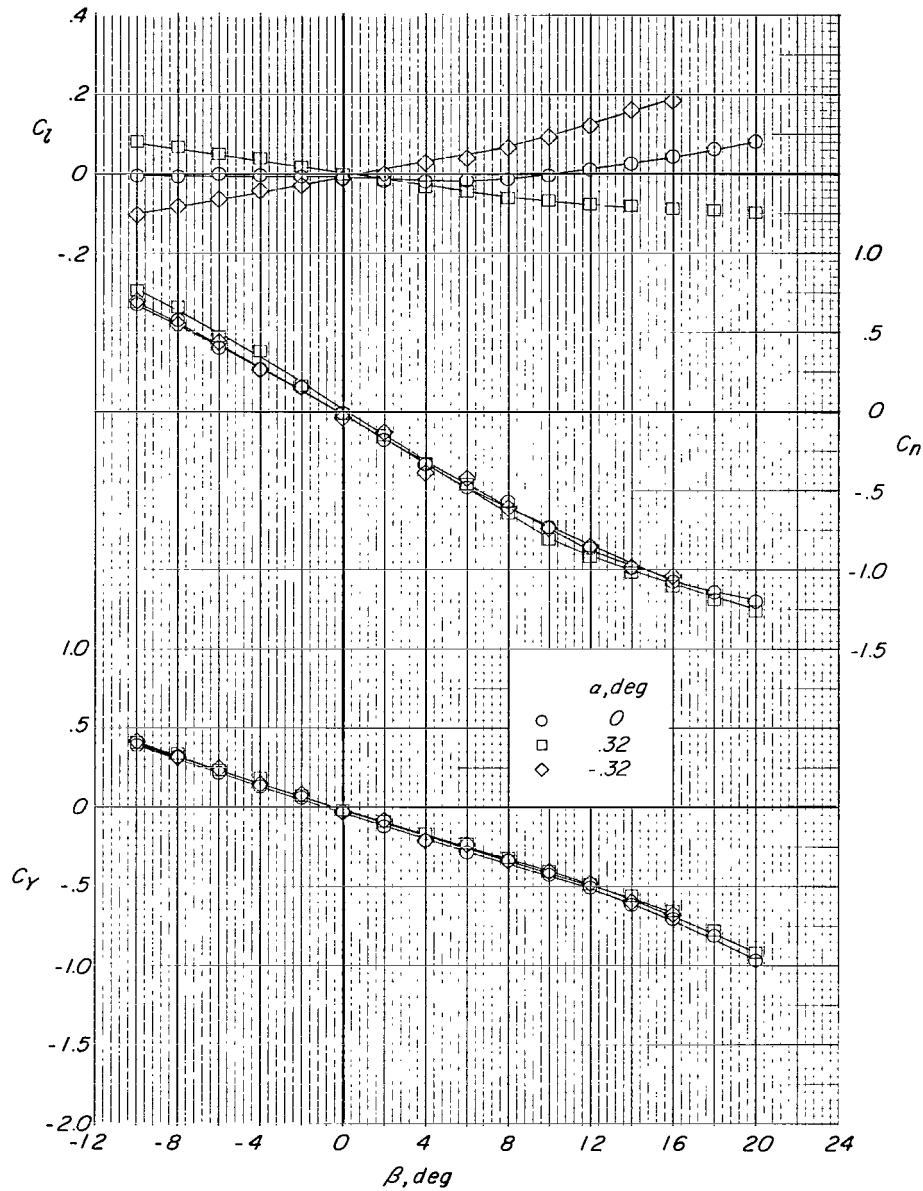
Half-circle cross-section configuration, $H/d_e = .03$



(b) Lift, drag, and pitching-moment coefficients with base pressure corrections.

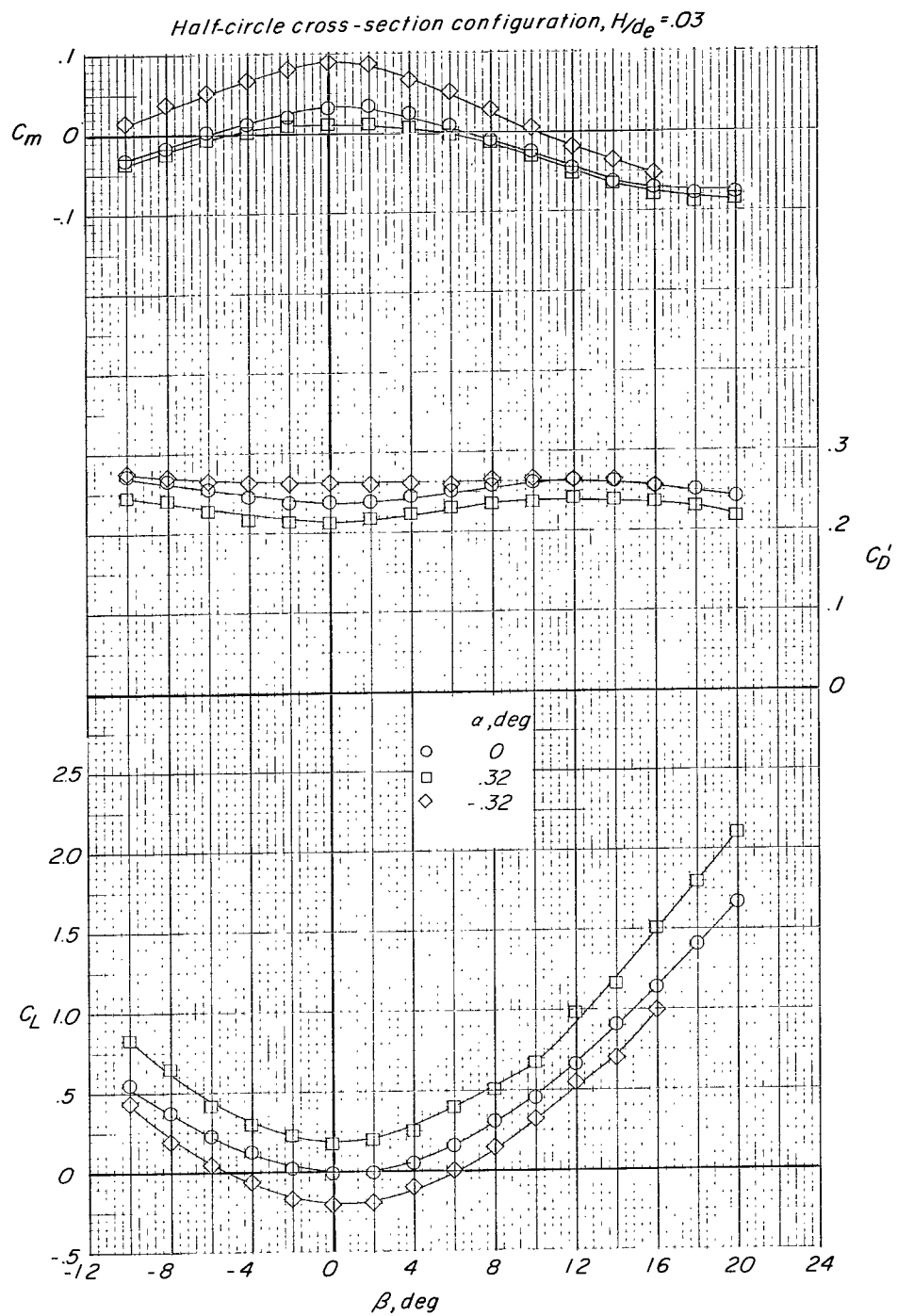
Figure 42.- Continued.

Half-circle cross-section configuration, $H/d_e = .03$



(c) Rolling-moment, yawing-moment, and side-force coefficients.

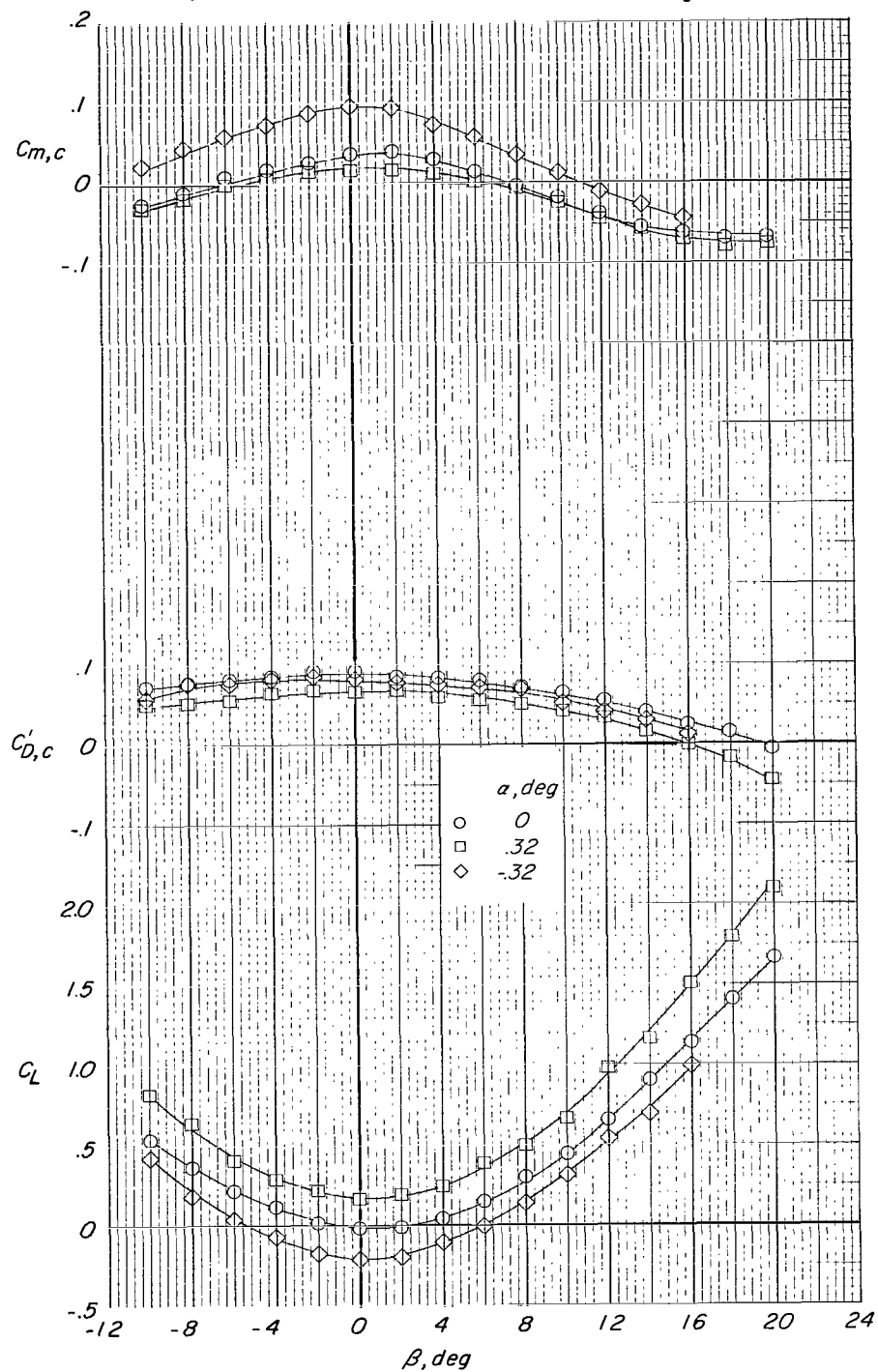
Figure 42.- Concluded.



(a) Lift, drag, and pitching-moment coefficients.

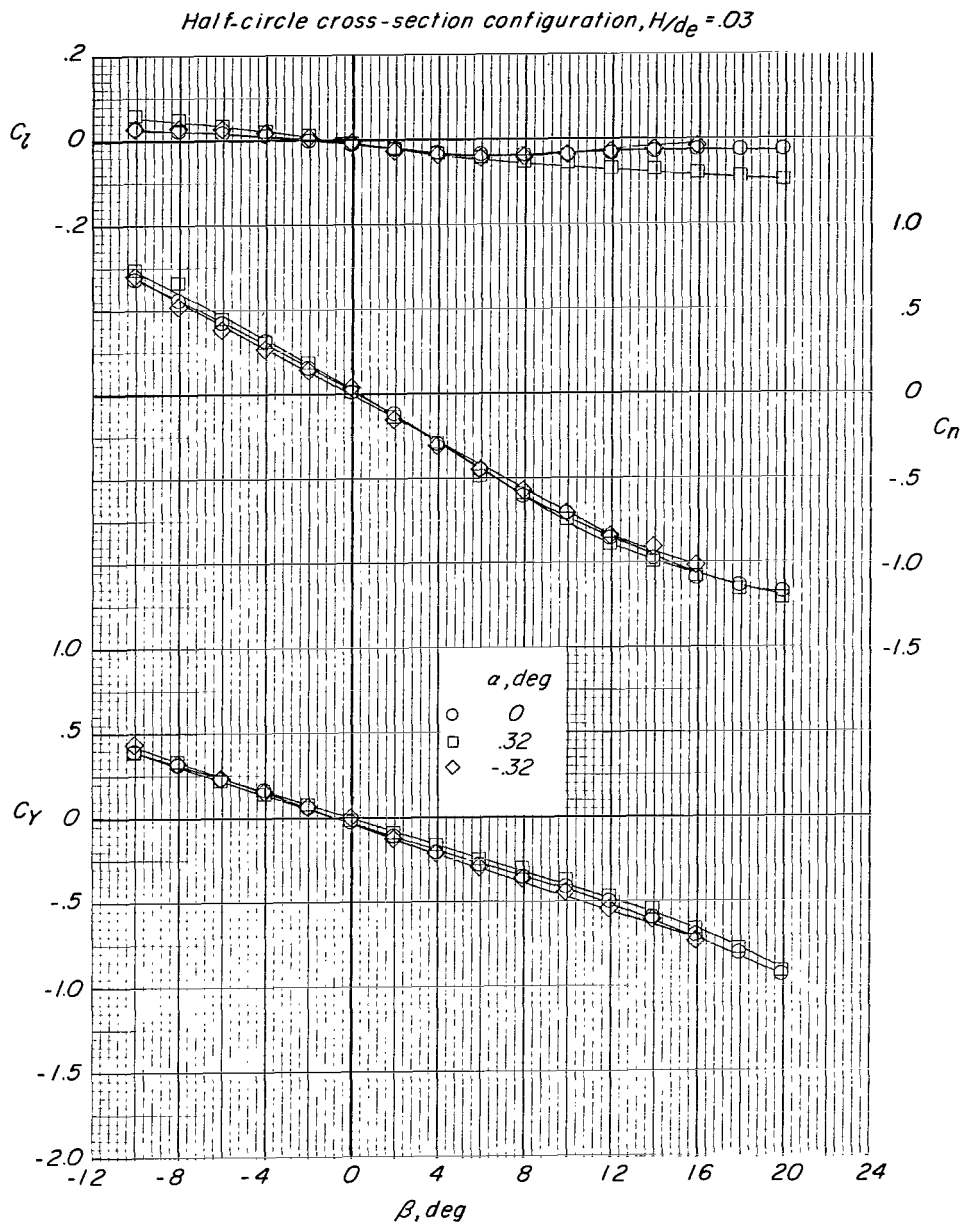
Figure 43.- Effect of angle of attack α on the aerodynamic characteristics of half-circle configuration. Ground belt stopped.

Half-circle cross-section configuration, $H/d_e = .03$



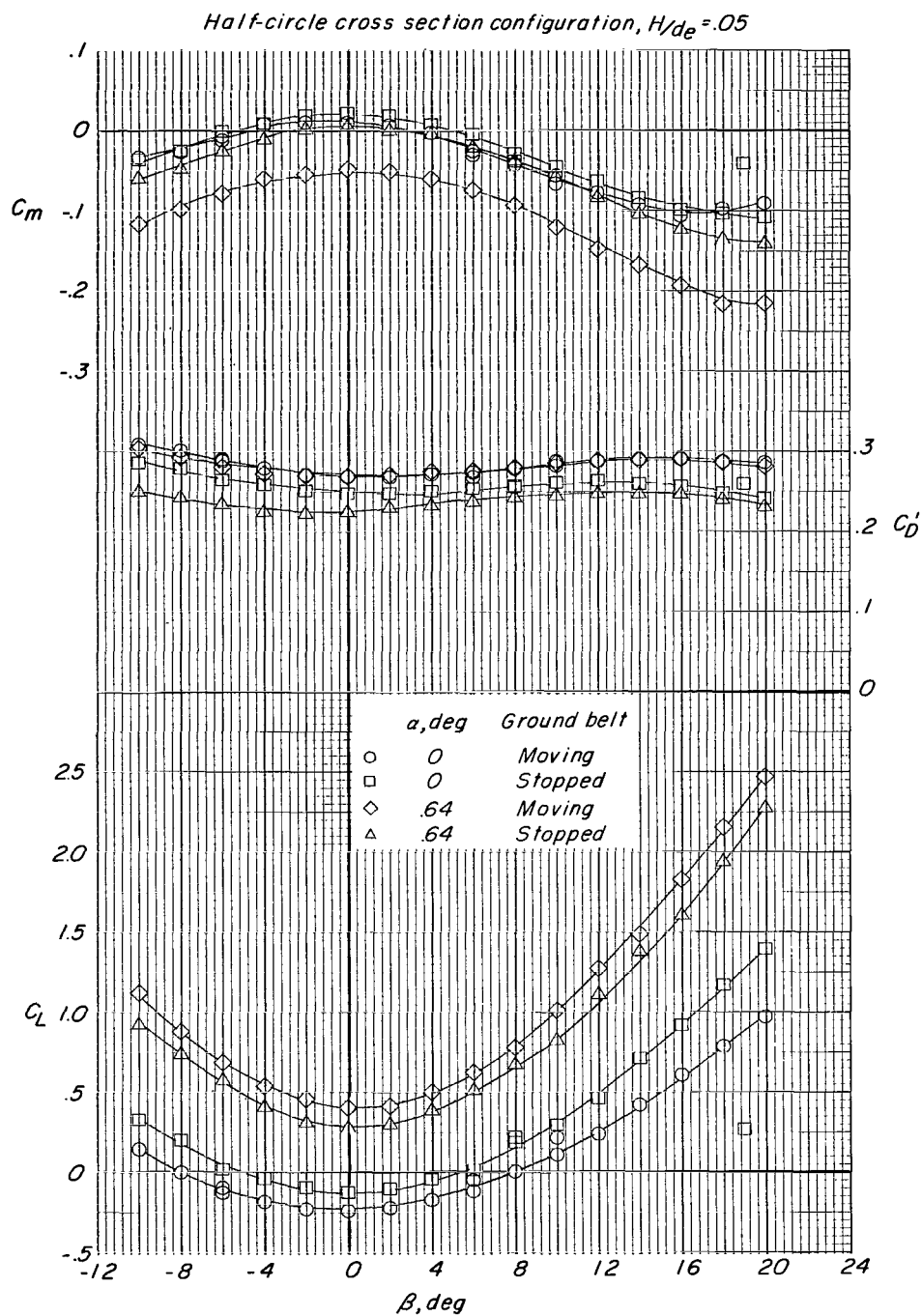
(b) Lift, drag, and pitching-moment coefficients with base pressure corrections.

Figure 43.- Continued.



(c) Rolling-moment, yawing-moment, and side-force coefficients.

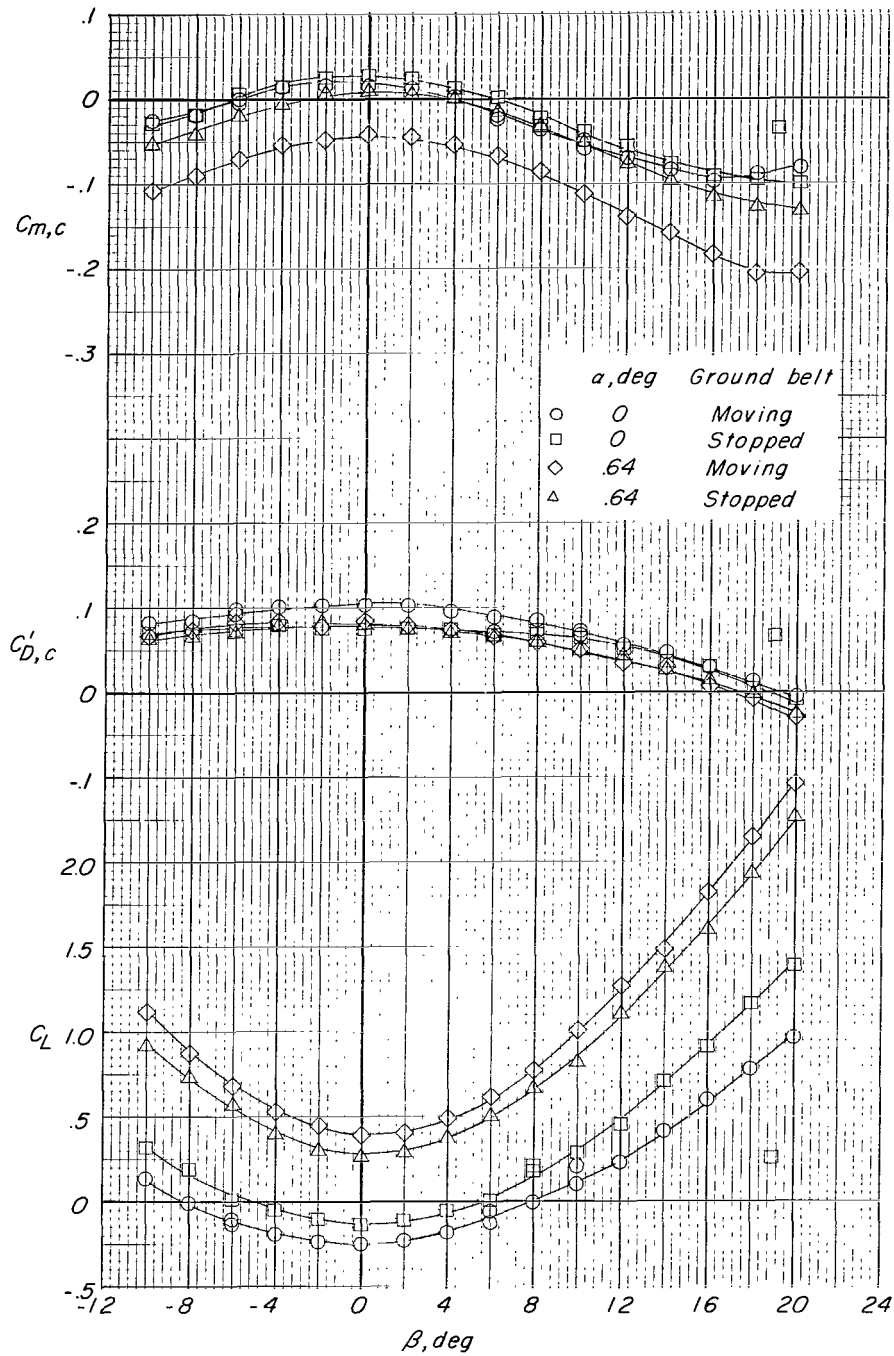
Figure 43.- Concluded.



(a) Lift, drag, and pitching-moment coefficients.

Figure 44.- Effect of angle of attack α on the aerodynamic characteristics of half-circle configuration.

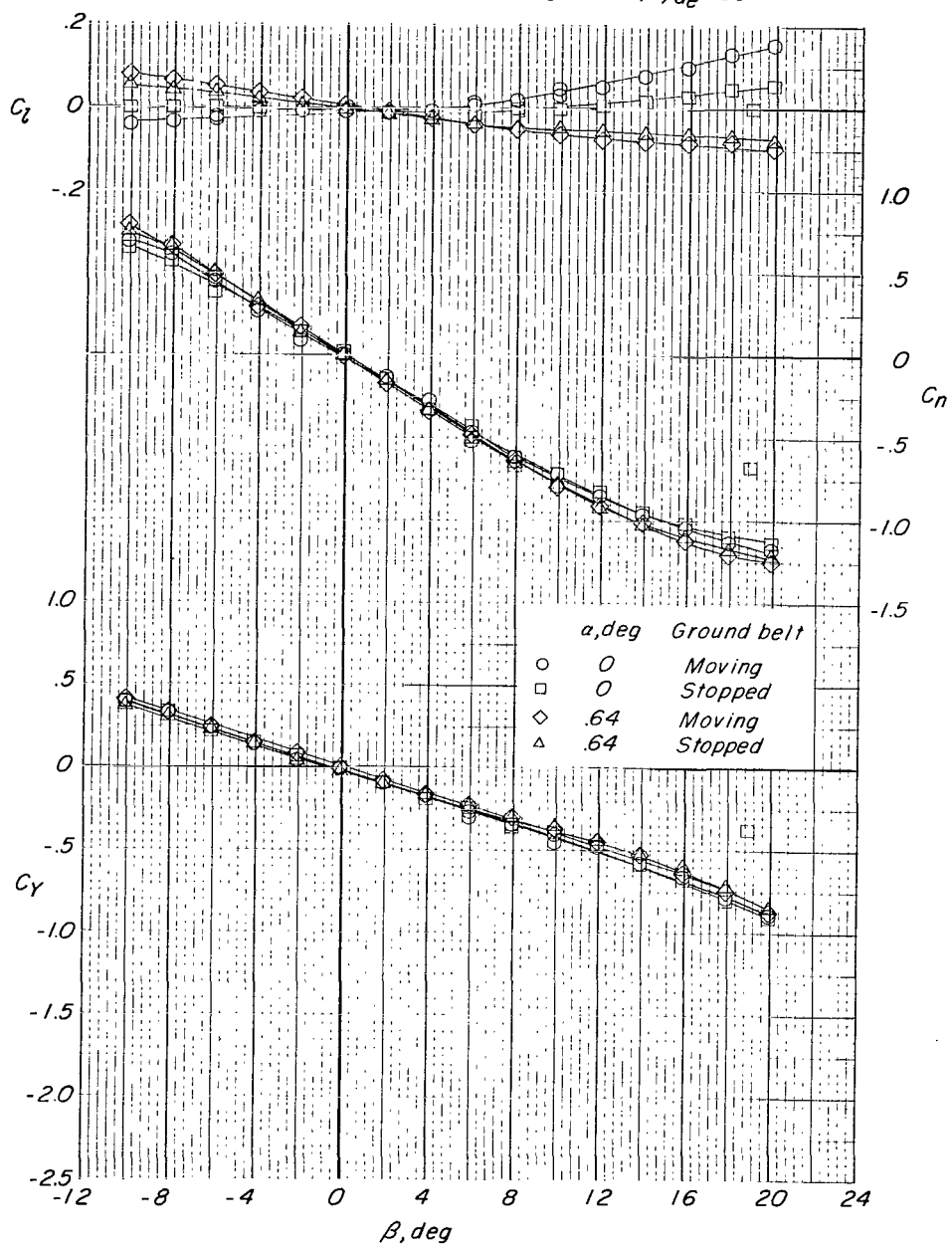
Half-circle cross-section configuration, $H/d_e = .05$



(b) Lift, drag, and pitching-moment coefficients with base pressure corrections.

Figure 44.- Continued.

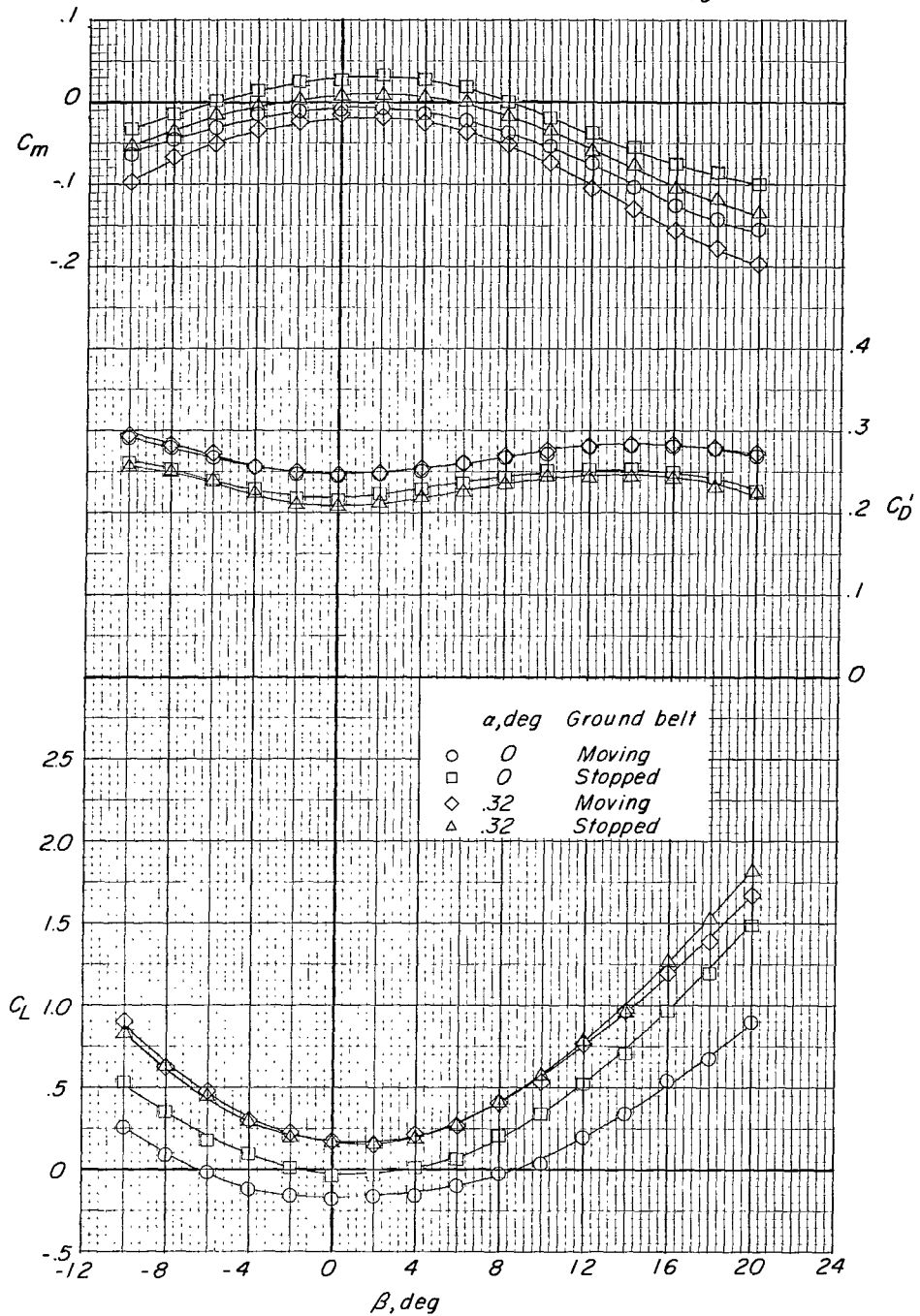
Half-circle cross-section configuration, $H/d_e = 0.05$



(c) Rolling-moment, yawing-moment, and side-force coefficients.

Figure 44.- Concluded.

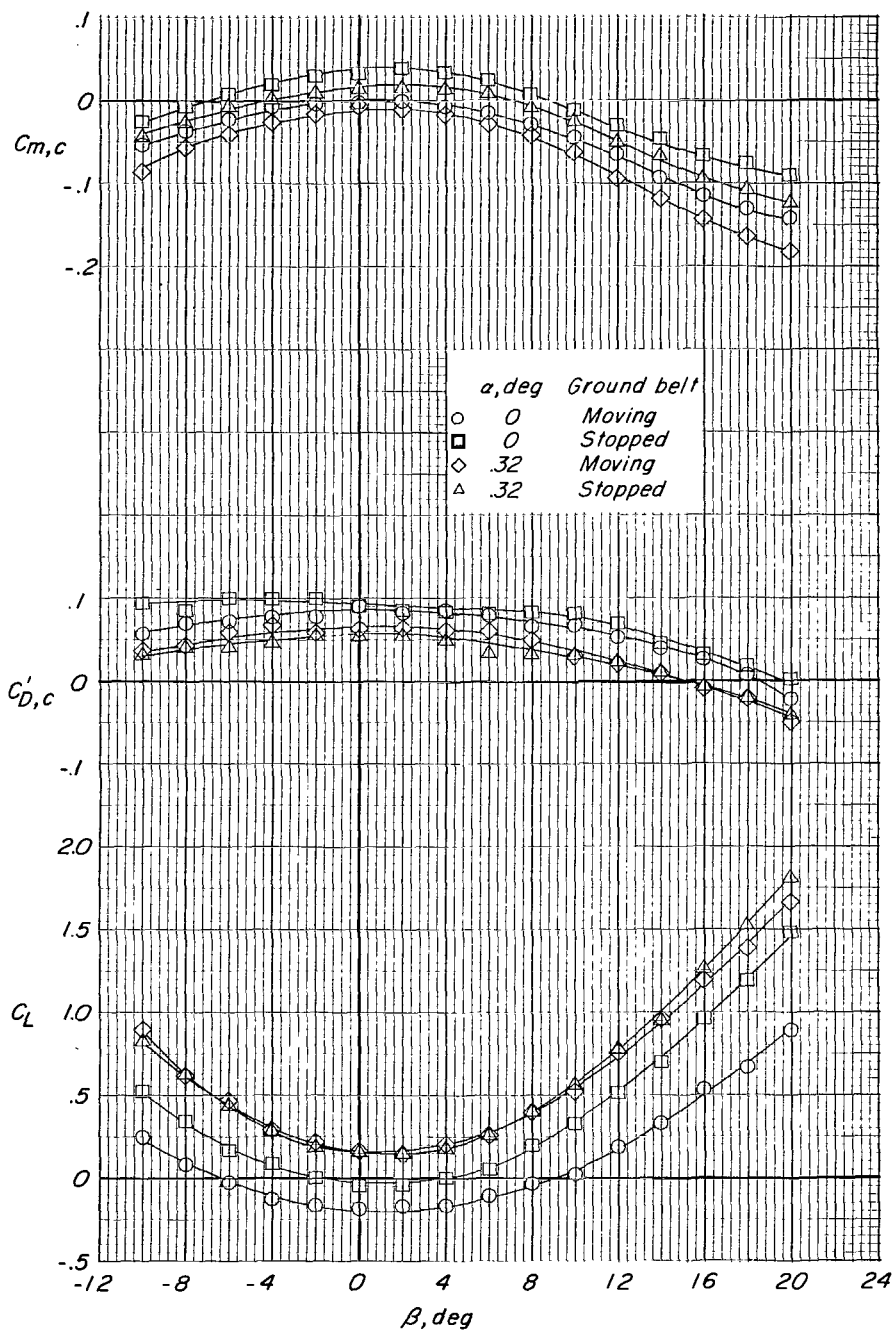
Half-circle(short extended sides)cross section, $H_{de} = .03$



(a) Lift, drag, and pitching-moment coefficients.

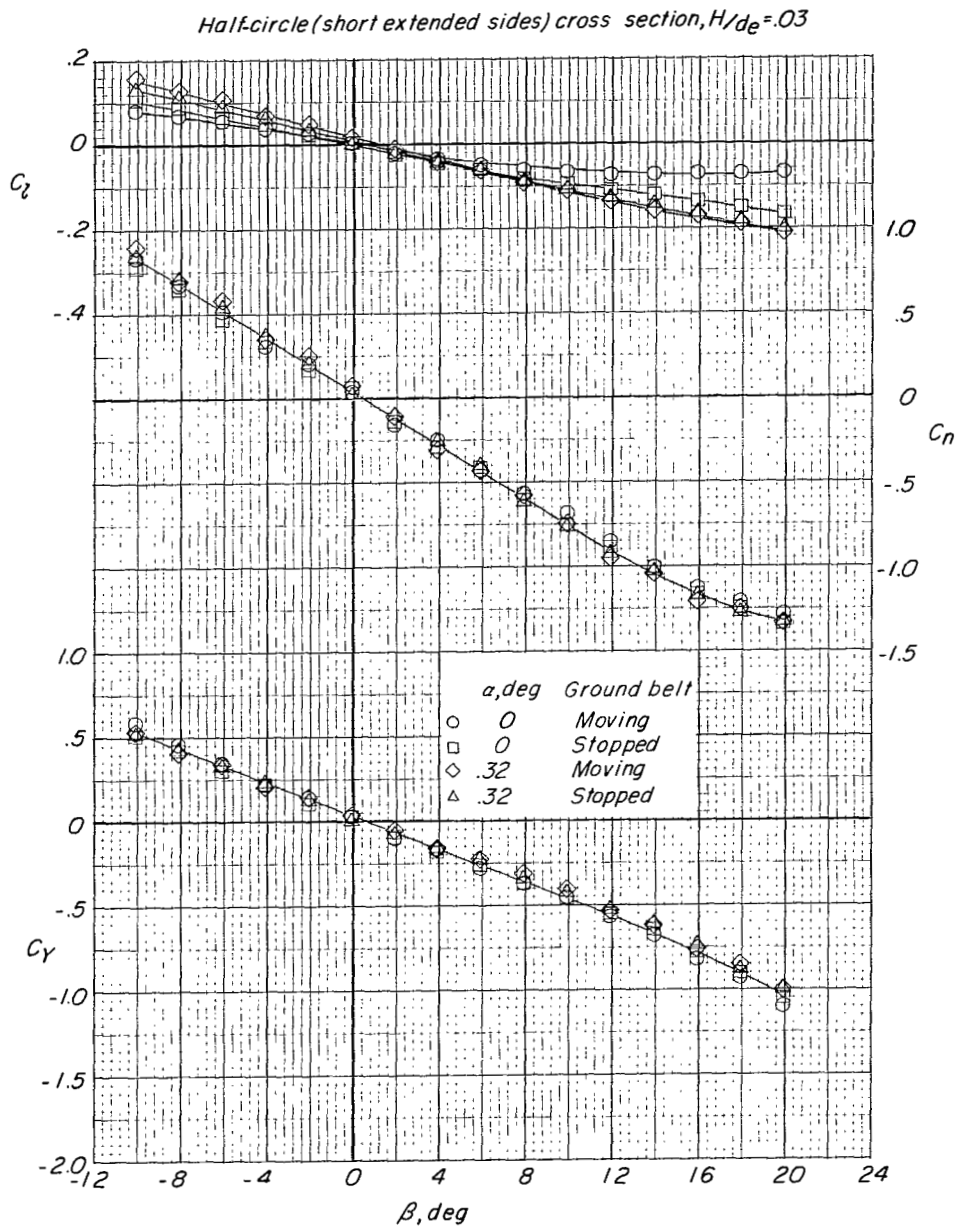
Figure 45.- Effect of angle of attack α on the aerodynamic characteristics of half-circle (short extended sides) configuration.

Half-circle(short extended sides) cross section, $H/d_e = 0.3$



(b) Lift, drag, and pitching-moment coefficients with base pressure corrections.

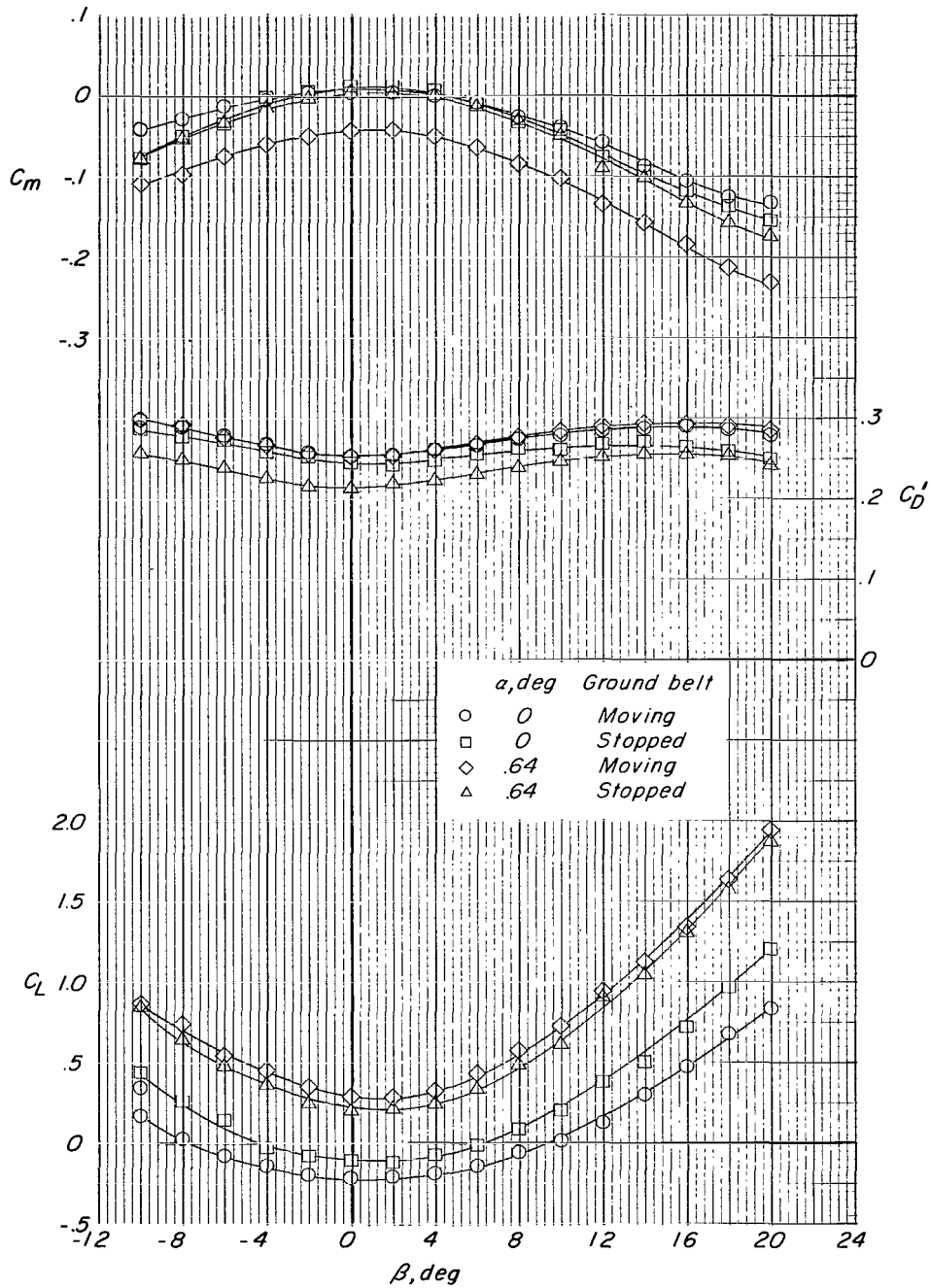
Figure 45.- Continued.



(c) Rolling-moment, yawing-moment, and side-force coefficients.

Figure 45.- Concluded.

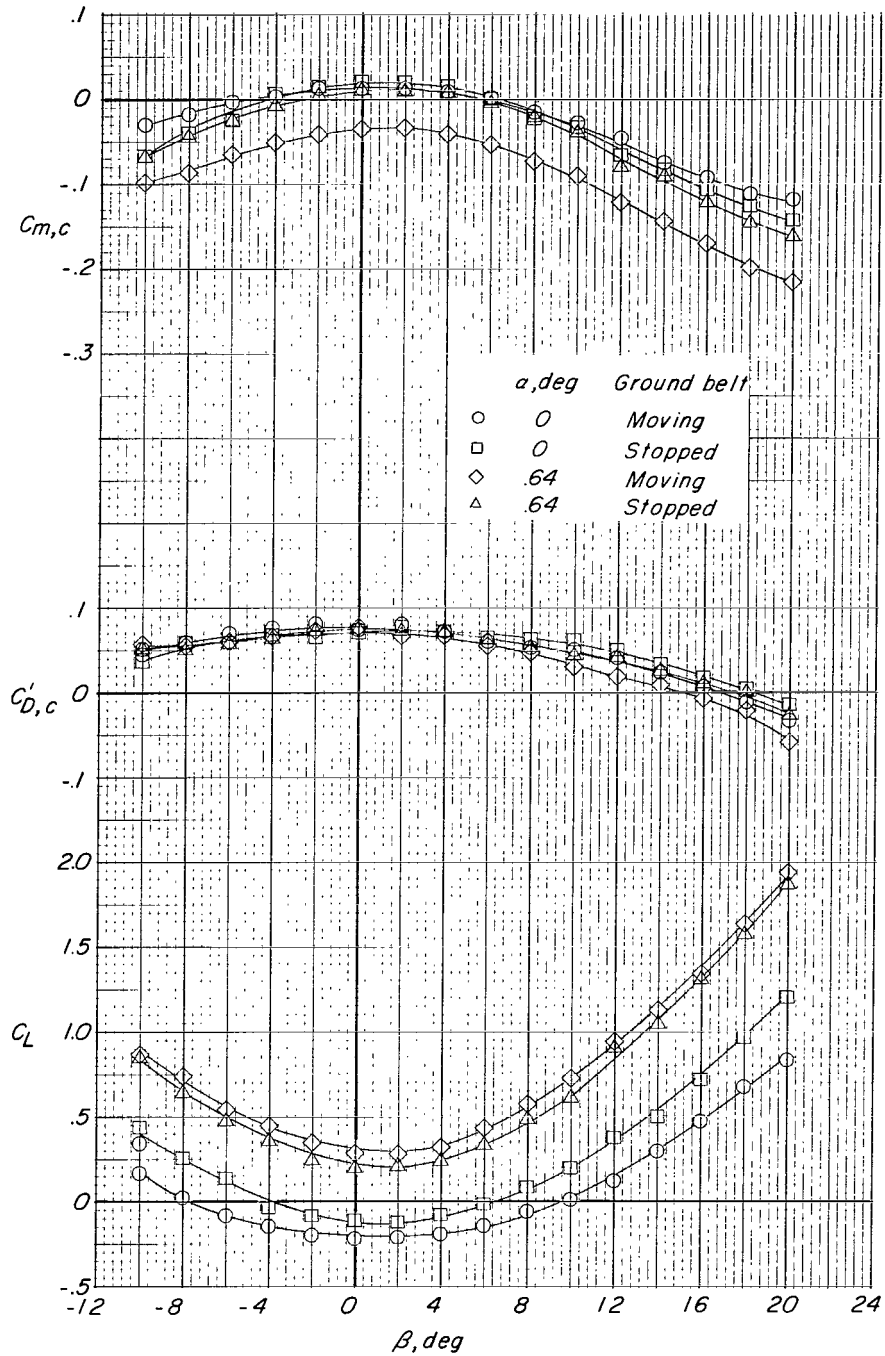
Half-circle(short extended sides) cross section, $H/d_e = .05$



(a) Lift, drag, and pitching-moment coefficients.

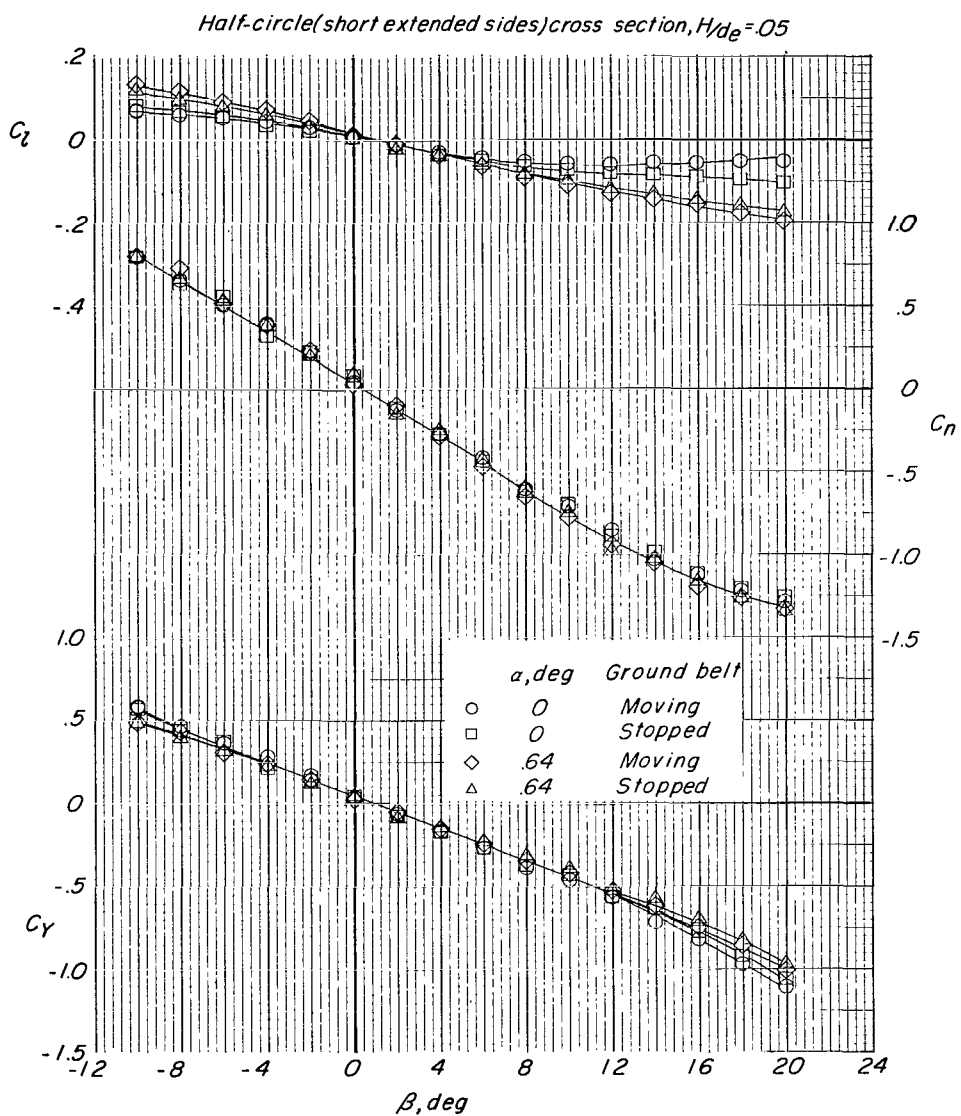
Figure 46.- Effect of angle of attack α on the aerodynamic characteristics of half-circle (short extended sides) configuration.

Half-circle(short extended sides) cross section, $H/d_e = .05$



(b) Lift, drag, and pitching-moment coefficients with base pressure corrections.

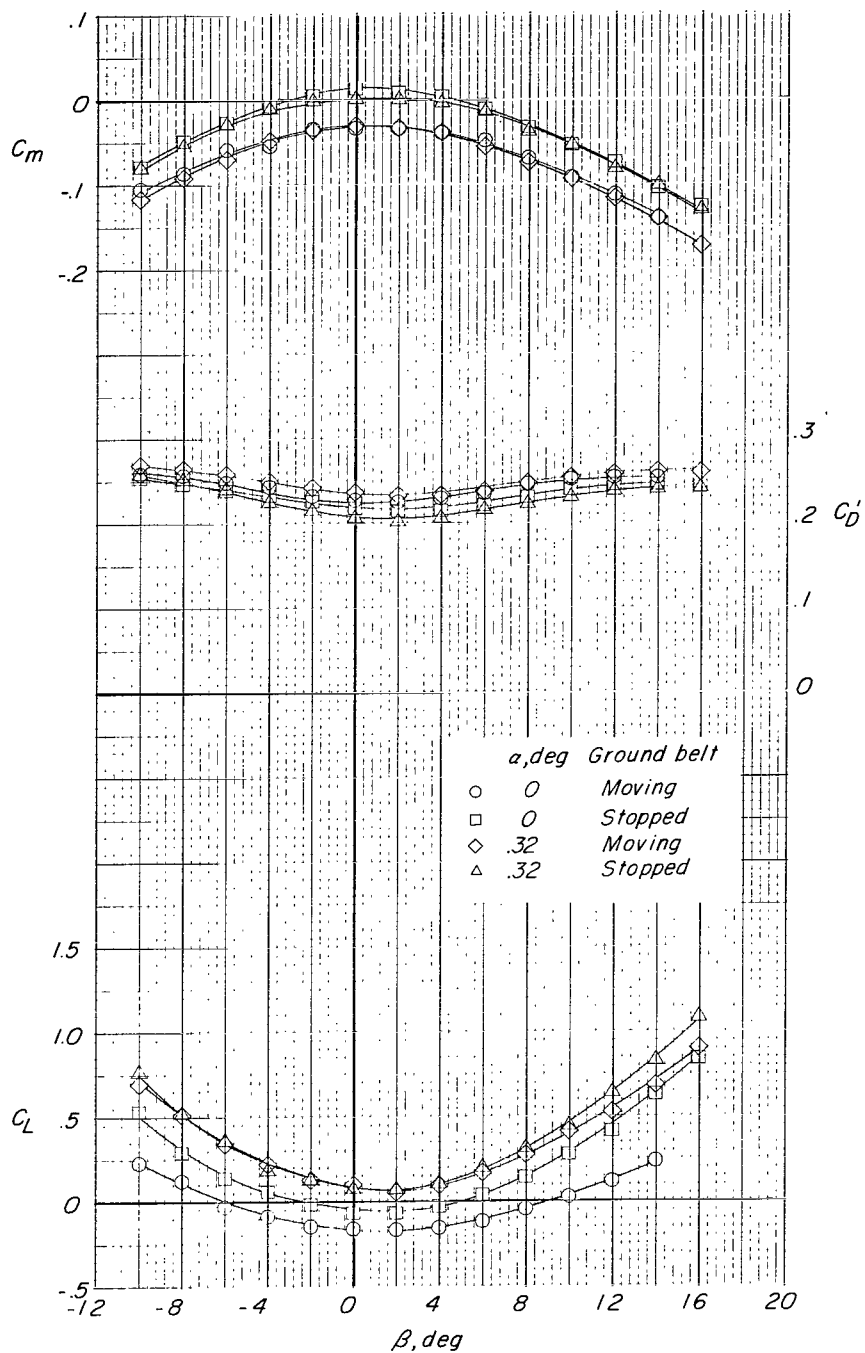
Figure 46.- Continued.



(c) Rolling-moment, yawing-moment, and side-force coefficients.

Figure 46.- Concluded.

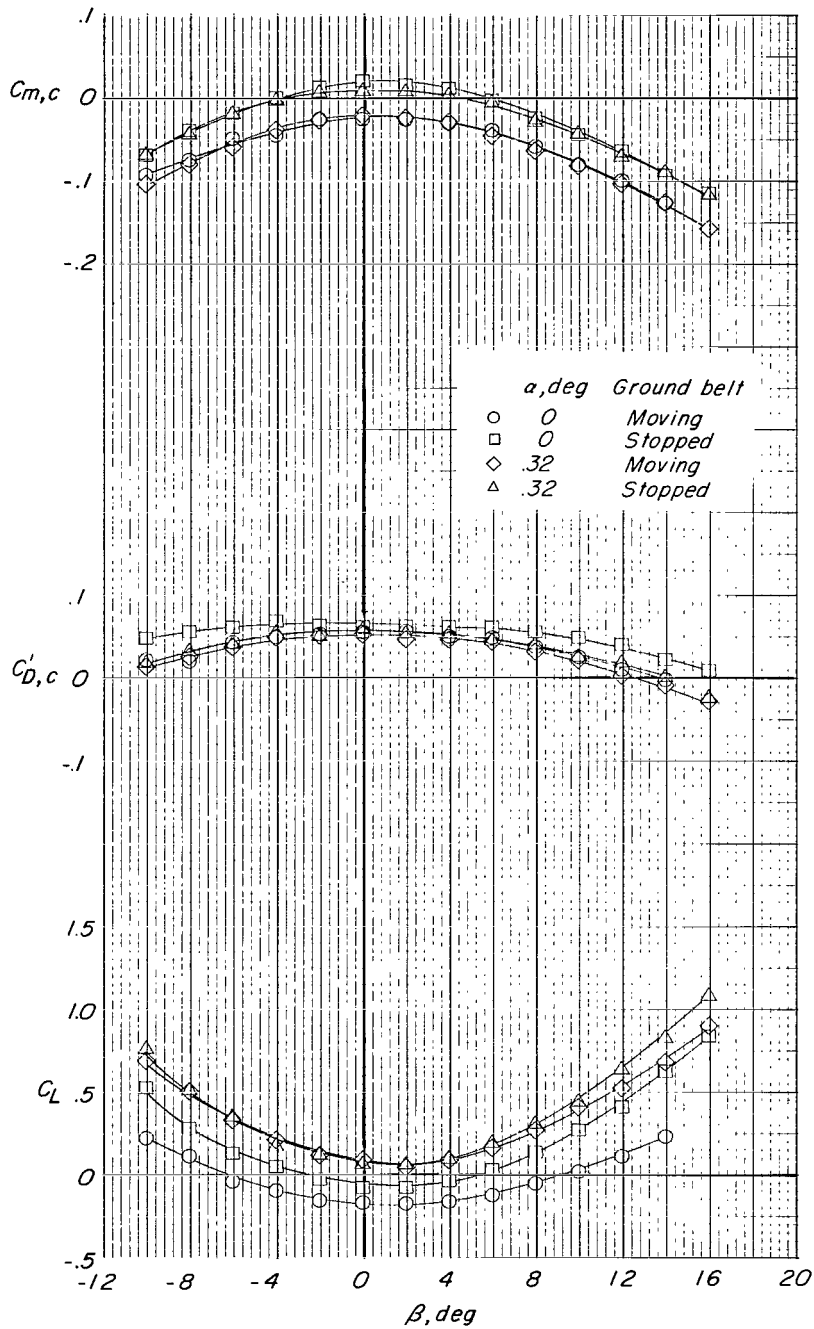
Half-circle(long extended sides)cross section, $H/d_c=.03$



(a) Lift, drag, and pitching-moment coefficients.

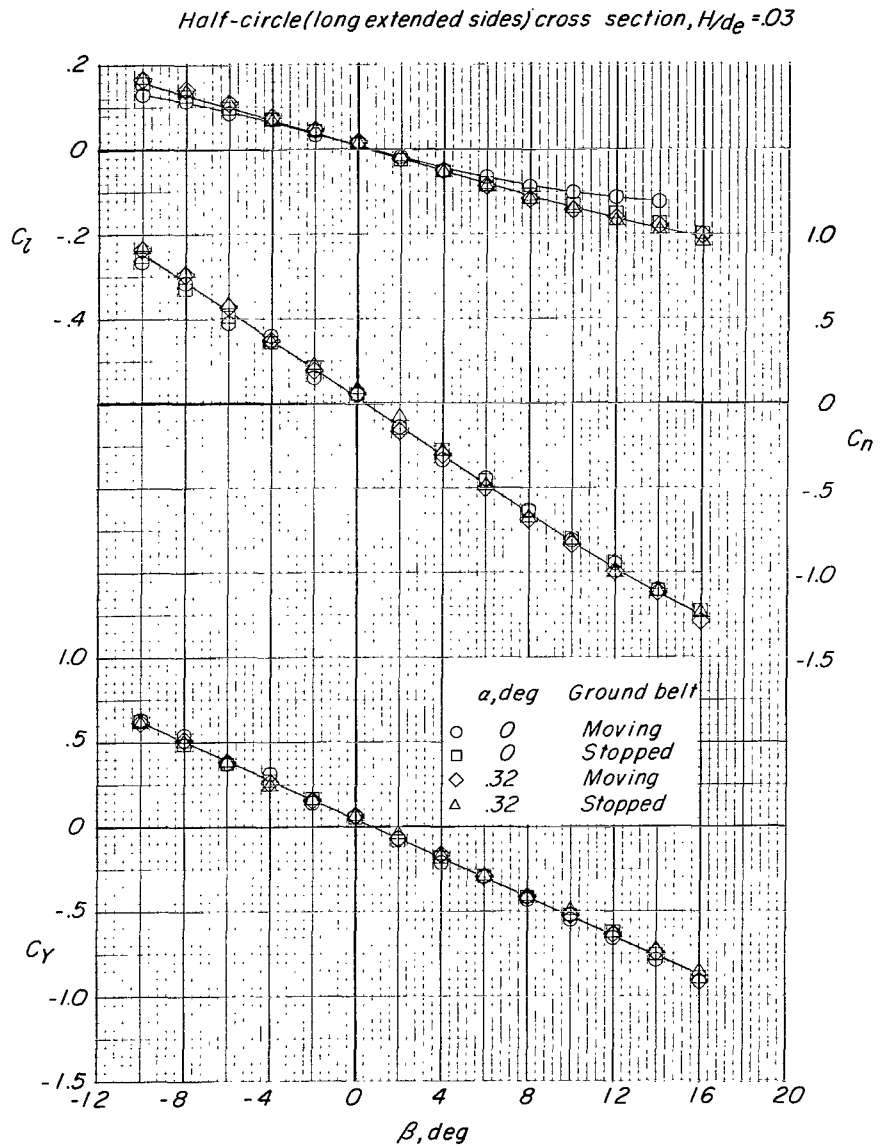
Figure 47.- Effect of angle of attack α on the aerodynamic characteristics of half-circle (long extended sides) configuration.

Half-circle (long extended sides) cross section, $H/d_e = .03$



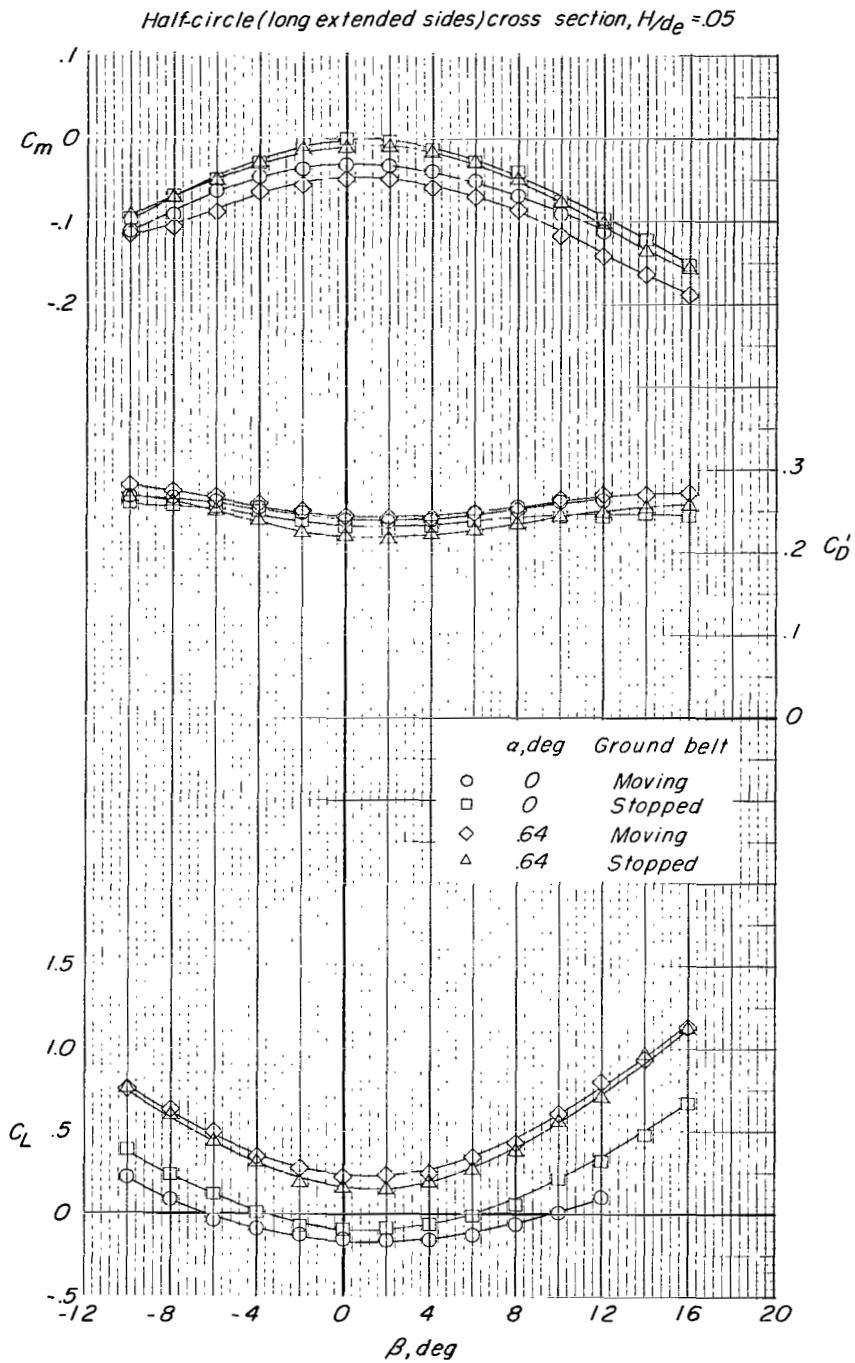
(b) Lift, drag, and pitching-moment coefficients with base pressure corrections.

Figure 47.- Continued.



(c) Rolling-moment, yawing-moment, and side-force coefficients.

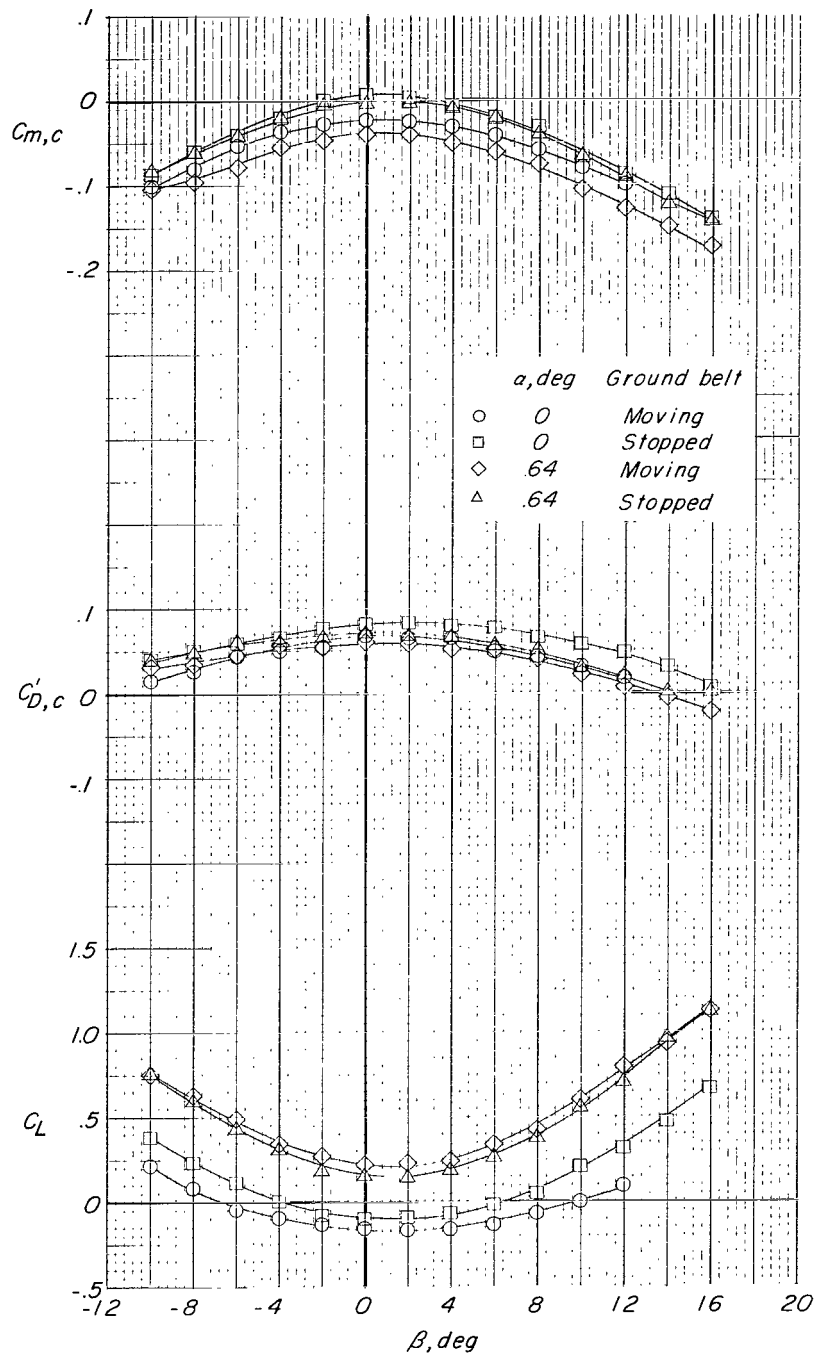
Figure 47.- Concluded.



(a) Lift, drag, and pitching-moment coefficients.

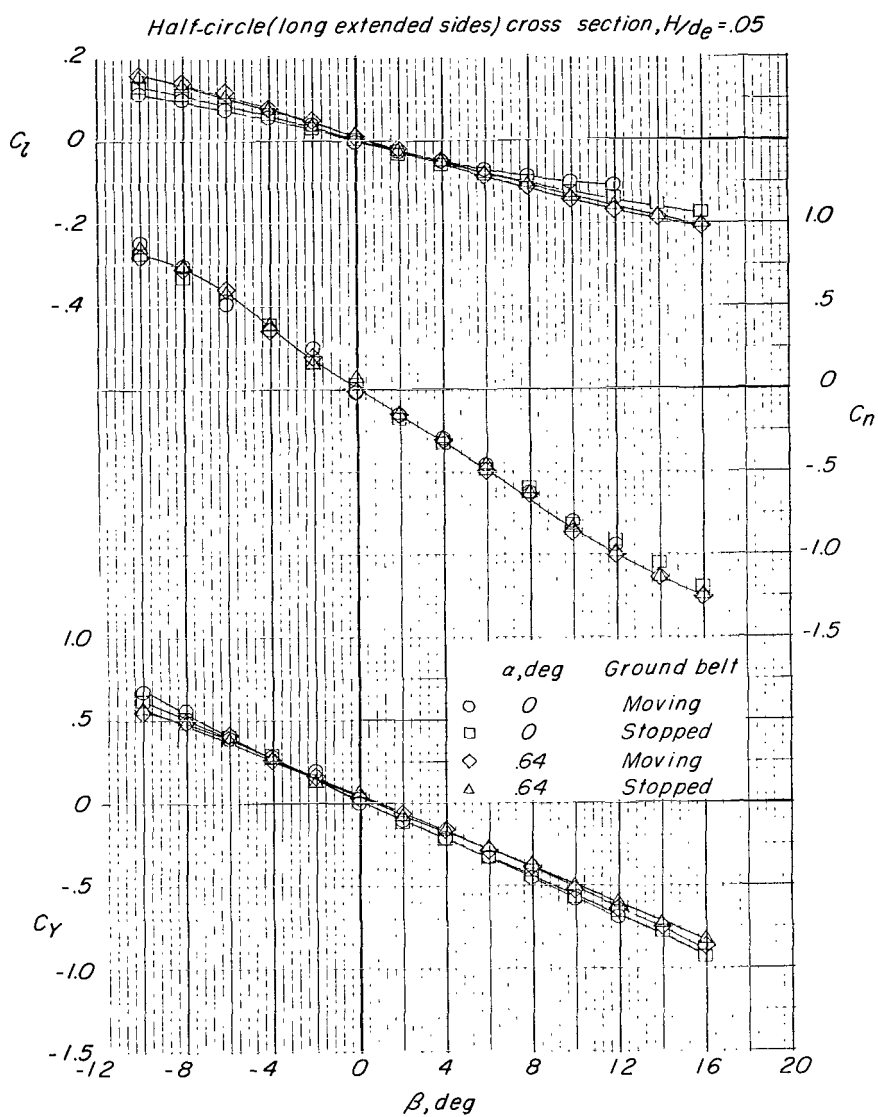
Figure 48.- Effect of angle of attack α on the aerodynamic characteristics of half-circle (long extended sides) configuration.

Half-circle (long extended sides) cross section, $H/d_e = 0.05$



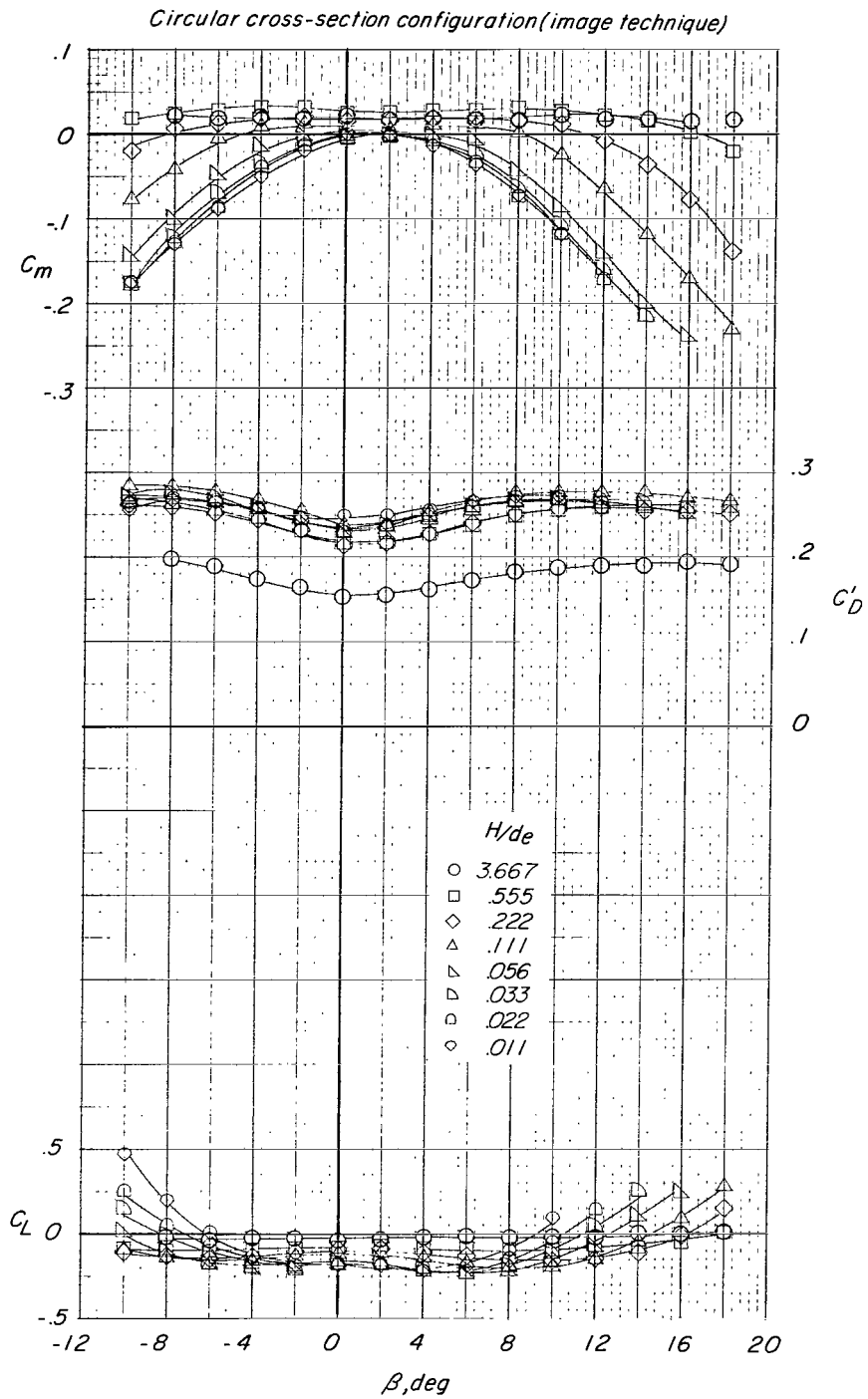
(b) Lift, drag, and pitching-moment coefficients with base pressure corrections.

Figure 48.- Continued.



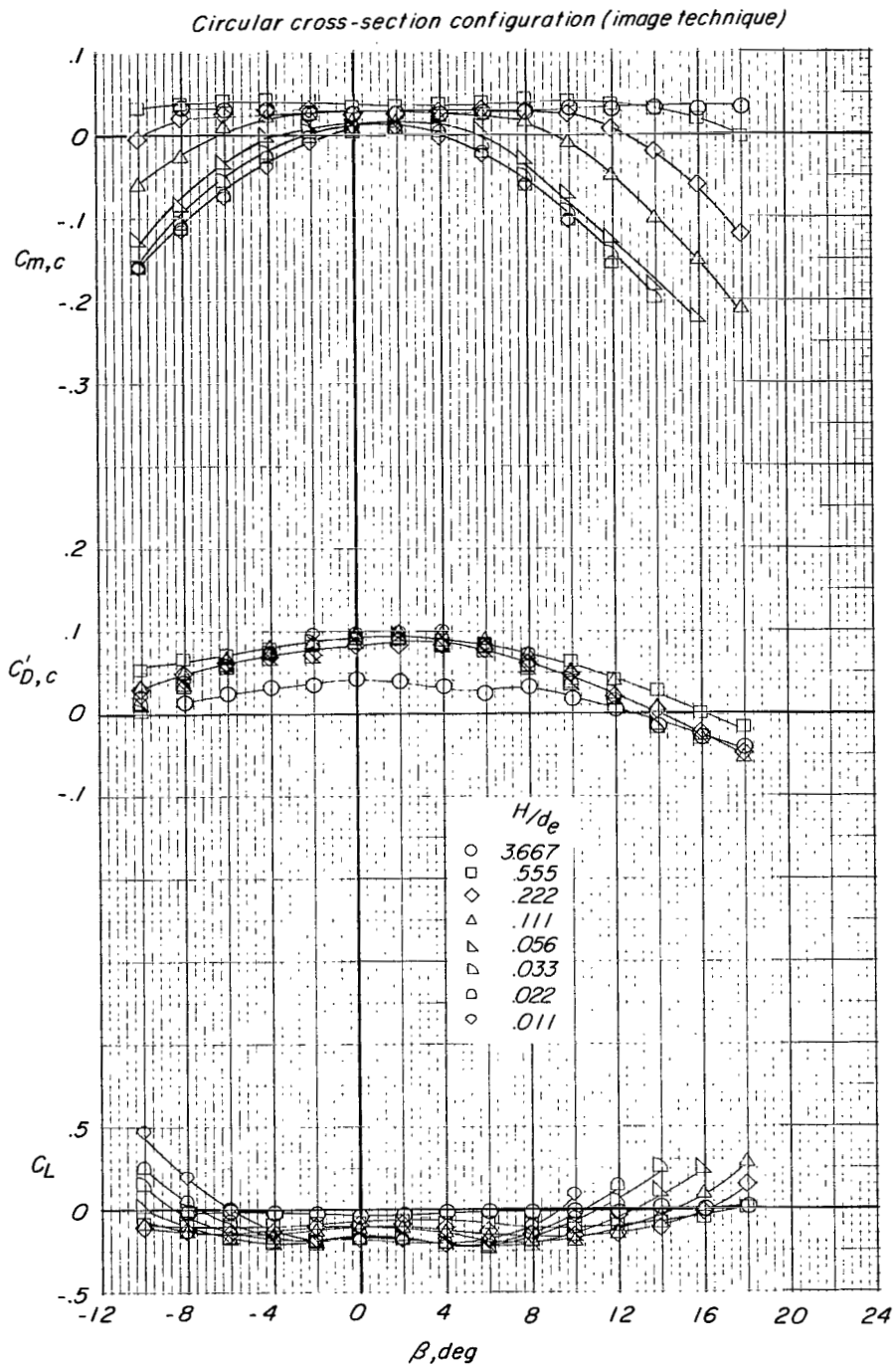
(c) Rolling-moment, yawing-moment, and side-force coefficients.

Figure 48.- Concluded.



(a) Lift, drag, and pitching-moment coefficients.

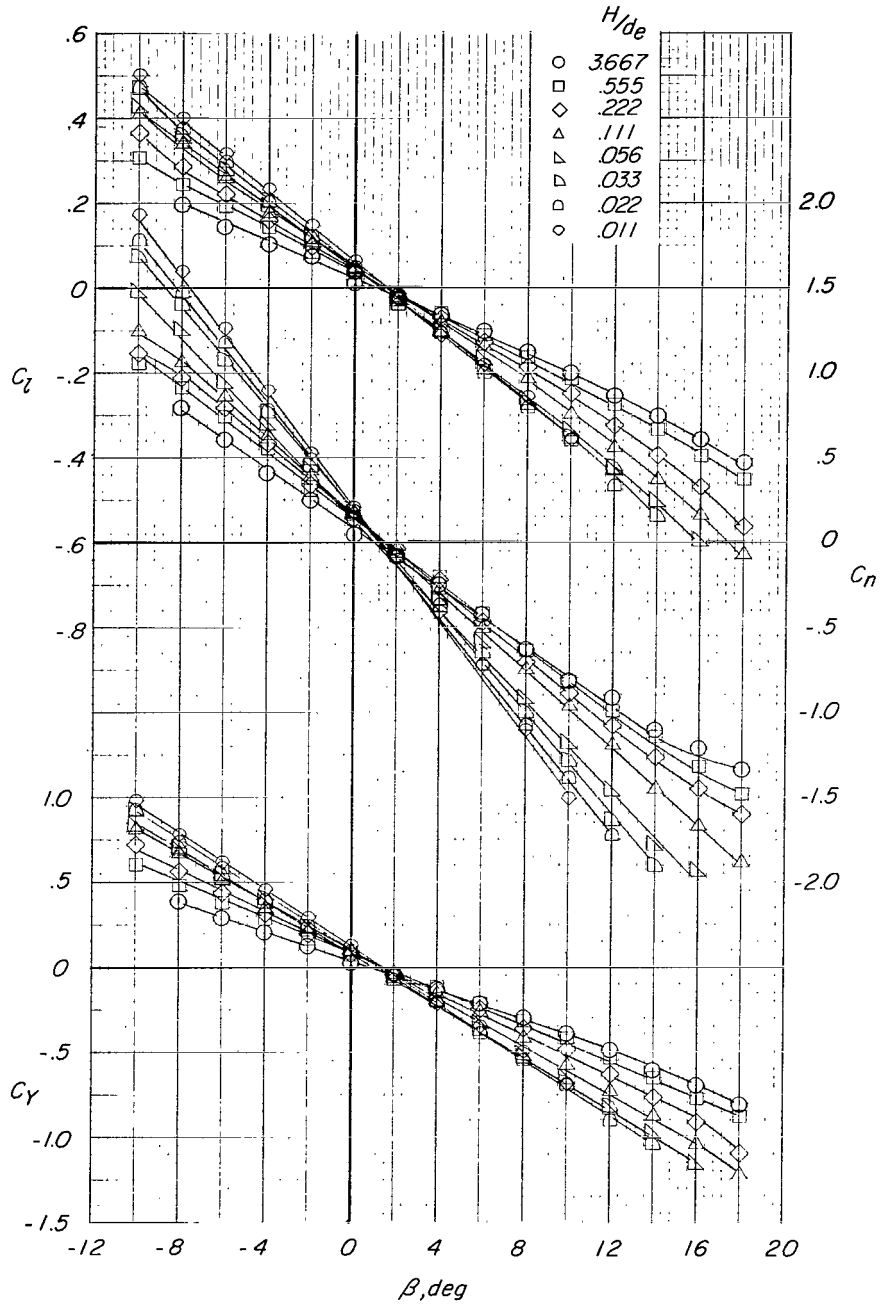
Figure 49.- Effect of height, by using image-model ground-simulation technique, on the aerodynamic characteristics of circular configuration.
 $\alpha = 0^\circ$.



(b) Lift, drag, and pitching-moment coefficients with base pressure corrections.

Figure 49.- Continued.

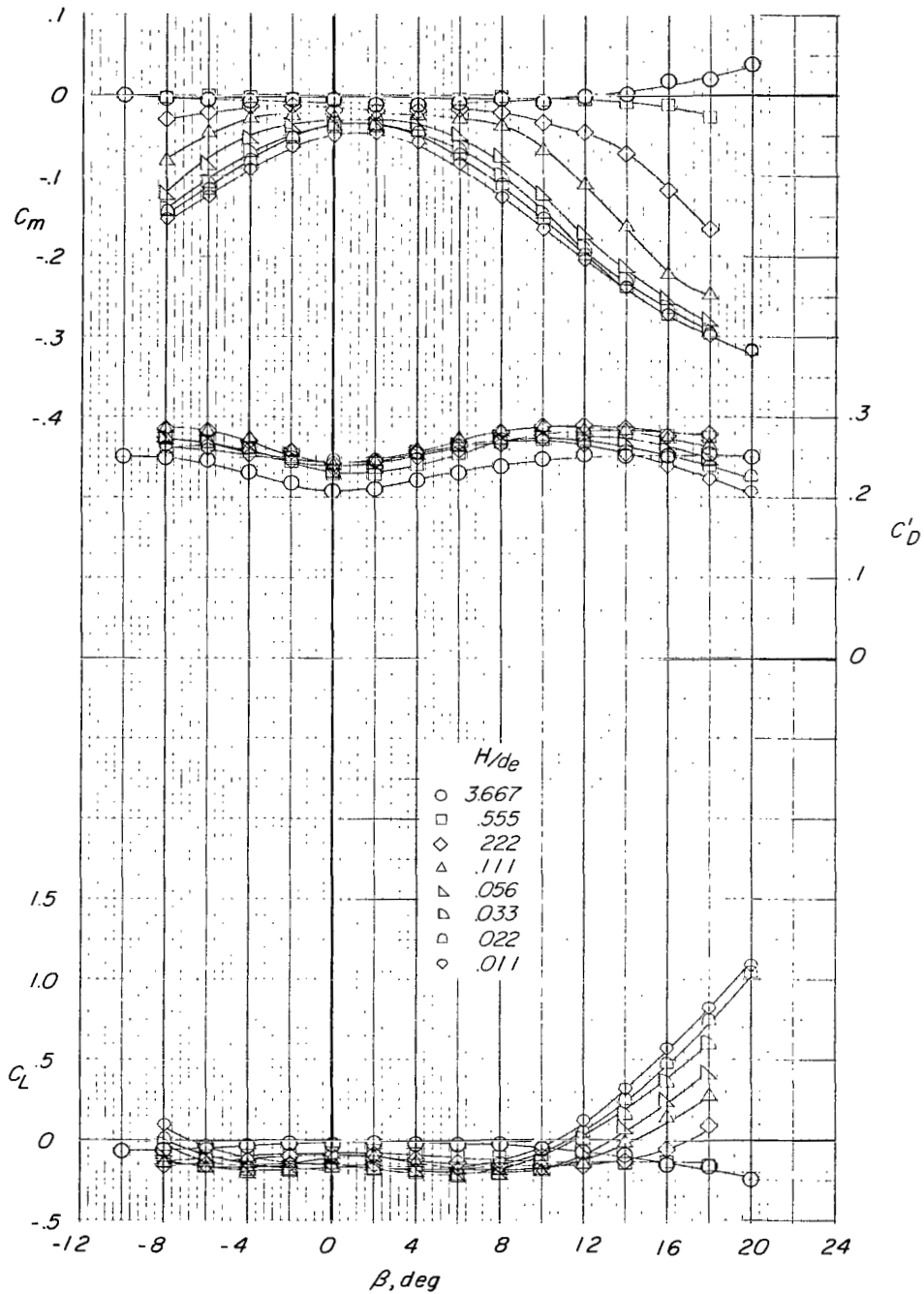
Circular cross-section configuration(image technique)



(c) Rolling-moment, yawing-moment, and side-force coefficients.

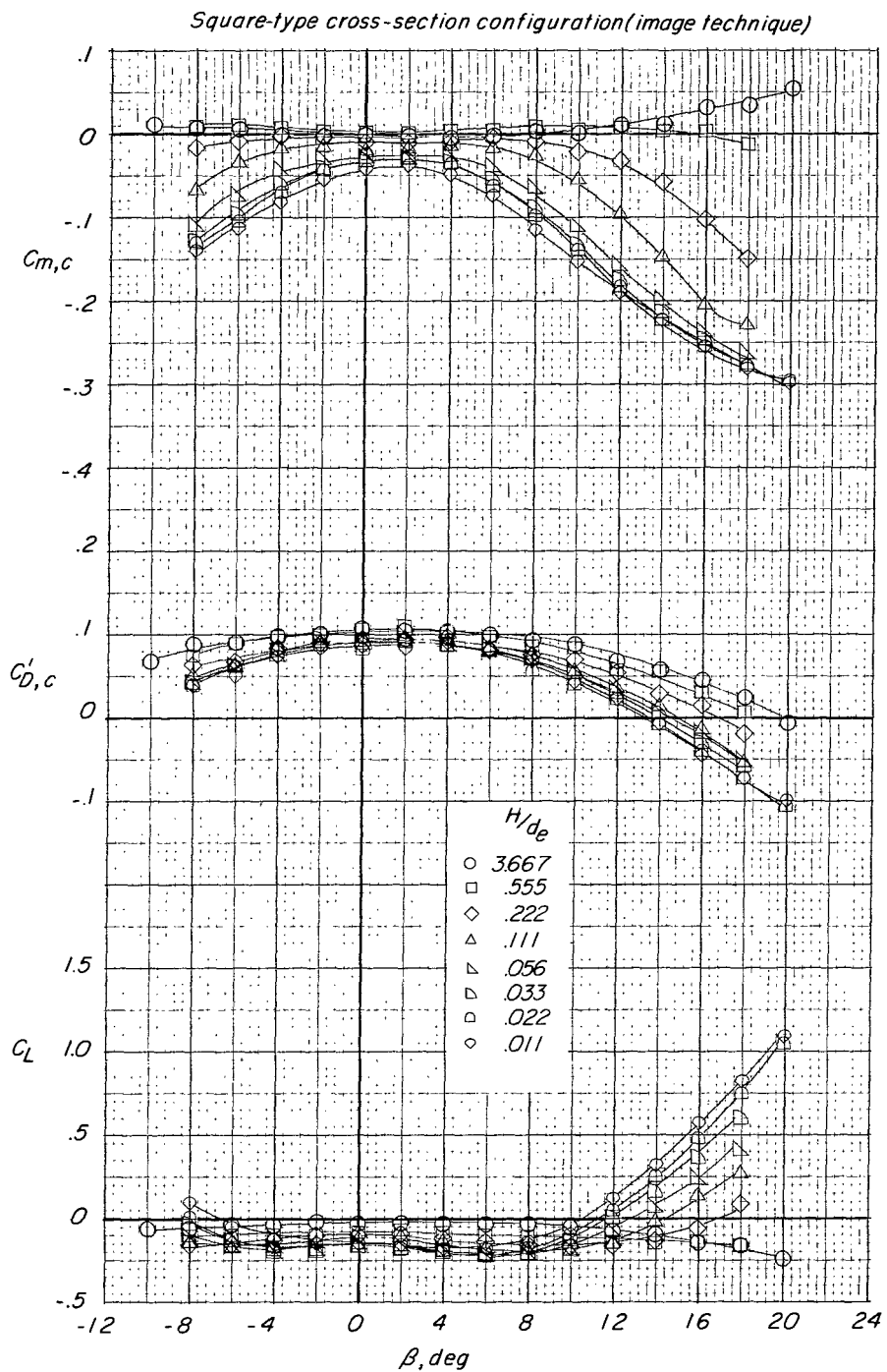
Figure 49.- Concluded.

Square-type cross-section configuration (image technique)



(a) Lift, drag, and pitching-moment coefficients.

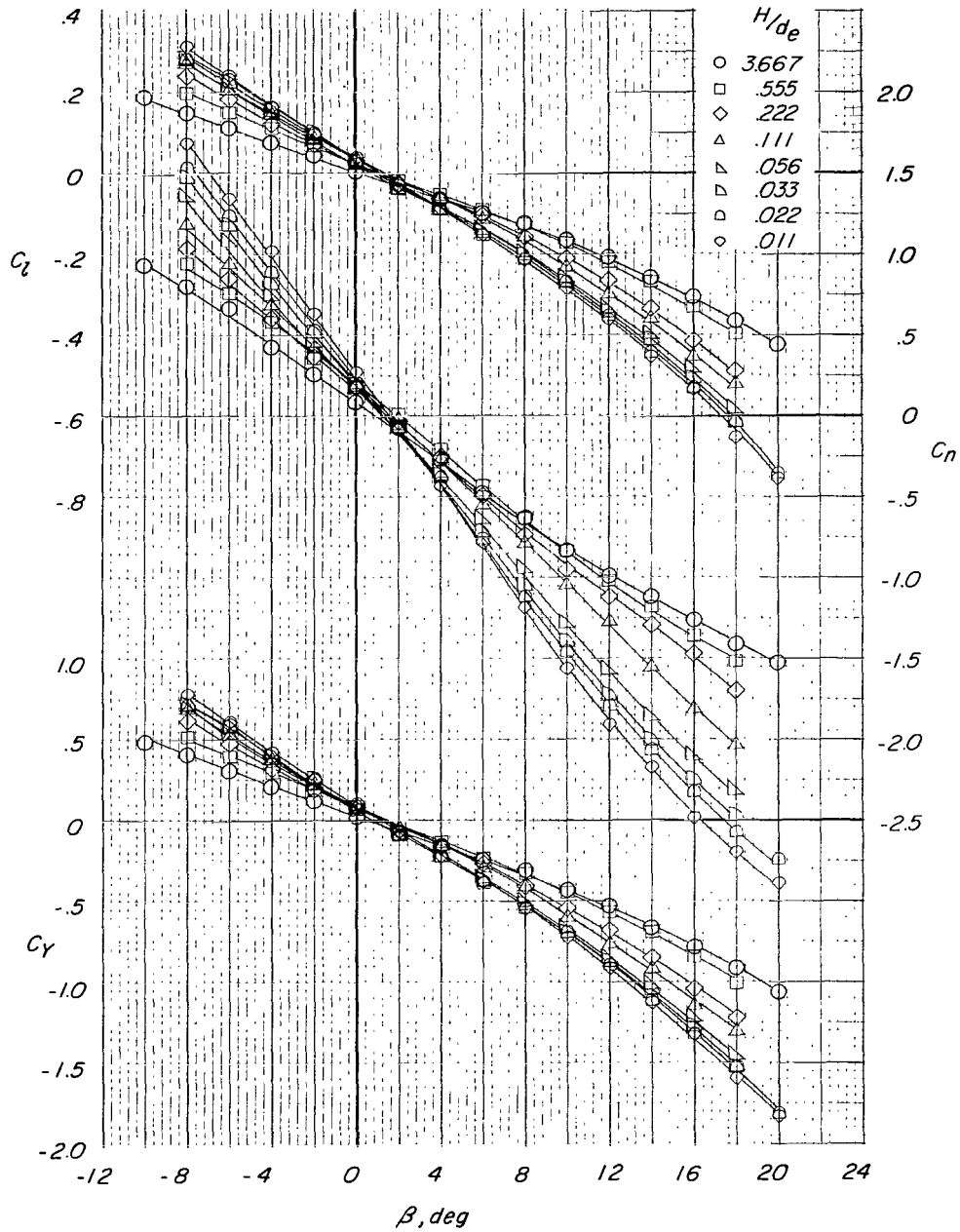
Figure 50.- Effect of height, by using image-model ground-simulation technique, on the aerodynamic characteristics of square-type configuration. $\alpha = 0^\circ$.



(b) Lift, drag, and pitching-moment coefficients with base pressure corrections.

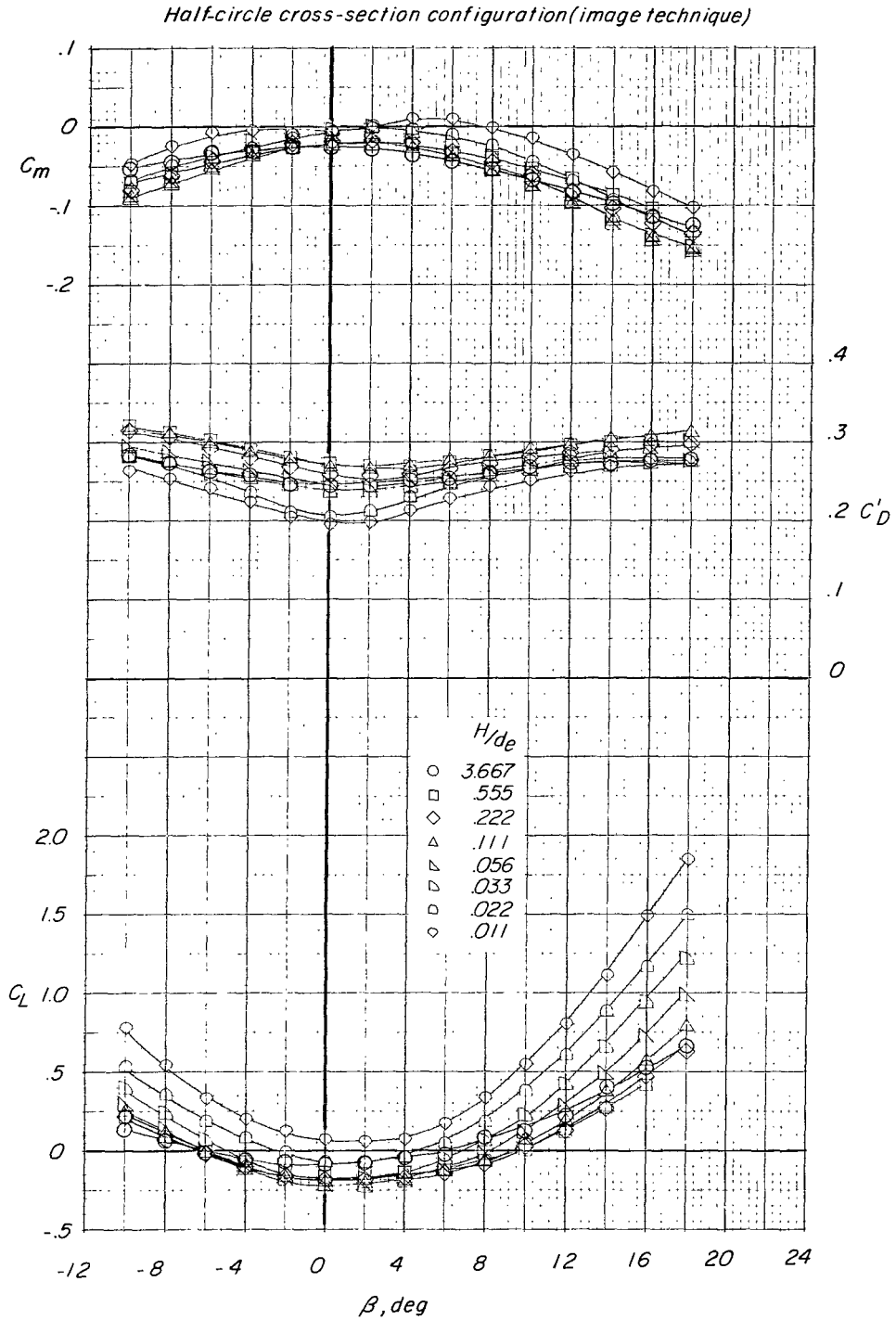
Figure 50.- Continued.

Square-type cross-section configuration (image technique)



(c) Rolling-moment, yawing-moment, and side-force coefficients.

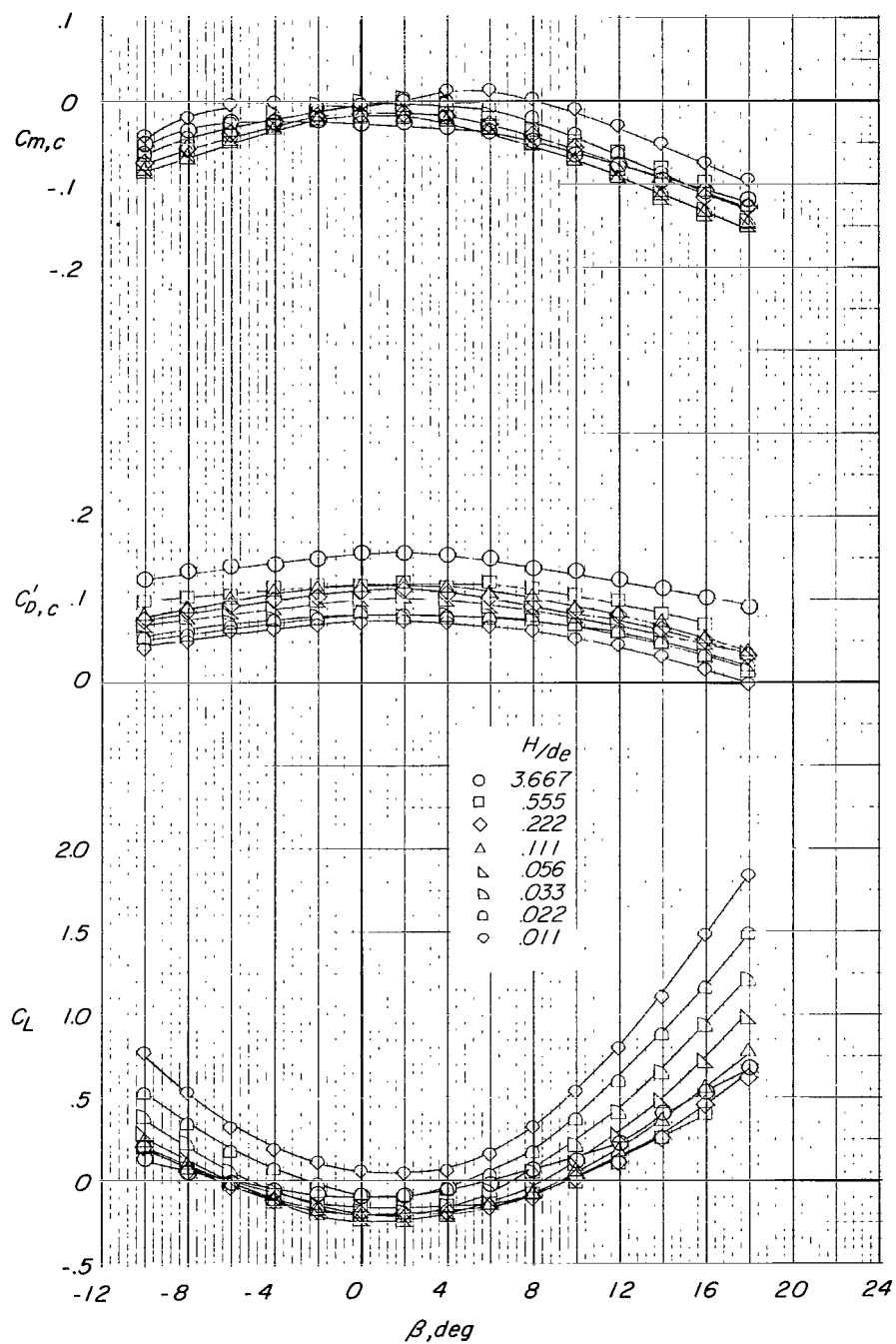
Figure 50.- Concluded.



(a) Lift, drag, and pitching-moment coefficients.

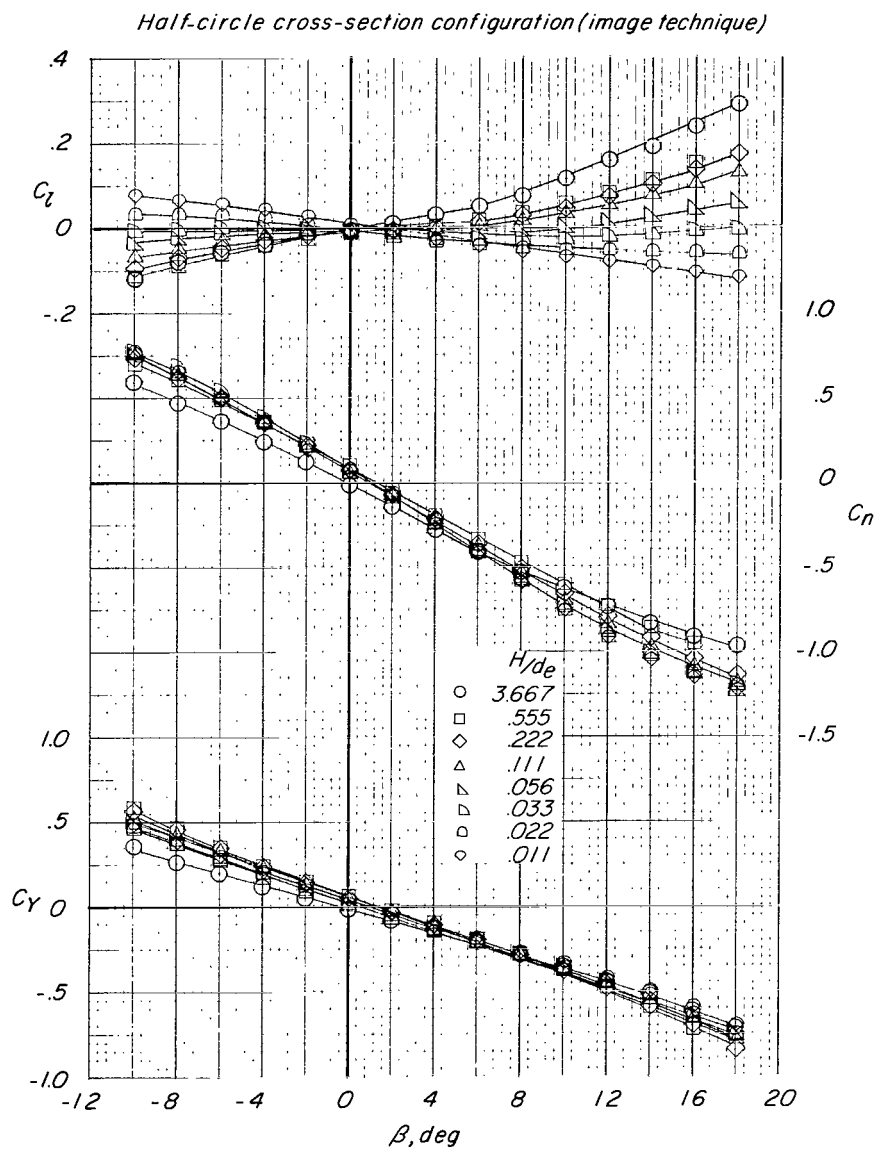
Figure 51.- Effect of height, by using image-model ground-simulation technique, on the aerodynamic characteristics of half-circle configuration.

Half-circle cross-section configuration (image technique)



(b) Lift, drag, and pitching-moment coefficients with base pressure corrections.

Figure 51.- Continued.



(c) Rolling-moment, yawing-moment, and side-force coefficients.

Figure 51.- Concluded.

NATIONAL AERONAUTICS AND SPACE ADMINISTRATION
WASHINGTON, D. C. 20546
OFFICIAL BUSINESS

FIRST CLASS MAIL



02U 001 26 51 3DS 70225 00903
AIR FORCE WEAPONS LABORATORY /WLUL/
KIRTLAND AFB, NEW MEXICO 87117

NO FEES PAID
AERONAUTICS
ADMINISTRATION

ATTN: E. LOU BOWMAN, CHIEF, TECH. LIBRARY

POSTMASTER: If Undeliverable (Section 1
Postal Manual) Do Not Return

"The aeronautical and space activities of the United States shall be conducted so as to contribute . . . to the expansion of human knowledge of phenomena in the atmosphere and space. The Administration shall provide for the widest practicable and appropriate dissemination of information concerning its activities and the results thereof."

— NATIONAL AERONAUTICS AND SPACE ACT OF 1958

NASA SCIENTIFIC AND TECHNICAL PUBLICATIONS

TECHNICAL REPORTS: Scientific and technical information considered important, complete, and a lasting contribution to existing knowledge.

TECHNICAL NOTES: Information less broad in scope but nevertheless of importance as a contribution to existing knowledge.

TECHNICAL MEMORANDUMS: Information receiving limited distribution because of preliminary data, security classification, or other reasons.

CONTRACTOR REPORTS: Scientific and technical information generated under a NASA contract or grant and considered an important contribution to existing knowledge.

TECHNICAL TRANSLATIONS: Information published in a foreign language considered to merit NASA distribution in English.

SPECIAL PUBLICATIONS: Information derived from or of value to NASA activities. Publications include conference proceedings, monographs, data compilations, handbooks, sourcebooks, and special bibliographies.

TECHNOLOGY UTILIZATION PUBLICATIONS: Information on technology used by NASA that may be of particular interest in commercial and other non-aerospace applications. Publications include Tech Briefs, Technology Utilization Reports and Technology Surveys.

Details on the availability of these publications may be obtained from:

SCIENTIFIC AND TECHNICAL INFORMATION DIVISION
NATIONAL AERONAUTICS AND SPACE ADMINISTRATION
Washington, D.C. 20546